Dryland rivers and hydroclimatic change: past, present and future

Okavango River, Botswana

Warrego River, Australia

Zacchary T. Larkin BEnv (Hons) MRes

Department of Environmental Sciences, Macquarie University

Thesis submitted for the degree of Doctor of Philosophy, January 2019

MACQUARIE
University

"Study the past, if you would divine the future"

- *Confucius*

TABLE OF CONTENTS

ABSTRACT

Rivers and wetlands in drylands are vital components of the landscape that provide countless beneficial services to humans and ecosystems. The hydrological and geomorphological diversity of rivers across time and space makes comprehensive understanding of fluvial systems and prediction of future change very difficult. A long-term perspective, however, can improve our ability to assess the sensitivity of dryland rivers to extrinsic forcing, such as climate-driven hydrological (hydroclimatic) changes, and contextualises the natural range of variability defining modern rivers. This thesis aims to understand: 1) how dryland rivers have responded to past hydroclimatic changes, 2) the processes that define the natural range of variability of modern rivers, and 3) how dryland rivers will respond to future hydroclimatic change. Hydroclimatic change has affected dryland rivers differently around the world, but evidence from eastern Australia and southern Africa suggests a relatively synchronous period of enhanced fluvial activity during the early to mid-Holocene (~8–4 ka) followed by relative quiescence of fluvial activity in the late Holocene. An inter-continental approach allows an improved understanding of how hydroclimatic changes manifest in dryland rivers in very different settings. The fan-shaped alluvial plain of the lower Warrego River in eastern Australia has preserved evidence for large (~160 m), sinuous, laterally migrating palaeochannels that were transporting ~20 times the discharge of the modern river and were active until ~5 ka. The modern Warrego River has a markedly different planform, with narrower, straighter anabranching channels in the equivalent position on the plain. Similarly, in the Panhandle region of the Okavango Delta, northern Botswana, large (~120 m), sinuous, laterally migrating palaeochannels conveyed up to ~9 times the discharge of the modern system during a period of enhanced rainfall over the headwaters that lasted until ~3.5 ka. The response of the Okavango River to subsequent declining discharge has been to contract considerably and, in the Panhandle, processes of channel adjustment by avulsion now dominate over lateral migration. A range of hydroclimatic drivers, related to orbital variations and climatic teleconnections, have likely been responsible for declining fluvial activity and dramatic transformations of river style in the late Holocene. The geomorphological sensitivity of the Warrego and Okavango rivers to relatively modest Holocene hydroclimatic change highlights that improving understanding of how rivers will respond to future climate change is of critical importance. Prediction of future fluvial change in dryland settings requires consideration of the intrinsic processes of river adjustment and the influence of extrinsic, hydroclimatic forcing on these processes. Catchment aridity strongly influences the geomorphology of Australian dryland rivers. By defining thresholds of aridity and modelling future climatic conditions, this research indicates that many Australian dryland rivers will likely undergo profound changes to their physical character and behaviour over coming decades/centuries, most likely in the form of increased likelihood of flow disconnection and channel breakdown.

CERTIFICATE

This thesis comprises original research performed by Zacchary T. Larkin, and has not previously been submitted for a degree or diploma at any university or institution. To the best of my knowledge and belief, this thesis contains no material previously published or written by another person except where due reference is made in the thesis itself.

The Introduction section of this thesis details the contributions of fellow authors to the four data chapters prepared, or under review, for publication. Non-author contributions to this thesis are detailed in the acknowledgements section of each data chapter. The sources of data used in this thesis are detailed in the methods and acknowledgements sections of each data chapter.

Zacchary T. Larkin

18 January, 2019

ACKNOWLEDGEMENTS

x

CHAPTER 1

Introduction

Rivers are vital components, and architects, of the landscape. They provide countless beneficial functions to humans and ecosystems, and throughout history have been lifelines along which civilisations, agriculture, industry, and trade have flourished (Costanza et al., 1997; Macklin and Lewin, 2015). This is particularly true of rivers in the Earth's drylands where scarcity of surface water makes rivers disproportionately important for ecosystems and people. Nevertheless, the geomorphological and hydrological variability of dryland rivers across time and space is well recognised by geologists, geomorphologists, engineers, and managers, and often makes comprehensive understanding of systems and prediction of change very difficult (Schumm, 1977; 2005). In particular, the sensitivity of dryland rivers to climate-driven hydrological (hydroclimatic) change in the past is poorly understood, making it difficult to assess how these critical and complex systems will respond to future hydroclimatic change. As such, this thesis is guided by three main research questions that address how hydroclimatic change affects past, present and future river response: 1) How have dryland rivers responded to hydroclimatic change in the past?; 2) What processes define the natural range of variability of modern dryland rivers?; and 3) How will dryland rivers respond to future hydroclimatic change?

1.1 Geomorphology of dryland rivers

Drylands are regions with subhumid, semiarid, arid or hyperarid climates and cover ~40 % of the Earth's land surface (UNEP, 1992). They are characterised by net moisture deficits with generally low amounts of highly variable rainfall and runoff, and, given significant atmospheric water demand, high rates of evapotranspiration. Despite this, drylands support large river and wetland systems on most continents (Tooth, 2000; Tooth and McCarthy, 2007). These dryland rivers are highly variable in terms of their character and behaviour. River character refers to the physical structure of a river incorporating channel pattern, planform and cross-sectional morphology, while river behaviour refers to the set of processes responsible for producing the characteristic morphology and planform of the river (Brierley and Fryirs, 2005). Some dryland rivers have perennial or seasonal flow regimes and maintain a single, commonly sinuous through-going channel to base level (Fig. 1.1A). Others are characterised by sinuous or straight channels with dramatic downstream declines in discharge and channel size. These downstream declining rivers can breakdown completely, forming unchannelled wetlands or floodouts when channelised flow can no longer be maintained (Fig. 1.1B-F).
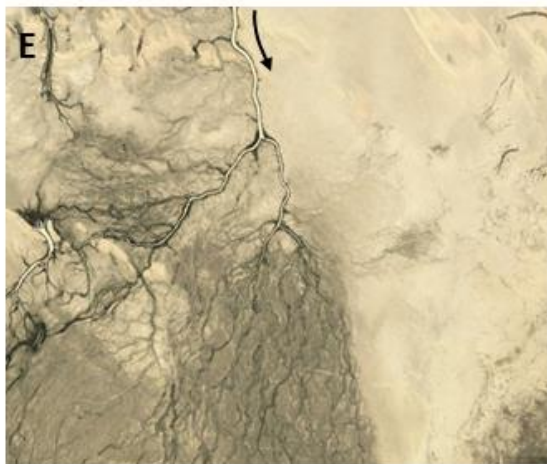
Figure 1.1. Diversity of dryland rivers. Arrows show flow direction.

The 2005 Millennium Ecosystem Assessment (MEA) identified that, given their location in otherwise dry landscapes, rivers and wetlands in drylands are disproportionately important providers of ecosystem

services. Ecosystem services can be defined as benefits provided to humans by the presence and functioning of a natural system (Clarkson et al., 2010). For rivers and wetlands, these services fall into four categories which are: 1) provisioning (e.g. food, water, and raw materials); 2) regulating (e.g. flood attenuation, water quality improvement, and maintenance of soil fertility); 3) habitat (hotspots of biodiversity and habitat complexity); and 4) cultural (e.g. recreation/tourism, art, spiritual experience) (MEA, 2005; Costanza et al., 1997). The physical characteristics of the dryland fluvial landscape (i.e. a single channel, multiple anastomosing and distributary channels, unchannelled wetlands, or discontinuous channel segments, Fig. 1.1) are defined by the character and behaviour of dryland rivers, and influence the type of ecosystem services provided by the river, as well as influencing ecosystem structure and functioning, and guiding agricultural and other land use practices (Kotze et al., 2009). By taking a long-term perspective of dryland river evolution and understanding how these systems respond to extrinsic forcing, we can better define thresholds of change and improve our ability to predict future change in these fundamentally important and highly complex systems.

1.2 Late Quaternary climate change and fluvial response in drylands

The Earth's climate has changed significantly over the late Quaternary (last ~100 ka) in response to a range of drivers and feedbacks, from Milankovitch-scale orbital variations that pace glacial-interglacial cycles to regional-scale impacts of atmospheric and oceanic circulation changes (Petit et al., 1999; Meadows, 2001; Fitzsimmons et al., 2013). Proxy records derived from marine or lacustrine sediment cores, ice cores, speleothems, tree rings, and corals are invaluable for reconstructing climate conditions over a range of spatial and temporal scales and resolutions (McCarroll, 2015). Organic-based proxy records in the world's extensive drylands however, are relatively scarce (a notable exception is the use of hyrax middens to reconstruct climatic conditions in the southern African drylands, Chase et al., 2010, 2012, 2013). As such, landform records or geoproxies, such as palaeochannels and palaeolake shorelines provide the most promising record of past climate change (Tooth, 2012). For example, in southeastern Australia, much of what we know about climate in the dryland interior over the past ~50 ka has been interpreted from geoproxy records (Nanson et al., 1992, 1995; Page et al., 2009; Cohen et al., 2012, 2015; Hesse et al., 2018a, b; Mueller et al., 2018). It is from this perspective that most palaeofluvial research is conducted; with the view to understand past climates. Understanding thresholds and feedbacks defining river response to such climate change is often a secondary consideration, particularly when modern channels and palaeochannels have similar morphology but are scaled differently due to different prevailing hydrological regimes. In some dryland systems, however, palaeochannels and their modern counterparts have striking differences in character, providing a good opportunity to understand both past regional hydroclimatic change and also the threshold responses to extrinsic forcing that drive dramatic changes in river character and behaviour. Holocene palaeofluvial records are relatively rare, likely because the warm, wet Holocene interglacial was characterised by relatively modest climatic

changes compared with other glacial and interglacial periods in the late Quaternary and, as such, are thought to be less useful for understanding long-term past climate change (Petit et al., 1999; McCarroll, 2015). Also, high-resolution organic and inorganic proxy records from depositional settings other than rivers that yield Holocene records are generally more numerous and well preserved than for periods earlier in the Quaternary (McCarroll, 2015).

In Australia, exceptions exist. For example, one of the most continuous palaeo-fluvial records in southeastern Australia is derived from an array of palaeochannels on the Macquarie River floodplain. During Marine Isotope Stage 3 (MIS3, ~60–27 ka), the Macquarie River was a very large, meandering river transporting ~270 times the discharge of the modern system (Hesse et al., 2018a, b). From about 50 ka, the Macquarie River declined markedly in size, but maintained a consistent planform (single-thread, meandering channel) until the mid Holocene (Hesse et al., 2018a, b). However, after ~5.5 ka, the Macquarie River underwent a dramatic change in character and behaviour, forming a complex system of disintegrating distributary channels and unchannelled floodplain wetlands. During its larger, higher energy phases, the behaviour of the Macquarie River was relatively consistent as it maintained a meandering channel to base level, but towards the lower energy end of its evolution around 5.5 ka, the Macquarie River crossed an extrinsic geomorphic threshold, triggering a dramatic change in the character and behaviour of the river as it became a very low-energy, discontinuous river type with extensive floodplain wetlands. Interestingly, the Murrumbidgee River a few hundred kilometres south of the Macquarie River underwent a similar decline in size and discharge from MIS2 to the present-day, but it has maintained a through-going, meandering channel (Hesse et al., 2018b; Mueller et al., 2018). The Murrumbidgee River did not cross a similar extrinsic geomorphic threshold to that which resulted in the dramatic response of the Macquarie River. Defining these types of thresholds will improve our ability to forecast future changes to the character and behaviour of dryland rivers around the world.

1.3 Intrinsic processes and extrinsic forcing

One challenge in understanding geomorphological sensitivity of dryland fluvial systems is that alluvial rivers are dynamic, non-linear, and self-adjusting systems that are controlled both by intrinsic processes of adjustment and extrinsic forces (Schumm, 1977; Phillips, 1992; Phillips, 2003). Intrinsic processes are related to the balance between discharge, slope, and sediment supply, and drive river adjustment within a range of variability (Lane, 1955) even in the absence of changes to the external environment. However, extrinsic forces such as climate and hydrology, tectonics, lithology, and human activities have an overarching control on the environmental parameters (or flux boundary conditions, Fryirs et al., (2012)) of a system (e.g. flow regime, slope, sediment load), and largely define the natural range of variability. The complex spatial and temporal response of fluvial systems to both intrinsic process of adjustment and to extrinsic forcing makes it difficult to understand how rivers have responded to hydroclimatic change in the past and how they may respond in the future (Schumm, 1973, 1979). There

is an urgent need for research that attempts to disentangle intrinsic processes of adjustment from extrinsic forcing, and/or that highlights their interplay.

1.3.1 Geomorphic thresholds and complex response

Intrinsic geomorphic thresholds define the behaviour of a river, and are responsible for landform change associated with river adjustment in the absence of extrinsic forcing (Schumm, 1973; 1979). Examples of fluvial processes characterised by intrinsic geomorphic thresholds include progressive meander bend migration and eventual cut-off, and levee and alluvial ridge building and eventual avulsion. Lateral channel migration is an inherent form of lateral instability, although intrinsic geomorphic thresholds related to declining channel slope may trigger meander bend cut-off, locally increasing channel bed slope and maintaining or improving sediment transport efficiency. The types and rates of such intrinsic geomorphic threshold responses, define the natural (or historical) range of variability of a system (Wohl, 2011; Fryirs et al., 2012; Wohl and Rathburn, 2013). The natural/historical range of variability is typically defined as encompassing the period of generally stable hydroclimatic variables consistent with the late 20th century climate (Fryirs et al., 2012; Wohl and Rathburn, 2013). It is used to understand the way in which rivers adjust in the absence of changes to extrinsic forcing. In other words, rivers adjust within a natural range but relationships between fluvial landforms and processes remain the same such that river type is consistent despite intrinsic variability and complex response (Brierley and Fryirs, 2005; Fryirs et al., 2012). However, change in river type (i.e. character and behaviour), resulting in changed landform-process relationships, will often occur when an extrinsic geomorphic threshold is crossed (Schumm, 1973). Extrinsic geomorphic thresholds are crossed when the changing environmental variables of a system, brought about by climate change, base-level fall or human activities for example, result in changes to river character and behaviour as landform-process relationships are redefined under 'new' environmental parameters. The dramatic climate-driven decline of the Macquarie River leading to channel breakdown and floodplain wetland formation is a good example of the impact of crossing an extrinsic geomorphic threshold for river character and behaviour (Hesse et al., 2018a, b).

In complex natural systems such as alluvial rivers, adjustments to intrinsic geomorphic threshold responses or to extrinsic forcing will be spatially and temporally variable and may occur after a considerable lag time (Schumm and Lichty, 1965; Schumm, 1973; Chappell, 1983). Complex response is a concept introduced by Schumm (1973, 1979) that describes how a single event or geomorphic threshold response can trigger multiple, subsequent morphological adjustments, and was originally defined in reference to terrace formation in incising catchments (Schumm and Parker; 1973; Schumm, 1973, 1979). The term is used here to refer more generally to the complicated, sometimes non-linear, behaviour of fluvial systems. The phenomenon of complex response means that the fluvial response to regional or global environmental change (e.g. climate change) will not necessarily result in equifinality, nor be temporally synchronous between catchments or even within a system (Schumm, 1973; Phillips, 1992). Whether extrinsic forcing is abrupt or gradual will also influence the complexity of river response to

extrinsic forcing. The varying sensitivity of landforms to forcing, and lags within the geomorphic system are responsible for the complex response to intrinsic and extrinsic geomorphic threshold crossing (Schumm, 1973; Chappell, 1983; Phillips, 2003; Fryirs, 2017). The same magnitude disturbance event (e.g. a flood) may have different geomorphic effectiveness (Wolman and Miller, 1960), depending on antecedent conditions and the level of priming of a landform or reach for adjustment (e.g. avulsion) (Schumm, 1973; Schumm and Parker, 1973; Wolman and Gerson, 1978). The scale at which one investigates a system, therefore is an important consideration when attempting to determine river response to extrinsic forcing (Schumm and Lichty, 1965). For example, at the reach or landform scale over short (sub-decadal) time periods, the complex response to fluvial systems may make it difficult to disentangle adjustments brought about by intrinsic processes or by extrinsic forcing. The complex response of fluvial systems precludes high-resolution analysis of fluvial response to extrinsic forcing in the way that other proxies such as tree rings or coral can record seasonal or annual changes. However, historical analyses help to illuminate process-form relationships and intrinsic geomorphic thresholds under modern conditions. Conversely, a longer-term, late Quaternary approach targeting step changes in river character and behaviour provides a good method to understand and define extrinsic geomorphic thresholds and to identify associated river responses.

1.3.2 Factors responsible for channel pattern

The broad spectrum of channel patterns includes straight, meandering, braided, and anabranching (Schumm, 1977; Tooth and Nanson, 2004). Channel pattern refers to the planform geometry of a river and is controlled by a range of factors such as climate and hydrology, valley slope, degree of confinement, and sediment calibre and load (Lewin and Brewer, 2001; Tooth and Nanson 2004; Kleinhans, 2010; Kleinhans and van den Berg, 2011). While channel patterns are known to occur across a continuum, there has been much research to determine thresholds between channel patterns based on the factors listed above (e.g. Leopold and Wolman, 1957; Lewin and Brewer, 2001; Kleinhans and van den Berg, 2011). Stream power is an explicit combination of channel slope (potential energy) and discharge and is often used to differentiate channel patterns by plotting against median channel bed grain size (Lewin and Brewer, 2001; Tooth and McCarthy, 2004). Sediment calibre has a significant influence on channel pattern. For example, for an equivalent stream power, a suspended-load river transporting fine-grained sediment will have a different channel pattern to a coarse-sand bed river transporting dominantly bedload. Fine-grained, cohesive sediment may preclude lateral channel adjustment in the form of lateral channel migration but encourage lateral adjustment in the form of channel avulsion. Conversely, coarse-grained sand bed rivers are more easily able to migrate laterally in more easily erodible substrate, and thus will have a different channel pattern. Similarly, bank and floodplain vegetation can have a disproportionately important influence on channel pattern in certain settings (e.g. Tooth and Nanson, 2004).

1.3.3 Maximum flow efficiency

In many rivers, intrinsic processes adjust channel forms in such a way that flow efficiency is maximised. Maximum flow efficiency can be defined as the ratio of sediment transported to the stream power expended (Huang and Nanson, 2000). The Least Action Principle (LAP) maintains that natural systems tend toward the most economical or efficient pathway in terms of energy expenditure (Huang et al., 2004; Nanson and Huang, 2008; 2017; 2018). Rivers evolve to become the most energy efficient and stable form possible given the extrinsic characteristics of its catchment (i.e. climate, lithology, tectonics) by self-regulating the amount of energy expended or conserved (Nanson and Huang, 2017). Intrinsic processes and their associated geomorphic thresholds and feedbacks are the mechanisms controlling this self-regulation. Alluvial rivers have a degree of freedom to self-adjust within a range of conditions to maximise flow efficiency, such that energy surplus to the requirements of the most efficient sediment transport in a river can be expended (e.g. through frictional losses and reduction in bed slope by meandering), which could otherwise lead to erosional instability. Conversely, adjustment can be made to conserve energy in the case of rivers with a deficit of energy. In rivers that have a deficit of energy relative to that needed to maintain onward transport of the supplied sediment load (a characteristic of many dryland rivers that lose discharge downstream), sediment deposition is inevitable and energy must therefore be conserved in order to attempt to maximise sediment transport efficiency and not be characterised by excessive deposition and channel instability (Nanson and Huang, 2017). This can occur through straightening which maximises channel gradient for a given regional slope and reduces frictional resistance and energy loss at bends (Nanson and Huang, 2017). Where a channel is already straight, the channel cross-section may be adjusted by reducing the width/depth ratio. This can be achieved by the formation of relatively narrower and deeper, multiple (anabranching) channels which have been shown to have greater sediment transport capacity per unit of available stream power than a single channel (Nanson and Knighton, 1996; Nanson and Huang, 1999; Jansen and Nanson, 2004; Huang and Nanson, 2007). In some rivers, such intrinsic processes maintain restorative, negative feedbacks and adjust in a way that maximises throughput of their imposed water and sediment load (e.g. cycle of progressive lateral meander migration leading to the point of failure and meander bend cut-off), other rivers display a nonequilibrium response where the transport of water and sediment from upstream cannot be maintained, despite formation of a multichannelled planform, resulting in channel instability or breakdown (Ralph and Hesse, 2010). These systems are typically characterised by a deficit of energy which is exacerbated by dramatic downstream declines in discharge and stream power, leading to sediment sequestration within and adjacent to the channel. Intrinsic geomorphic thresholds and feedbacks in these systems act to encourage channel avulsion in an effort to improve flow efficiency (Huang and Nanson, 2007), but ultimately sediment throughput cannot be maintained. Such feedbacks that act to reduce discharge and stream power can ultimately result in channel breakdown and termination of channelised flow and sediment transport.

Crucially, while intrinsic processes and related geomorphic threshold responses drive ongoing adjustment of a river, the suite of processes, and the rate at which they occur, are defined by extrinsic forces acting on the catchment. As such, changes to extrinsic forcing can lead to crossing of extrinsic geomorphic thresholds, resulting in changes to form-process relationships and rates of internal processes, and therefore the overall character and behaviour of a river. This concept will form the crux of this thesis, which investigates the response of dryland rivers to Holocene climate changes, the intrinsic processes that define modern rivers, and the potential impacts of future climate change on dryland rivers.

1.4 Forecasting future change to dryland rivers

Global climate models tend to project future increases in aridity in many drylands around the world as well as an increase in the extent of drylands (Greve and Seneviratne, 1999; Feng and Fu, 2013; Schewe et al., 2013; Seager et al., 2013; Cook et al., 2014; Fu and Feng, 2014; IPCC, 2014; CSIRO and BoM, 2015; Gosling and Arnell, 2016). Regional declines in rainfall are not the only driver of this projected trend, but rising temperatures are expected to increase atmospheric demand for water through evapo-transpiration, and so regions that may not experience a net reduction in rainfall will likely experience higher overall aridity (Cook et al., 2014). Some tropical regions are expected to have higher annual rainfall totals although the interannual variability of this rainfall is expected to increase (Nijssen et al., 2001; Milly et al., 2005). Areas which are projected to experience declines in rainfall due to changing circulation patterns (e.g. southward shift of the southern hemisphere westerlies (Cai and Cowan, 2013)) as well as increased temperatures will likely experience the most pronounced increases in aridity. For example, southwestern Australia, the southeastern highlands of Australia and the Southern Cape of southern Africa are expected to experience significant declines in seasonal winter rainfall due to the southwards contraction of the mid-latitude westerlies and associated rain-bearing systems. Indeed, these regions have seen reduced precipitation over the last few decades (Milly et al., 2005; Potter et al., 2010; de Wit and Stankiewicz, 2006; Cai and Cowan, 2013; Pekel et al., 2016; Rodell et al., 2018).

Unsurprisingly, projected increases in aridity are expected to alter flow regimes and reduce surface water availability in many of the world's drylands (Arnell, 1999; Nijssen et al., 2001; Milly et al., 2005; de Wit and Stankiewicz, 2006; CSIRO, 2007; Schewe et al., 2013). Mid-latitude regions in southern Africa, western North America, and the Middle East are expected to experience a 10–30 % decline in annual runoff by 2050 (Milly et al., 2005). Similarly, for the Murray-Darling Basin in southeastern Australia, runoff is projected to decline by between 12–35 % by the 2050s (Arnell, 1999; Hughes, 2003). There is considerable uncertainty associated with specific regional projections of rainfall and runoff but the agreement of many global climate models indicates that coming decades will be characterised by increasing water scarcity and reduced streamflow in drylands around the world (Arnell, 1999; Nijssen et al., 2001; Milly et al., 2005; CSIRO, 2007; Schewe et al., 2013; Gosling and Arnell, 2016). A key gap in

understanding of the future impacts of climate change on dryland rivers relates to their geomorphological response (Lane, 2013; Fryirs, 2017). It is as yet unclear just how geomorphologically sensitive dryland rivers are to the magnitude of hydroclimatic changes projected for coming decades.

1.5 Study areas

To address the research issues identified above, this thesis focusses on two mid-latitude dryland catchments; the Warrego River in eastern Australia and the Okavango River in southern Africa (Fig. 1.2). Both are large, regionally important systems and while poorly known in terms of their late Quaternary history and palaeohydrology, both have palaeochannels that indicate a marked change in river behaviour to form the modern system. The Warrego and Okavango differ significantly in their hydrology, geomorphology and tectonic setting, but provide independent records of river response to climate change in the Holocene. Advantages of an inter-continental comparison include an improved understanding of how hydroclimatic changes manifest in dryland rivers in vastly different settings, and the ability to potentially identify synchronous fluvial responses at the hemispheric or global scale. These records are presented in Chapters 2 and 3, and collectively help to illuminate continental or global scale synchronicity of Holocene climate and hydrological change, and associated river response. Intrinsic processes of adjustment of the modern Warrego and Okavango rivers are also placed into the context of this Holocene evolution using detailed field and desktop analyses (Chapters 2, 3 and 4). A wider analysis of dryland river catchments in the Murray-Darling Basin and Lake Eyre Basin of central and eastern Australia, including geomorphological analysis and climate modelling is undertaken to improve our understanding of the projected geomorphological response of these Australian dryland rivers to future climate change (Chapter 5).
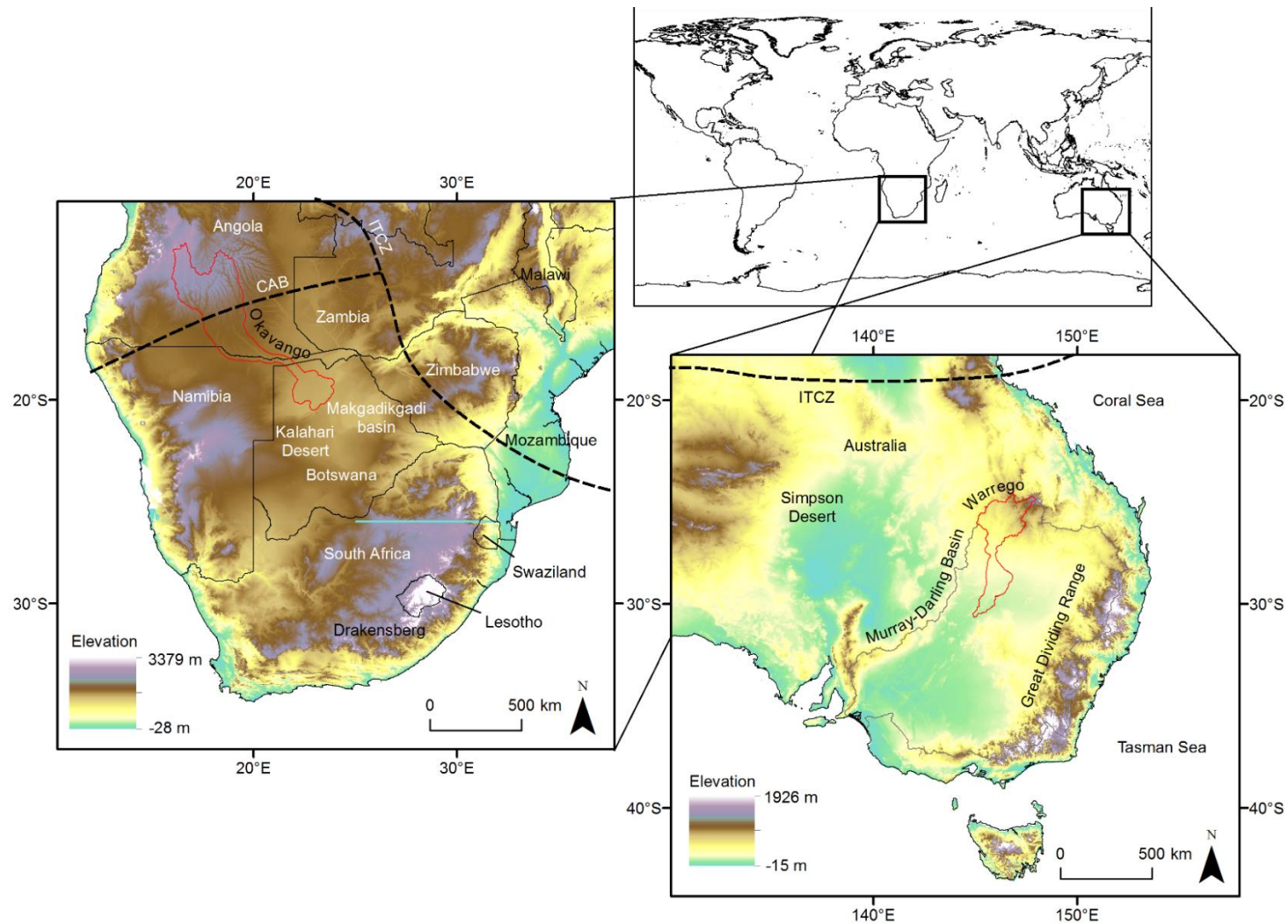
Figure 1.2. Southern Africa and central-eastern Australia. The Okavango and Warrego catchments are outlined in red. The mean January location of the intertropical convergence zone (ITCZ) and the Congo air boundary (CAB) are shown with black dashed lines. Elevation data provided by continental-scale 30 m Shuttle Radar Topography Mission (SRTM) Digital Elevation Models (DEMs).

10

1.5.1 The Warrego River, eastern Australia

Australia is a dry, generally low elevation continent with large dryland catchments at its interior. The Great Dividing Range is a broad belt of mountainous terrain extending roughly north-to-south near the east coast (Fig. 1.2). At its highest it rises to over 2,000 m.a.s.l. in the southeast. Many of eastern Australia's dryland rivers, particularly in the Murray-Darling Basin, have headwaters that drain the western flanks of the Great Dividing Range with orographic rainfall providing the majority of runoff. Farther west, the inland regions are characterised by low elevation, low relief alluvial plains and local bedrock ranges.

The Warrego River is a large intermittent/seasonal river in the northern Murray-Darling Basin of eastern Australia. The ~75,000 km^2 catchment has headwaters in the Carnarvon Ranges in central Queensland which rise to ~600 m.a.s.l. In its lower reaches, the Warrego River flows across a large, low-angled, fan-shaped fine-grained alluvial floodplain; a floodplain-fan (Fig. 1.2). At its downstream end, the floodplain abuts a northeast-southwest trending bedrock ridge which forces the Warrego River into narrower, bedrock-confined lower reaches prior to its confluence with the Darling River, just downstream of Bourke. The Warrego River has a highly variable, 'boom and bust' hydrology, characterised by long periods of zero or low flow and periods of extensive flooding that can inundate up to 3,000 km^2 of intermittent and ephemeral floodplain wetlands. The entire Warrego catchment is semiarid. Approximately 600 mm of annual rainfall over the headwaters falls during the austral summer months, but rainfall declines to ~250 mm over the lower catchment. However, there is significant interannual variability of rainfall and runoff (BoM, 2018) that is largely related to the El Niño-Southern Oscillation (ENSO). Synoptic conditions that typically promote widespread flooding in the Warrego are large monsoonal troughs that extend southwards from the Intertropical Convergence Zone (ITCZ) lying to the north of the catchment (Fig. 1.2) and result in long-duration rainfall events (Grootemaat, 2008). Smaller minor and moderate flooding typically occurs as a result of localised convective thunderstorms during the summer months, as moist southeast trade winds from the Coral Sea promote orographic rainfall over the central Queensland parts of the Great Dividing Range (Grootemaat, 2008).

There has been no previous geomorphological investigation of the Warrego River or its floodplain, not even in the form of cursory, catchment-scale geomorphic mapping, and the late Quaternary dynamics of the system are entirely undocumented. However, hydrological modelling has been undertaken as part of the CSIRO's Sustainable Yields project to understand impacts of future climate change and future water resource development on hydrology within the Murray-Darling Basin (CSIRO, 2007). There has been relatively little water resource development in the Warrego catchment, and modelling to 2030 suggests that water use will not considerably impact flows in the river (CSIRO, 2007). However, projected climate changes are likely to reduce flows beneficial for the maintenance of riverine and floodplain wetlands by ~10 % (CSIRO, 2007). The predominant land use in the catchment is cattle and sheep grazing with only small amounts of dryland and irrigated cropping due to the highly variable

rainfall and streamflow. For much of the time during dry periods, the Warrego River persists only as a string of irregularly-spaced, disconnected, semi-permanent waterholes, but which nonetheless provide refugia for waterbirds, fish and other aquatic animals (Kingsford et al., 2001). Against this backdrop, research presented in this thesis improves our understanding of the geomorphological character of the modern Warrego River. The palaeofluvial record derived from optically stimulated luminescence (OSL) dating of Warrego River palaeochannels improves our understanding of past climate change in eastern Australia, and the response of the Warrego River, and other similar dryland rivers, to such change.

1.5.2 The Okavango River, southern Africa

The southern African subcontinent is characterised by a prominent plateau >1,000 m.a.s.l. (Fig. 1.2). The Drakensberg in the southeast is the highest and steepest mountain region, while much of the central plateau, particularly in the Kalahari Desert, has relatively low relief (Fig. 1.2). The endorheic Makgadikgadi basin in the central and northern Kalahari is fed by catchments with headwaters in the Angolan highlands (e.g. the Okavango and Kwando). A southwest-northeast trending half-graben thought to be associated with the East African Rift system (McCarthy, 2013) forms a regional depocentre and is responsible for the formation of the Okavango and Linyanti wetlands, respectively.

The Okavango is a perennial but strongly seasonal river which flows into the Okavango Delta in the northern Kalahari Desert of Botswana. Its headwater channels rise in the tropical Angolan highlands and provide the majority of runoff within the Okavango (Fig. 1.2). The Okavango Delta is one of the largest and most pristine wetland wilderness areas in the world and was inscribed as a World Heritage site in 2014. The Delta itself is a large (>40,000 km^2) alluvial fan formed in a half-graben, with a roughly 10 km wide 'entry corridor' known as the Panhandle (McCarthy and Ellery, 1998; McCarthy, 2013). The Okavango River system is unusual due to its sediment load and the dominant role of vegetation in the channels and wetlands (McCarthy, 2013). The Kalahari sand sheet mantles much of the catchment, meaning that sediment supply is predominantly ~300 μm sand transported as bedload with very small amounts of finer-grained suspended sediment (McCarthy, 2013). Channel banks are comprised of permeable peat and living vegetation which allows considerable leakage of water from channels into surrounding wetlands (Ellery et al., 2003; Tooth and McCarthy, 2004; McCarthy, 2013). The Okavango is a flood pulse system with one large seasonal flood per year. Monsoonal rainfall over the Angolan headwaters during the austral summer is attenuated in low gradient swamps and dambos, and the peak of the flood arrives at the head of the Okavango Panhandle around April and maximum extent of flooding occurs during the austral winter dry season around August (McCarthy and Ellery, 1998; McCarthy et al., 2000; McCarthy, 2013).

The geomorphology and hydrology of the Okavango Delta has been extensively studied (see McCarthy et al., 1992; Stanistreet et al., 1993; Smith et al., 1997; McCarthy and Ellery, 1998; McCarthy et al., 2000; Ellery et al., 2003; Gumbricht et al., 2004; Tooth and McCarthy, 2004; McCarthy et al., 2012; McCarthy,

2013; Thito et al., 2016; Fryirs et al., 2018), but the late Quaternary dynamics of the Okavango River are poorly documented. This thesis will present one of the first suites of OSL ages obtained to understand the palaeohydrology of the Okavango River in the Panhandle. These ages will help to provide temporal context for a study of the patterns and processes of adjustment that have characterised the Okavango River over the historical period.

1.6 Thesis objectives and structure

The overarching aim of this thesis is to investigate and define the response of dryland rivers, particularly in Australia and southern Africa, to hydroclimatic change over a range of spatial and temporal scales and, in the process, to contextualise the behaviour of dryland rivers under modern conditions. The research is guided by three research questions, introduced earlier, which relate to the influence of climate on river behaviour in the *past* (how have dryland rivers responded to climate-driven hydrological change in the past?), *present* (what processes define the natural range of variability of modern dryland rivers?) and the *future* (how will dryland rivers respond to future climate change?).

To address the overarching aim and provide answers to these questions, this thesis has five objectives:

1) Determine the timing of Holocene phases of enhanced fluvial activity in the Warrego and Okavango catchments.
2) Reconstruct the character and behaviour of the palaeo-Warrego and palaeo-Okavango.
3) Define the character and behaviour of the modern Warrego and Okavango rivers and compare and contrast the modern river styles with the palaeo rivers.
4) Quantify patterns and mechanisms of a key driver of fluvial change, namely channel avulsion in the Okavango River.
5) Use global climate model projection data to assess future Australian dryland river response to climate change.

These objectives are addressed in Chapters 2, 3, 4 and 5, which are written and formatted as journal articles and are sequenced according to the thesis objectives and the key themes that are emphasised in each chapter along the way (Fig. 1.3). Chapters 2, 3 and 4 have not yet been submitted for publication, but Chapter 5 is under review (and formatted accordingly for *Nature Geoscience*).

1.7 Author contributions

Data analysis, interpretation, and writing of this thesis has been undertaken by me, but there have been many collaborators who have contributed to data collection in the field and data analysis, particularly with optically stimulated luminescence dating undertaken by Geoff Duller at the Aberystwyth Luminescence Research Laboratory (Table 1.1).

RESEARCH QUESTIONS | RESEARCH OBJECTIVES | CHAPTER 2 | CHAPTER 3 | CHAPTER 4 | CHAPTER 5 | CHAPTER 6 | APPENDIX 1 | APPENDIX 2 | APPENDIX 3

RESEARCH QUESTIONS

1) HOW HAVE DRYLAND RIVERS RESPONDED TO CLIMATE-DRIVEN HYDROLOGICAL CHANGE IN THE *PAST*?

2) WHAT PROCESSES DEFINE THE NATURAL RANGE OF VARIABILITY OF *MODERN* DRYLAND RIVERS?

3) HOW WILL DRYLAND RIVERS RESPOND TO *FUTURE* CLIMATE CHANGE?

RESEARCH OBJECTIVES

1) Determine the timing of Holocene phases of enhanced fluvial activity in the Warrego and Okavango catchments.

2) Reconstruct the character and behaviour of the palaeo-Warrego and palaeo-Okavango.

3) Define the character and behaviour of the modern Warrego and Okavango rivers, and compare and contrast the modern river styles with the palaeo-rivers

4) Quantify patterns and mechanisms of a key driver of fluvial change, namely, avulsion in the Okavango River.

5) Use global climate model projection data to assess future Australian dryland river response to climate change.

CHAPTER 2
- Holocene climate change
- River evolution
- Extrinsic geomorphic thresholds
- Palaeo-geomorphology, palaeohydrology
- Modern geomorphology and hydrology

CHAPTER 3
- Holocene climate change
- River evolution
- Extrinsic geomorphic thresholds
- Palaeo-geomorphology, palaeohydrology
- Modern geomorphology and hydrology
- Historical patterns of channel adjustment; avulsion

CHAPTER 4
- Modern geomorphology and hydrology
- Historical patterns of channel adjustment; avulsion
- Mechanisms of channel avulsion

CHAPTER 5
- Character and behaviour of Australian dryland rivers
- Future climate change
- River response

CHAPTER 6
- Holocene climate change
- Global dryland river evolution
- Extrinsic geomorphic thresholds
- Palaeo-geomorphology, palaeohydrology
- Modern geomorphology and hydrology
- Interaction between extrinsic forces and intrinsic processes
- Future climate change
- River response

APPENDIX 1
- Holocene climate change
- River evolution
- Extrinsic geomorphic thresholds
- Palaeo-geomorphology, palaeohydrology

APPENDIX 2
- Holocene climate change
- River evolution
- Extrinsic geomorphic thresholds
- Palaeo-geomorphology, palaeohydrology

APPENDIX 3
- Modern geomorphology

Figure 1.3. Structure of the thesis in relation to research questions, objectives and thesis chapters, and the themes addressed in each chapter.

Table 1.1. Author contributions to chapters within this thesis.

	Intellectual contribution				Manuscript preparation		
	Chapter/paper conception	Data collection	Data analysis	Data interpretation	Writing	Figures	Tables
Chapter 1 Introduction	ZL (100%)	ZL	ZL (100%)	ZL (100%)	ZL (100%) wrote all text (TR, ST, and KF provided feedback).	ZL (100%)	ZL (100%)
Chapter 2	ZL (50%), TR (50%)	ZL, TR, AW	ZL (80%), GD (20%) undertook the analysis to provide OSL ages.	ZL (100%)	ZL (90%) drafted all text, TR (5%) and ST (5%) edited the manuscript and provided feedback.	ZL (100%)	ZL (100%)
Chapter 3	ZL (33%), ST (33%), TR (33%)	ZL, TR, ST, KF, PH, MH, EM, IM	ZL (80%), GD (20%) undertook the analysis to provide OSL ages.	ZL (100%)	ZL (85%) drafted all text, TR (5%), ST (5%), and KF (5%) edited the manuscript and provided feedback.	ZL (100%)	ZL (100%)
Chapter 4^	TM (50%), TR (30%), ZL (20%)	ZL, TR, ST, KF, PH, MH, EM, IM	ZL (55%), TR (35%), MH (10%)	TR (50%), ZL (50%)	TR (50%) and ZL (50%) drafted all text and edited the manuscript.	ZL (90%), TR (10%)	ZL (100%)
Chapter 5	ZL (50%), TR (50%)	ZL	ZL (95%) performed the vast majority of data analysis and AC (5%) assisted with statistical analyses.	ZL (100%)	ZL (85%) drafted all text, TR (5%), ST (5%), KF (3%), and AC (2%) edited the manuscript and provided feedback.	ZL (100%)	ZL (100%)
Chapter 6 Discussion	ZL (100%)	ZL	ZL (100%)	ZL (100%)	ZL (100%) wrote all text (TR, ST, and KF provided feedback).	ZL (100%)	ZL (100%)

*ZL = Zacchary Larkin, TR = Timothy Ralph, ST = Stephen Tooth, KF = Kirstie Fryirs, GD = Geoff Duller, PH = Paul Hesse, MH = Marc Humphries, EM = Edwin Mosimanyana, IM = Ineelo Mosie, TM = Terence McCarthy, AC = Alexandra Carthey, AW = Adam Wethered

^Chapter 4 presents unpublished data collected in 1995 by Terence McCarthy (some published in Smith et al., 1997), plus unpublished data collected in 2008 by Terence McCarthy and Piotr Wolski, as well as data collected during this PhD in 2016.

References

Arnell NW, 1999. Climate change and global water resources. Global Environmental Change, 9, 31–49.

Brierley GJ and Fryirs KA, 2005. Geomorphology and River Management: Applications of the River Styles Framework. Blackwell Publications: Oxford; 398 pp.

Bureau of Meteorology (BoM), 2018. Long range weather and climate. Available online at: http://www.bom.gov.au/climate/. Date last accessed: 15/01/2019.

Cai W, and Cowan T, 2013. Southeast Australia autumn rainfall reduction: A climate-change-induced poleward shift of ocean-atmosphere circulation. Journal of Climate, 26(1), 189–205.

Chappell J, 1983. Thresholds and lags in geomorphologic changes. Australian Geographer. 15, 357–366.

Chase BM, Boom A, Carr AS, Meadows ME, and Reimer PJ, 2013. Holocene climate change in southernmost South Africa: Rock hyrax middens record shifts in the southern westerlies. Quaternary Science Reviews, 82, 199–205.

Chase BM, Meadows ME, Carr AS, and Reimer PJ, 2010. Evidence for progressive Holocene aridification in southern Africa recorded in Namibian hyrax middens: Implications for African Monsoon dynamics and the 'African Humid Period.' Quaternary Research, 74(1), 36–45.

Chase BM, Scott L, Meadows ME, Gil-Romera G, Boom A, Carr AS, Reimer PJ, Truc L, Valsecchi V, and Quick LJ, 2012. Rock hyrax middens: A palaeoenvironmental archive for southern African drylands. Quaternary Science Reviews, 56, 107–125.

Clarkson BR, Ausseil AE, and Gerbeaux P, 2013. Wetland ecosystem services. In Dymond JR ed. Ecosystem services in New Zealand – conditions and trends. Manaaki Whenua Press, Lincoln, New Zealand.

Cohen TJ, Jansen JD, Gliganic LA, Larsen JR, Nanson GC, May JH, Jones BG, and Price DM, 2015. Hydrological transformation coincided with megafaunal extinction in central Australia. Geology, 43(3), 195–198.

Cohen TJ, Nanson GC, Jansen JD, Jones BG, Jacobs Z, Larsen JR, May JH, Treble P, Price DM, Smith AM, 2012. Late Quaternary mega-lakes fed by the northern and southern river systems of central Australia: Varying moisture sources and increased continental aridity. Palaeogeography, Palaeoclimatology, Palaeoecology, 356–357, 89–108.

Cook BI, Smerdon JE, Seager R, and Coats S, 2014. Global warming and 21st century drying. Climate Dynamics, 43(9-10), 2607-2627.

Costanza R, D'Arge R, de Groot R, Farber S, Grasso M, Hannon B, Limburg K, Naeem S, O'Neill RV, Paruelo J, Raskin RG, Sutton P, and van den Belt M, 1998. The value of the world's ecosystem services and natural capital. Nature, 387, 253–260.

CSIRO, 2007. Water availability in the Warrego. A report to the Australian Government from the CSIRO Murray-Darling Basin Sustainable Yields Project. CSIRO, Australia. 89pp.

CSIRO and Bureau of Meteorology (BoM), 2015. Projections: Atmosphere and the land, Climate Change in Australia Information for Australia's Natural Resource Management Regions: Technical Report.

De Wit M and Stankiewicz J, 2006. Changes in surface water supply across Africa with predicted climate change. Science, 311, 1917–1921.

Ellery WN, McCarthy TS, Smith ND, and Hall B, 2003. Vegetation, hydrology, and sedimentation patterns on the major distributary system of the Okavango fan, Botswana. Wetlands, 23(2), 357–375.

Feng S, and Fu Q, 2013. Expansion of global drylands under a warming climate. Atmospheric Chemistry and Physics, 13(19), 10081–10094.

Fitzsimmons KE, Cohen TJ, Hesse PP, Jansen J, Nanson GC, May JH, Barrows TT, Haberlah D, Hilgers A, Kelly T, Larsen J, Lomax J, and Treble, P, 2013. Late Quaternary palaeoenvironmental change in the Australian drylands. Quaternary Science Reviews, 74, 78–96.

Fryirs KA, 2017. River sensitivity: A lost foundation concept in fluvial geomorphology. Earth Surface Processes and Landforms, 42(1), 55-70.

Fryirs K, Brierley GJ, and Erskine WD, 2012. Use of ergodic reasoning to reconstruct the historical range of variability and evolutionary trajectory of rivers. Earth Surface Processes and Landforms, 37(7), 763–773.

Fryirs KA, Ralph TJ, Larkin ZT, Tooth S, Humphries M, McCarthy T, Hesse PP, and Mosimanyana E, 2018. A nested hierarchical perspective to enhance interpretations and communication in fluvial geomorphology for use in water resources management: Lessons from the Okavango Delta, Botswana. Geographical Journal, 184(2), 192–207.

Fu Q and Feng S, 2014. Responses of terrestrial aridity to global warming. Journal of Geophysical Research: Atmospheres, 119(13), 1–13.

Gosling SN, and Arnell NW, 2016. A global assessment of the impact of climate change on water scarcity. Climatic Change, 134(3), 371–385.

Greve P, and Seneviratne SI, 1999. Assessment of future changes in water availability and aridity. Geophysical Research Letters, 42, 5493–5499.

Grootemaat GD, 2008. The relationship of flooding in Australian dryland rivers to synoptic weather patterns, El Niño southern oscillation, sea surface temperatures and rainfall distribution, unpubl. PhD thesis, University of Wollongong.

Gumbricht T, McCarthy J, and McCarthy TS, 2004. Channels, wetlands and islands in the Okavango Delta, Botswana, and their relation to hydrological and sedimentological processes. Earth Surface Processes and Landforms, 29(1), 15–29.

Hesse PP, Williams R, Ralph TJ, Fryirs KA, Larkin ZT, Westaway KE, and Farebrother W, 2018a. Palaeohydrology of lowland rivers in the Murray-Darling Basin, Australia. Quaternary Science Reviews, 200, 85–105.

Hesse PP, Williams R, Ralph TJ, Larkin ZT, Fryirs KA, Westaway KE, and Yonge D, 2018b. Dramatic reduction in size of the lowland Macquarie River in response to Late Quaternary climate-driven hydrologic change. Quaternary Research, 90(2), 360–379.

Huang HQ, Chang HH, and Nanson GC, 2004. Minimum energy as the general form of critical flow and maximum flow efficiency and for explaining variations in river channel pattern. Water Resources Research, 40(4), 1–13.

Huang HQ, and Nanson GC, 2000. Hydraulic geometry and maximum flow efficiency as products of the principle of least action. Earth Surface Processes and Landforms, 25, 1–16.

Huang HQ, and Nanson GC, 2007. Why some alluvial rivers develop an anabranching pattern. Water Resources Research, 43(7), 1–12.

Huang HQ, and Nanson GC, 2008. Least action principle, equilibrium states, iterative adjustment and the stability of alluvial channels. Earth Surface Processes and Landforms, 33, 923–942.

Hughes L, 2003. Climate change and Australia: Trends, projections and impacts. Austral Ecology, 28(4), 423–443.

IPCC, 2014. Climate Change 2014: Synthesis Report. Contribution of Working Groups I, II and III to the Fifth Assessment Report of the Intergovernmental Panel on Climate Change [Core Writing Team, R.K. Pachauri and L.A. Meyer (eds.)]. IPCC, Geneva, Switzerland, 151 pp.

Jansen JD, and Nanson GC, 2004. Anabranching and maximum flow efficiency in Magela Creek, northern Australia. Water Resources Research, 40(4), 1–12.

Kingsford RT, Thomas RF, and Curtin AL, 2001. Conservation of wetlands in the Paroo and Warrego River catchments in arid Australia. Pacific Conservation Biology, 7(1), 21–33.

Kleinhans MG, 2010. Sorting out river channel patterns. Progress in Physical Geography, 34(3), 287-326.

Kleinhans, van den Berg JH, 2011. River channel and bar patterns explained and predicted by an empirical and a physics-based method. Earth Surface Processes and Landforms, 36(6), 721-738.

Kotze DC, Marneweck G, Batchelor A, Lindley D, Collins N, 2009. WET-EcoServices: a technique for rapidly assessing ecosystem services supplied by wetlands. Wetland Management Series, Water Research Commission Report No. TT 339/09. Water Research Commission, Pretoria.

Lane EW, 1955. The importance of fluvial morphology in hydraulic engineering. Proceedings of the American Society of Civil Engineers 81, 1–17.

Lane SN, 2013. 21st Century climate change: Where has all the geomorphology gone? Earth Surface Processes and Landforms, 38(1), 106–110.

Leopold LB, Wolman MG, 1957. River channel patterns: braided, meandering, and straight. US Geological Survey Professional Paper 282-B.

Lewin J, Brewer PA, 2001. Predicting channel patterns. Geomorphology, 40(3-4), 329-339.

Macklin MG. and Lewin J., 2015. The rivers of civilization. Quaternary Science Reviews, 114, 228–244.

McCarroll D, 2015. "Study the past, if you would divine the future": A retrospective on measuring and understanding Quaternary climate change. Journal of Quaternary Science, 30(2), 154–187.

McCarthy TS, Cooper GRJ, Tyson PD, and Ellery WN, 2000. Seasonal flooding in the Okavango Delta, Botswana - Recent history and future prospects. South African Journal of Science, 96, 25–33.

McCarthy TS, and Ellery WN, 1998. The Okavango Delta. Transactions of the Royal Society of South Africa, 53(2), 157–182.

McCarthy TS, Humphries MS, Mahomed I, Le Roux P, and Verhagen BT, 2012. Island forming processes in the Okavango Delta, Botswana. Geomorphology, 179, 249–257.

McCarthy TS, 2013. The Okavango Delta and its place in the geomorphological evolution of southern Africa. South African Journal of Geology, 116(1), 3–54.

McCarthy TS, Ellery WN, and Stanistreet IG, 1992. Avulsion mechanisms on the Okavango fan, Botswana: the control of a fluvial system by vegetation. Sedimentology, 39, 779–795.

Meadows ME, 2001. The role of Quaternary environmental change in the evolution of landscapes: case studies from southern Africa. Catena, 42, 39–57.

Millennium Ecosystem Assessment (MEA). 2005. Ecosystems and Human Well-being: Wetlands and Water. World Resources Institute: Washington, DC.

Milly PCD, Dunne KA, and Vecchia AV, 2005. Global pattern of trends in streamflow and water availability in a changing climate. Nature, 438, 347–350.

Mueller D, Jacobs Z, Cohen TJ, Price DM, Reinfelds IV, and Shulmeister J, 2018. Revisiting an arid LGM using fluvial archives: a luminescence chronology for palaeochannels of the Murrumbidgee River, south-eastern Australia. Journal of Quaternary Science, 33(7), 777–793.

Nanson GC, Chen XY, and Price DM, 1995. Aeolian and fluvial evidence of changing climate and wind patterns during the past 100 ka in the western Simpson Desert, Australia. Palaeogeography, Palaeoclimatology, Palaeoecology, 113(1), 87–102.

Nanson GC, and Huang HQ, 1999. Anabranching rivers: divided efficiency leading to fluvial diversity. In: Varieties of fluvial form, 7, 477–494.

Nanson GC, and Huang HQ, 2017. Self-adjustment in rivers: Evidence for least action as the primary control of alluvial-channel form and process. Earth Surface Processes and Landforms, 42(4), 575–594.

Nanson GC, and Huang HQ, 2018. A philosophy of rivers: Equilibrium states, channel evolution, teleomatic change and least action principle. Geomorphology, 302, 3–19.

Nanson GC, and Knighton DA, 1996. Anabranching rivers: Their cause, character and classification. Earth Surface Processes and Landforms, 21(3), 217–239.

Nanson CG, Price DM, and Short SA, 1992. Wetting and drying of Australia over the past 300,000 years. Geology, 20, 791–794.

Nijssen B, O'Donnell GM, Hamlet AF, and Lettenmaier DP, 2001. Hydrologic sensitivity of global rivers to climate change. Climatic Change, 50(1–2), 143–175.

Page KJ, Kemp J, and Nanson GC, 2009. Late Quaternary evolution of Riverine Plain paleochannels, southeastern Australia. Australian Journal of Earth Sciences, 56, S19–S33.

Pekel J-F, Cottam A, Gorelick N, and Belward AS, 2016. High-resolution mapping of global surface water and its long-term changes. Nature, 540, 418–422.

Petit RJ, Raynaud D, Basile I, Chappellaz J, Ritz C, Delmotte M, Legrand M, Lorius C, and Pe L, 1999. Climate and atmospheric history of the past 420,000 years from the Vostok ice core, Antarctica. Nature, 399, 429–413.

Phillips JD, 1992. The end of equilibrium. Geomorphology 5, 195–201.

Phillips JD, 2003. Sources of Nonlinearity and Complexity in Geomorphic Systems. Progress in Physical Geography, 27, 1–23.

Potter NJ, Chiew FHS, and Frost AJ, 2010. An assessment of the severity of recent reductions in rainfall and runoff in the Murray-Darling Basin. Journal of Hydrology, 381(1–2), 52–64.

Ralph TJ, and Hesse PP, 2010. Downstream hydrogeomorphic changes along the Macquarie River, southeastern Australia, leading to channel breakdown and floodplain wetlands. Geomorphology, 118(1–2), 48–64.

Rodell M, Famiglietti JS, Wiese DN, Reager JT, Beaudoing HK, Landerer FW, and Lo M-H, 2018. Emerging trends in global freshwater availability. Nature, 557, 651–659.

Schewe J, Heinke J, Gerten D, Haddeland I, Arnell NW, Clark DB, Dankers R, Eisner S, Fekete BM, Colón-González FJ and Gosling SN, 2014. Multimodel assessment of water scarcity under climate change. Proceedings of the National Academy of Sciences, 111(9), 3245-3250.

Schumm SA, and Lichty RW, 1965. Time, space, and causality in geomorphology. American Journal of Science, 263, 110–119.

Schumm SA, 1973. Geomorphic thresholds and the complex response of drainage systems. In Fluvial Geomorphology, Morisawa M (ed). State University of New York: Binghampton, NY; 299–310.

Schumm SA., 1977. The fluvial system (Vol. 338). New York: Wiley.

Schumm SA, 1979. Geomorphic thresholds: the concept and its applications. Transactions of the Institute of British Geographers 4: 485–515.

Schumm SA, and Parker RS, 1973. Implications of complex response of drainage systems for Quaternary alluvial stratigraphy. Nature 243: 99–100.

Schumm SA., 2005. River variability and complexity. University Press, Cambridge.

Seager R, Ting M, Li C, Naik N, Cook B, Nakamura J, and Liu H, 2013. Projections of declining surface-water availability for the southwestern United States. Nature Climate Change, 3(5), 482–486.

Smith ND, McCarthy TS, Ellery WN, Merry CL, and Rüther H, 1997. Avulsion and anastomosis in the panhandle region of the Okavango Fan, Botswana. Geomorphology, 20(1–2), 49–65.

Stanistreet IG, Cairncross B and McCarthy TS, 1993. Low sinuosity and meandering bedload rivers of the Okavango Fan: channel confinement by vegetated levees without fine sediment. Sedimentary Geology, 85(1-4), pp.135–156.

Thito K, Wolski P, and Murray-Hudson M, 2016. Mapping inundation extent, frequency and duration in the Okavango Delta from 2001 to 2012. African Journal of Aquatic Science, 41(3), 267–277.

Tooth S, 2000. Process, form and change in dryland rivers: A review of recent research. Earth Science Reviews, 51(1–4), 67–107.

Tooth S, 2012. Arid geomorphology: Changing perspectives on timescales of change. Progress in Physical Geography, 36(2), 262–284.

Tooth S, and McCarthy TS, 2004. Controls on the transition from meandering to straight channels in the wetlands of the Okavango Delta, Botswana. Earth Surface Processes and Landforms, 29(13), 1627–1649.

Tooth S, and McCarthy TS, 2007. Wetlands in drylands: geomorphological and sedimentological characteristics, with emphasis on examples from southern Africa. Progress in Physical Geography, 31(1), 3–41.

United Nations Environment Programme (UNEP), 1992. World Atlas of Desertification. Edward Arnold: London; 15–45.

Wohl E, 2011. What should these rivers look like? Historical range of variability and human impacts in the Colorado Front Range, USA. Earth Surface Processes and Landforms, 36(10), 1378–1390.

Wohl E, and Rathburn S, 2013. Guest Editorial: Introduction to special issue on historical range of variability. Earth Surface Processes and Landforms, 38(2), 213–216.

Wolman MG and Gerson R, 1978. Relative scales of time and effectiveness of climate in watershed geomorphology. Earth Surface Processes 3(2), 189–208.

Wolman MG, and Miller JP, 1960. Magnitude and frequency of forces in geomorphic processes. The Journal of Geology 68(1), 54–74.

CHAPTER 2

From a sinuous to a straight 'river of sand': the profound response of the dryland Warrego River, eastern Australia, to Holocene hydroclimatic change

Larkin Z.T.[1], Ralph T.J.[1], Tooth S.[2,3], Duller G.A.T.[2]*

[1] Department of Environmental Sciences, Macquarie University, NSW Australia

[2] Department of Geography and Earth Sciences, Aberystwyth University, Aberystwyth, UK

[3] School of Geosciences, University of the Witwatersrand, Johannesburg, South Africa

*See Table 1.1 in chapter 1 for author contributions.

Abstract

In dryland regions, the typical scarcity of organic-based proxies that traditionally are used to reconstruct Quaternary environmental changes means that geomorphological features such as palaeochannels commonly provide some of the most promising alternative proxy records. The ~850 km long Warrego River and its floodplain is well-placed to improve our understanding of Holocene climate change in semi-arid eastern Australia, particularly because the catchment is largely isolated from extratropical sources of moisture that can complicate other Australian palaeofluvial records. The mid Holocene Warrego River, active between ~8–5 ka, transported up to 20 times the discharge of the modern river and maintained a large (~160 m wide), moderate energy (~10 W m^{-2}), likely perennial, meandering channel. Prevailing La Niña conditions during the early-mid Holocene were responsible for this enhanced discharge, which probably enabled the channel to maintain a continuous course to its confluence with the Darling River. After ~5 ka, the modern El Niño-Southern Oscillation climate mode established, with stronger and more frequent El Niño events leading to greater catchment aridity and reduced discharge. This climate transition forced the Warrego River across an extrinsic geomorphic threshold, resulting in a step-change in its character and behaviour and establishment of the modern system. The modern Warrego is a much smaller, lower-energy (<4 W m^{-2}), intermittent to ephemeral river with straight, laterally stable, fine-grained anabranching and distributary channels. Marked downstream declines in discharge and stream power mean that many channels now terminate downstream in unchannelled wetlands. The Warrego River's dramatic response to the relatively modest mid-late Holocene climate change, and its synchronicity with the transformations experienced by other Australian dryland rivers, demonstrate high sensitivity to climate-driven hydrological change in this important inland system.

Introduction

Drylands are terrestrial environments with sub-humid, semiarid, arid and hyperarid climates that collectively cover ~40 % of the Earth's land surface (UNEP, 1992). Despite pronounced moisture deficits and highly variable rainfall and runoff (McMahon et al., 1987; 2007), many drylands support perennial, intermittent and ephemeral rivers and wetlands (Tooth and McCarthy, 2007; Tooth and Nanson, 2011; Jaeger et al., 2017). Given their location in otherwise dry environments, these rivers and wetlands are disproportionately important in terms of ecosystem service delivery (MEA, 2005). However, their geomorphology and hydrology are less well understood compared to rivers in more humid regions (Tooth, 2013), despite the fact that more than 2 billion people live in the world's drylands and rely to some degree on dryland rivers for water, food, agriculture and cultural practices, and other amenities (MEA, 2005; Van der Esch, 2017).

The processes that drive dryland river adjustment and development are related to the balance between discharge, sediment supply and slope (Lane, 1955). For example, sediment volume and calibre, and the amount and frequency of water available to transport that sediment, are controlled by extrinsic characteristics of the catchment such as lithology and climate. Within these constraints, intrinsic processes determine how efficiently the river transports water and sediment towards its base level (Huang and Nanson, 2000, 2008). A long-term perspective on dryland river adjustment and development can improve understanding of the relationships between extrinsic forces and intrinsic processes, particularly by defining how they interact to influence thresholds (or tipping points) of river behaviour (Larkin et al., 2017a). This is particularly important considering future projections of increasing aridity and declining freshwater availability in many drylands globally (Schewe et al., 2013; Cook et al., 2014; Fu and Feng, 2014; Pekel et al., 2016; Rodell et al., 2018), as such extrinsic changes may significantly alter the balance of intrinsic processes and induce changes in dryland river character and behaviour (Larkin et al., in prep [Chapter 5]).

Many previous studies of dryland rivers have focussed on the role of extrinsic forcing, such as tectonic activity or hydroclimatic change, in inducing adjustments in river character and behaviour (Bowler, 1978; Nanson et al., 1992; Nanson et al., 2008; Page et al., 2009; Pietsch et al., 2013; Woodward et al., 2015; Hesse et al., 2018a, b; Mueller et al., 2018). In tectonically stable settings, many dryland river floodplains have preserved evidence of late Quaternary climate change in the form of palaeochannels substantially larger than the modern rivers and in some cases indicating a significantly different channel planform. This is certainly the case in the drylands of southern and northern Africa (Woodward et al., 2015; Larkin et al., in prep) and eastern Australia (Hesse et al., 2018a, b; Mueller et al., 2018). In southeastern Australia, such palaeochannels have long been exploited as robust, but indirect, proxies of late Quaternary climate change (e.g. Bowler, 1967; Nanson et al., 1992; Nanson et al., 2008; Page et al., 2009; Pietsch et al., 2013; Hesse et al., 2018a, b; Mueller et al., 2018). Most recently, Hesse et al. (2018a) showed that Murray-Darling Basin rivers had very large channels and high discharges during

Marine Isotope Stage (MIS) 3 and MIS2, but that this was followed by a significant decline in fluvial activity in the Holocene. The palaeochannel record in the southern Murray-Darling Basin (e.g. Murrumbidgee and Goulburn rivers) correlates well with Antarctic temperature records, indicating that discharge in these systems was mediated by temperature (i.e. enhancement of orographic rainfall, fraction of precipitation stored as snow, and CO_2 feedbacks with vegetation) without requiring large net changes in precipitation. However, northern Murray-Darling Basin palaeochannel records do not correlate as well with the temperature record, suggesting that other mechanisms for increasing available moisture are required to explain high palaeodischarges, particularly in MIS3 (Hesse et al., 2018b). Similarly, in the Lake Eyre Basin in central Australia, palaeoshoreline research has shown substantial hydrological declines since MIS3 (Nanson et al., 1995, 2008; Cohen et al., 2012, 2015). Given the substantial latitudinal range of the Lake Eyre Basin, however, which extends from the winter rainfall zone in the south into the summer monsoon-influenced zone in the north, determining the climatic drivers of both increased discharge and high lake levels and subsequent hydrological declines remains difficult (Cohen et al., 2012).

In parts of the Murray-Darling Basin, explanations for past periods of enhanced flow are also problematic. For instance, rivers are influenced by extratropical sources of enhanced moisture related to the mid-latitude westerlies and the Southern Annular Mode (SAM) as well as tropical sources of moisture related to the Australian summer monsoon and the El Niño-Southern Oscillation (ENSO). The size and latitudinal extent of some northern Murray-Darling Basin catchments can make it difficult to determine the relative influence of these sources. However the north-to-south flowing Warrego River and its extensive fan-shaped floodplain in the northern Murray-Darling Basin is well placed to yield palaeofluvial records that can be used to isolate late Quaternary changes to tropical sources of moisture related to climate modes such as the Australian monsoon and the ENSO, but has not been studied previously. The hydrology of the Warrego River is tied strongly to the ENSO and the summer monsoon (Grootemaat, 2008), but is much less influenced by the SAM-moderated, moisture-bearing winter westerlies that intersect southern Australia. For this reason, the palaeofluvial record of the Warrego River will enhance our understanding of late Quaternary climate change in the Australian drylands, while also providing the opportunity to examine the role of extrinsic forcing by hydroclimatic change and the response of intrinsic processes that govern dryland river morphology.

The overall aim of this paper is to reconstruct, for the first time, the response of the Warrego River to Holocene hydroclimatic change. This paper has four objectives: i) to characterise the contemporary hydrology and geomorphology of the Warrego River; ii) to determine the age of large palaeochannels on the surface of the Warrego floodplain-fan and to characterise their palaeohydrology and geomorphology; iii) to synthesise these findings to reconstruct the processes underlying the Holocene development of the Warrego; and iv) to discuss the findings in the wider context of Australian dryland river response to Holocene hydroclimatic change.

Study system and setting

The Warrego (an indigenous word meaning 'river of sand') is located in the northern Murray-Darling Basin in central-eastern Australia (Fig. 1). The catchment area is approximately 75,000 km^2 and the river extends for over 850 km from -24.838109° S /147.891700° E to -30.404947° S /145.344853° E at its confluence with the Darling River near Bourke. The semi-arid headwaters in the Carnarvon Ranges of central Queensland receive 400-600 mm of rainfall per year during the austral summer months (BOM, 2018). Rainfall decreases downstream and the lower areas of the catchment receive only 250-300 mm of rainfall per year. Owing to dramatic transmission losses (evapotranspiration and groundwater recharge) and distributary channels that flow into wetlands or connect to adjacent basins (e.g. Cuttaburra Creek, Paroo River, Nebine Creek, Culgoa River), the modern Warrego River only establishes a hydrologic connection with the Darling River during occasional large floods. The Warrego River is largely unregulated except for a weir at Cunnamulla that supplies town water and dryland and irrigated agriculture, and that is used to divert flow into Cuttaburra Creek and the Paroo River further west. Land use in the region is predominantly grazing of cattle and sheep and dryland cropping, with only small areas of irrigated cropping.

The Warrego River can be divided into four broad sections: i) the bedrock confined and partly-confined headwaters; ii) the alluvial partly-confined 'panhandle' (i.e. entry-corridor upstream of the fan) and upper fan; iii) the unconfined lower fan; and iv) the partly-confined lower wetland reaches (Fig. 1). At present, downstream of the headwaters (section i), the Warrego River in sections ii-iv is a straight, mostly fine-grained, anabranching river within a distributary fluvial system (DFS) that flows across a low-angled fan-shaped floodplain (Figs. 1 and 2). The Warrego floodplain-fan has an area of ~16,000 km^2. The floodplain is comprised of a complex mosaic of fine sandy and cracking clay alluvial deposits, low sand hills and dunes, partly buried bedrock outcrops, numerous shallow channels and abandoned palaeochannels, and up to 3,000 km^2 of intermittent and ephemeral wetlands (Fig. 2). Much of the Warrego catchment falls within the Mulga Lands Bioregion, where mulga acacia (*Acacia* spp.) plains are interspersed with eucalypt woodlands (Wilson, 1999). River red gums (*Eucalpytus camaldulensis*) and coolibahs (*Eucalyptus coolabah*) line the channels and wetlands. River red gums and lignum (*Muehlenbeckia florulenta*) also locally grow on the bed of the channel.
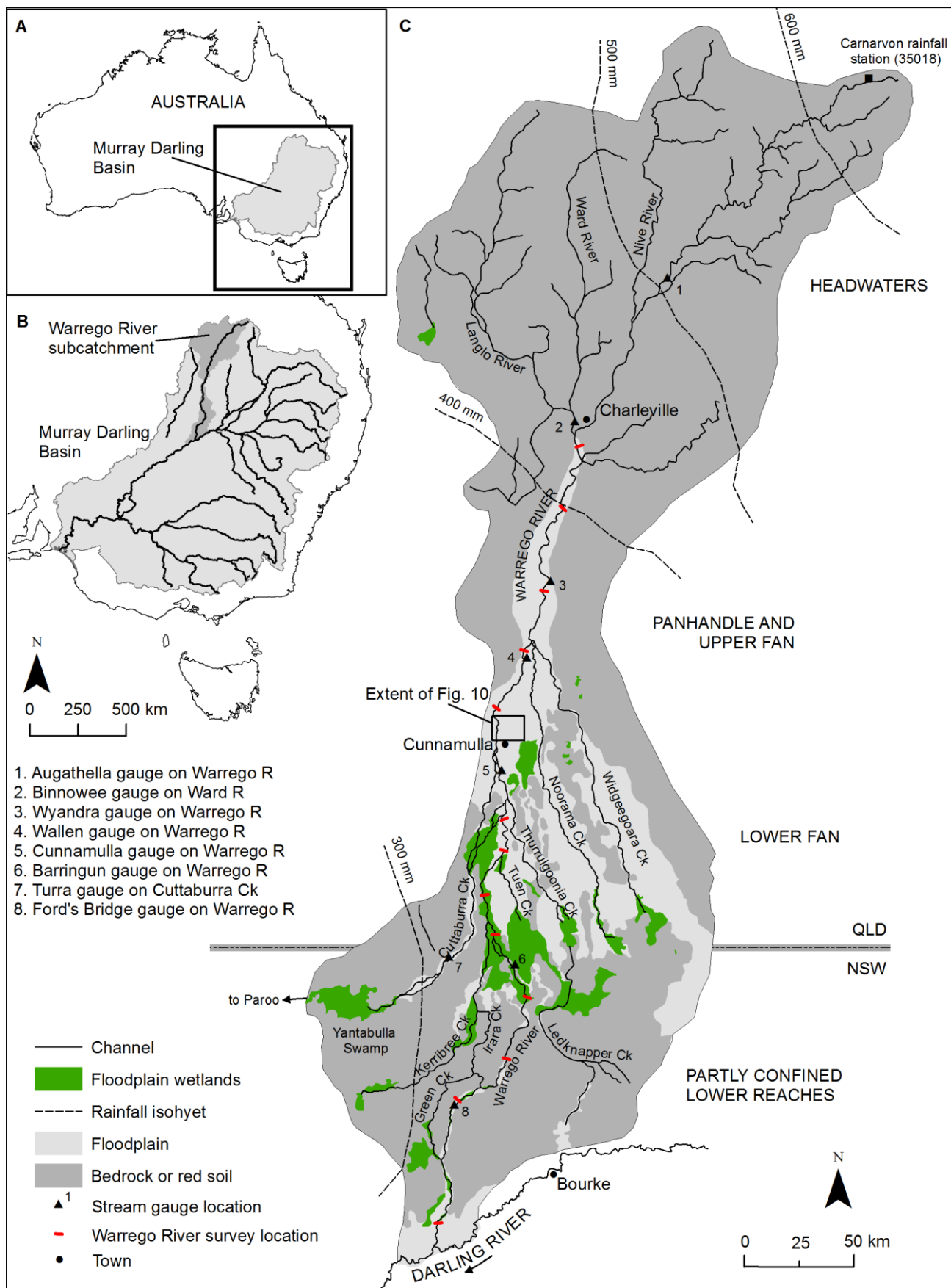
Figure 1. (A, B) Australia and the Murray-Darling Basin. (C) The Warrego River catchment in the northern Murray-Darling Basin showing the major channels, areas of intermittent floodplain wetlands, and river survey locations mentioned in the text.

(A) Warrego River in the panhandle/upper fan

(B) Warrego River in the panhandle/upper fan

(C) Warrego River on the lower fan
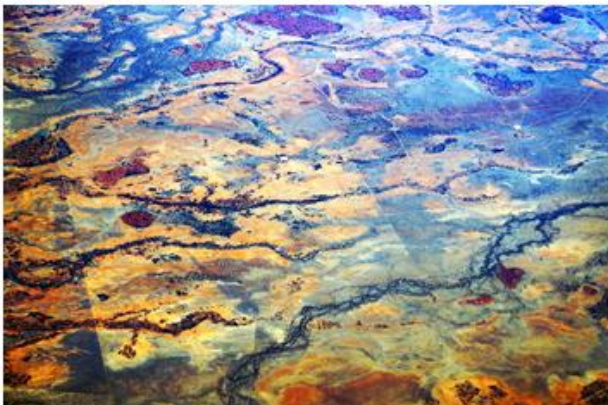
(D) Warrego River on the lower fan

(E) Warrego River in the lower confined reaches

(F) Burrenbilla palaeochannel

(G) Burrenbilla palaeochannel
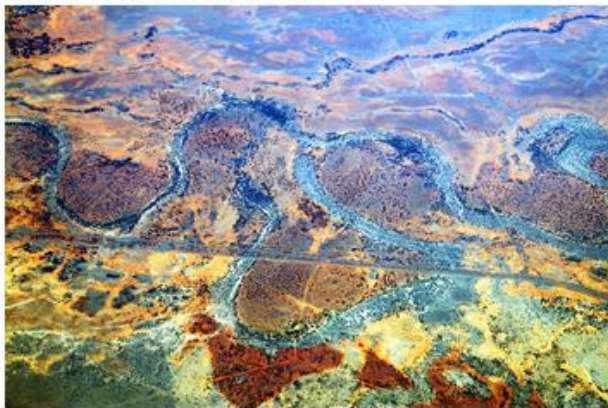
(H) Burrenbilla and Coongoola palaeochannels

Figure 2. Oblique aerial photographs of the modern Warrego River and palaeochannels on the Warrego floodplain-fan. Flow direction is from left to right in all images. Photos used with permission. Credit: Michael Thirnbeck.

Methods

For this study, data were derived from a mixture of secondary sources, field investigation and laboratory analytical methods.

Modern climate and hydrology

Hydrological time-series data were sourced from the Queensland government Water Information System (DNRME, 2018), and the New South Wales Department of Primary Industries Office of Water (Water NSW, 2018). Inundation extent and frequency data created by Mueller et al. (2016) are publicly available from the Australian Flood Risk Information Portal (www.ga.gov.au/wofs). Monthly southern oscillation index (SOI) data and annual rainfall data for the Carnarvon rainfall station (35018) was sourced from the Australian Bureau of Meteorology (BoM, 2018).

Mapping and channel morphometrics

Geomorphological mapping of the Warrego floodplain, the modern river and palaeochannels was carried out using ESRI basemap satellite imagery and a 30 m Shuttle Radar Topography Mission (SRTM) Digital Elevation Model (DEM) (Geoscience Australia, 2011).

In the field, standard automatic level methods were used to survey the topography of the Warrego River channel at 13 locations spaced downstream from Charleville to Toorale National Park near the junction with the Darling River (Figs. 1 and 3). Channel morphometric parameters were calculated from the survey data, including bankfull width, depth, width/depth ratio, and cross-sectional area. At points where the trunk stream of the Warrego was multi-channelled, total channel width and total channel area were calculated. The same survey methods were used to measure the floodplain and channel topography at meander bends of two large palaeochannels, which we have named 'Burrenbilla' and 'Coongoola' after nearby localities or station names.

Figure 3. Photographs from the 13 Warrego River field sites showing the downstream transition of the trunk stream from a densely vegetated channel with multiple thalwegs, to a large, well-defined single channel, to a shallow and increasingly indistinct channel with wetland vegetation. All photos are looking downstream.

Bankfull discharge and palaeodischarge estimates

Due to the and the lack of flow in the system during fieldwork and the dramatic downstream declines in channel size, survey data from 13 sites along the modern river were used in conjunction with roughness estimates (after Gardiner and Dackombe, 1983) to estimate flow velocity, bankfull discharge and stream power using Manning's equation. Slope estimates derived from a 30 m SRTM DEM were also used to calculate gross and unit bankfull stream power for the 13 sites on the modern channel and for the two palaeochannels studied.

Palaeodischarge estimates for the Warrego palaeochannels were made using the empirical regime equation using bankfull channel width derived by Hesse et al. (2018a) for similar rivers in the Murray-Darling Basin, which, like the Warrego palaeochannels, are also sinuous/meandering dryland rivers with equivalent form-process relationships. The log regression equation is:

$$\log_{10} Q_{bf} = 2.2412 \log_{10} W_{bf} - 1.7224$$

where Q_{bf} is bankfull discharge and W_{bf} is mean bankfull width for the reach. Confidence intervals at 95 % were also calculated to account for the error associated with extrapolation.

Sediment sampling

Sediment samples were collected from the Burrenbilla and Coongoola palaeochannels at pronounced scroll ridges on the inside of large, well-defined meander bends. In all, nine palaeochannel samples from four meander bends on the two palaeochannels, and one source-bordering dune sample were collected for optically stimulated luminescence (OSL) dating. Palaeochannel samples were collected by hand augering ~1 m into the top of each scroll ridge, a depth below the usual level of bioturbation and anthropogenic disturbance. Following the approach adopted in similar studies (Rodnight et al., 2005, 2006; Munyikwa et al., 2011; Larkin et al., 2017b), a ~30 cm long, ~7 cm diameter metal tube was then attached to the end of the auger extension rods. The metal tube was pushed into the undisturbed sand at the base of the auger hole, and the sample retrieved without mixing, contamination or exposure to sunlight. All OSL sample tubes were sealed to prohibit exposure to light, and then wrapped in light-tight black plastic for transport to the laboratory, where subsequent sample treatment took place in subdued red-light conditions.

Optically stimulated luminescence (OSL)

OSL samples were processed in the Aberystwyth Luminescence Research Laboratory at Aberystwyth University, U.K. Standard methods were used to isolate the 125–212 µm quartz fraction of sediment, to dissolve carbonates and organics (hydrochloric acid and hydrogen peroxide, respectively), to remove heavy minerals and feldspars by density mineral separations, and to etch grains with 40 % hydrofluoric acid in order to remove the alpha irradiated outer grain surface (see Aitken 1998).

Luminescence measurements were made on a Risø automated TL/OSL reader equipped with a single-grain system based on a 532 nm green laser (Bøtter-Jensen et al. 2003). Luminescence emitted by grains was detected with an EMI 9235QA photomultiplier, with the light filtered through 2.5 mm of U-340 to reject the stimulation source. Prior to single-grain OSL analysis, a dose response and preheat test was performed to determine the optimum thermal treatment for the samples to be used in the single aliquot regenerative dose (SAR) procedure (Wintle and Murray 2006). All samples were measured with a preheat temperature of 200 °C for 10 seconds and a cut-heat of 160 °C for 10 seconds. One thousand grains were analysed for each sample and individual grains were accepted based on criteria outlined in Jacobs et al. (2006), which are: recycling ratio within 10 % of unity, test dose error less than 10 %, T_n signal greater than three times the standard deviation of the background, and an IR-OSL depletion ratio within 10 % of unity (Duller 2003). After application of these criteria, between 120 and 254 individual equivalent dose (D_e) values were determined using Analyst software (Duller 2015). The samples display equivalent dose (D_e) distributions with relatively high degrees of overdispersion, and some include an anomalous young population of grains centred on ~1 Gy (see Supplementary Fig. 1). The D_e distributions do not suggest incomplete bleaching at burial, which would necessitate the use of the minimum age model (MAM). Rather, two discrete populations are identified which suggests contamination either during sampling or prior to sampling due to bioturbation. The finite mixture model (FMM) was used to isolate the anomalous youngest population of grains and to provide an age estimation based on the older population of grains which are more representative of the most recent deposition of these scroll bar samples. Although sites were chosen carefully in the field, it is possible that bioturbation accounts for the anomalous younger populations of D_e values in the samples.

The environmental dose rate was calculated by thick source alpha counting and beta counting of dried and milled material taken from the ends of sample tubes, as this is representative of sediment surrounding the OSL sample. The cosmic ray contribution was estimated from the data given by Prescott and Hutton (1994), taking into account altitude, geomagnetic latitude and thickness of sediment overburden. Water content was kept constant for palaeochannel scroll bar samples at 5 ± 5 % given the prevailing dry climate and distance from the modern Warrego river channel (see Supplementary Table 1 for dosimetry data). Equivalent dose is divided by the dose rate to derive an OSL age estimate (Duller 2004).

Results

Hydrological and geomorphological data to characterise the modern Warrego River, including downstream trends, are presented in Figures 2–9, and geochronology and palaeohydrology data are presented in Figure 10 and Tables 1 and 2.

Hydrology of the modern Warrego River

The Warrego River has a highly variable flow regime with occasional large floods separated by several years of low or no flow (Fig. 4). Interannual fluctuations between La Niña (wet in eastern Australia) and El Niño (dry in eastern Australia) conditions correlate with some of the large floods and dry spells, respectively, particularly in the early 1970s and the 2010–2012 La Niña (Fig. 4A). Precipitation over the headwaters in the Carnarvon Ranges is distinctly seasonal but with a high amount of interannual variability (Fig. 4B). Rain falls over the headwaters largely during the austral summer months (November to March) and the winter months (May to September) are much drier. In conjunction with a significant attenuation of flow downstream, the passage of the flood wave is quite slow highlighting the long-duration floods that are characteristic of large, low-gradient dryland systems, particularly in Australia (cf. Knighton and Nanson, 1994a). For example, the 2010 and 2012 floods had peak discharges of ~3000 $m^3 s^{-1}$ at Wyandra (Fig. 4), but peak discharge at the downstream end of the system (Ford's Bridge, ~300 km downstream) occurred 2–3 months later, having diminished by over 97 % to ~80 $m^3 s^{-1}$ (Fig. 4F). At Wyandra, there was no flow for ~43 % of the time in the period between 1972 and 2016 (Fig. 5). The steepness of the flood duration curve for Wyandra demonstrates the boom and bust hydrology of the modern Warrego River with long dry periods separated by large floods (Fig. 5).
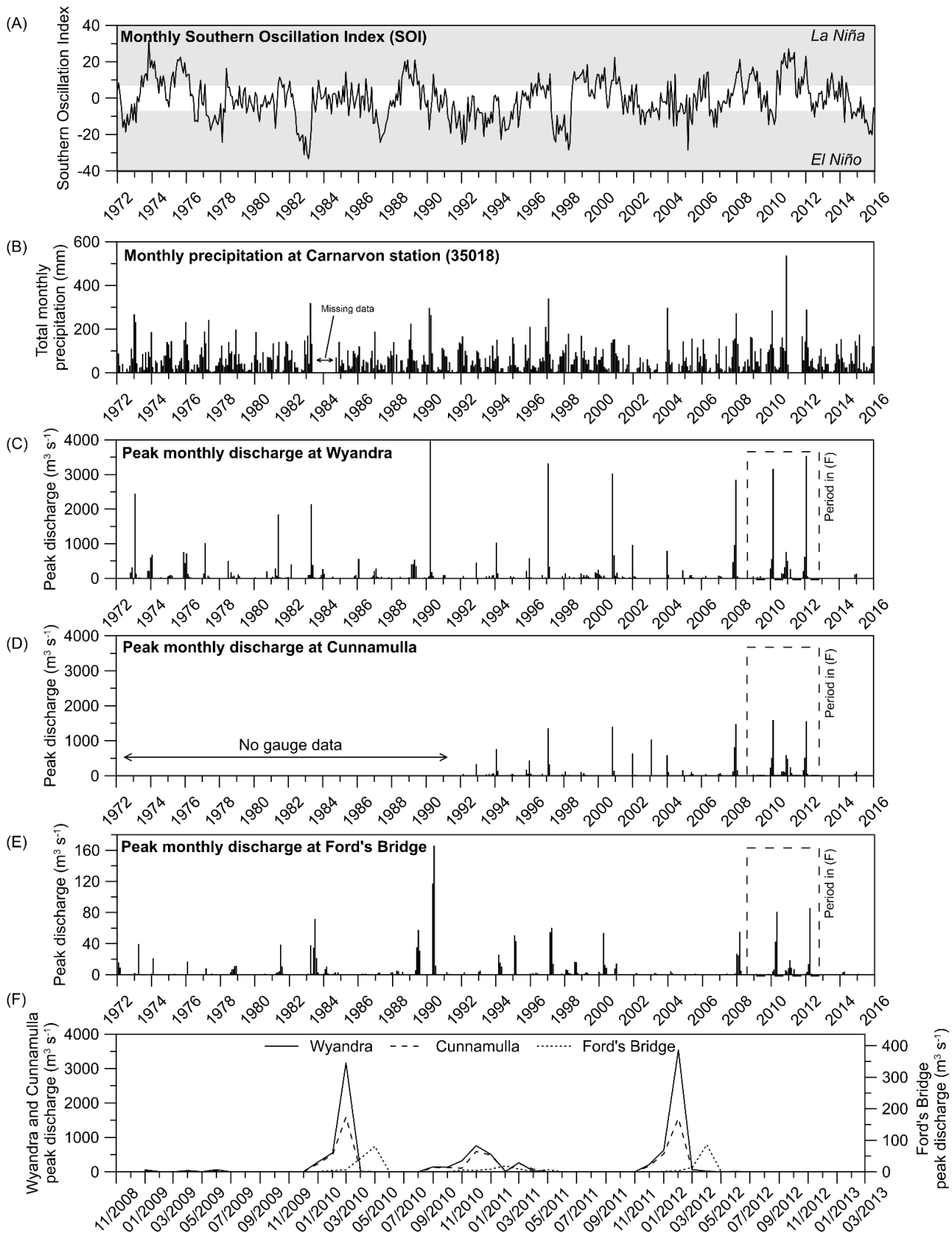
Figure 4. (A) Monthly Southern Oscillation Index (SOI) values between 1972 and 2016. A SOI index value of greater than 7 (less than -7) is associated with La Niña (El Niño) conditions in the western Pacific Ocean. (B) Total monthly precipitation at the Carnarvon Station in the Warrego River headwaters. Note the seasonality of rainfall in the headwater catchments, but also substantial interannual variability. (C) Peak monthly discharge at Wyandra in the Warrego panhandle (1972–2016). (D) Peak monthly discharge at Cunnamulla on the upper fan (1992–2016). (E) Peak monthly discharge at Ford's Bridge and Bywash (combined) in the partly confined lower reaches (1972–2016). (F) Peak monthly discharge at Wyandra, Cunnamulla and Ford's Bridge during the La Niña floods of 2010, 2011, and 2012 (data shown from late 2008–2013). Note that the data for Ford's Bridge is shown at 1/10 axis scale

and that there is a 2–3 month lag between peak flooding at Wyandra and Cunnamulla and peak flow towards the downstream end of the system at Ford's Bridge.
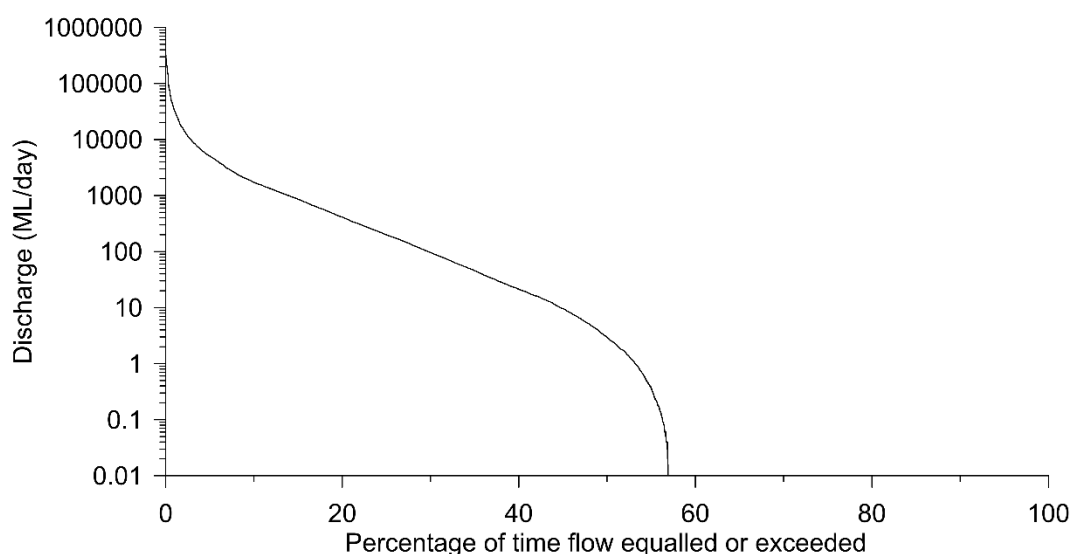
Figure 5. Flood duration curve for the Warrego River at Wyandra, calculated from hydrological time-series data from 1972–2016.

Inundation mapping shows the extent and frequency of flooding on the Warrego floodplain-fan during the 27 years between 1987 and 2014 (Fig. 6; Mueller et al., 2016). Inundation extent and frequency data was created by Mueller et al. (2016) by creating a water detection algorithm and determining the presence of water across the entire Australian continent for each of the 27 years of satellite imagery available. In the panhandle and upper fan, flooding is generally confined within the channel belt (Fig. 6B), while extensive inundation of the floodplain occurs further downstream on the lower fan, particularly on the western portion of the fan where the modern Warrego River is situated. Distributary channels are well defined but have low inundation frequency, as do the unchannelled wetlands at their downstream ends, only being flooded for up to ~5 % of the observations between 1987 and 2014 (Fig. 6). Cuttaburra Creek which transports water to Yantabulla Swamp and the Paroo River is relatively frequently flooded compared to some of the other distributary channels on the eastern side of the fan (e.g. Widgeegoara and Noorama creeks). Palaeochannel depressions near Cunnamulla carry water during overbank flooding, although infrequently (~1 % of observations between 1987 and 2014), while the Cunnamulla weir holds almost permanent water and the irrigated pastures near Cunnamulla are also frequently flooded (Fig. 6C). Yantabulla Swamp is among the largest and most regularly flooded wetlands in the area, assisted by diversions from Cunnamulla Weir. To the northeast of the fan, numerous rain-fed pans in the bedrock hills are inundated in ~5–10 % of observations (Fig. 6).

37
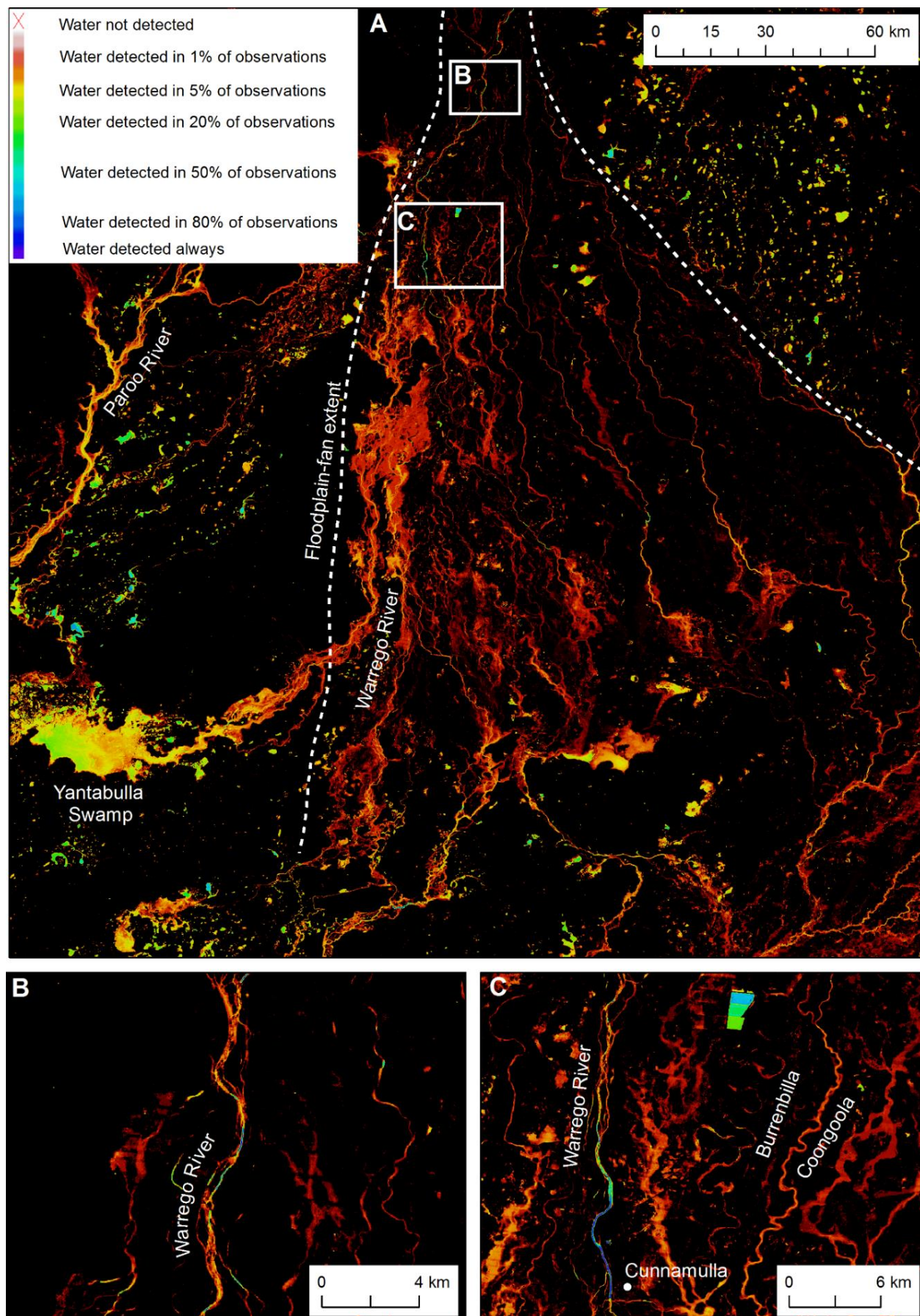
Figure 6. Inundation frequency of (A) the Warrego floodplain-fan, (B) the Warrego River in the panhandle, and (C) the Warrego River and palaeochannels on the upper fan near Cunnamulla. Inundation extent and frequency based on 27 years of Landsat satellite imagery from 1987 to 2014 (Mueller et al., 2016). Data source: Mueller et al. (2016).

Modern downstream trends in discharge and stream power

The Warrego River is characterised by substantial downstream declines in discharge and stream power (Fig. 7). Total and bankfull discharge and bankfull stream power (both gross and unit) peak in the panhandle and upper floodplain-fan around Wyandra and Wallen before declining dramatically across the lower floodplain-fan (Fig. 7). In the panhandle and upper fan, the channel is inset into the floodplain and while bankfull discharge ranges up to ~100 $m^3\,s^{-1}$ (Fig. 7) the flow required to overtop the inset channel and inundate the floodplain is substantially higher at between ~310 and 1400 $m^3\,s^{-1}$ (Fig. 8). Inundation mapping for the period 1987–2014 highlights this as flows are largely constrained within the channel belt (Fig. 6B). Cuttaburra Creek, which branches from the Warrego River near Cunnamulla, is the only distributary channel that is gauged and is a particularly important distributary as it diverts ~200 x10^6 m^3 a year towards the ecologically important Yantabulla Swamp (a Ramsar wetland) and eventually connects to the Paroo River. Across the fan, bankfull discharge diminishes from ~90 $m^3\,s^{-1}$ to ~10 $m^3\,s^{-1}$, and in the lower confined reaches of the Warrego River, bankfull discharge is less than 4 $m^3\,s^{-1}$. Bankfull gross (unit) stream power similarly declines across the fan from ~200 W m^{-1} (~4 W m^{-2}) to less than ~13 W m^{-1} (~1 W m^{-2}) in the lower reaches (Fig. 7).
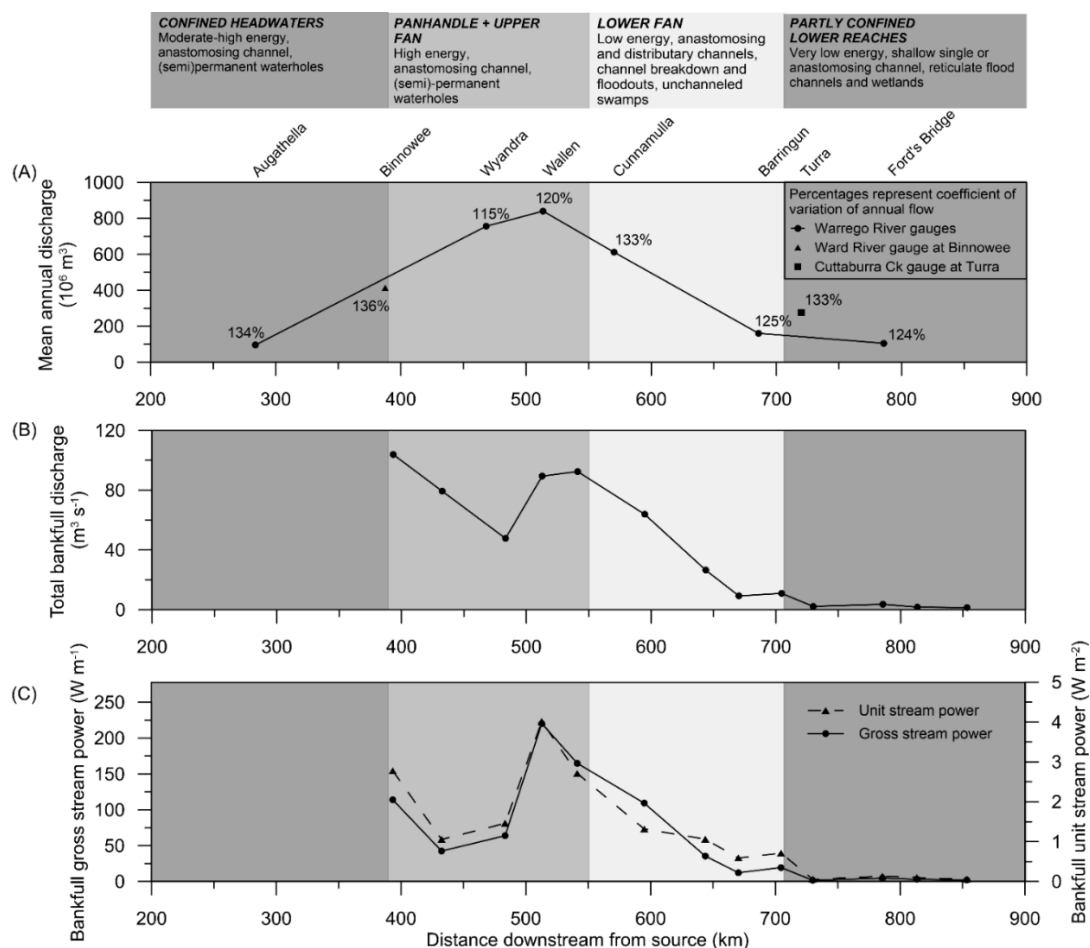
Figure 7. Downstream discharge and stream power trends for the Warrego River. (A) Mean annual discharge from eight flow gauge locations in the Warrego catchment plus labels indicating coefficient of variation of annual flow

(standard deviation/mean annual discharge) values given as a percentage. There are six gauges on the main Warrego River, one on a tributary (Ward River at Binnowee) and one on a distributary (Cuttaburra Ck at Turra). (B) Total bankfull discharge estimated using Manning's equation and data from surveys conducted in the field at 13 sites along the Warrego River. (C) Bankfull gross and unit stream power at the 13 Warrego River sites.

Modern channel pattern and morphology

The very low gradient Warrego floodplain (mean slope ~0.0003 m m^{-1}) is traversed by the modern Warrego River and at least nine major distributary or anabranching channels that either join adjacent river systems (e.g. Paroo River, Nebine Creek), terminate in wetlands, or in some cases, re-join the Warrego (e.g. Green Creek). The morphology of the Warrego River changes dramatically downstream (Figs. 2, 3, 8, and 9). In the upper reaches of the panhandle, the Warrego River is significantly inset into the floodplain and is laterally stable along much of this section (Fig. 8). In these reaches, the Warrego has a complex ridge-form anabranching planform characterised by several straight channels separated by heavily-vegetated, sandy ridges forming a channel tract (Fig. 8). In the panhandle and upper floodplain-fan, the Warrego gradually transitions to a largely single-thread channel (i.e. single main channel with high-flow flood channels and anabranches) characterised by a series of deep waterholes, isolated during low flow, that hold permanent water (e.g. WR7, Fig. 8). These single-thread reaches are also inset into the floodplain and have the highest bankfull discharge and gross and unit bankfull stream power values in the modern Warrego system (Fig. 7). Downstream of Cunnamulla on the lower floodplain-fan, the Warrego is less inset into the floodplain and several major distributary channels divert from the main channel (e.g. Cuttaburra Creek, Woggonora Creek, Thurrulgoonia Creek, and Tuen Creek; Fig. 8). Subsequently, the main Warrego channel declines rapidly in size and generally becomes shallower and wider (Fig. 8). On the lower floodplain, the Warrego has a complex planform of generally one or two low sinuosity main channels and numerous, smaller flood channels and shallow flow paths on the floodplain, with reticulate channel patterns occurring in backswamp locations and where channels break down. Vegetation invades the channels and distributaries disintegrate into splay complexes (see Tooth, 2005), eventually forming unchannelled, intermittent wetlands. At the very downstream end of the system in the confined reaches, the channel is very shallow and indistinct in places with poorly coordinated drainage patterns and unchannelled wetlands (Figs. 2, 3, and 8).
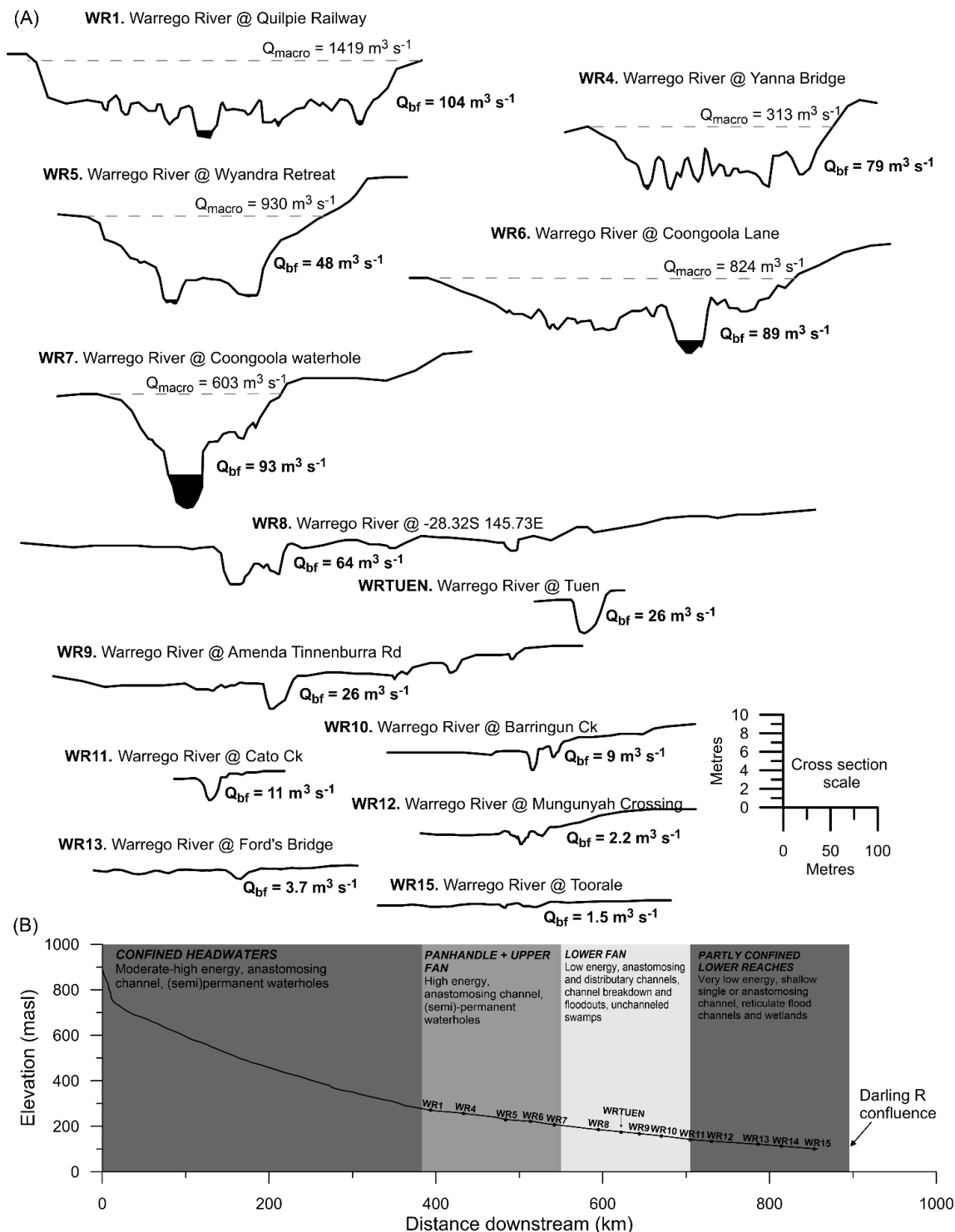
Figure 8. Downstream changes in channel size and morphology along the Warrego River. (A) Channel cross sections from 13 locations along the main Warrego River. Q_{bf} is total bankfull discharge. Q_{macro} is the minimum discharge required to overtop the macrochannel and inundate the surrounding floodplain. (B) Longitudinal profile of the Warrego River including the locations of the cross sections shown in (A).

Modern channel downstream morphometric trends

At its maximum, floodplain width on the fan extends to ~130 km before it abuts a bedrock ridge and the Warrego River enters the lower confined reaches (Fig. 9). Total bankfull channel width declines from ~200 m near the head of the panhandle to less than ~40 m on the lower floodplain-fan (Fig. 9). The

depth of main channel increases until the upper floodplain-fan near the town of Wyandra, where the channel is characterised by irregularly-spaced, deep waterholes (see Fig. 3), before declining gradually in the middle and lower reaches (Fig. 9C). Total bankfull channel area is variable in the panhandle and upper floodplain-fan but overall declines substantially downstream, from ~300 m^2 at the head of the panhandle to < 35 m^2 on the lower floodplain-fan and in the lower confined reaches (Fig. 9D). The size of flood channels is relatively constant throughout the lower half of the Warrego River, being generally ~20–40 m wide and ~1–2 m deep (Fig. 9B, C). The width/depth ratio of channels is relatively constant until the lower confined reaches where it begins to increase as shallow channels enter the wetlands (Figs. 3 and 9E).
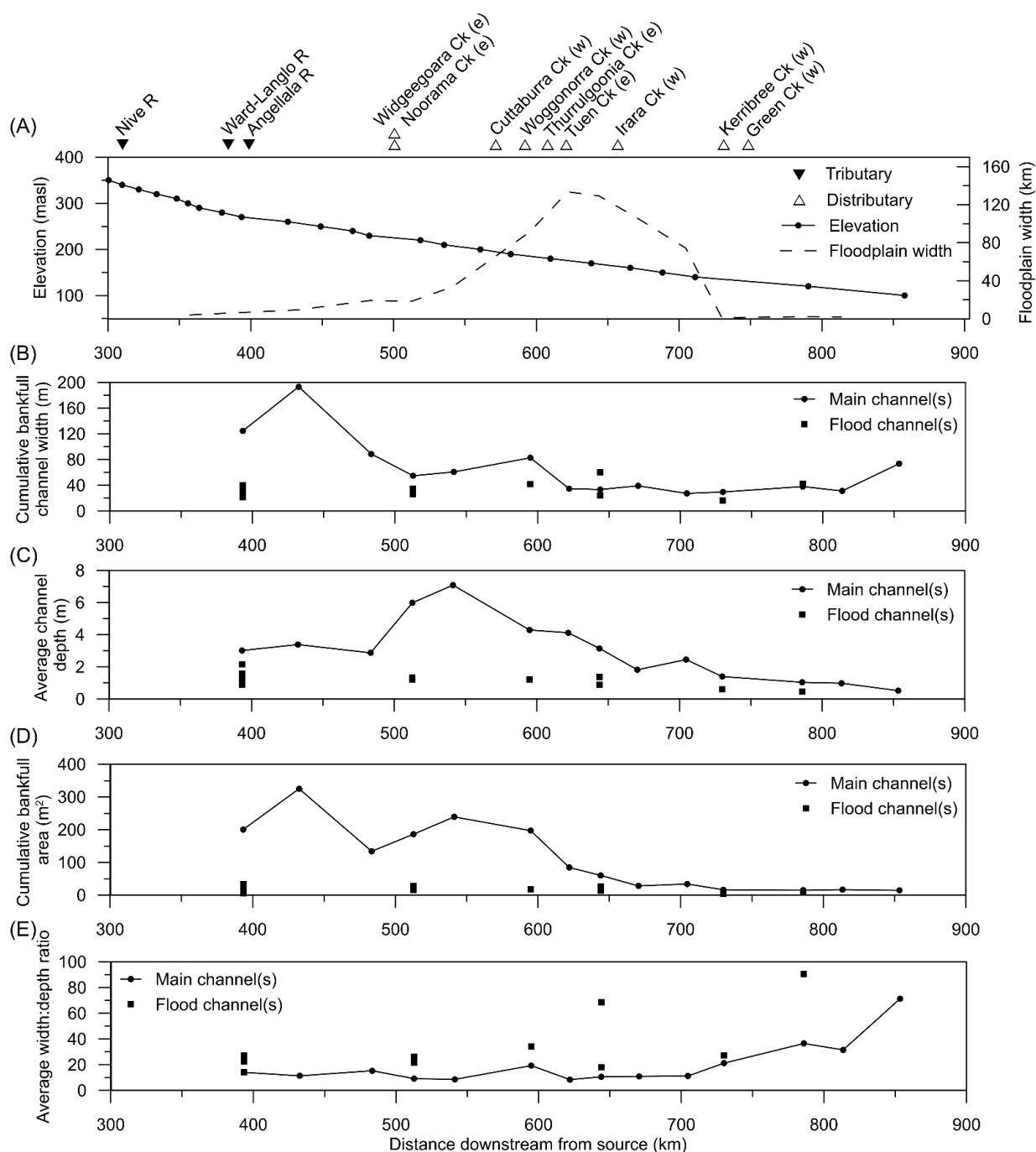
Figure 9. Downstream morphological characteristics of the Warrego River. (A) Longitudinal profile and floodplain width. Locations of tributaries and distributaries marked with closed and open triangles respectively. Letters in

brackets represent the direction the distributary channel diverts from the main channel (w – western side of main channel, e – eastern side of main channel) (B) Cumulative bankfull channel width of main channel(s) and flood channel(s). (C) Average channel depth of main and flood channel(s). (D) Cumulative bankfull cross sectional area of main and flood channel(s). (E) Average width/depth ratio of main and flood channel(s).

Palaeochannel morphometrics and palaeohydrology

The Burrenbilla palaeochannel has an average width of ~161 m and an estimated bankfull discharge of ~1669 m^3 s^{-1} (95 % CI ~526–5292 m^3 s^{-1}, Table 1). Bankfull gross and unit stream power was ~1636 W m^{-1} (95 % CI ~516–5186 W m^{-1}) and ~10.2 W m^{-2} (95 % CI ~3.2–32.3 W m^{-2}), respectively. Burrenbilla was a meandering river with regular meanders, cutoffs and a pronounced alluvial ridge (Fig. 10). The Coongoola palaeochannel has an average width of ~116 m and an estimated bankfull discharge of ~810 m^3 s^{-1} (95 % CI ~268–2452 m^3 s^{-1}, Table 1). Bankfull gross and unit stream power was ~962 W m^{-1} (95 % CI ~318–2912 W m^{-1}) and ~8.3 W m^{-2} (95 % CI ~2.7–25 W m^{-2}), respectively. Compared to Burrenbilla, Coongoola was a lower-energy, lower-sinuosity meandering river with irregular meanders (Fig. 10).

Table 1. Summary of morphological and hydraulic characteristics of the Warrego palaeochannels.

Palaeochannel	Channel width (m)	Average floodplain slope (m m^{-1})	Average sinuosity	Channel discharge (m^3 s^{-1}) [95 % CI]	Gross stream power (W m^{-1}) [95 % CI]	Unit stream power (W m^{-2}) [95 % CI]
Burrenbilla	160.7	0.0002	~2	1669 [526–5292]	1636 [516–5186]	10.2 [3.2–32.3]
Coongoola	116.4	0.0002	~1.65	810 [268–2452]	962 [318–2912]	8.3 [2.7–25]
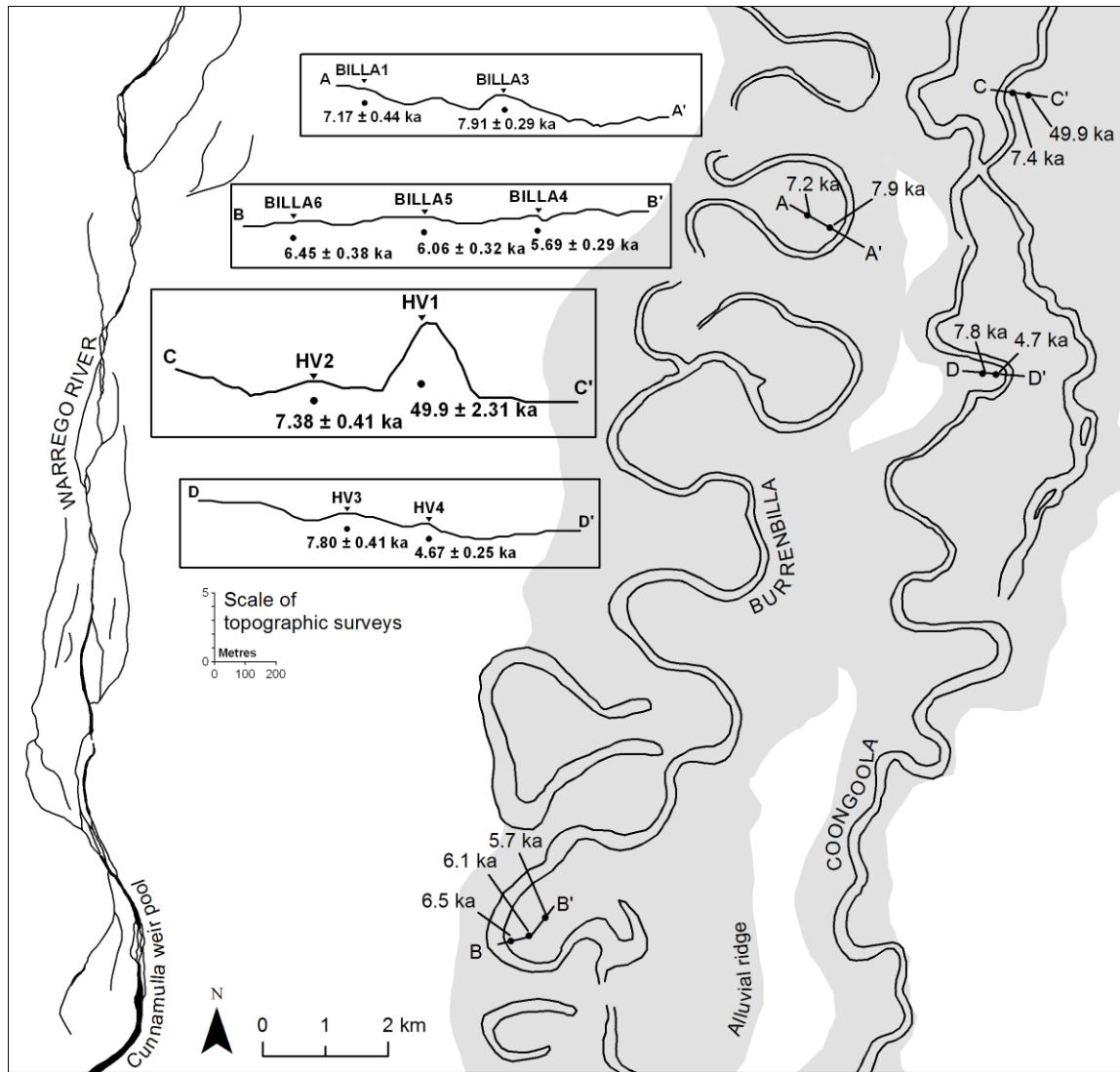
Figure 10. Sample locations and OSL ages for the Burrenbilla and Coongoola palaeochannels. Flow in the Warrego and its palaeochannels is from top to bottom (i.e. north to south; see Fig. 1 for location).

Palaeochannel chronology

OSL ages of buried sediment samples collected from palaeochannel scroll-ridge deposits indicate that the Burrenbilla and Coongoola palaeochannels were active during the early-mid Holocene (Table 2, Fig. 10). The large Burrenbilla palaeochannel has a median age of ~6.5 ka and was actively migrating laterally across the floodplain between ~7.9 ka and ~5.7 ka (Fig. 10). The scroll-ridge deposits comprised of upwardly-fining, fine-medium (~125-300 µm) sand. It is not possible to estimate rates of lateral channel migration as the mid-points of the OSL ages are in the inverse order to that which would be expected for both meander bends (i.e. scroll ridge OSL age midpoints are older closer to the channel rather than younger, Fig. 10), however there is overlap in the error of the ages and so they can be accepted with confidence. OSL dates from the smaller Coongoola palaeochannel show that it was active between ~7.8 and ~4.7 ka, indicating that it may have been contemporaneously active with the Burrenbilla channel – perhaps as a smaller distributary channel – and that it persisted for ~1000 years longer than Burrenbilla. The modern, much smaller and straighter Warrego River evolved into its current planform after ~4.7 ka.

Table 2. OSL sample details and single grain analysis results.

Sample	Sample type	Depth (m)	n	Age model	Equivalent dose (Gy)	Dose Rate (Gy ka^{-1})	Age (ka)
BILLA1	Palaeo-scroll ridge	1 ± 0.1	254	FMM	11.17 ± 0.43	1.56 ± 0.07	7.17 ± 0.44
BILLA3	Palaeo-scroll ridge	1 ± 0.1	185	FMM	7.79 ± 0.24	0.99 ± 0.04	7.91 ± 0.43
BILLA4	Palaeo-scroll ridge	1 ± 0.1	137	FMM	6.15 ± 0.14	1.08 ± 0.05	5.69 ± 0.29
BILLA5	Palaeo-scroll ridge	1 ± 0.1	214	FMM	6.46 ± 0.17	1.07 ± 0.05	6.06 ± 0.32
BILLA6	Palaeo-scroll ridge	1 ± 0.1	194	FMM	8.12 ± 0.30	1.26 ± 0.06	6.45 ± 0.38
HV1	Aeolian dune	3 ± 0.1	182	FMM	25.53 ± 0.44	0.51 ± 0.02	49.9 ± 2.31
HV2	Palaeo-scroll ridge	1.1 ± 0.1	212	FMM	12.67 ± 0.36	1.72 ± 0.08	7.38 ± 0.41
HV3	Palaeo-scroll ridge	1 ± 0.1	147	FMM	6.9 ± 0.22	0.89 ± 0.04	7.8 ± 0.41
HV4	Palaeo-scroll ridge	1 ± 0.1	120	FMM	4.06 ± 0.12	0.87 ± 0.04	4.67 ± 0.25

Interpretation

The Warrego River has undergone profound changes to its hydrology and geomorphology during the Holocene. As evidenced by its palaeochannels, the Warrego River during the early-mid Holocene, between ~8 and ~5 ka, was a large, high-energy and highly sinuous meandering river. The Burrenbilla and Coongoola channels were actively migrating laterally across the floodplain and building a super-elevated, sandy alluvial ridge. The Burrenbilla palaeochannel transported >20 times the total bankfull discharge of the modern river at the equivalent position downstream. The Coongoola palaeochannel transported >10 times the discharge of the modern river at the equivalent position downstream. The ages of the Burrenbilla and Coongoola palaeochannels overlap considerably indicating that the Coongoola channel was a smaller, contemporaneous, distributary channel which had avulsed from the larger Burrenbilla trunk channel (together capable of transporting up to ~2400 $m^3 s^{-1}$). The Coongoola palaeochannel, however, appears to have been active until ~4.7 ka, ~1000 years longer than the Burrenbilla palaeochannel, suggesting that perhaps the smaller, and less sinuous Coongoola channel became the main channel as discharge waned heading into the late Holocene and the Burrenbilla channel was abandoned. This interpretation is limited by the number and spread of fluvial ages we have for the Warrego palaeochannels and, therefore, further dating is required to fully understand the timing of the abandonment of the Burrenbilla and Coongoola channels.

Nevertheless, after ~4.7 ka, an extrinsically-driven threshold was crossed, leading to the collapse of the higher energy, meandering palaeochannels and the formation of the modern Warrego River. The contemporary Warrego River is vastly different in terms of its channel planform, morphology and behaviour, being a lower-energy, intermittent river with relatively straight, laterally stable, anabranching and distributary channels, many of which terminate in unchannelled wetlands. In the modern Warrego system, a strong correlation exists between hydrology and geomorphology, with pronounced downstream trends. The persistent downstream decline in discharge and stream power

manifests in downstream declines in channel size as well as changes in river behaviour. In the upper and middle reaches, the modern Warrego River is inset into the floodplain and has a ridge-form anabranching planform where multiple parallel channels are separated by well vegetated, sandy ridges. Ridge-form anabranching channels have been described in central Australian rivers (Tooth and Nanson, 1999). This channel pattern is thought to be a mechanism which improves sediment transport efficiency (Jansen and Nanson, 2004; Huang and Nanson, 2007). Vegetation also plays a role in these reaches as bars and ridges form in the lee of trees that colonise the channel bed to take advantage of intermittent flows. Where discharge and stream power are highest, in the panhandle and upper floodplain-fan, the channel is largely straight and single-thread with deep, scoured waterholes. These waterholes are similar to those seen on Cooper Creek in the Lake Eyre Basin (Knighton and Nanson, 1994b), which form where local stream power is highest, for example, at the junction of two or more channels or constriction between dunes or bedrock. The Warrego waterholes do not form due to flow constriction but due to the inset channel and locally high discharge and stream power (Figs. 7 and 8). Further downstream on the middle and lower floodplain, the channel is less inset into the floodplain and dramatic declines in discharge and stream power promote significant downstream declines in channel size, initiation of channel anabranching and distributary channel formation due to avulsion, which act to further reduce flow in the main channel. The distributary channels are generally characterised by gradual declines in flow and sediment transport competence, and eventually break down into unchannelled, intermittent wetlands. When the Warrego River enters the lower confined reaches, it is considerably weakened by the magnitude of downstream declines in flow and stream power and persists as discontinuous channel segments and unchannelled wetlands (e.g. lignum swamps). It is also likely that local runoff from adjacent hillslopes plays an important role in maintaining wetlands in these confined reaches.

The evolutionary trajectory of fluvial change in this system is clear: in the mid-late Holocene a decline occurred from the high-discharge and high-sinuosity meandering Burrenbilla channel, to the lower-discharge and lower-sinuosity meandering Coongoola channel, followed by a step-change in the character and behaviour of the Warrego River to the modern low-energy, straight, and anabranching river. A major extrinsic driver must have forced this system over a threshold triggering dramatic river response, and the predominant hydroclimatic drivers thought to be responsible are discussed below.

Discussion

The dramatic contrast between the character and behaviour of the Holocene palaeochannels and the modern river provides interesting insight into the dominant control that catchment hydroclimate has on fluvial geomorphology in this setting.

Drivers of Holocene hydroclimatic conditions in Australia

Holocene climate conditions and their changes over time are relatively well understood in the Northern Hemisphere, with the well-documented, orbitally-controlled northward shift of the intertropical convergence zone (ITCZ) during the early-mid Holocene having significant impacts on rivers and wetlands, ecosystems, and human civilisations in the northern mid-latitudes (Giosan et al., 2012; Macklin and Lewin, 2015; Yang et al., 2015). However, the drivers of Holocene hydroclimatic change in the southern hemisphere are relatively less well documented. The Warrego River catchment lies within the Australian summer rainfall zone, but just south of the extent of the true monsoon. The source of moisture in the Warrego catchment is typically the Coral Sea off the northeast coast of Australia, where moisture-laden southeast trade winds bring summer rainfall over Warrego headwaters (and other regions of the Great Dividing Range) due to orographic forcing, or the Gulf of Carpentaria when large troughs extend south from the ITCZ, often triggering widespread flooding (Grootemaat, 2008). Given the influence of the ENSO on both sea surface temperatures (SST) in the Coral Sea (cooler during El Niño and warmer during La Niña) and the likelihood of deep monsoonal troughs developing over northern Australia (more likely during La Niña), rainfall and runoff in the Warrego catchment is strongly correlated with ENSO (Verdon et al., 2004; Grootemaat, 2008). The Warrego River is otherwise isolated from the SAM-moderated mid-latitude westerlies which intersect southern Australia and complicate the interpretation of fluvial records in catchments that are affected by both the ENSO and the SAM (e.g. the Macquarie River).

A range of high-resolution climate proxies indicate that the Pacific Ocean during the early-mid Holocene was characterised by a reduction in ENSO variability and El Niño events, with a La Niña-like mean state or otherwise wetter conditions (Shulmeister and Lees, 1995; Liu et al., 2000; Rein et al., 2005; Koutavas et al., 2006; Shin et al., 2006; Conroy et al., 2008; Carré et al., 2012; 2014; McGowan et al., 2012; Chen et al., 2016; Leonard et al., 2016; Pausata et al., 2017; Tian et al., 2017, 2018). A more northerly ITCZ during the early-mid Holocene meant that cross-equatorial, southeasterly trade winds in the eastern Pacific were more permanent, encouraging upwelling near the South American coast and reducing SST and the thermocline depth (Koutavas et al., 2006). Between ~8–5 ka, eastern Pacific Ocean SSTs were between 1–4 °C cooler than present as a result of upwelling (Carré et al., 2012), while maximum temperatures (~0.5–1 °C warmer) in the western Pacific occurred simultaneously between ~8–5.5 ka, increasing the zonal SST gradient across the Pacific Ocean by ~30 % (Koutavas et al., 2006; Reeves et al., 2013a, b). This enhanced the Pacific Walker circulation and lead to a mean La Niña state, therefore strengthening the Australian-Indonesian monsoon as well as increasing rainfall over eastern Australia including the Warrego catchment (Shulmeister, 1999; Chen et al., 2016). An enhanced East Asian monsoon and associated deep convection over the western Pacific has been suggested as another mechanism acting to strengthen the Walker circulation during the mid Holocene (Liu et al., 2000). While many proxy records support this interpretation, modelling efforts thus far have been unsuccessful in

replicating this (Braconnot et al., 2012). As such, more work is required to fully understand the evolution of the ENSO throughout the Holocene and potential impacts on Australia's hydroclimate. There is also the possibility of Northern Hemisphere high-latitude forcing on the latitudinal extent of the ITCZ and the Australian monsoon. Cooling in the Northern Hemisphere has been correlated with southward excursions of the ITCZ (Bayon et al., 2017; Collins et al., 2017; Liu et al., 2017). The 8.2 ka event was a period of pronounced cooling in the northern high latitudes and may have been associated with the shift of the ITCZ and monsoonal rainfall further south over the Australian continent in the early Holocene (Muller et al., 2008). However, the period of enhanced fluvial activity in the Warrego catchment (~8–4.5 ka) is longer than the relatively short-lived climatic impacts thought to be associated with the 8.2 ka event (Muller et al., 2008). Nonetheless, proxy evidence from the Pacific Ocean indicates a La Niña mean state of the Pacific Ocean during the early-mid Holocene, and given the control ENSO has on rainfall and runoff in the Warrego catchment, we suggest that climatic changes related to ENSO are most responsible for the enhanced fluvial activity in the Warrego catchment during the early-mid Holocene, and the subsequent decline in fluvial activity and change in river character and behaviour after ~4.5 ka.

Gradual southward retreat and contraction of the ITCZ driven by precession of the Earth's orbit increased instability and the likelihood of westerly wind anomalies required to initiate El Niño events by around 5–4.5 ka, which correlates well with the timing of the reduction in activity and ultimate failure of the Burrenbilla and Coongoola palaeochannels (Koutavas et al., 2006). At this transition to a late Holocene climate regime around 5–4.5 ka, ENSO began to resemble the modern-day ENSO with more frequent and stronger El Niño events (Shulmeister and Lees, 1995; Koutavas et al., 2006; Asmussen and McInnes, 2013). The late Holocene/modern ENSO is much more variable than during the early-mid Holocene and essentially led to an increase in aridity across eastern Australia and the Warrego catchment. Interestingly, the Holocene climate changes that were responsible for enhanced discharge and higher-energy fluvial activity in the Warrego catchment were relatively modest and regional in scale, especially compared to other periods of climate change in the late Quaternary, suggesting that the Warrego River is highly geomorphologically sensitive to climate-driven hydrological changes in its catchment.

The Warrego in the context of wider response of Australian rivers to Holocene hydroclimatic change

High-resolution proxies are relatively scarce in the vast dryland regions of Australia, as such, geoproxies such as palaeochannels and palaeo-lake shorelines have provided the most promising evidence of past climate changes (Nanson et al., 2008; Page et al., 2009; Pietsch et al., 2013; Hesse et al., 2018a, b; Mueller et al., 2018). The past ~50 ka has seen dramatic hydroclimatic changes influence Australian dryland fluvial and lacustrine systems (Nanson et al., 1992, 1995; Cohen et al., 2015; Hesse et al., 2018a, b), and there has been a particular focus on fluvial activity during the enigmatic last glacial maximum (LGM), and the apparent contradiction of (geo)proxy records which simultaneously suggest enhanced

discharge in rivers but also regionally drier conditions (Kemp and Spooner, 2007; Page et al., 2009; Hesse et al., 2018b; Mueller et al., 2018). Less focus has been placed on Holocene fluvial responses, likely because Holocene climate changes were relatively modest compared to changes at other times in the late Quaternary. However, there is scattered, but robust, evidence of enhanced fluvial activity in eastern and central Australia during the mid-Holocene followed by a subsequent decline in fluvial activity in the late Holocene supporting the palaeoclimatic interpretation outlined earlier (Cohen and Nanson, 2007; Hesse et al., 2018a, b). The relative synchronicity of the fluvial records of dryland Australia suggest that the change in the behaviour of ENSO over the last ~8 ka has had widespread hydrological impacts. Changes in the mean state of ENSO explain mid to late Holocene fluvial records in central and eastern Australia without the need to invoke large southward fluctuations of the ITCZ or sustained northward penetration of the mid-latitude westerlies, neither of which are supported by palaeoclimatic proxy data (Shulmeister et al., 2004), with the possible exception of a short-lived southward shift of the ITCZ associated with the 8.2 ka event (Muller et al., 2008). The mid-Holocene fluvial decline of the Macquarie River, near the Warrego in the northern Murray-Darling Basin, is one of the better constrained Holocene palaeochannel records in Australia (Hesse et al., 2018a, b). In the mid Holocene, the Macquarie River was a single, through-going meandering channel transporting >18 times the discharge of the modern river (Mundadoo palaeochannel; Hesse et al., 2018a, b). Around 5.5 ka, hydrological declines in the catchment triggered the disintegration of the Macquarie River and the formation of the modern anastomosing and distributary system characterised by channel breakdown and extensive unchannelled floodplain wetlands (>2,000 km^2; Ralph and Hesse, 2010; Ralph et al., 2011, 2016; Hesse et al., 2018a). The modern Gwydir, Namoi, and Lachlan rivers are similarly characterised by channel breakdown and extensive wetlands, however the timing of their formation is less well-constrained (Kemp and Rhodes, 2010; Pietsch and Nanson, 2011).

In the drier Lake Eyre Basin of central Australia, there is also evidence to suggest increased fluvial activity during the early-mid Holocene. A large palaeochannel on the Cooper Creek floodplain with bankfull discharge of 7–11 times the modern channel was active from ~8–7 ka (Nanson et al., 2008). This palaeochannel did not re-work the extensive Cooper Creek floodplain and declined to its modern size between ~4.6–3 ka (Nanson et al., 2008). Given a lack of further evidence of early-mid Holocene fluvial activity elsewhere on the Cooper Creek floodplain, it is thought that the early-mid Holocene palaeochannel was formed by a series of erratic, catastrophic floods rather than a systematic change in flow regime (Nanson et al., 2008). Nevertheless, dating of the Finke River in the western Lake Eyre Basin also suggests increased fluvial activity during the period between ~9–5 ka, with active lateral channel migration and floodplain formation correlating with a hiatus in dune-building (Nanson et al., 1995). From ~5 ka, source-bordering dunes became more active and the Finke River became relatively inactive and infilled, while rates of vertical floodplain aggradation were significantly reduced (Nanson et al., 1995). There is also emerging evidence of a hiatus in dune-building and increased frequency of large

floods on the central Australian Hale River during the mid Holocene (Tooth et al., 2017). These results accord with evidence of increased early-mid Holocene fluvial activity in tropical Australian rivers such as the Gilbert River (Nanson et al., 1991, 2005), East Alligator River and Magela Creek (Nanson et al., 1993), and plunge pool records from various rivers near Darwin (Nott and Price, 1994; 1999; Nott et al., 1996).

Upland swamps and floodplains in the southeastern Australian tablelands also provide a record of fluvial activity during the Holocene, albeit not in a dryland setting (Cohen and Nanson, 2007; Woodward et al., 2014; 2017). Many valleys in these tablelands are currently characterised by fine-grained, vertically accreting floodplains, but investigation of 23 different systems reveals a prominent and widespread gap in the alluvial record between ~8.5–4 ka (Cohen and Nanson, 2007). This period is thought to represent a period of enhanced runoff and sediment transport with reduced sediment sequestration in these upland valleys. Similarly, Little Llangothlin Lagoon in the northern NSW tablelands persisted as a lake during the early-mid Holocene (~9-6 ka), before drying out from ~ 6 ka to 1 ka (Woodward et al., 2014; 2017). Further south and slightly later drier conditions from ~4.5 ka promoted the lateral stabilisation of channels and the vertical accretion of fine-grained floodplains (Cohen and Nanson, 2007). While these records are not from dryland rivers, many Australian dryland rivers have their headwaters in similar valleys on the western flanks of the Great Dividing Range, and increased runoff and sediment transport in these upland catchments would have influenced the dryland rivers on the lowland alluvial plains.

Conclusion

The modern Warrego River is a complex dryland river characterised by substantial downstream changes in channel behaviour brought about by persistent downstream declines in discharge and stream power. The dramatic change of the Warrego River from large, sinuous channels to narrow, straight channels in response to mid Holocene climate change demonstrates the high geomorphological sensitivity of the system to relatively modest climate-driven hydrological change. This is intriguing and raises questions about how future changes to hydrological regimes brought about by anthropogenic climate change will affect the Warrego and other dryland rivers. Many climate projections suggest an increase in terrestrial aridity and declining water availability in the world's drylands, which is bound to affect fluvial systems in as yet unquantified ways (Feng and Fu, 2013; Schewe et al., 2013; Cook et al., 2014; Fu and Feng, 2014; Rodell et al., 2018). Major change to the physical structure, planform and behaviour of dryland rivers would have fundamental knock-on effects for ecosystems, agriculture and communities which exist in already marginal environments. The geomorphological sensitivity of dryland rivers to climate change has not been assessed in a systematic way, and so improving our understanding of how dryland rivers may respond to future hydroclimatic change by quantifying extrinsic and intrinsic thresholds for dryland rivers is an urgent priority.

Acknowledgements

References

Aitken MJ, 1998. An introduction to optical dating: the dating of Quaternary sediments by the use of photon-stimulated luminescence: Oxford University Press, Oxford.

Asmussen B, and McInnes P, 2013. Assessing the impact of mid-to-late Holocene ENSO-driven climate change on toxic Macrozamia seed use: A 5000 year record from eastern Australia. Journal of Archaeological Science 40, 471–480.

Bayon G, De Deckker P, Magee JW, Germain Y, Bermell S, Tachikawa K, and Norman MD, 2017. Extensive wet episodes in Late Glacial Australia resulting from high-latitude forcings. Scientific Reports 7, 1–7.

Bøtter-Jensen L, Andersen CE, Duller GAT, and Murray AS, 2003. Developments in radiation, stimulation and observation facilities in luminescence measurements. Radiation Measurements 37: 535-541.

Bowler JM, 1967. Quaternary chronology of Goulburn valley sediments and their correlation in southeastern Australia. Journal of the Geological Society of Australia 14, 287–292.

Bowler JM, 1978. Quaternary climate and tectonics in the evolution of the Riverine Plain, southeastern Australia In: Davies JL, Williams MAJ (Eds.), Landform Evolution in Australasia. ANU Press, Canberra, Australia, pp. 70–112.

Braconnot P, Luan Y, Brewer S, and Zheng W, 2012. Impact of Earth's orbit and freshwater fluxes on Holocene climate mean seasonal cycle and ENSO characteristics. Climate Dynamics 38, 1081–1092.

Bureau of Meteorology (BoM), 2018. Long range weather and climate. Available online at: http://www.bom.gov.au/climate/

Carré, M., Sachs, J.P., Purca, S., Schauer, A.J., Braconnot, P., Falcón, R.A., Julien, M. and Lavallée, D., 2014. Holocene history of ENSO variance and asymmetry in the eastern tropical Pacific. Science, 345(6200), 1045-1048.

Carré M, Azzoug M, Bentaleb I, Chase BM, Fontugne M, Jackson D, Ledru MP, Maldonado A, Sachs JP, and Schauer AJ, 2012. Mid-Holocene mean climate in the south eastern Pacific and its influence on South America. Quaternary International 253, 55–66.

Chen S, Hoffmann SS, Lund DC, Cobb KM, Emile-Geay J, and Adkins JF, 2016. A high-resolution speleothem record of western equatorial Pacific rainfall: Implications for Holocene ENSO evolution. Earth and Planetary Science Letters 442, 61–71.

Cohen TJ, Jansen JD, Gliganic LA, Larsen JR, Nanson GC, May JH, Jones BG, and Price DM, 2015. Hydrological transformation coincided with megafaunal extinction in central Australia. Geology, 43(3), 195–198.

Cohen TJ, Nanson GC, Jansen JD, Jones BG, Jacobs Z, Larsen JR, May JH, Treble P, Price DM, Smith AM, 2012. Late Quaternary mega-lakes fed by the northern and southern river systems of central Australia: Varying moisture sources and increased continental aridity. Palaeogeography, Palaeoclimatology, Palaeoecology, 356–357, 89–108.

Cohen TJ, and Nanson GC, 2007. Mind the gap: an absence of valley-fill deposits identifying the Holocene hypsithermal period of enhanced flow regime in southeastern Australia. The Holocene 17, 411–418.

Collins JA, Prange M, Caley T, Gimeno L, Beckmann B, Mulitza S, Skonieczny C, Roche D, and Schefuß E, 2017. Rapid termination of the African Humid Period triggered by northern high-latitude cooling. Nature Communications 8(1372), 1-11.

Conroy JL, Overpeck JT, Cole JE, Shanahan TM, and Steinitz-Kannan M, 2008. Holocene changes in eastern tropical Pacific climate inferred from a Galápagos lake sediment record. Quaternary Science Reviews 27, 1166–1180.

Cook BI, Smerdon JE, Seager R, and Coats S, 2014. Global warming and 21st century drying. Climate Dynamics, 43(9-10), 2607-2627.

Department of Natural Resources, Mines and Energy (DNRME), 2018. Water Monitoring Information Portal. Date last accessed: 15/01/2019, URL: water-monitoring.information.qld.gov.au/

Duller GAT, 2003. Distinguishing quartz and feldspar in single grain luminescence measurements. Radiation Measurements 37: 161-165.

Duller GAT, 2004. Luminescence dating of Quaternary sediments: recent advances. Journal of Quaternary Science 19: 183-192.

Duller GAT, 2015. The Analyst software package for luminescence data: overview and recent improvements. Ancient TL 33: 35-42.

Feng S, and Fu Q, 2013. Expansion of global drylands under a warming climate. Atmospheric Chemistry and Physics, 13(19), 10081–10094.

Fu Q and Feng S, 2014. Responses of terrestrial aridity to global warming. Journal of Geophysical Research: Atmospheres, 119(13), 1–13.

Gardiner V, and Dackombe RV, 1983. Geomorphological field manual. Allen and Unwin, London.

Geoscience Australia, 2011. SRTM-derived 1 Second Digital Elevation Models Version 1.0. Date last accessed: 15/01/2019, URL:
https://ecat.ga.gov.au/geonetwork/srv/eng/catalog.search?node=srv#/metadata/72759

Giosan L, Clift PD, Macklin MG, Fuller DQ, Constantinescu S, Durcan JA, Stevens T, Duller GAT, Tabrez AR, Gangal K, Adhikari R, Alizai A, Filip F, VanLaningham S, and Syvitski JPM, 2012. Fluvial landscapes of the Harappan civilization. Proceedings of the National Academy of Sciences 109, 1688–1694.

Grootemaat GD, 2008. The relationship of flooding in Australian dryland rivers to synoptic weather patterns, El Niño southern oscillation, sea surface temperatures and rainfall distribution, unpubl. PhD thesis, University of Wollongong.

Hesse PP, Williams R, Ralph TJ, Fryirs KA, Larkin ZT, Westaway KE, and Farebrother W, 2018a. Palaeohydrology of lowland rivers in the Murray-Darling Basin, Australia. Quaternary Science Reviews, 200, 85–105.

Hesse PP, Williams R, Ralph TJ, Larkin ZT, Fryirs KA, Westaway KE, and Yonge D, 2018b. Dramatic reduction in size of the lowland Macquarie River in response to Late Quaternary climate-driven hydrologic change. Quaternary Research, 90(2), 360–379.

Huang HQ, and Nanson GC, 2000. Hydraulic geometry and maximum flow efficiency as products of the principle of least action. Earth Surface Processes and Landforms, 25, 1–16.

Huang HQ, and Nanson GC, 2007. Why some alluvial rivers develop an anabranching pattern. Water Resources Research, 43(7), 1–12.

Huang HQ, and Nanson GC, 2008. Least action principle, equilibrium states, iterative adjustment and the stability of alluvial channels. Earth Surface Processes and Landforms, 33, 923–942.

Jacobs Z, Duller GAT, and Wintle AG, 2006. Interpretation of single grain De distributions and calculation of De. Radiation Measurements 41: 264-277.

Jaeger KL, Sutfin NA, Tooth S, Michaelides K, and Singer M, 2017. Geomorphology and sediment regimes of intermittent rivers and ephemeral streams. In Intermittent Rivers and Ephemeral Streams pp. 21-49.

Jansen JD, and Nanson GC, 2004. Anabranching and maximum flow efficiency in Magela Creek, northern Australia. Water Resources Research, 40(4), 1–12.

Kemp J, and Rhodes EJ, 2010. Episodic fluvial activity of inland rivers in southeastern Australia: Palaeochannel systems and terraces of the Lachlan River. Quaternary Science Reviews 29, 732–752.

Kemp J, and Spooner NA, 2007. Evidence for regionally wet conditions before the LGM in southeast Australia: OSL ages from a large palaeochannel in the Lachlan Valley. Journal of Quaternary Science 22, 423–427.

Knighton AD, and Nanson GC, 1994a. Flow transmission along an arid zone anastomosing river, Cooper Creek, Australia. Hydrological Processes 8, 137–154.

Knighton AD, Nanson GC, 1994b. Waterholes and their significance in the anastomosing channel system of Cooker Creek, Australia. Geomorphology 9, 311–324.

Koutavas A, deMenocal PB, Olive GC, and Lynch-Stieglitz J, 2006. Mid-Holocene El Niño-Southern Oscillation (ENSO) attenuation revealed by individual foraminifera in eastern tropical Pacific sediments. Geology 34, 993–996.

Lane EW, 1955. The importance of fluvial morphology in hydraulic engineering. Proceedings of the American Society of Civil Engineers 81, 1–17.

Larkin ZT, Ralph TJ, Tooth S, Fryirs KA, and Carthey AJR, in review. Threshold responses to future hydroclimatic change. Nature Geoscience.

Larkin ZT, Ralph TJ, Tooth S, and McCarthy TS, 2017a. The interplay between extrinsic and intrinsic controls in determining floodplain wetland characteristics in the South African drylands. Earth Surface Processes and Landforms 42, 1092–1109.

Larkin ZT, Tooth S, Ralph TJ, Duller GAT, McCarthy T, Keen-Zebert A, and Humphries MS, 2017b. Timescales, mechanisms, and controls of incisional avulsions in floodplain wetlands: Insights from the Tshwane River, semiarid South Africa. Geomorphology, 283, 158–172.

Leonard ND, Welsh KJ, Lough JM, Feng Y, Pandolfi JM, Clark TR, and Zhao J, 2016. Evidence of reduced mid-Holocene ENSO variance on the Great Barrier Reef, Australia. Paleoceanography 31, 1248–1260.

Liu Z, Kutzbach J, and Wu L, 2000. Modelling climate shift of El Nino variability in the Holocene. Geophysical Research Letters 27, 2265–2268.

Liu X, Rendle-Bühring R, Kuhlmann H, and Li A, 2017. Two phases of the Holocene East African Humid Period: Inferred from a high-resolution geochemical record off Tanzania. Earth and Planetary Science Letters 460, 123–134.

Macklin MG, Lewin J, 2015. The rivers of civilization. Quaternary Science Reviews 114, 228–244.

McGowan H, Marx S, Moss P, and Hammond A, 2012. Evidence of ENSO mega-drought triggered collapse of prehistory Aboriginal society in northwest Australia. Geophysical Research Letters 39.

McMahon TA, Finlayson BL, Haines A, and Srikanthan R, 1987. Runoff variability: a global perspective. IASH-AISH, 168, pp.3-11.

McMahon TA, Peel MC, Vogel RM, and Pegram GGS, 2007. Global streamflows - Part 3: Country and climate zone characteristics. Journal of Hydrology 347, 272–291.

Millennium Ecosystem Assessment (MEA). 2005. Ecosystems and Human Well-being: Wetlands and Water. World Resources Institute: Washington, DC.

Mueller D, Jacobs Z, Cohen TJ, Price DM, Reinfelds IV, and Shulmeister J, 2018. Revisiting an arid LGM using fluvial archives: a luminescence chronology for palaeochannels of the Murrumbidgee River, south-eastern Australia. Journal of Quaternary Science, 33(7), pp.777-793.

Mueller N, Lewis A, Roberts D, Ring S, Melrose R, Sixsmith J, Lymburner L, McIntyre A, Tan P, Curnow S, and Ip A, 2016. Water observations from space: Mapping surface water from 25years of Landsat imagery across Australia. Remote Sensing of Environment, 174, 341–352.

Muller J, Kylander M, Wüst RAJ, Weiss D, Martinez-Cortizas A, LeGrande AN, Jennerjahn T, Behling H, Anderson WT, and Jacobson G, 2008. Possible evidence for wet Heinrich phases in tropical NE Australia: the Lynch's Crater deposit. Quaternary Science Reviews 27, 468–475.

Munyikwa K, Telfer MW, Baker I, and Knight C, 2011. Core drilling of Quaternary sediments for luminescence dating using the Dormer Drillmite. Ancient TL, 29(1), 15-23.

Nanson GC, Chen XY, and Price DM, 1995. Aeolian and fluvial evidence of changing climate and wind patterns during the past 100 ka in the western Simpson Desert, Australia. Palaeogeography, Palaeoclimatology, Palaeoecology, 113(1), 87–102.

Nanson GC, East TJ, and Roberts RG, 1993. Quaternary stratigraphy, geochronology and evolution of the Magela Creek catchment in the monsoon tropics of northern Australia. Sedimentary Geology 83, 277–302.

Nanson GC, Jones BG, Price DM, and Pietsch TJ, 2005. Rivers turned to rock: Late Quaternary alluvial induration influencing the behaviour and morphology of an anabranching river in the Australian monsoon tropics. Geomorphology 70, 398–420.

Nanson GC, Price DM, Jones BG, Maroulis JC, Coleman M, Bowman H, Cohen TJ, Pietsch TJ, Larsen, J. R, 2008. Alluvial evidence for major climate and flow regime changes during the middle and late Quaternary in eastern central Australia. Geomorphology, 101(1–2), 109–129.

Nanson GC, Price DM, Short SA, Young RW, and Jones BG, 1991. Comparative uranium-thorium and thermoluminescence dating of weathered Quaternary alluvium in the tropics of northern Australia. Quaternary Research, 35(3), 347-366.

Nanson CG, Price DM, and Short SA, 1992. Wetting and drying of Australia over the past 300,000 years. Geology, 20, 791–794.

Nott J, and Price D, 1994. Plunge pools and paleoprecipitation. Geology 22, 1047–1050.

Nott JF, Price DM, and Bryant EA, 1996. A 30,000 year record of extreme floods in tropical Australia from relict plunge-pool deposits : Implications for future climate change. Geophysical Research Letters 23, 379–382.

Nott J, and Price D, 1999. Waterfalls, floods and climate change: Evidence from tropical Australia. Earth and Planetary Science Letters 171, 267–276.

Page KJ, Kemp J, and Nanson GC, 2009. Late Quaternary evolution of Riverine Plain paleochannels, southeastern Australia. Australian Journal of Earth Sciences, 56, S19–S33.

Pausata FSR, Zhang Q, Muschitiello F, Lu Z, Chafik L, Niedermeyer EM, Stager JC, Cobb KM, Liu Z, 2017. Greening of the Sahara suppressed ENSO activity during the mid-Holocene. Nature Communications 8, 16020.

Pekel J-F, Cottam A, Gorelick N, and Belward AS, 2016. High-resolution mapping of global surface water and its long-term changes. Nature, 540(7633), 418–422.

Pietsch TJ, and Nanson GC, 2011. Bankfull hydraulic geometry; the role of in-channel vegetation and downstream declining discharges in the anabranching and distributary channels of the Gwydir distributive fluvial system, southeastern Australia. Geomorphology 129, 152–165.

Pietsch TJ, Nanson GC, and Olley JM, 2013. Late Quaternary changes in flow-regime on the Gwydir distributive fluvial system, southeastern Australia. Quaternary Science Reviews 69, 168–180.

Prescott JR, and Hutton JT, 1994. Cosmic ray contributions to dose rates for luminescence and ESR dating: large depths and long-term time variations. Radiation Measurements 23: 497–500.

Reeves JM, Bostock HC, Ayliffe LK, Barrows TT, De Deckker P, Devriendt LS, Dunbar GB, Drysdale RN, Fitzsimmons KE, Gagan MK, Griffiths ML, Haberle SG, Jansen JD, Krause C, Lewis S, McGregor H V., Mooney SD, Moss P, Nanson GC, Purcell A, and van der Kaars S, 2013a. Palaeoenvironmental change in tropical Australasia over the last 30,000 years - a synthesis by the OZ-INTIMATE group. Quaternary Science Reviews 74, 97–114.

Ralph TJ, Kobayashi T, García a., Hesse PP, Yonge D, Bleakley N, and Ingleton T, 2011. Paleoecological responses to avulsion and floodplain evolution in a semiarid Australian freshwater wetland. Australian Journal of Earth Sciences 58, 75–91.

Ralph TJ, and Hesse PP, 2010. Downstream hydrogeomorphic changes along the Macquarie River, southeastern Australia, leading to channel breakdown and floodplain wetlands. Geomorphology, 118(1–2), 48–64.

Ralph TJ, Hesse PP, and Kobayashi T, 2016. Wandering wetlands: spatial patterns of historical channel and floodplain change in the Ramsar-listed Macquarie Marshes, Australia. Marine and Freshwater Research, 67(6), 782-802.

Reeves JM, Barrows TT, Cohen TJ, Kiem AS, Bostock HC, Fitzsimmons KE, Jansen JD, Kemp J, Krause C, Petherick L, Phipps SJ, and OZ-INTIMATE Members, 2013b. Climate variability over the last 35,000 years recorded in marine and terrestrial archives in the Australian region: An OZ-INTIMATE compilation. Quaternary Science Reviews 74, 21–34.

Rein B, Lückge A, Reinhardt L, Sirocko F, Wolf A, and Dullo WC, 2005. El Niño variability off Peru during the last 20,000 years. Paleoceanography 20, 1–18.

Rodell M, Famiglietti JS, Wiese DN, Reager JT, Beaudoing HK, Landerer FW, and Lo M-H, 2018. Emerging trends in global freshwater availability. Nature, 557, pp. 651-659.

Rodnight H, Duller GAT, Tooth S, Wintle AG, 2005. Optical dating of a scroll-bar se- quence on the Klip River, South Africa, to derive the lateral migration rate of a mean- der bend. The Holocene 15, 802–811.

Rodnight H, Duller GAT, Wintle AG, Tooth S, 2006. Assessing the reproducibility and accuracy of optical dating of fluvial deposits. Quaternary Geochronology 1:109–120.

Schewe J, Heinke J, Gerten D, Haddeland I, Arnell NW, Clark DB, Dankers R, Eisner S, Fekete BM, Colón-González FJ and Gosling SN, 2014. Multimodel assessment of water scarcity under climate change. Proceedings of the National Academy of Sciences, 111(9), pp.3245-3250.

Shin SI, Sardeshmukh PD, Webb RS, Oglesby RJ, and Barsugli JJ, 2006. Understanding the mid-Holocene climate. Journal of Climate 19, 2801–2817.

Shulmeister J, and Lees BG, 1995. Pollen evidence from tropical Australia for the onset of an ENSO-dominated climate at c. 4000 BP. The Holocene 5(1), 10-18.

Shulmeister J, 1999. Australasian evidence for mid-Holocene climate change implies precessional control of Walker Circulation in the Pacific. Quaternary International 57–58, 81–91.

Shulmeister J, Goodwin I, Renwick J, Harle K, Armand L, McGlone MS, Cook E, Dodson J, Hesse PP, Mayewski P, and Curran M, 2004. The Southern Hemisphere westerlies in the Australasian sector over the last glacial cycle: A synthesis. Quaternary International 118–119, 23–53.

Tian Z, Li T, Jiang D, and Chen L, 2017. Causes of ENSO weakening during the mid-Holocene. Journal of Climate 30, 7049–7070.

Tian Z, Li T, and Jiang D, 2018. Strengthening and westward shift of the tropical Pacific walker circulation during the mid-Holocene: PMIP simulation results. Journal of Climate 31, 2283–2298.

Tooth S, Nanson GC, 1999. Anabranching rivers on the Northern Plains of arid central Australia. Geomorphology 29, 211–233.

Tooth S. 2013. Dryland Fluvial Environments: Assessing Distinctiveness and Diversity from a Global Perspective. Treatise on Geomorphology (Vol. 9).

Tooth S, Craddock RA, Durcan J, Maxwell T, and Wilson Purdy S, 2017. Late Quaternary aeolian-fluvial interactions in arid central Australia: implications for models of dryland river floodplain and linear dune development, Annual Conference Programme and Abstract, British Society for Geomorphology Annual Meeting, University of Hull, 4-6 September 2017, p.55.

Tooth S, and McCarthy TS, 2007. Wetlands in drylands: geomorphological and sedimentological characteristics, with emphasis on examples from southern Africa. Progress in Physical Geography, 31(1), 3–41.

Tooth S, and Nanson GC, 2011. Distinctiveness and diversity of arid zone river systems. In: Arid Zone Geomorphology: Process, Form and Change in Drylands, pp.269-300.

United Nations Environment Programme (UNEP), 1992. World Atlas of Desertification. Edward Arnold: London; 15–45.

Van der Esch S, ten Brink B, Stehfest E, Bakkenes M, Sewell A, Bouwman A, Meijer J, Westhoek H and van den Berg, M., 2017. Exploring future changes in land use and land condition and the impacts on food, water, climate change and biodiversity: Scenarios for the Global Land Outlook. PBL Netherlands Environmental Assessment Agency, The Hague.

Verdon DC, Wyatt AM, Kiem AS, and Franks SW, 2004. Multidecadal variability of rainfall and streamflow: Eastern Australia. Water Resources Research 40, 1–8.

Water NSW, 2018. Real Time Data – Rivers and Streams. Date last accessed: 15/01/2019. URL: realtimedata.waternsw.com.au/water.stm

Wilson, B. A. 1999. Mulga Lands. In: P.S. Sattler and R. D. Williams, editors. The conservation status of Queensland's Bioregional Ecosystems. Environmental Protection Agency, Brisbane.

Wintle AG, and Murray AS, 2006. A review of quartz optically stimulated luminescence characteristics and their relevance in single-aliquot regeneration dating protocols. Radiation Measurements 41: 369-391.

Woodward C, Shulmeister J, Bell D, Haworth R, Jacobsen G, Zawadzki A, 2014. A Holocene record of climate and hydrological changes from Little Llangothlin Lagoon, south eastern Australia. Holocene 24, 1665–1674.

Woodward C, Shulmeister J, Zawadzki A, Child D, Barry L, Hotchkis M, 2017. Holocene ecosystem change in Little Llangothlin Lagoon, Australia: implications for the management of a Ramsar-listed wetland. Hydrobiologia 785, 337–358.

Woodward J, Macklin M, Fielding L, Millar I, Spencer N, Welsby D, and Williams M, 2015. Shifting sediment sources in the world's longest river: A strontium isotope record for the Holocene Nile. Quaternary Science Reviews 130, 124–140.

Yang X, Scuderi LA, Wang X, Scuderi LJ, Zhang D, Li H, Forman S, Xu Q, Wang R, Huang W, and Yang S, 2015. Groundwater sapping as the cause of irreversible desertification of Hunshandake Sandy Lands, Inner Mongolia, northern China. Proceedings of the National Academy of Sciences 112, 702–706.

Supplementary Material
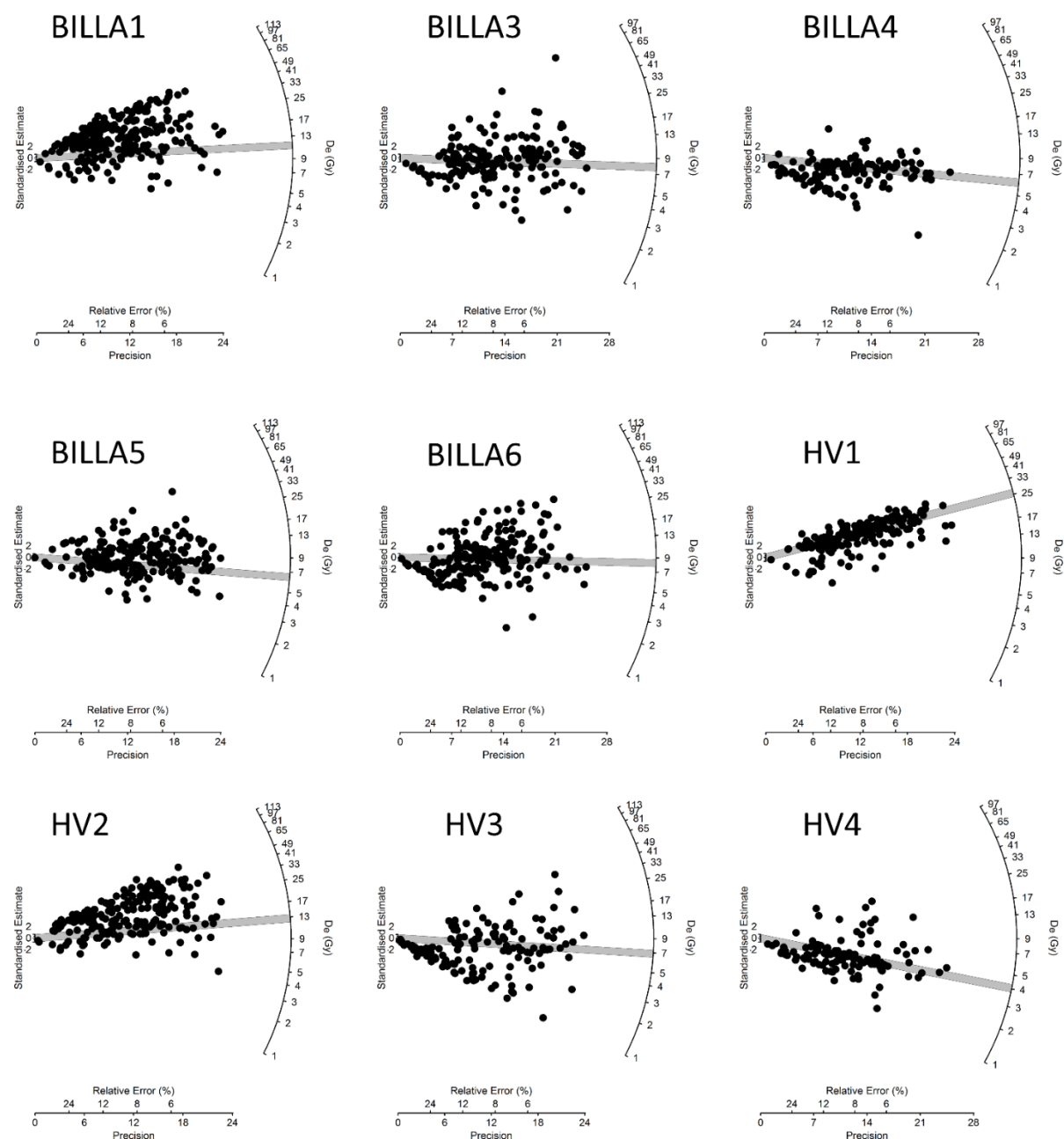
Supplementary Figure 1. Radial plots of equivalent dose (D_e) values from individual grains of quartz for the Warrego River OSL samples. The grey shaded bar represents the D_e used for age calculation based on the finite mixture model (FMM), which is able to account for and exclude the anomalous young population of grains evident in many samples.

Supplementary Table 1. OSL dosimetry data for the Warrego River samples.

Sample	Depth (m)	Water content (%)	Grain size (μm)	Beta dose (Gy ka^{-1})	Gamma dose (Gy ka^{-1})	Cosmic dose (Gy ka^{-1})	Total dose rate (Gy ka^{-1})
BILLA1	1.00 ± 0.1	5 ± 5	180 − 250	0.83 ± 0.06	0.56 ± 0.05	0.17 ± 0.01	1.56 ± 0.07
BILLA3	1.00 ± 0.1	5 ± 5	180 − 212	0.48 ± 0.03	0.33 ± 0.03	0.17 ± 0.01	0.99 ± 0.04
BILLA4	1.00 ± 0.1	5 ± 5	180 − 212	0.52 ± 0.04	0.39 ± 0.03	0.17 ± 0.01	1.08 ± 0.05
BILLA5	1.00 ± 0.1	5 ± 5	180 − 212	0.53 ± 0.04	0.37 ± 0.03	0.17 ± 0.01	1.07 ± 0.05
BILLA6	1.00 ± 0.1	5 ± 5	180 − 212	0.63 ± 0.04	0.46 ± 0.04	0.17 ± 0.01	1.26 ± 0.06
HV1	3.00 ± 0.1	5 ± 5	180 − 250	0.21 ± 0.02	0.17 ± 0.02	0.14 ± 0.01	0.51 ± 0.02
HV2	1.10 ± 0.1	5 ± 5	180 − 250	0.90 ± 0.06	0.65 ± 0.05	0.17 ± 0.01	1.72 ± 0.08
HV3	1.00 ± 0.1	5 ± 5	180 − 212	0.43 ± 0.03	0.28 ± 0.02	0.17 ± 0.01	0.89 ± 0.04
HV4	1.00 ± 0.1	5 ± 5	180 − 212	0.39 ± 0.03	0.31 ± 0.03	0.17 ± 0.01	0.87 ± 0.04

CHAPTER 3

River response to Holocene hydroclimatic change in the Okavango Panhandle, Botswana

Larkin Z.T.[1], Ralph T.J.[1], Tooth S.[2,3], Duller G.A.T.[2], Fryirs K.A.[1] *

[1] Department of Environmental Sciences, Macquarie University, NSW Australia

[2] Department of Geography and Earth Sciences, Aberystwyth University, Aberystwyth, UK

[3] School of Geosciences, University of the Witwatersrand, Johannesburg, South Africa

*See Table 1.1 in chapter 1 for author contributions.

Abstract

Fluvial systems adjust in response to internal processes and to external forcing. Understanding the interplay between these forcing factors in driving fluvial adjustment is critical for assessing past, present and future changes and for developing associated river management strategies. The Okavango Delta is one of the world's largest and most pristine wetland wilderness areas and preserves a long but poorly resolved record of substantive fluvial adjustment in a critical region of central southern Africa. Here, we use aerial image interpretations, field surveys, and optically stimulated luminescence (OSL) dating to quantify the dramatic, mid Holocene transition of the Okavango River in the Panhandle region of the Delta from a single-channel, meandering river to its present form as a multi-channel, anastomosing river. OSL ages demonstrate that the largest palaeochannels in the Panhandle were active until ~4–3.5 ka when channel width and discharge were ~5 times that of the modern river and the primary mechanism of fluvial adjustment was lateral migration (rates >6 m a^{-1}). In contrast, the smaller, modern Okavango River has limited capacity for lateral migration (rates below detection over the last 40 years), and instead is characterised by periodic lateral instability due to avulsion which rapidly creates secondary channels that may co-exist for many decades. We propose that the mid Holocene palaeochannels were fed by enhanced seasonal flows associated with intensified Atlantic-sourced monsoonal rainfall over the Okavango's headwater catchments, and that the subsequent transition to relatively quiescent flows has driven the dramatic width contraction of the modern channel, and the associated change to hyperavulsive river behaviour. Demonstration of the natural range of variability of channels in the Okavango Panhandle, and explanations of this variability in the context of river response to Holocene hydroclimate change, provide insights to improve projections of future changes and enhance management planning.

Introduction

Dryland rivers and floodplain wetlands are distinctive environments, yet highly variable in terms of their geomorphology, hydrology, and ecology (Tooth and McCarthy, 2007; Tooth, 2013; Jaeger et al., 2017). The geomorphology of dryland rivers and wetlands is controlled by a range of factors including climate and hydrology, valley gradient, and sediment calibre (Tooth and Nanson, 2004; Kleinhans, 2010; Klienhans and van den Berg, 2011), and the interplay between these factors results in a remarkable variability of fluvial forms and processes. Many such rivers and wetlands undergo profound changes over various spatial and temporal scales; for example, by adjusting from single to multiple channels, or by experiencing shifts from regular to more irregular discharge and inundation regimes. The factors driving these changes are varied but include extrinsic forces such as hydrological regime shifts resulting from climatic change (Hesse et al., 2018a, b; Woodward et al., 2015a, b) base-level change associated with neotectonic activity (Bowler, 1967) or habitat degradation associated with human impacts (Kingsford, 2000), as well as intrinsic forces related to processes such as sedimentation, erosion, and river avulsion (Tooth et al., 2007; Ralph et al., 2011; Larkin et al., 2017).

The spatial and temporal variability of river and wetland changes creates difficulties for managers, conservationists, and the communities that rely on the systems for their water and livelihoods. Key questions that are commonly asked (Tooth et al., 2009) include: 1) what should these rivers/wetlands look like?; 2) how long have these rivers/wetlands persisted in their present form?; 3) how do these rivers/wetlands adjust to environmental change?; 4) what is the expected future trajectory of change for these rivers/wetlands? In these complex systems, establishing the natural, or historical, range of variability – defined as the natural adjustments that occur in the absence of extrinsic forcing, typically measured over historical timeframes with climatic conditions relatively similar to the late 20th Century climate (Wohl, 2011; Wohl and Rathburn, 2013) – as well as understanding the way systems have responded to extrinsic forcing can help to answer such questions and therefore be critical for implementing successful management strategies. Knowledge of past fluvial adjustments can help contextualise contemporary dynamics and allow more accurate projections of future trajectories of change resulting from climatic and/or land use changes. Providing such insights has become a critical issue given the projections of future decreases in water availability globally (Pekel et al., 2016; Rodell et al., 2018), especially given the fundamental importance of surface water in dryland regions for riparian ecosystem functioning and human activities.

In recent decades, dating techniques such as radiocarbon (^{14}C) and optically stimulated luminescence (OSL) have revolutionised palaeoenvironmental reconstructions and helped to develop robust chronologies of dryland landscape change over long timescales (Tooth, 2012). In many drylands, historical accounts by European explorers, missionaries and early colonists (mid 19th century onwards) and aerial photography (mid 20th century onwards) can provide a complementary time series that can also provide important insight into historical fluvial dynamics with practical implications for

management (Tooth et al., 2007; Ralph et al., 2016; Larkin et al., 2017; Fryirs et al., 2018). In this paper, we use single-grain (SG) OSL dating of palaeochannels and modern bank deposits in conjunction with an examination of historical channel change of the Okavango River and its anabranches in the Panhandle region of the Okavango Delta, northern Botswana (Fig. 1, inset), to quantify and interpret the nature of channel change in this iconic dryland wetland from the mid Holocene to the present. This is an important management challenge because the perennial, but highly seasonal, inflow of water to the Okavango Delta is vital for local communities, and the Botswanan economy more widely, owing to the significant tourism industry that is based upon the Delta (Mbaiwa, 2003; Mendelsohn et al., 2010). For instance, given the close relationship between channel locations, the extent of permanent swamps, and the siting of local communities and tourism lodge operations, an understanding of the likely timing, processes, and spatial extent of future channel changes is important. At present, there are concerns over changes to the inflow of water and channel activity resulting from climate change (Andersson et al., 2006), and also as a result of upstream agricultural developments, water extraction, and proposed dam building (Ramberg, 1997; Andersson et al., 2006; King et al., 2014). Against this backdrop, the aims of this paper are to: i) determine the timing and nature of palaeochannel activity in the Panhandle region of the Delta; ii) contrast this activity with historical (last 60–70 years) and contemporary channel activity; iii) interpret the various channel adjustments over the late Holocene in terms of extrinsic and intrinsic forcing; iv) discuss the key drivers of fluvial change in the Okavango and Africa more widely over these timescales; and v) assess possible future changes and the implications for conservation and management policies and practices.

Study Area

The Okavango Delta is a large (c. 40,000 km^2) fan-shaped distributive fluvial system (*sensu* Weismann et al., 2010) hosting >12,000 km^2 of wetlands in the northern Kalahari Desert (Fig. 1A). The Delta is flooded annually by monsoonal rainfall that falls during the austral summer months (November through March), most prominently over the headwaters in the Angolan highlands (McCarthy 2013). The seasonal monsoonal rainfall is largely modulated by the Congo Air Boundary which is a convergence of air masses over central and southern Africa which separates the southeasterly trade winds that bring moisture from the Indian Ocean from the West African monsoonal system that brings moisture from the Atlantic Ocean. The Delta is one of the world's most pristine large, dryland wetlands in the world and, in 2014 was inscribed as the 1000th World Heritage site. The Delta has formed in a half-graben and is a tectonically active area (Hutchins et al., 1976). The Delta is comprised of two main regions: the Panhandle and the Fan (Fig. 1A). The Panhandle is a relatively confined valley up to ~12 km wide with extensive permanent swamps, bounded by perpendicular northwest-southeast trending faults. This faulting, and subsidence of the Panhandle, creates accommodation space for channels to distribute and deposit sediment within the Panhandle (Hutchins et al., 1976). Downstream, the river crosses the

Gumare fault and emerges onto the unconfined Fan, which is bounded at its southeasterly end by northeasterly trending faults. On the Fan, the Okavango divides into numerous distributary channels that feed a complex mosaic of permanent, seasonal and ephemeral wetlands. In the Panhandle, inundation is relatively regular and uniform, with water levels rising and falling with the passage of the annual flood, while across the Fan, inundation is more spatially and temporally variable, depending on the size of the annual flood and channel dynamics (Thito et al., 2016).

Palaeochannels of the Okavango River are widespread and well preserved, particularly on the northeastern margins of the Panhandle (Fig. 1B) and across the Fan, where they range in width from ~120–160 m. Through the Panhandle, the modern Okavango River is highly sinuous, with regular and irregular meanders, scroll bars, point bars, and cutoffs. In the middle of the Panhandle, an anastomosing reach has developed where the Filipo channel bifurcates from the Okavango before reconverging ~26 km downstream (Fig. 1B). The Filipo channel alternates downstream between sections with small and highly tortuous irregular meanders, and sections with straighter, wider channels, generally contrasting with the larger and more regular meanders of the Okavango River in this reach (Fig. 1B). Dense vegetation (typically *Cyperus papyrus* and *Phragmites* spp.) rooted in peat and occasionally sandy sediment forms the greater part of the channel margins, allowing lateral water diffusion into the adjacent wetlands (Ellery et al., 2003). Locally, the channels are encroached upon by hippo grass (*Vossia cuspidata*); for example, along some reaches of the Okavango downstream of the Filipo channel bifurcation. The channels in the Panhandle are bedload-dominated and transport fine-medium sand (median grain size ~300 µm), with some minor finer grained clastic sediment (i.e. clay, silt) and organic matter being deposited in standing water environments (e.g. backswamps and abandoned channels) and/or being filtered out of suspension by leakage through the vegetated, peat-rich channel margins (McCarthy, 2013).
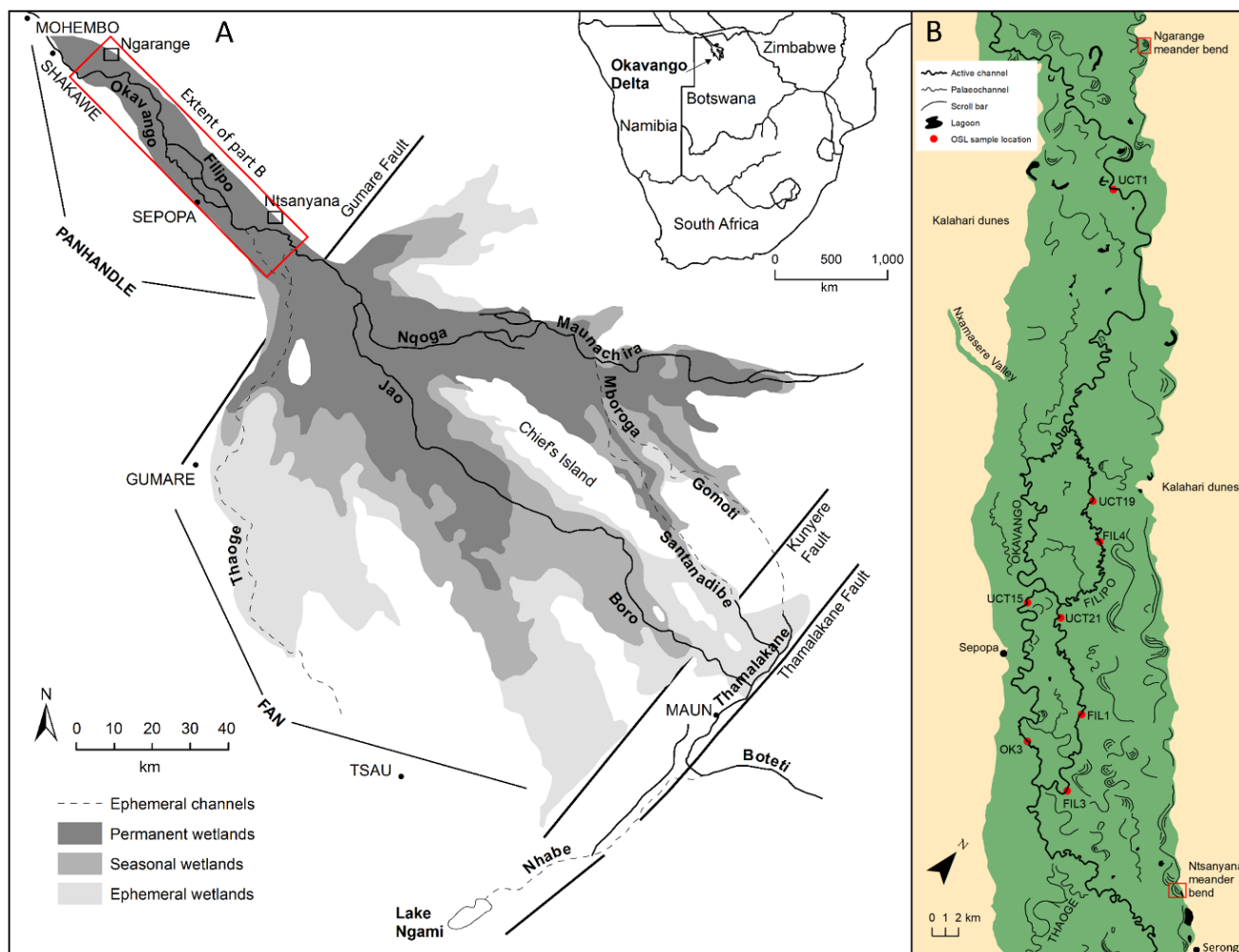
Figure 1. (A) The Okavango Delta in Botswana, showing the extent of the Panhandle and Fan, and major faults, channels, and areas of permanent, seasonal and ephemeral wetlands. The extent of permanent, seasonal, and ephemeral wetlands is adapted from recent inundation mapping by Thito et al. (2016). (B) Map of the Panhandle showing the localities mentioned in the text, as well as active channels (black lines; flow from top to bottom) and numerous meander scars and palaeochannels (grey lines). OSL sample locations are shown (red dots and boxes). The palaeochannel sites (red boxes) have been named after nearby communities, i.e. 'Ngarange' (upstream site) and 'Ntsanyana' (downstream site).

Historical accounts of the Okavango Delta highlight the inherent channel and wetland variability. The first maps and written accounts describing the Delta were from explorers and missionaries such as David Livingstone, Charles Andersson, Thomas Baines, Siegfried Passarge, and Captain Almar Stigand (Andersson 1856; Livingstone, 1858; Baines 1864; Oswell 1900; Passarge, 1904; Stigand, 1923; VanderPost, 2005). In 1849, when Livingstone and his fellow explorers visited Lake Ngami at the southern end of the Okavango system (Fig. 1A), it was a large, deep (up to 6 m) expanse of water (Livingstone 1858; Stigand 1923). Lake Ngami was fed by the Thaoge distributary, which ceased to flow completely by the 1880s (Shaw 1985; Chapman, 1886). The failure of the Thaoge and subsequent desiccation of Lake Ngami in the second half of the 19th century was initially thought to be due to climatic changes reducing flow in the Okavango River but Stigand (1923, p.402) observed that the drying of Lake Ngami was caused by "silting up of the bed" of the Thaoge and blockage by papyrus. More recent studies have also shown that climatic change was not responsible for the desiccation of Lake

Ngami, but rather resulted from greater water diversion along the northern Nqoga channel, leading to gradual vegetation encroachment, blockage and failure of the Thaoge (McCarthy et al., 1992). The Nqoga functioned as the main distributary for several decades but in the mid 1900s, the lower reaches of the Nqoga-Mboroga-Santanadibe branch became progressively more prone to blockages and slowly failed, resulting in more water being diverted to the more northerly Maunachira branch (Fig. 1A and 2). More recent annual inundation mapping (Thito et al., 2016) indicates that the central Jao/Boro branch may now be overtaking the Nqoga/Maunachira branch as the dominant distributary (Fig. 1A and 2). Such accounts – both historical and more contemporary – serve to illustrate the frequency and significance of large-scale water redistribution in the Delta, with associated work outlining the processes of avulsion driving the channel formation and abandonment (e.g. McCarthy et al., 1992). Compared to the Fan, the timing and patterns of historical and longer-term channel and wetland change in the Panhandle are poorly documented, nevertheless are needed to understand the full historical range of variability in the Delta as a whole, and to provide insights to help with projections of future change and management recommendations.
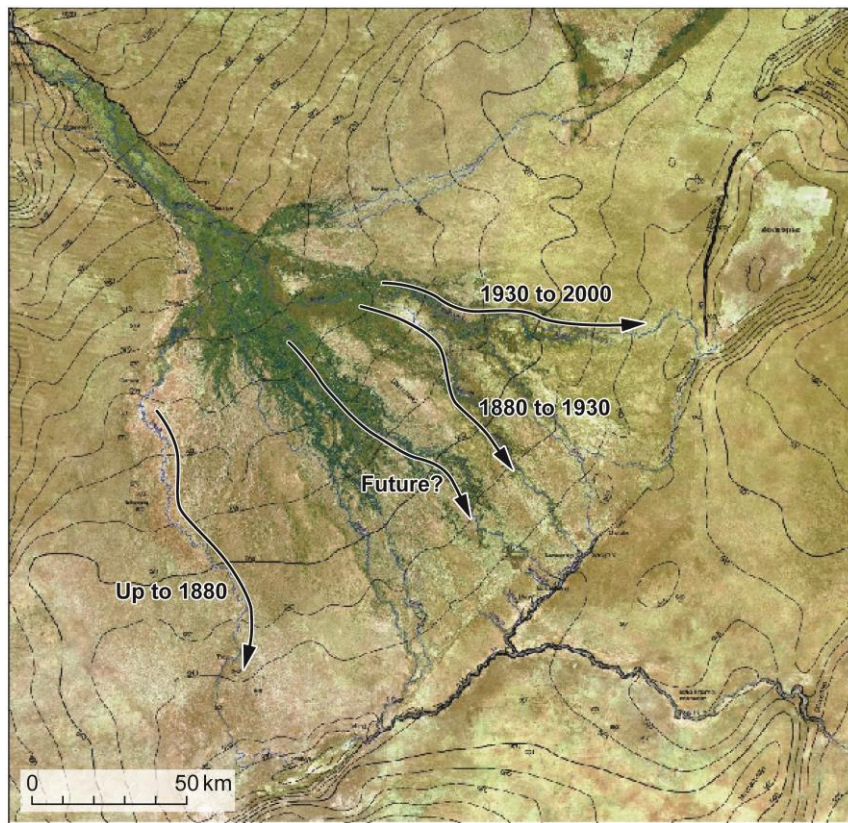
Figure 2. Decadal to centennial scale changes in the location of the main distributary channels of the Okavango Delta. Source of figure: Tooth et al. (2015).

Methods

Focussing on both palaeochannels and modern channels in the Panhandle, this study employed a combination of aerial image interpretations, field data collection, and OSL dating.

Palaeochannel mapping and OSL sampling

Using aerial photographs, the largest, best preserved and most accessible palaeochannel segments on the northeastern margin of the Panhandle were identified and mapped, and two specific sites were targeted for collection of samples for OSL dating (four palaeochannel samples in all). At each site, samples were collected from slightly elevated scroll bar ridges on the inside of an abandoned meander bend. Following the approach adopted in previous similar studies (Rodnight et al., 2005, 2006; Munyikwa et al., 2011), samples were collected by hand augering or digging pits to a depth of ~1 m, before a ~30 cm long, ~7 cm diameter metal tube was pushed or hammered into the undisturbed, typically sandy sediment at the base of the auger hole or on the pit face to retrieve sealed samples without exposure to sunlight. While these samples are from below the depth of most forms of surface disturbance by large mammals such as elephants, bioturbation is always a risk. The shallow water table at ~1.25 m precluded sampling from greater depths. Nevertheless, these samples are interpreted as representative of the last time that the palaeochannels were actively depositing bedload on point bars that eventually became incorporated into wider scroll bar sequences.

For the modern system, two samples were collected from active channel margins along the Okavango and Filipo channels, while an additional two samples were collected from (assumed older) alluvium through which the Filipo channel is presently cutting and exposing on bends. OSL sample tubes were hammered into the exposures as close to water level as possible (typically 0.85–1 m depth), and extracted and sealed without exposing the sediment to light.

OSL laboratory methods

OSL samples were processed in the Aberystwyth Luminescence Research Laboratory at Aberystwyth University, U.K. Standard methods were used to isolate the 125–212 µm quartz fraction of sediment by dissolving carbonates and organics (hydrochloric acid and hydrogen peroxide, respectively) and removing heavy minerals and feldspars by density mineral separations. Quartz grains were then etched in 40 % hydrofluoric acid to remove the alpha-irradiated outer grain surface (see Aitken 1998).

Luminescence measurements were made on a Risø automated TL/OSL reader equipped with a single-grain system based on a 532 nm green laser (Bøtter-Jensen et al. 2003). Luminescence emitted by grains was detected with an EMI 9235QA photomultiplier, with the light filtered through 2.5 mm of U-340 to reject the stimulation source. Prior to single-grain OSL analysis, a dose response and preheat test was performed to determine the optimum thermal treatment for the samples to be used in the single aliquot regenerative dose (SAR) procedure (Wintle and Murray 2006). All samples were measured with a preheat temperature of 220 °C for 10 seconds and a cut-heat of 160 °C for 10 seconds. At least 1000 grains were analysed for each sample and individual grains were accepted based on criteria outlined in Jacobs et al. (2006), which are: recycling ratio within 10 % of unity; test dose error less than 10 %; T_n

signal greater than three times the standard deviation of the background; and an IR-OSL depletion ratio within 10 % of unity (Duller 2003). After application of these criteria, between 43 and 74 individual equivalent dose (D_e) values were determined using Analyst software (Duller 2015). The central age model (CAM) was applied to most samples as their D_e distributions indicate the samples were well bleached prior to burial (see Supplementary Fig. 1 for radial plots). In the case of particularly young samples, the unlogged CAM was applied. Samples MQ7 and MQ10 displayed D_e distributions that indicate heterogeneous bleaching prior to burial (see Supplementary Fig. 1 for radial plots), so for these samples, the minimum age model (MAM) was used to calculate D_e values (Galbraith et al. 1999) as implemented in the R package 'Luminescence' (Fuchs et al. 2015). For both MQ7 and MQ10, the majority of grains fall in the presumably well-bleached population and there is a scattering of older, poorly bleached grains. In this case, the MAM is the most appropriate model to calculate burial age (Supplementary Fig. 1).

The environmental dose rate was calculated by thick source alpha counting and beta counting of dried and milled material taken from the ends of sample tubes, as this is representative of sediment surrounding the OSL sample. The cosmic ray contribution was estimated from the data given by Prescott and Hutton (1994), taking into account altitude, geomagnetic latitude and thickness of sediment overburden. Water content was measured and kept constant for palaeochannel samples at 25 ± 5 %, and at 15 ± 5 % for channel margin samples, which dry out more readily and regularly than samples in abandoned palaeochannels. These water content estimates align with the measured field water contents of the samples and have been applied in previous dating efforts in the Okavango Delta (see Tooth et al., in prep). Equivalent dose is divided by the dose rate to derive an OSL age estimate (Duller 2004).

Historical channel analysis and field measurements

To complement the palaeochannel mapping and OSL sample collection and analysis, aerial photographs and satellite imagery were used to map modern channels in the Panhandle and quantify key morphometric parameters such as channel width. Particular attention focussed on the Okavango and Filipo channels in a ~26 km anastomosing reach of the Panhandle (Fig. 1B) that had been investigated previously by Smith et al. (1997). Extending this previous investigation, aerial photographs from 1955, 1962, and 1991 (1:40 000) and satellite imagery from 2011 and 2016 (2.5 m resolution), were georectified and overlain to provide the basis for detailed geomorphological mapping and development of a time series of channel change over the second half of the 20th century and the early 21st century. This was supplemented by the Google Earth Engine Landsat imagery from 1984 to the present (Google Earth Engine Team, 2015). The key focus of mapping was to identify changes in channel configuration and planform, so the main features mapped were active trunk channels and secondary channels, abandoned trunk and secondary channels, and oxbows. In addition to mapping, morphological and longitudinal analysis was undertaken to define both temporal and downstream trends. Bankfull channel

width was the most important variable considered due to the well-defined width-discharge and width-depth relationships (Tooth and McCarthy, 2004), but meander wavelength, and vegetation encroachment were also measured. To assess the accuracy of the remotely sensed channel width measurements, field measurements of channel widths using rangefinders and measuring tapes were also made at 30 sites throughout the Panhandle. Three measurements were made at each site, the average of which was compared with the average of three measurements made at the same location using Google Earth satellite imagery from the same year as fieldwork was conducted (2016). There is a very strong positive linear correlation (R^2 = 0.99, p<0.00001) between channel width measured in the field and width measured from satellite imagery (Fig. 3) indicating that a high level of confidence can be placed in using remotely sensed channel width measurements over longer channel reaches.
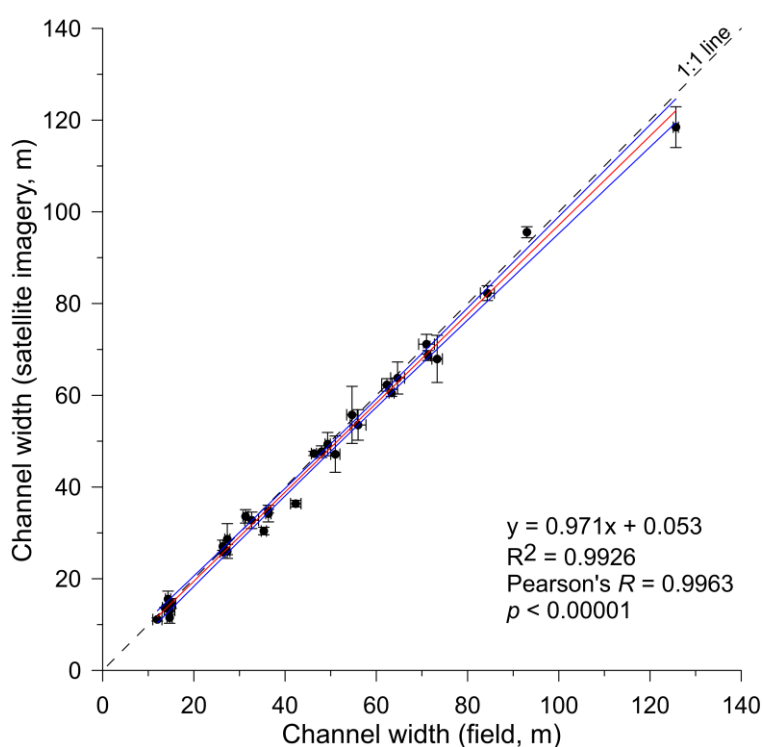
Figure 3. Comparison of field measured channel width using a rangefinder and tapes at 30 sites in the Okavango Panhandle with channel widths measured remotely at the same sites using Google Earth 2016 satellite imagery.

Results

OSL and palaeohydrology data are presented in Figs. 4–5, Supplementary Fig. 1, Tables 1–2, and Supplementary Table 1. Historical channel mapping and morphometric analysis data are presented in Figs. 6–11 and Table 2.

Palaeochannel chronology, morphometrics and palaeohydrology

At the two palaeochannel sampling sites (Fig. 1B), OSL ages were anticipated to provide an indication of the timing of channel belt activity at these locations, including the palaeochannel lateral migration rate (cf. Rodnight et al., 2006). The OSL ages demonstrate that the Ngarange meander bend was laterally migrating and depositing sediment around 4 ka, while the Ntsanyana meander bend was laterally migrating and depositing sediment between ~3.5–3.6 ka (Table 1 and Fig. 4). The scroll bars from which OSL samples were collected comprise of medium-sized (~300 μm) clean sand, with organic rich sand containing small roots in the top 25 cm. The water table at ~1.25 m depth precluded sampling below this depth. At Ntsanyana, the mid-points of the ages are in the order expected given the direction of lateral migration, and the ages overlap within error. Sample MQ10 on the Ngarange meander bend does not follow this pattern, likely due to reworking by later channel activity (see Fig. 4C). Stratigraphy does not provide an explanation for this as the scroll ridge is comprised of massive, unstructured medium sand, but imagery indicates that a meander bend has partially overprinted the southern portion of the Ngarange scroll bar sequence and may be responsible for reworking the sediment at site MQ10 (see Fig. 4C). The relatively high overdispersion of the MQ10 sample supports this interpretation (Supplementary Fig. 1).

Given the overlap in errors between individual scroll bar ages, it is not possible to precisely quantify palaeochannel lateral migration rate, but it was likely quite rapid given that sediments of similar age were deposited hundreds of metres apart in a laterally accreting sequence. For example, using the mid points of the ages, the palaeochannel at Ntsanyana appears to have migrated ~906 m within a period of just ~150 years, yielding a minimum migration rate of ~6 m a^{-1} (Fig. 4).

Table 1. Single grain OSL sample details and analytical results. See Fig. 1B for sample locations. Ages are expressed as years (ka unless otherwise noted) before the measurement date of 2017 AD. See Supplementary Fig. 1 and Supplementary Table 1 for radial plots and dosimetry data, respectively.

Sample	Sample type	Depth (m)	Equivalent dose (Gys)	Age model	Dose Rate (Gy ka $^{-1}$)	Age (ka)
MQ1	Scroll ridge	1.10 ± 0.10	4.97 ± 0.29	CAM	1.44 ± 0.06	3.45 ± 0.25 ka
MQ6	Scroll ridge	1.10 ± 0.10	1.49 ± 0.07	CAM	0.41 ± 0.02	3.60 ± 0.22 ka
MQ7	Scroll ridge	1.10 ± 0.10	2.18 ± 0.43	MAM	0.54 ± 0.02	4.05 ± 0.82 ka
MQ10	Scroll ridge	1.12 ± 0.13	2.20 ± 0.39	MAM	1.24 ± 0.05	1.77 ± 0.32 ka
FIL1	Sandy levee	0.90 ± 0.10	0.005 ± 0.003	CAM	0.46 ± 0.02	11 ± 7 years
FIL4	Island	0.90 ± 0.10	0.054 ± 0.005	CAM	0.37 ± 0.01	0.15 ± 0.02 ka
UCT19	Island/old alluvium	1.05 ± 0.10	3.50 ± 0.16	CAM	1.25 ± 0.05	2.81 ± 0.17 ka
OK3	Sandy levee	0.85 ± 0.10	0.36 ± 0.01	CAM	1.42 ± 0.06	0.25 ± 0.01 ka
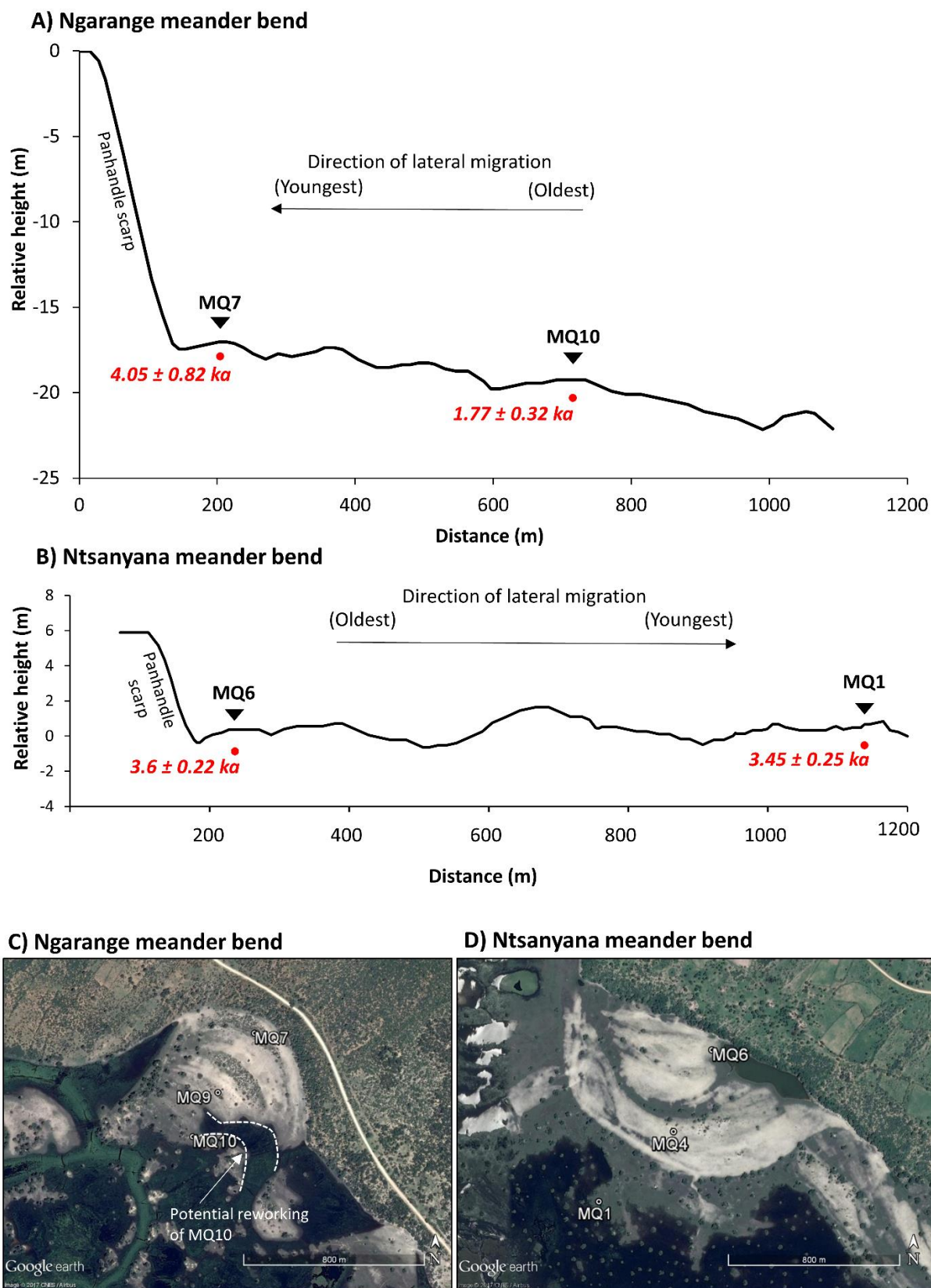
Figure 4. Topographic survey with OSL ages from: A) Ngarange meander bend scroll bar sequence; and B) Ntsanyana meander bend scroll bar sequence. Satellite image of: C) Ngarange meander bend; and D) Ntsanyana meander bend. See Fig. 1B for locations of Ngarange and Ntsanyana scroll sequences in the wider Panhandle context.

Given the similar size, morphology and OSL ages of the Ngarange and Ntsanyana bends (Fig. 1B), they are interpreted as being part of the same palaeochannel belt despite having a discontinuous palaeochannel trace in this region of the Panhandle. This palaeochannel belt declines downstream from ~160 m wide to ~120 m over a distance of ~60 km (Fig. 5A). Extrapolating from the tightly defined hydraulic geometry relationships developed by Tooth and McCarthy (2004) for channels in the Panhandle, bankfull palaeodischarge of this channel belt is estimated to be between 450–500 $m^3 s^{-1}$ at the upstream Ngarange scroll bar sequence, and between 275–400 $m^3 s^{-1}$ at the downstream Ntsanyana scroll bar sequence (Fig. 5B; Table 2).
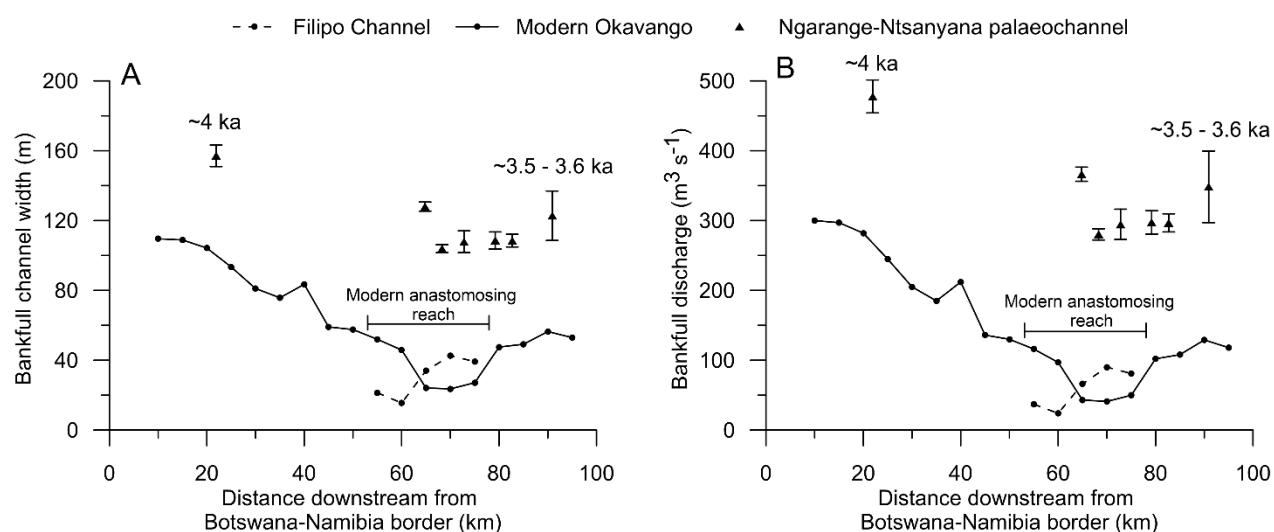
Figure 5. Downstream trends of A) bankfull channel width, and B) bankfull discharge (extrapolated using hydraulic geometry relationships developed by Tooth and McCarthy (2004)) for the Okavango Delta).

Table 2. Average morphometric and hydraulic data for modern and palaeochannels of the Okavango Panhandle. Ranges given indicate upstream to downstream trends.

Channel	Channel width (m)	Average depth (m)	Width/ Depth	Average meander wavelength (m)	Average floodplain slope (m m^{-1})	Average sinuosity	Channel discharge (m^3 s^{-1})	Gross stream power (W)	Unit stream power (W m^{-2})	Average bed shear (N m^{-2})
Ngarange-Ntsanyana	~160–110	~3.52*	~46–31	1919	0.00018	1.5	500–300	555–272	2.7–3.4	3.53
Okavango	~90–20	3.52*	~25–6	791	0.00018	1.8	230–30	228–33	2.5–1.7	2.73
Filipo	~20–50	3.52*	~6–14	441	0.00018	1.7	30–100	34–110	1.7–2.2	2.61

*Depth does not vary systematically with discharge in channels of the Okavango (Tooth and McCarthy, 2004). The average channel depth measured in the field by Tooth and McCarthy (2004) is ~3.52 m, and is therefore used as an estimate in this analysis.

Contemporary channel chronology, morphometrics and hydrology

The OSL ages from the modern course of the Okavango and Filipo channels were anticipated to provide an indication of the timing and rates of channel activity more widely across the Panhandle, including over recent decades. The modern Okavango River mainly occupies the southwestern side of the middle-

lower Panhandle (Fig. 1A) and the OSL ages suggest that channels have been active in this region for at least 250 years (see OK3, Table 1 and Fig. 1). Aerial photographs (Fig. 6) show that the channel from which sample OK3 was collected on formed after 1962, and so the channel appears to be cutting through slightly older alluvium that dates to ~0.25 ka. The modern Filipo channel occupies the central portion of the Panhandle and is cutting through even older alluvium that dates to ~2.8 ka (UCT19). Conversely, and as expected, sediment that has been deposited by the modern Filipo channel on channel margins is relatively young, with ages of ~11 and ~150 years (FIL1 and FIL4, respectively). The modern Okavango channel declines downstream from ~90–20 m wide, with discharge showing a corresponding decrease from ~100–30 m^3 s^{-1} (Fig. 5, Table 2). The Filipo channel is slightly straighter than the modern Okavango channel and gradually increases in width and discharge downstream (Fig. 5, Table 2), although this may partly be an artefact of the reoccupation of older, abandoned channel segments during development of the Filipo's lower reaches. The uppermost reach of the Filipo channel has a lower discharge than the Okavango channel but in the lowermost reaches, discharge is higher than in the Okavango channel (Fig. 5, Table 2). In both channels, unit stream power remains low at between ~1.7–2.5 W m^{-2} (Table 2).

Historical channel records

The historical dynamism of the Okavango River channel and its anabranches are demonstrated by the aerial photographs that provide a time series of channel change for the ~26 km long anastomosing reach (see also Smith et al. 1997). In the 49 years between 1962 and 2011, the meander bends in this reach have been relatively stable, with low to negligible rates of bend migration and only one meander bend cutoff occurring between 1962 and 2011 on the Okavango and two cutoffs occurring along the Filipo channel (Fig. 6). Locally, however, there have been some significant channel width adjustments, largely as a result of vegetation encroachment into the channels, especially by hippo grass (Fig. 7). Measurements of an abandoned channel segment in the southeastern region of the anastomosing reach (bottom of Fig. 10 panels), indicate a vegetation encroachment rate of ~0.9 m a^{-1} once a channel has been completely abandoned.

The aerial photographs also show that while several small secondary channels have formed due to avulsion, some have been abandoned relatively quickly (within a few decades) due to subsequent channel failure (Fig. 6). Some of these new channels have reoccupied old meander bends and straighter palaeochannels segments, and others appear to have formed along hippopotami (*Hippopotamus amphibious*) trails, which are very common throughout the Panhandle. More generally, channel reoccupation seems to be a common feature in the anastomosing reach in particular; for instance, along the present Filipo channel (~54 km river distance), reoccupied channel segments account for at least ~33 % (~18 km) of the total channel length.
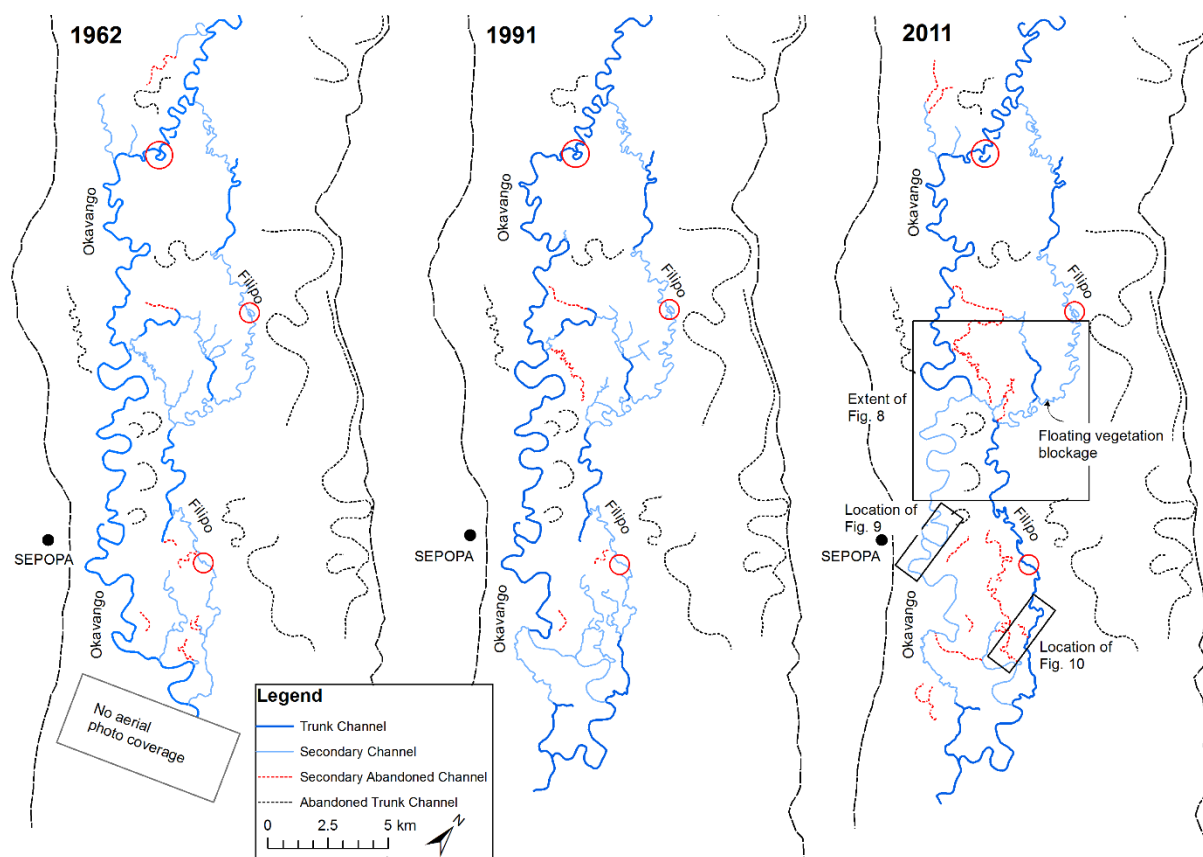
Figure 6. Time series maps of the anastomosing reach of the Okavango River in the middle Panhandle using aerial photographs from 1962 and 1991, and satellite imagery from 2011. Meander cutoffs occurring during this 49-year record are indicated by a red circle.
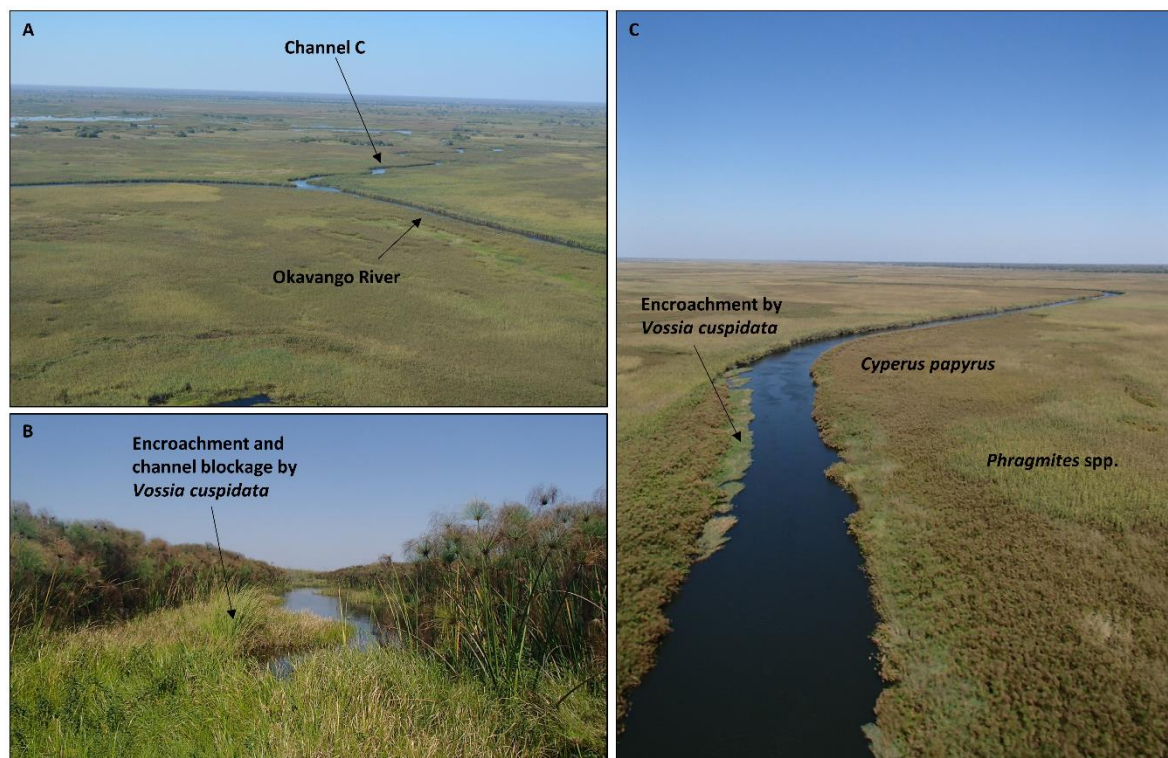
Figure 7. (A) The Okavango River and channel C joining the Okavango to the Filipo. Flow in the Okavango is from middle left to middle right, and flow in channel C is away from the camera. (B) Encroachment of hippo grass

(*Vossia cuspidata*) in standing water forming a complete blockage across a failed channel in the Panhandle (former flow direction is away from the camera). (C) Encroachment of hippo grass into the main Okavango channel near Sepopa. Flow direction in all images is toward the camera.

A substantial change to the size of both the Okavango and Filipo channels has been driven by the formation of a short 'breakaway' channel (here named channel C to remain consistent with Smith et al. 1997 and our subsequent study of channel avulsion in this reach) that joins the Okavango and Filipo (Fig. 6 - centre of 2011 panel, Fig. 8). Google Earth Engine Landsat imagery since 1984 shows that this channel initially formed around 1995 (Google Earth Engine Team, 2015). Prior to the formation of channel C, the Okavango near Sepopa was from 40–50 m wide. In 2011, just 10–15 years after the formation of channel C, the Okavango near Sepopa was only ~20 m wide (Fig. 8) and channel width was much more irregular due to the uneven encroachment of vegetation into the channel (Fig. 9). This reduction of channel width and increase in width irregularity continued through to 2016 (Fig. 9) and the present day.

Upstream of the channel C junction, the Filipo remains relatively narrow (~20–30 m), and in some locations (Fig. 8 - sites x, xi, and xv) has even declined in size. These decreases in width are associated with other channel changes; for instance, by 2011, there was a complete blockage of floating vegetation upstream of the channel C junction (Fig. 8). By contrast, the Filipo downstream of channel C is significantly wider (~40–50 m) than in the reach upstream (Figs. 8 and 10). Overall, along the anastomosing reach there has been a significant net reduction in the width of the Okavango channel, but a slight net increase in the width of the Filipo (Fig. 11). In 2011 and 2016, most sections of the Okavango channel were substantially narrower than the Filipo (Fig. 11).
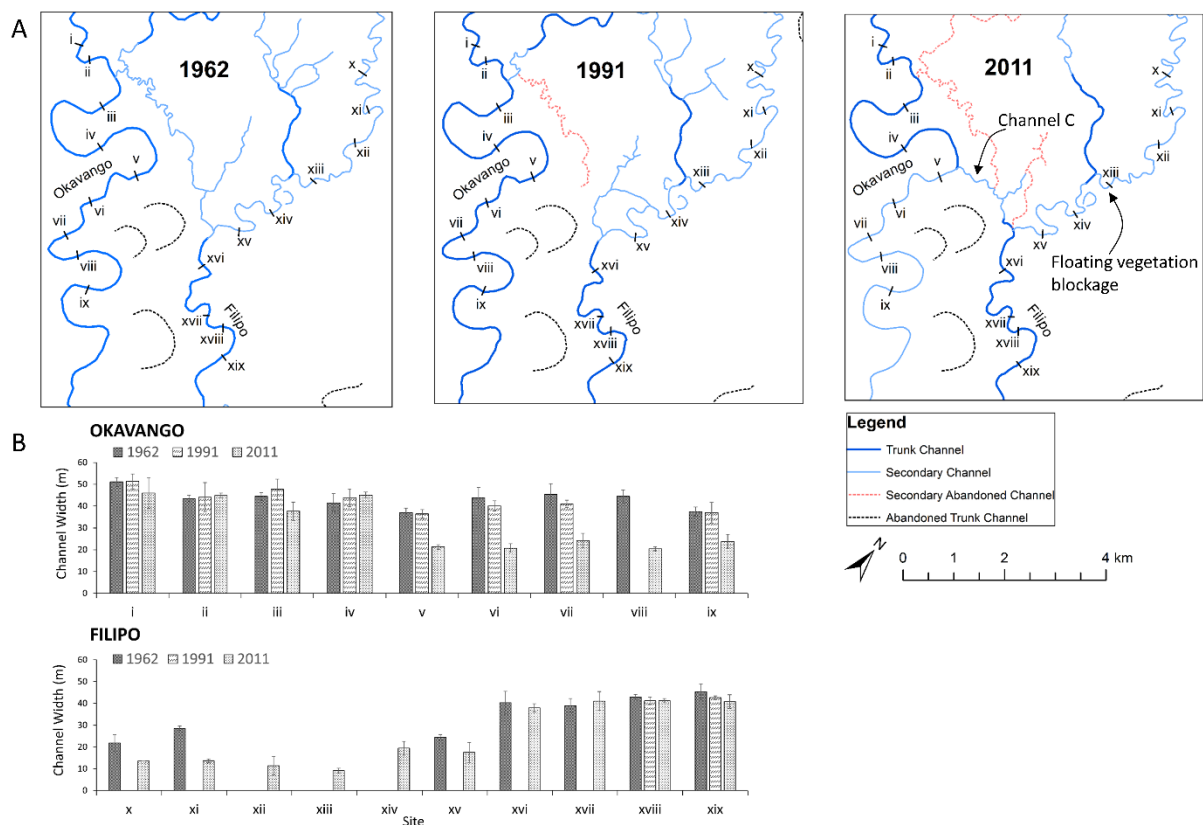
Figure 8. A) Maps showing the formation of channel C between 1991 and 2011. Google Earth Engine Landsat imagery (Google Earth Engine Team, 2015) (1984–2016) shows that channel C first formed around 1995. The panels are mapped using aerial photographs from 1962 and 1991, and satellite imagery from 2011. Flow direction is from top to bottom. Using the aerial imagery in A, channel widths were measured at locations indicated by roman numerals. B) Graphs indicating both the downstream and temporal trend in channel widths along the Okavango and Filipo channels along the reaches shown in A. Where a channel width measurement is absent, aerial photograph resolution was too poor to accurately measure width.
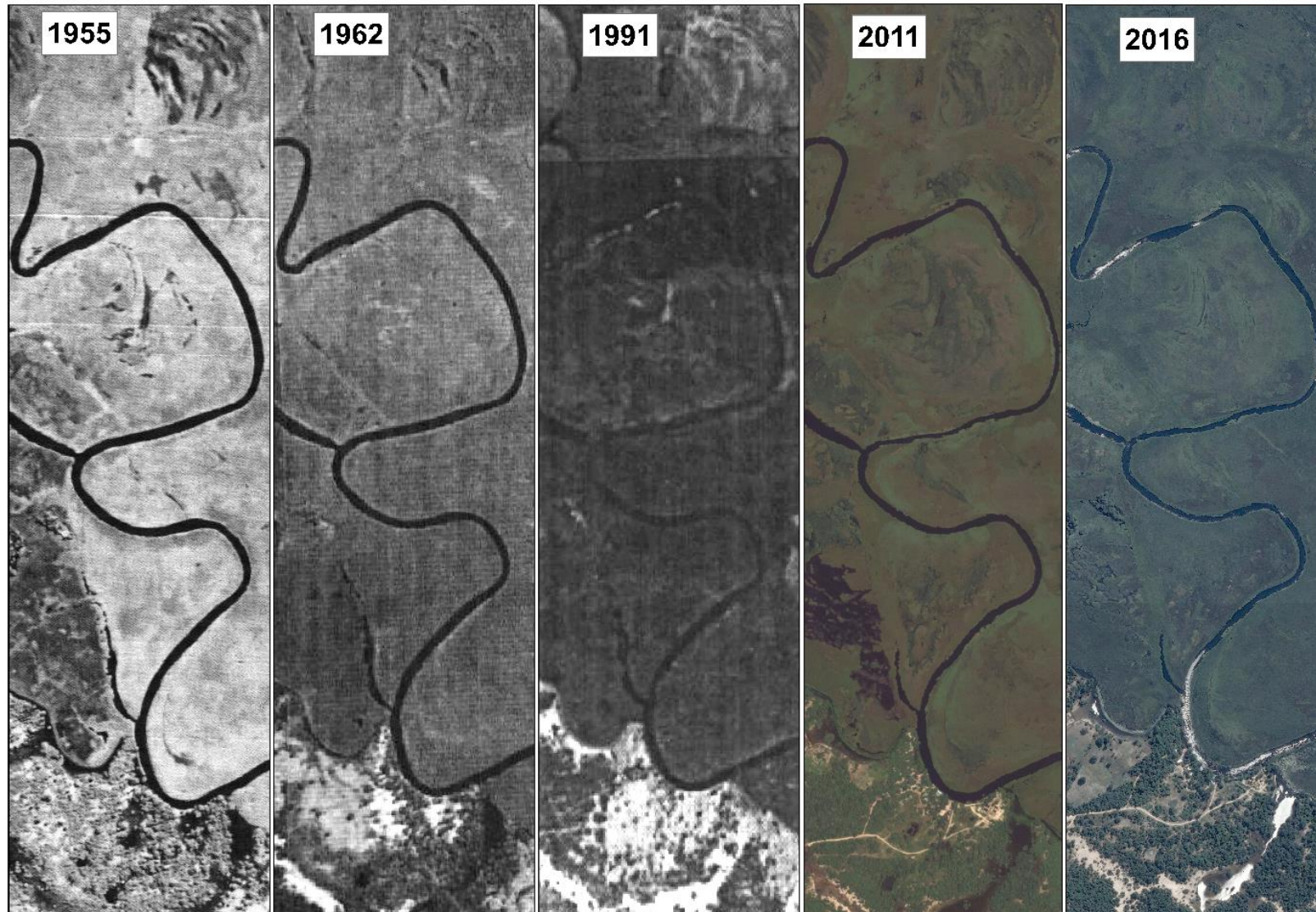
Figure 9. Historical aerial photographs from 1955, 1962, and 1991, and satellite imagery from 2011 and 2016 of the Okavango channel near Sepopa (see Fig. 6 for location and orientation of panels; north is towards the top of the images). Flow direction is from top left to bottom right of images. Panel width is ~1 km.
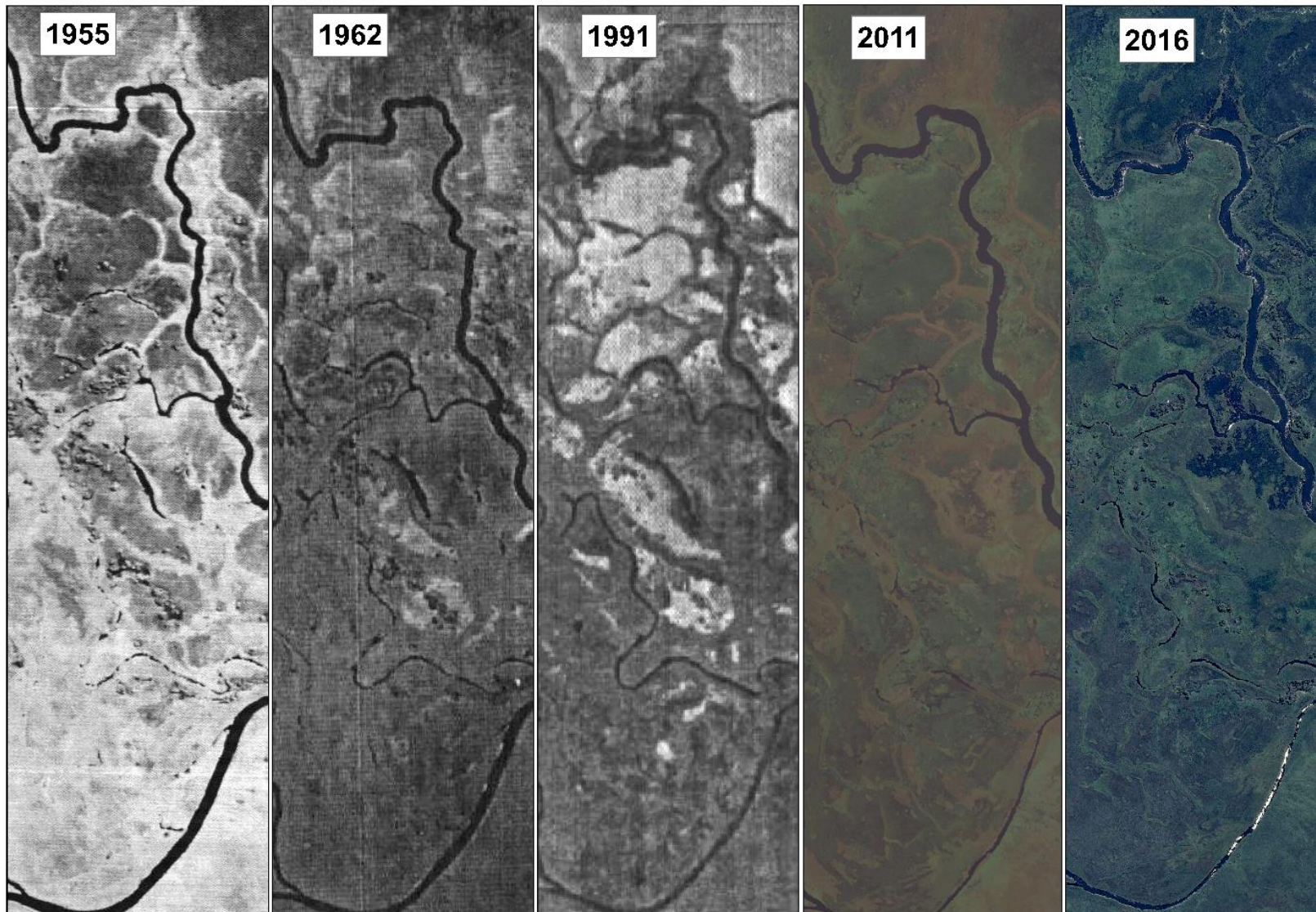
Figure 10. Historical aerial photographs from 1955, 1962, and 1991, and satellite imagery from 2011 and 2016 of the Filipo channel near Sepopa (see Fig. 6 for location and orientation of panels; north is towards the top of the images). Flow direction in the Filipo is from top left to middle right of image. The clearly narrowing channel in the bottom portion of the panels is a section of the Okavango River abandoned between 1962 and 1991. Panel width is ~1 km.
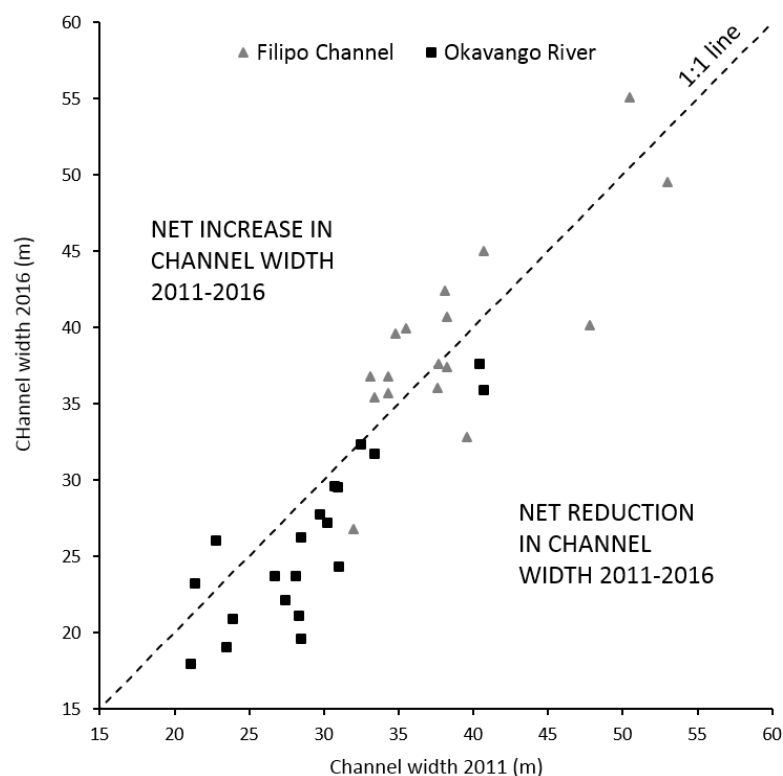
Figure 11. Net change in channel width along the Okavango and Filipo channels between 2011 and 2016. Channel widths were measured using satellite imagery along the sections shown in Figs 9 and 10. The 1:1 line represents zero net change in channel width between 2011 and 2016.

Interpretation

OSL dating of fluvial deposits along the northeastern margin of the Okavango Panhandle establishes the timing of enhanced fluvial activity (wider channels, higher discharges, faster lateral migration) within a major palaeochannel belt at ~4 to 3.5 ka. By contrast, OSL dating along the modern Okavango and Filipo channels in the more central and western part of the Panhandle shows reduced fluvial activity (narrower channels, lower discharges, slower lateral migration) over the last ~250 years. Historical analysis of channel change demonstrates the short-term dynamics (last 60–70 years) associated with anastomosing channels in the middle reach of the Panhandle. Together, these findings allow us to synthesise the mid to late Holocene development of the Okavango River in the Panhandle and explain the changing nature of channel dynamics.

Holocene evolution of the Okavango River

Our findings show that the Okavango River in the Panhandle has undergone dramatic reductions in width and discharge, as well as changes in the rates and dominant types of channel adjustment. At ~4– 3.5 ka, the large, rapidly laterally migrating Ngarange-Ntsanyana palaeochannel was active. It migrated laterally across the floodplain at least ~6 m a^{-1}, which is comparable to lateral migration rates in some

modern sand-bed rivers of similar size in others parts of central southern Africa (e.g. Luangwa River, Zambia – Gilvear et al., 1999). The Ngarange-Ntsanyana palaeochannel was ~5 times the width of the modern Okavango channel but width also decreased downstream (Fig. 5, Table 2), most likely as a result of water leakage through vegetation- and peat-lined channel margins to flanking wetlands. However, this palaeochannel did not decrease in width at the same rate as the modern river. The Ngarange-Ntsanyana palaeochannel declined from ~160 m to ~120 m over ~60 km (i.e. ~0.67 m km^{-1}, or ~0.42 % km^{-1}), while the modern channel declines from ~100 m to ~50 m over ~40 km, after which the anastomosing reach starts (i.e. 1.25 m km^{-1}, or 1.25 % km^{-1}; Fig. 5A). Discharge in the Ngarange-Ntsanyana palaeochannel was between 2.5–9.2 times greater than the modern channels at equivalent locations downstream (Fig. 5B), indicating a substantially greater capacity for lateral channel activity and associated sediment transport. Along the smaller, modern channels, lateral migration has substantially decreased with many bends now essentially static and with only three examples of cutoffs occurring in the anastomosing reach over the last 60–70 years (Fig. 6). Nevertheless, lateral instability is still a feature of the modern channels, in the form of periodic avulsions. OSL ages from along the modern Okavango and Filipo channels show that in some locations active deposition is taking place on channel margins, but in other locations, sections of channel that have formed by avulsion are now eroding through older alluvium that dates to at least 2.8 ka (Table 1).

Clearly, the findings suggest that a dramatic change in river behaviour has occurred during the transition from the mid to the late Holocene. In the Okavango Panhandle, the degree of lateral migration and propensity for avulsion may be linked. Previous research has shown the sandy sediment is transported mainly as bedload in the base of ~3–4 m deep channels, with very little sediment in suspension (McCarthy et al., 1992; Tooth and McCarthy, 2004). As discharge decreases downstream owing to leakage through the vegetation- and peat-lined channel margins, sediment transport capacity declines downstream leading to net channel aggradation. In large channels with rapid lateral migration (such as the Ngarange-Ntsanyana palaeochannel), bedload is readily incorporated into channel margin and near-channel deposits (i.e. point bar sediments and ultimately scroll bar sequences), whereas in channels with slower lateral migration, bedload remains confined within the channel. This acts to more quickly raise the channel bed and water surface relative to the surrounding wetlands (permanent swamps), which increases the potential for avulsion because the hydraulic advantage promotes new channel formation in areas away from the aggrading channel, commonly by the widening of pre-existing pathways like hippopotami trails or older palaeochannel sections (see McCarthy et al., 1992; McCarthy, 2013).

Historical and future channel dynamics

There is an apparent paradox within the contemporary channels of the Okavango Panhandle, in that the trunk channels are characterised both by relative bend stability yet locally have undergone pronounced changes in width and are subject to periodic lateral relocation by avulsion. The limited or negligible

lateral migration can be explained, however, by considering channel width/depth ratios. Based on analysis of modern Delta channels, Tooth and McCarthy (2004) highlighted a threshold in width/depth ratios of ~10, below which channels cease to migrate laterally as the proportionally enhanced roughness from bank vegetation precludes the development of the secondary circulation cells that are essential precursors to outer bend erosion and inner bend deposition, particularly in low stream power channels. Indeed, modern channels in the anastomosing reach of the Panhandle typically have width/depth ratios between 6 and 14 (Table 2), so are just above or below this threshold, as suggested by the aerial image evidence for relative meander bend stability and only minor local cutoffs over the last 60–70 years (Fig. 6). The lateral stability of channels in the Panhandle had also been noted previously by Wilson (1973), who highlighted a tortuous sequence of bends near Seronga (Fig. 1A) that had remained unchanged for at least 35 years (exact years unspecified). Comparisons between Wilson's (1973) aerial photo (Wilson 1973, his Fig. 2), and contemporary satellite imagery (2016) indicates that there is still no discernible lateral adjustment in this reach.

By contrast with the relative bend stability, local adjustments in width of the trunk channels and the formation and abandonment of secondary channels can be a rapid, near-continuous process (Figs. 6 and 8). In particular, marked adjustments result from shifts in water balance between incipient channels that have formed along hippopotami trails or older palaeochannel sections, and sections constricted by vegetation encroachment. For instance, despite pronounced lateral stability, the progressive dominance of the Filipo channel (Smith et al., 1997) in the middle Panhandle has led to a shifting water balance and significant width decreases of 50–60% along many sections of the Okavango channel in just a few decades (Fig. 9), particularly downstream of the channel C bifurcation (Figs. 8 and 9).

Upstream of the channel C junction, the Filipo channel also had decreased in width and is blocked by vegetation in at least one location (Fig. 8). The future configuration of the single-thread Okavango River is thus likely to incorporate the current Okavango channel upstream of channel C, channel C itself, and the Filipo downstream of the channel C junction. The current anastomosing configuration pattern may well only be a transitional pattern as the lower Filipo overtakes part of the Okavango as the main channel in the Panhandle downstream of channel C, and this section of the modern Okavango channel is gradually abandoned. Reorganisation of the channels in this part of the middle Panhandle will likely continue until a single channel captures all of the flow, whereupon meander development will continue to progress slowly (see also Smith et al., 1997). If this interpretation is correct, this example of 'transitional anastomosis' will contrast with the long-term 'stable anastomosis' that characterises some other dryland rivers and wetlands, especially in Australia (e.g. Knighton and Nanson, 1993; Huang and Nanson, 2000; 2007). In this respect, the Okavango River in the Panhandle may be more similar to avulsive rivers that abandon their former channels after avulsion such as the Tshwane and Klip rivers in South Africa (Tooth et al., 2007; Larkin et al., 2017). In the Okavango, however, the process of abandonment takes considerably longer and results in temporary, or transitional, anastomosis.

Discussion

Our understanding of the evolution of the Okavango River during the Holocene not only provides an important record of palaeoclimatic change, but also has implications for assessments of future trajectories of change for the Okavango River under future climate change and potential water resource development.

Holocene hydroclimatic controls in the Okavango catchment

Given the magnitude of changes to hydrological and channel dynamics in the Okavango Panhandle, with evidence for substantially enhanced mid Holocene fluvial activity and an overall decrease in late Holocene activity, and given that tectonic activity or other extrinsic forcing cannot feasibly account for these changes, a palaeoclimatic explanation is required. The two major controls on rainfall patterns in the summer rainfall zone (SRZ) of the southern African interior (i.e. excluding the winter rainfall zone and all seasons rainfall zone around the southern Cape) are the Intertropical Convergence Zone (ITCZ) and the Congo Air Boundary (CAB) (Burrough and Thomas, 2013; Cordova et al., 2017). The ITCZ and its associated rain belt migrates north and south annually and brings rainfall to southern Africa during the austral summer months. The CAB is an unstable, northeast to southwest convergence of air over Zambia and Angola (Burrough and Thomas, 2013) and separates the southeasterly trade winds that bring moisture from the Indian Ocean from the West African monsoonal system that brings moisture from the Atlantic Ocean. The CAB migrates meridionally with the annual movement of the ITCZ. The dynamics of these air masses are responsible for the early-mid Holocene African Humid Period (AHP), which is recognised in the palaeoclimatic and wider palaeoenvironmental records of western and northern Africa, and the complex palaeoenvironmental Holocene records from central and southern Africa. In northern Africa, the AHP resulted from increased boreal summer insolation related to precession of the Earth's orbit (Singarayer and Burrough, 2015). The termination of the AHP in northern Africa ~5 ka is thought to have been triggered by high-latitude northern hemisphere cooling in the North Atlantic Ocean, which slowed the Atlantic Meridional Overturning Circulation and encouraged cold anomalies in the mid-low latitudes. In combination with declining northern hemisphere summer insolation, cold anomalies reduced the northern extent of the monsoon, and initiated a relatively rapid end to the Holocene AHP (Burrough and Thomas, 2013; Singarayer and Burrough, 2015; Collins et al., 2017). In southern Africa, however, Holocene palaeoenvironmental records are complex and, with respect to links to the AHP, appear contradictory in some cases (Thomas and Shaw, 2002; Chase et al., 2010; Schefuß et al., 2011; Thomas and Burrough, 2012). Fluvial and lake shoreline records from the Okavango and central Kalahari suggest wetter conditions during the mid Holocene, coincident with the end of the AHP, but some other proxies from the region indicate locally drier conditions during the same period (Burrough and Thomas, 2008; Burrough and Thomas, 2013; Tooth et al., in prep).

For instance, dating of large palaeochannels in the Xugana region of the northeastern part of the Okavango Fan has also provided evidence for significantly enhanced discharges (up to 9–10 times that of the modern channels in the same part of the Fan) during the period 7–4 ka (Tooth et al., in prep). This correlates well with the last major palaeolake highstand in the Mababe depression between ~6.6–5.2 ka (Burrough and Thomas, 2008). Our dating of the Ngarange-Ntsanyana palaeochannel belt in the Panhandle indicates enhanced fluvial activity extended to ~3.5 ka, perhaps reflecting the tail end of fluvial activity associated with the Xugana palaeochannel belt. Along the Ngarange-Ntsanyana palaeochannel belt, located within the relatively confined setting of the Panhandle, slightly older evidence for fluvial activity more tightly coincident with activity in the Xugana region may have been lost as a result of reworking by subsequent river migration activity, as suggested by the anomalously young age for MQ10 from the innermost edge of the Ngarange scroll bar sequence (Fig. 4A). Nevertheless, it remains possible that a continuous palaeochannel linking Ngarange, Ntsanyana and Xugana may once have been part of a longer palaeochannel supplying flow to support a palaeolake high-stand in the Mababe depression during the mid Holocene.

In contrast, an apparent contradictory line of evidence is provided by pollen analysis undertaken by Nash et al. (2006) in the Ncamasere valley that joins the western margin of the northern Panhandle. This record has been interpreted as indicating generally drier conditions during the 7–4 ka period, albeit with a short wet interval around 6 ka (Nash et al., 2006). Our OSL dating, however, indicates that a larger Okavango River was flowing close to the northeastern margin of the Panhandle at and perhaps before ~4 ka. As such, it is possible that the pollen record reflects a reduction in backflooding of the Ncamasere valley during the mid Holocene, as the main Okavango River perhaps may have been >11 km away on the other side of the Panhandle at this time. Further investigation and dating of channel features is required to fully constrain the position and activity of the Okavango River at various times during the Holocene.

Other proxy records from aeolian dunes and impact crater infill sediments in central and eastern southern Africa also indicate drier conditions at intervals during the mid Holocene (e.g. Partridge et al., 1997; O'Connor and Thomas, 1999; Kristen et al., 2007; Burrough et al, 2012; Burrough and Thomas, 2013). For instance, barchan dunes are thought to have been active on the floor of the Ntwetwe Pan in the Makgadikgadi basin of the central Kalahari Desert ~200 km southeast of the Okavango Delta during the mid Holocene, although there is some debate surrounding the interpretation of these features, with alternative explanations suggesting that these features are actually sub-aqueously formed or reworked (Macfarlane and Long, 2015; Burrough et al., 2012; Burrough and Thomas, 2013). Dune building associated with regional aridity between ~5–4 ka has been recorded in the linear dunes of western Zambia just north of the Okavango Delta (O'Connor and Thomas, 1999). High-resolution geochemistry on a core extracted from the Tswaing impact crater in northeastern South Africa also indicates reduced precipitation during the mid Holocene (Partridge et al., 1997; Kristen et al., 2007) and has been

attributed to a weakened summer monsoon in eastern South Africa that brought less moisture from the Indian Ocean (Partridge et al., 1997).

Overall, these apparently contradictory records support the argument that the mid Holocene period was characterised by substantial climatic and environmental variability in central southern Africa (Burrough and Thomas, 2013). The dynamics of the ITCZ and the CAB, and thus the relative importance of either Atlantic derived (West African monsoon) rainfall or Indian Ocean derived (East African monsoon) rainfall, likely account for the variability in proxy records in this region, and the apparent zonal dichotomy of contemporaneously relatively drier conditions in the Kalahari and eastern southern Africa compared with relatively wetter conditions in the northwestern region around Angola. The drier conditions in the northern Kalahari and eastern southern Africa during the mid Holocene are thought to be due to weakened southeast trade winds bringing less moisture from the Indian Ocean (Burrough and Thomas, 2013). Conversely, the significantly enhanced fluvial activity in the Okavango during the mid Holocene may have been related to an increase in Atlantic Ocean derived rainfall over the Angolan headwaters, as has been hypothesised for substantially enhanced mid Holocene palaeochannel activity in the Xugana region of the Okavango Fan (Tooth et al., in prep.) and the last major megalake phase (palaeolake Makgadikgadi) in the early Holocene (Burrough and Thomas, 2013). Isotopic analysis of Lake Tanganyika records indicates an increase in Atlantic derived West African monsoon rainfall around 6 ka, which likely shifted the CAB farther southeast over the Okavango catchment, particularly given the presumed weakened southeast trades (Tierney et al., 2011). This argument is supported by offshore pollen records near Angola which show a shift from savannah to miombo/closed woodland between ~7.8–3.7 ka in the Angolan highlands, including the upper Okavango catchment, and is interpreted as an ecological response to increased rainfall and more humid conditions (Dupont et al., 2008). Burrough and Thomas (2013) argue that the stabilisation of the Makgadikgadi barchan dunefield at ~2 ka by vegetation growth on the dunes reflects an increased dominance of moisture supplied by southeast trade winds from the Indian Ocean and a stabilisation of the climate with conditions that are more similar to the present. In the Okavango Panhandle, and perhaps across the Delta more widely, this hydroclimatic shift, as well as the decline in the strength of the West African monsoon, appears to be responsible for the disappearance of large, rapidly laterally migrating palaeochannels and their replacement by smaller, more slowly migrating channels characterised by periodic avulsion.

Implications of future climate change and water resource development activities for channel adjustments in the Okavango Panhandle

Our analysis of mid-late Holocene channel dynamics provides context for understanding contemporary fluvial dynamics in the Okavango Panhandle, with implications for assessments of future changes and associated management strategies. A long-term perspective has allowed us to more fully understand the boundary conditions and historical range of variability in the system, and given our improving understanding of the Okavango River's response to changing hydroclimatic conditions over the last ~4

ka, we can identify a range of possible future pathways of change. In the short term, local impacts resulting from ongoing avulsion in the middle Panhandle will continue, with increasing flow diversion from the Okavango to the Filipo channel likely leading to the abandonment of the Okavango channel near Sepopa. Given recent rapid rates of width decrease along the Okavango channel near Sepopa (Figs. 8 and 9), we predict that abandonment of this segment could occur within the next two decades. In the longer term, climate and land use changes will also begin to have tangible impacts on the Okavango, possibly by the mid to late 21st century. Expansion of the tropical belt and the subtropical ridge may increase rainfall totals over part of the Okavango headwaters, but many global climate models indicate increased climatic variability superimposed on an overall drying trend throughout southern Africa in the future (Arnell et al., 2003; Engelbrecht et al., 2009; Shongwe et al., 2009; Milzow et al., 2010; Wolski et al., 2012). In the Okavango catchment, increased climatic and hydrological variability, combined with increased temperatures and evapotranspiration, is projected to reduce mean streamflows (Andersson, 2006). Additionally, in the upper catchment, future increases in irrigated agriculture and other water resource developments (e.g. water extraction, dam building) will also likely reduce streamflows, possibly suppressing or curtailing the natural river dynamics that sustain the wetland ecosystem (Mbaiwa, 2004; Andersson et al., 2006). For instance, dam building will likely lead to a downstream reduction in sediment supply, possibly affecting channel-bed aggradation, the key driver of avulsion, which is an essential process for regular redistribution of water and sediment and associated ecosystem health (McCarthy, 2013). Changes to nutrient balances due to upstream agricultural developments may also have large impacts, given that the Okavango is naturally a very low nutrient system (McCarthy, 2013). Increases in nutrients like nitrogen and phosphorus would likely affect the growth dynamics and patterns of key channel-margin vegetation types like papyrus, phragmites and hippo grass, with severe potential impacts on channel dynamics. For example, increased nutrients, in conjunction with lower mean streamflows, may drive increased vegetation encroachment into channels and more rapid closure of failed or failing channels. This may have knock-on impacts for local communities and tourist lodges who may find that they have less reliable access to channels for fresh water and transport.

Conclusion

The Okavango River in the Panhandle has undergone substantial changes to its size and behaviour in response to mid-late Holocene hydroclimatic changes. We argue that enhanced mid Holocene rainfall over the northern headwaters resulted in higher discharges along large, rapidly laterally migrating palaeochannels that were active until ~4–3.5 ka. A subsequent decline in rainfall and discharges led to substantial reduction in channel width and decreased lateral migration. As a consequence, channels in the Panhandle are now susceptible to a different form of lateral instability, namely avulsion, which proceeds at a rapid rate. An appreciation of the key drivers and processes of these profound changes helps to establish the historical range of variability in the Panhandle and the Okavango Delta more

widely. This information provides vital context for an examination of contemporary and potential future trajectories of change under future climate change or water development scenarios, hopefully informing development of sustainable management strategies in this iconic dryland wetland.

The evidence presented here suggests that the Okavango has exhibited considerable geomorphological sensitivity to mid-late Holocene hydroclimatic changes. More research is required to understand the response of other large African, and global, dryland fluvial systems to Holocene climate change. Having a more spatially comprehensive, and temporally-constrained, understanding of the response of dryland rivers to Holocene hydroclimatic changes will improve assessment of the relative sensitivity of dryland rivers to hydroclimatic change. This is particularly important in light of future climate change, which is likely to reduce surface water availability in drylands around the world, and will therefore have impacts on the hydrology, geomorphology, and ecology of dryland rivers in as yet poorly understood ways.

Acknowledgements

References

Aitken MJ, 1998. An introduction to optical dating: the dating of Quaternary sediments by the use of photon-stimulated luminescence: Oxford University Press, Oxford.

Andersson CJ, 1856. Lake Ngami; or explorations and discoveries during four years' wanderings in the wilds of south western Africa. London, Hurst and Blackett.

Andersson L, Wilk J, Todd MC, Hughes DA, Earle A, Kniveton D, Layberry R, and Savenije HHG, 2006. Impact of climate change and development scenarios on flow patterns in the Okavango River. Journal of Hydrology, 331(1–2), 43–57.

Arnell NW, Hudson DA, and Jones RG, 2003. Climate change scenarios from a regional climate model: Estimating change in runoff in southern Africa. Journal of Geophysical Research, 108, 4519.

Baines T, 1864. Explorations in southwest Africa: being an account of a journey in the years 1861-1862 from Walvisch Bay on the western coast, to Lake Ngami and the Victoria Falls. London, Longman.

Bøtter-Jensen L, Andersen CE, Duller GAT, and Murray AS, 2003. Developments in radiation, stimulation and observation facilities in luminescence measurements. Radiation Measurements 37: 535-541.

Bowler JM, 1967. Quaternary chronology of Goulburn valley sediments and their correlation in southeastern Australia. Journal of the Geological Society of Australia 14, 287–292.

Burrough SL, and Thomas DSG, 2008. Late Quaternary lake-level fluctuations in the Mababe Depression: Middle Kalahari palaeolakes and the role of Zambezi inflows. Quaternary Research 69, 388–403.

Burrough SL, and Thomas DSG, 2013. Central southern Africa at the time of the African Humid Period: A new analysis of Holocene palaeoenvironmental and palaeoclimate data. Quaternary Science Reviews 80, 29–46.

Burrough SL, Thomas DSG, Bailey RM, and Davies L, 2012. From landform to process: Morphology and formation of lake-bed barchan dunes, Makgadikgadi, Botswana. Geomorphology 161–162, 1–14.

Chapman J, 1886. Travels in the interior of South Africa. (2 volumes) London, Bell and Daldy.

Chase BM, Meadows ME, Carr AS, and Reimer PJ, 2010. Evidence for progressive Holocene aridification in southern Africa recorded in Namibian hyrax middens: Implications for African Monsoon dynamics and the "'African Humid Period.'" Quaternary Research 74, 36–45.

Cordova CE, Scott L, Chase BM, and Chevalier M, 2017. Late Pleistocene-Holocene vegetation and climate change in the Middle Kalahari, Lake Ngami, Botswana. Quaternary Science Reviews 171, 199–215.

Duller GAT, 2003. Distinguishing quartz and feldspar in single grain luminescence measurements. Radiation Measurements 37: 161-165.

Duller GAT, 2004. Luminescence dating of Quaternary sediments: recent advances. Journal of Quaternary Science 19: 183-192.

Duller GAT, 2015. The Analyst software package for luminescence data: overview and recent improvements. Ancient TL 33: 35-42.

Dupont LM, Behling H, Jahns S, Marret F, and Kim JH, 2007. Variability in glacial and Holocene marine pollen records offshore from west southern Africa. Vegetation History and Archaeobotany 16, 87–100.

Ellery WN, McCarthy TS, Smith N, and Hall B, 2003. Vegetation, hydrology, and sedimentation patterns on the major distributary system of the Okavango Fan, Botswana. Wetlands, 23, 357-375.

Engelbrecht FA, McGregor JL, and Engelbrecht CJ, 2009. Dynamics of the Conformal-Cubic Atmospheric Model projected climate-change signal over southern Africa. International Journal of Climatology, 29, 1013-1033.

Fryirs KA, Ralph TJ, Larkin ZT, Tooth S, Humphries M, McCarthy T, Hesse PP, Mosimanyana E, 2018. A nested hierarchical perspective to enhance interpretations and communication in fluvial geomorphology for use in water resources management: Lessons from the Okavango Delta, Botswana. Geographical Journal, 184, 192–207.

Fuchs MC, Kreutzer S, Burow C, Dietze M, Fischer M, Schmidt C, and Fuchs M, 2015. Data processing in luminescence dating analysis: An exemplary workflow using the R package 'Luminescence'. Quaternary International 362: 8-13.

Galbraith RF, Roberts RG, Laslett GM, Yoshida H, and Olley JM, 1999. Optical dating of single and multiple grains of quartz from Jinmium rock shelter, Northern Australia: Part I, Experimental design and statistical models. Archaeometry 41, 339–364.

Gilvear D, Winterbottom S, and Sichingabula H, 2000. Character of channel planform change and meander development: Luangwa River, Zambia. Earth Surface Processes and Landforms 25, 421–436.

Google Earth Engine Team, 2015. Google Earth Engine: A planetary-scale geospatial analysis platform. https://earthengine.google.com, date accessed: 6/12/16

Huang H, and Nanson G, 2000. Hydraulic geometry and maximum flow efficiency as products of the principle of least action. Earth Surface Processes and Landforms, 25, 1-16.

Huang H, and Nanson G, 2007. Why some alluvial rivers develop an anabranching pattern. Water Resources Research, 43, 1-12.

Hutchins DG, Hutton S, Jones CR, 1976. The geology of the Okavango Delta. In: Proceedings of the Symposium on the Okavango Delta and its Future Utilization. Botswana Society, National Museum, Gaborone, Botswana.

Jacobs Z, Duller GAT, and Wintle AG, 2006. Interpretation of single grain De distributions and calculation of De. Radiation Measurements 41: 264-277.

King J, Beuster H, Brown C, Joubert A, 2014. Pro-active management: the role of environmental flows in transboundary cooperative planning for the Okavango River system. Hydrological Sciences Journal 59, 786–800.

Kingsford RT, 2000. Ecological impacts of dams, water diversions and river management on floodplain wetlands in Australia. Austral Ecology, 25(2), 109–127.

Knighton AD, and Nanson GC, 1993. Anastomosis and the continuum of channel pattern. Earth Surface Processes and Landforms 18, 613–625.

Kristen I, Fuhrmann A, Thorpe J, Röhl U, Wilkes H, and Oberhänsli H, 2007. Hydrological changes in southern Africa over the last 200 ka as recorded in lake sediments from the Tswaing impact crater. South African Journal of Geology 110, 311-326.

Larkin ZT, Tooth S, Ralph TJ, Duller GAD, McCarthy T, Keen-Zebert A, and Humphries M, 2017. Timescales, mechanisms and controls of incisional avulsions in floodplain wetlands: Insights from the Tshwane River, semiarid South Africa. Geomorphology, 283, 158-172.

Livingstone D, 1858. Missionary travels and researches in South Africa. New York, Harper Bros.

McFarlane MJ, and Long CW, 2015. Pan floor "barchan" mounds, Ntwetwe Pan, Makgadikgadi, Botswana: Their origin and palaeoclimatic implications. Quaternary International 372, 108–119.

Mbaiwa JE, 2003. The socio-economic and environmental impacts of tourism development on the Okavango Delta, north-western Botswana. Journal of Arid Environments, 54, 447-467.

Mbaiwa JE, 2004. Causes and possible solutions to water resource conflicts in the Okavango River Basin: The case of Angola, Namibia and Botswana. Physics and Chemistry of the Earth, 29, 1319–1326.

McCarthy TS, Ellery WN, and Stanistreet IG, 1992. Avulsion mechanisms on the Okavango Fan, Botswana: the control of a fluvial system by vegetation. Sedimentology, 39, 779-795.

McCarthy TS, 2013. The Okavango Delta and it's place in the geomorphological evolution of southern Africa. South African Journal of Geology, 116, 3-54.

Mendelsohn JM, vanderPost C, Ramberg L, Murray-Hudson M, Wolski P, and Mosepele K, 2010. Okavango Delta: Floods of Life. RAISON, Windhoek, Namibia.

Milzow C, Burg V, and Kinzelbach W, 2010. Estimating future ecoregion distributions within the Okavango Delta Wetlands based on hydrological simulations and future climate and development scenarios. Journal of Hydrology 381, 89–100.

Munyikwa K, Telfer MW, Baker I, and Knight C, 2011. Core drilling of Quaternary sediments for luminescence dating using the Dormer Drillmite. Ancient TL, 29(1), 15-23.

Nash DJ, Meadows ME, and Gulliver VL, 2006. Holocene environmental change in the Okavango Panhandle, northwest Botswana. Quaternary Science Reviews. 25, 1302–1322.

O'Connor P, and Thomas D, 1999. The Timing and Environmental Significance of Late Quaternary Linear Dune Development in Western Zambia. Quaternary Research, 52(1), 44-55.

Oswell WC, 1900. William Cotton Oswell: hunter and explorer. New York

Paillou P, Schuster M, Tooth S, Farr T, Rosenqvist A, Lopez S, and Malezieux JM, 2009. Mapping of a major paleodrainage system in eastern Libya using orbital imaging radar: The Kufrah River. Earth and Planetary Science Letters 277, 327–333.

Paillou P, Tooth S, and Lopez S, 2012. The Kufrah paleodrainage system in Libya: A past connection to the Mediterranean Sea? Comptes Rendus - Geoscience 344, 406–414.

Partridge TC, Demenocal PB, Lorentz SA, Paiker M.J, and Vogel JC, 1997. Orbital forcing of climate over South Africa: A 200,000-year rainfall record from the Pretoria Saltpan. Quaternary Science Reviews 16, 1125–1133.

Passarge, S., 1904. Die Kalahari. Berlin, Dietrich Reimer (Ernst Vohsen)

Pekel J.-F, Cottam A, Gorelick N, Belward AS, 2016. High-resolution mapping of global surface water and its long-term changes. Nature 540, 418–422.

Prescott JR, and Hutton JT, 1994. Cosmic ray contributions to dose rates for luminescence and ESR dating: large depths and long-term time variations. Radiation Measurements 23: 497–500.

Ralph TJ, Hesse P, and Kobayashi T, 2016. Wandering wetlands: spatial patterns of historical channel and floodplain change in the Ramsar-listed Macquarie Marshes, Australia. Marine and Freshwater Research, 67, 782-802.

Ralph TJ, Kobayashi T, Garcia A, Hesse P, Yonge D, Bleakley N, and Ingleton T, 2011. Palaeoecological responses to to avulsion and floodplain evolution in a semiarid Australian freshwater wetland. Australian Journal of Earth Sciences, 58, 75-91.

Ramberg L, 1997. A pipeline from the Okavango River? Ambio 26: 129.

Rodell M, Famiglietti JS, Wiese DN, Reager JT, Beaudoing HK, Landerer FW, and Lo M-H, 2018. Emerging trends in global freshwater availability. Nature 557, 651-659.

Rodnight H, Duller GAT, Tooth S, and Wintle A, 2005. Optical dating of a scroll-bar sequence on the Klip River, South Africa, to derive the lateral migration rate of a meander bend. The Holocene 15: 802-811.

Rodnight H, Duller GAT, Wintle AG, Tooth S, 2006. Assessing the reproducibility and accuracy of optical dating of fluvial deposits. Quaternary Geochronology 1: 109-120.

Shaw P, 1985. The desiccation of Lake Ngami: An historical perspective. The Geographical Journal, 151, 318-326.

Shongwe ME, van Oldenborgh GJ, van den Hurk BJJM, de Boer B, Coelho CAS, van Aalst MK, 2009. Projected Changes in Mean and Extreme Precipitation in Africa under Global Warming. Part I: Southern Africa. Journal of Climate 22, 3819–3837.

Schefuß E, Kuhlmann H, Mollenhauer G, Prange M, and Pätzold J, 2011. Forcing of wet phases in southeast Africa over the past 17,000 years. Nature 480, 509–512.

Singarayer JS, and Burrough SL, 2015. Interhemispheric dynamics of the African rainbelt during the late Quaternary. Quaternary Science Reviews 124, 48–67.

Skonieczny C, Paillou P, Bory A, Bayon G, Biscara L, Crosta X, Eynaud F, Eacute BM, Revel M, Aleman N, Barusseau JP, Vernet R, Lopez S, Grousset F, 2015. African humid periods triggered the reactivation of a large river system in Western Sahara. Nature Communications 6, 1–6.

Smith N, McCarthy TS, Ellery WN, Merry C, and Rüther H, 1997. Avulsion and anastomosis in the Panhandle region of the Okavango Fan, Botswana. Geomorphology, 20, 49-65.

Stigand AG, 1923. Ngamiland. The Geographical Journal, 62, 402-419.

Stouthamer E, and Berendsen H, 2007. Avulsion: The relative roles of autogenic and allogenic processes. Sedimentary Geology, 198, 309-325.

Thito K, Wolski P, and Murray-Hudson M, 2016. Mapping inundation extent, frequency and duration in the Okavango Delta from 2001 to 2012. African Journal of Aquatic Science, 41, 267-277.

Thomas DSG, and Burrough SL, 2012. Interpreting geoproxies of late Quaternary climate change in African drylands: Implications for understanding environmental change and early human behaviour. Quaternary International 253, 5–17.

Thomas DSG, and Shaw PA, 2002. Late Quaternary environmental change in central southern Africa: New data, synthesis, issues and prospects. Quaternary Science Reviews 21, 783–797.

Tierney JE, Lewis SC, Cook BI, LeGrande AN, and Schmidt GA, 2011. Model, proxy and isotopic perspectives on the East African Humid Period. Earth and Planetary Science Letters 307, 103–112.

Tooth S, Ellery F, Grenfell M, Thomas A, Kotze D, and Ralph T, 2015. 10 reasons why the geomorphology of wetlands is important. Booklet produced after inaugural meeting of the Wetlands in Drylands Research Network. Available at www.wetlandsindrylands.net/downloads-2/

Tooth S, and McCarthy TS, 2004. Controls on the transition from meandering to straight channels in the wetlands of the Okavango Delta, Botswana. Earth Surface Processes and Landforms, 29, 1627-1649.

Tooth S, and McCarthy TS, 2007. Wetlands in Drylands: geomorphological and sedimentological characteristics, with emphasis on examples from southern Africa. Progress in Physical Geography, 31, 3-41.

Tooth S, Rodnight H, Duller G, McCarthy TS, Marren P, and Brandt D, 2007. Chronology and controls of avulsion along a mixed bedrock-alluvial river. Bulletin of the Geological Society of America, 119, 452-461.

Tooth S, 2012. Arid geomorphology: Changing perspectives on timescales of change. Progress in Physical Geography, 36, 262-284.

VanderPost C, 2005. Early maps of Ngamiland and the Okavango Delta. Botswana Notes and Records 37: 196-207.

Weissmann GS, Hartley AJ, Nichols GJ, Scuderi LA, Olson M, Buehler H, and Banteah R, 2010. Fluvial form in modern continental sedimentary basins: Distributive fluvial systems. Geology, 38(1), 39–42.

Wilson BH, 1973. Natural and man-made changes in the channels of the Okavango Delta, Botswana Notes and Records, 5, 132-153.

Wintle AG, and Murray AS, 2006. A review of quartz optically stimulated luminescence characteristics and their relevance in single-aliquot regeneration dating protocols. Radiation Measurements 41: 369-391.

Wohl E, 2011. What should these rivers look like? Historical of variability and human impacts in the Colorado Front Range, USA. Earth Surface Processes and Landforms, 36, 1378-1390.

Wohl E, and Rathburn S, 2013. Guest Editorial: Introduction to special issue on historical range of variability. Earth Surface Processes and Landforms, 38, 213-216.

Wolski P, Todd MC, Murray-Hudson MA, and Tadross M, 2012. Multi-decadal oscillations in the hydro-climate of the Okavango River system during the past and under a changing climate. Journal of Hydrology 475, 294–305.

Woodward JC, Williams MAJ, Garzanti E, Macklin MG, Marriner N, 2015a. From source to sink: Exploring the Quaternary history of the Nile. Quaternary Science Reviews 130, 3–8.

Woodward J, Macklin M, Fielding L, Millar I, Spencer N, Welsby D, Williams M, 2015b. Shifting sediment sources in the world's longest river: A strontium isotope record for the Holocene Nile. Quaternary Science Reviews 130, 124–140.

Supplementary Material
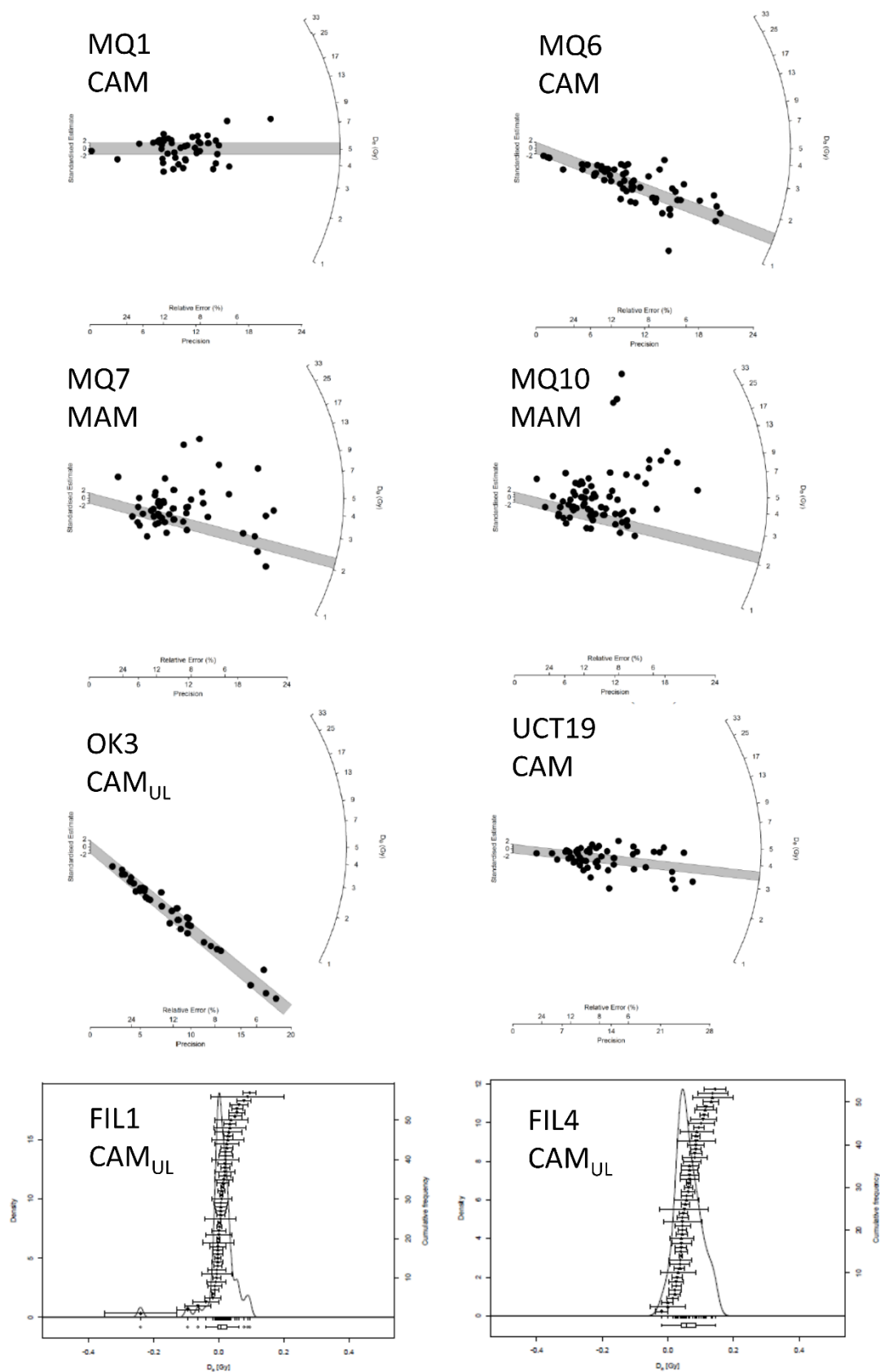
Supplementary Fig. 1. Radial plots of equivalent dose (D_e) values from individual grains of quartz for the Okavango OSL samples. The grey shaded bar represents the D_e used for age calculation based on the central age model (CAM), unlogged central age model (CAM_{UL}) or the minimum age model (MAM). D_e values for FIL1 and FIL4 are too young to display in a radial plot.

Supplementary Table 1. OSL dosimetry data for the Okavango samples. Ages are expressed as thousands of years (ka) before 2017 AD. Dose rate includes internal alpha dose of 0.026 ± 0.007 Gy ka^{-1}.

Sample	Depth (m)	Water content (%)	Grain size (μm)	Beta dose (Gy ka^{-1})	Gamma dose (Gy ka^{-1})	Cosmic dose (Gy ka^{-1})	Total dose rate (Gy ka^{-1})
MQ1	1.10 ± 0.1	25 ± 5	180–212	0.62 ± 0.04	0.61 ± 0.05	0.19 ± 0.01	1.44 ± 0.06
MQ6	1.10 ± 0.1	25 ± 5	180–250	0.10 ± 0.01	0.10 ± 0.01	0.19 ± 0.01	0.41 ± 0.02
MQ7	1.10 ± 0.1	25 ± 5	180–212	0.17 ± 0.01	0.16 ± 0.02	0.19 ± 0.01	0.54 ± 0.02
MQ10	1.12 ± 0.13	25 ± 5	180–212	0.54 ± 0.03	0.48 ± 0.04	0.19 ± 0.01	1.24 ± 0.05
FIL1	0.90 ± 0.1	25 ± 5	180–212	0.12 ± 0.01	0.12 ± 0.02	0.19 ± 0.01	0.46 ± 0.02
FIL4	0.90 ± 0.1	25 ± 5	180–120	0.08 ± 0.01	0.07 ± 0.01	0.19 ± 0.01	0.37 ± 0.01
UCT19	1.05 ± 0.1	25 ± 5	180–250	0.53 ± 0.03	0.50 ± 0.04	0.19 ± 0.01	1.25 ± 0.05
OK3	0.85 ± 0.1	25 ± 5	180–212	0.64 ± 0.04	0.56 ± 0.04	0.20 ± 0.01	1.42 ± 0.06

CHAPTER 4

Mechanisms of channel avulsion and failure in the Panhandle region of the Okavango Delta, Botswana

Ralph T.J.[1], Larkin Z.T.[1], McCarthy T.S.[2], Humphries M.[3], Tooth S.[2,4] *

[1] Department of Environmental Sciences, Macquarie University, NSW, Australia

[2] School of Geosciences, University of the Witwatersrand, Johannesburg, South Africa

[3] Molecular Sciences Institute, School of Chemistry, University of the Witwatersrand, Johannesburg, South Africa

[4] Department of Geography and Earth Sciences, Aberystwyth University, Aberystwyth, UK

*See Table 1.1 in chapter 1 for author contributions.

Abstract

Environmental boundary conditions control the flux of energy and materials within rivers. Intrinsic processes responsible for the transfer and deposition of sediment in rivers interact with resisting features such as vegetation to drive geomorphological changes, including channel formation, branching, and termination. Intrinsic mechanisms of channel adjustment in the Okavango River and its branches in the Panhandle region of the Okavango Delta, Botswana, are revealed using evidence collected from field campaigns spanning 21 years. In a ~26 km long reach of the middle Panhandle, the Okavango River is characterised by an anastomosing (multiple channel) pattern consisting of two named branches (Okavango, Filipo) and several cross branches (channel B, C, D-E, and D-F). From 1995-2016, the upper Filipo channel experienced significant declines in width, discharge, bedload transport and water-surface slope relative to the Okavango trunk stream, while the lower Filipo increased in all these respects owing to flow capture by the cross-cutting channel 'C'. Consequently, the upper Filipo and the Okavango downstream of channel C suffered significant hydro-geomorphological declines and are primed for abandonment. Overall, the anastomosing reach lost two active channels, two bifurcation nodes and one return junction due to consolidation of flow in the Okavango, Filipo and channel C, a net loss of at least ~15 km of channel length. Water-surface elevations in the Okavango and Filipo have largely equilibrated over time, despite significant local changes in width, discharge, bedload and slope. The current anastomosing pattern is likely a transitional state as channel C and the lower Filipo overtake adjacent failing channel segments. The mechanisms of avulsion and channel failure include both channel diversions and excision due to erosion in the early stages, and vegetation encroachment and bed aggradation in the later stages, but only a small proportion of new channels become stable and efficient and are therefore maintained. A threshold of discharge (~20 m^3 s^{-1}) exists, below which bedload sediment transport is minimal triggering channel failure. The mechanisms of channel initiation, development and failure are part of a cycle of avulsion leading to channel adjustment and realignment

in the system. In the absence of external forcing to influence avulsion, the river will likely continue its transition towards a single-thread planform, while the avulsion cycle may be reset if intrinsic fluvial inefficiency triggers channel instability and new flow diversions in the system. These insights into fluvial behaviour can inform river and ecosystem management, particularly in view of future projected climate and land use changes that may precipitate a dramatic fluvial response.

Introduction

Alluvial rivers are dynamic systems that adjust over time in response to pressures from extrinsic forces, such as climate and tectonics, and from intrinsic processes, such as sediment accumulation and erosion. Avulsion, the process of flow diversion to create a new channel on the floodplain, is one of the key mechanisms through which alluvial rivers can modify their planform to convey water and sediment downstream (Bridge and Leeder, 1979; Smith et al., 1989; Bryant et al., 1995; Nanson and Knighton, 1996; Slingerland and Smith, 2004; Stouthamer and Berendsen, 2007). Avulsion may be initiated by extrinsic factors, for example, base-level upsurge due to neotectonic activity or sea level rise (Bowler, 1967), intensified hydrological and sediment regimes, and/or altered riparian conditions. Avulsion may also be driven by hydraulic inefficiency. For example, when an existing channel cannot adjust its planform or otherwise increase its slope to maintain sediment transport, a marked reduction in transport capacity leads to formation of a new channel that bypasses the inefficient reach (reach-scale avulsion), or that conveys sediment around an obstructed segment (local avulsion, or channel cutoff). Avulsions are triggered by different factors including floods or other types of extreme events (e.g. mass movements, ice jams, log jams), animal activity (e.g. hippopotamus trails, beaver dams), and human activities (e.g. vegetation clearance, earth works) (McCarthy et al., 1998; Smith and Pearce, 2002; Tooth et al., 2007; Phillips, 2012; Polvi and Wohl, 2013). The closer a river system is to an avulsion threshold, the more likely an avulsion will occur; thus, the type and rate of biophysical processes responsible for priming a system are critical, and it is not always the largest or most significant event (e.g. a high magnitude, low frequency flood) that triggers an avulsion (Jones and Schumm, 1999).

Avulsion may lead to the formation of one or more new channels that coexist with older channels, to form an anabranching or distributary pattern, or new channel/s that eventually take over from older channel/s leading to channel abandonment in single-thread or multi-channelled systems. Anabranching rivers are differentiated on the basis of their hydrological, sedimentological and morphological traits, and may include relatively steep, high-energy wandering gravel bed rivers, laterally active mixed-load rivers, sand-dominated ridge-forming rivers, and low-energy, mud- and/or organic-dominated anastomosing rivers (Nanson and Knighton, 1996). Avulsion processes and alluvial architecture of anabranching rivers have been described in a range of settings globally, from the semi-arid and arid regions of inland Australia (e.g. Schumm, 1968; Tooth and Nanson, 1999; Ralph and Hesse, 2010; Ralph

et al., 2016), Africa (e.g. Jacobberger, 1987; McCarthy et al., 1991; 1992; Smith et al., 1997), North America (e.g. Schumann, 1989; Miller, 1991), the Middle East (e.g. Aqrawi, 2001; Morozova, 2005) and the Indian subcontinent (e.g. Jain and Sinha, 2004; Giosan et al., 2012), to the more humid settings of Canada (e.g. Makaske et al., 2002; Toonen et al., 2016), South America (e.g. Stevaux and Souza, 2004; Donselaar et al., 2013; Li et al., 2015) and Europe (e.g. Berendsen and Stouthamer, 2002). Indeed, anabranches characterise most large alluvial rivers of the world, and research suggests that in certain situations they have hydraulic advantages over single-thread rivers in equivalent settings (Jansen and Nanson, 2004; Huang and Nanson, 2007). In low-energy settings, alluvial rivers self-regulate their energy expenditure to create the maximally efficient flow pathway(s) possible (i.e. the highest possible ratio of sediment transported to stream power expended will tend to be the most stable channel form under the least action principle; Huang et al., 2004; Huang and Nanson, 2008; Nanson and Huang, 2017; 2018) which may have multi-channelled configurations if stream power and sediment transport efficiency cannot be maintained in a single channel (Nanson and Huang, 1999; Huang and Nanson, 2007). In other systems characterised by dramatic and persistent downstream declines in discharge and stream power, avulsion may not be able to improve flow and sediment transport efficiency enough, eventually leading to channel breakdown and floodout formation (e.g. Ralph and Hesse, 2010; Tooth, 2000).

Avulsion is a ubiquitous phenomenon leading to bifurcations and multi-channelled rivers globally, therefore it is critical to determine and quantify the types and rates of processes governing avulsion within the context of the natural (or anthropogenically altered) range of variability for such systems (Bryant et al., 1995). Key questions include: 1) what combination of extrinsic and intrinsic processes control avulsion leading to multiple channels and do these lead to establishment of a quasi-equilibrium condition over the long-term?; and 2) if avulsion in a river is cyclic, what are the thresholds that define the frequency of avulsion?. Understanding the mechanisms of avulsion and the after-effects leading alluvial channels to become stable or unstable are also critical for river and wetland management. Behavioural analysis of rivers can be used to more accurately predict future trajectories of fluvial change in systems that are pressured by water abstraction and other forms of anthropogenic activities. Rarely, however, are processes contributing to avulsion and anastomosis quantified through field campaigns over many years in large and/or remote catchments in semi-arid and arid landscapes (drylands). Such catchments also tend to have a dearth of hydrological data and relatively low-resolution digital elevation data, making robust measurement and modelling of avulsion processes a difficult undertaking. We address this deficit of information for an internationally significant dryland river, the Okavango River, in order to quantify and assess the mechanisms of avulsion, and the cause-effect relationships between discharge, bedload sediment transport, channel slope and channel initiation and abandonment due to avulsion.

The Okavango Delta in the northern Kalahari Desert of Botswana is an extensive (>40,000 km^2) World Heritage and Ramsar-listed riverine system with numerous channels that are highly susceptible to

avulsion (Fig. 1). The Delta has formed in response to incipient continental rifting and the graben that the present-day alluvial system occupies is slowly filling with sediment derived from the upstream catchment (McCarthy, 2013). The river receives perennial and highly seasonal discharge due to summer rainfall in the headwater catchments in central Angola. The Delta has two main geomorphic domains: the confined (up to 12 km wide) elongated depression known as the Panhandle, where the Okavango River and its branches meander through permanent wetlands; and the broader (up to 120 km wide) Fan, where water and sediment disperse through distributary channels into permanent and seasonal wetlands (Fryirs et al., 2018). Flow sometimes extends to the southeastern, peripheral region of the Delta, where the Boteti River occasionally receives flow and feeds into the Makgadikgadi lacustrine basin (Gumbricht et al., 2001).
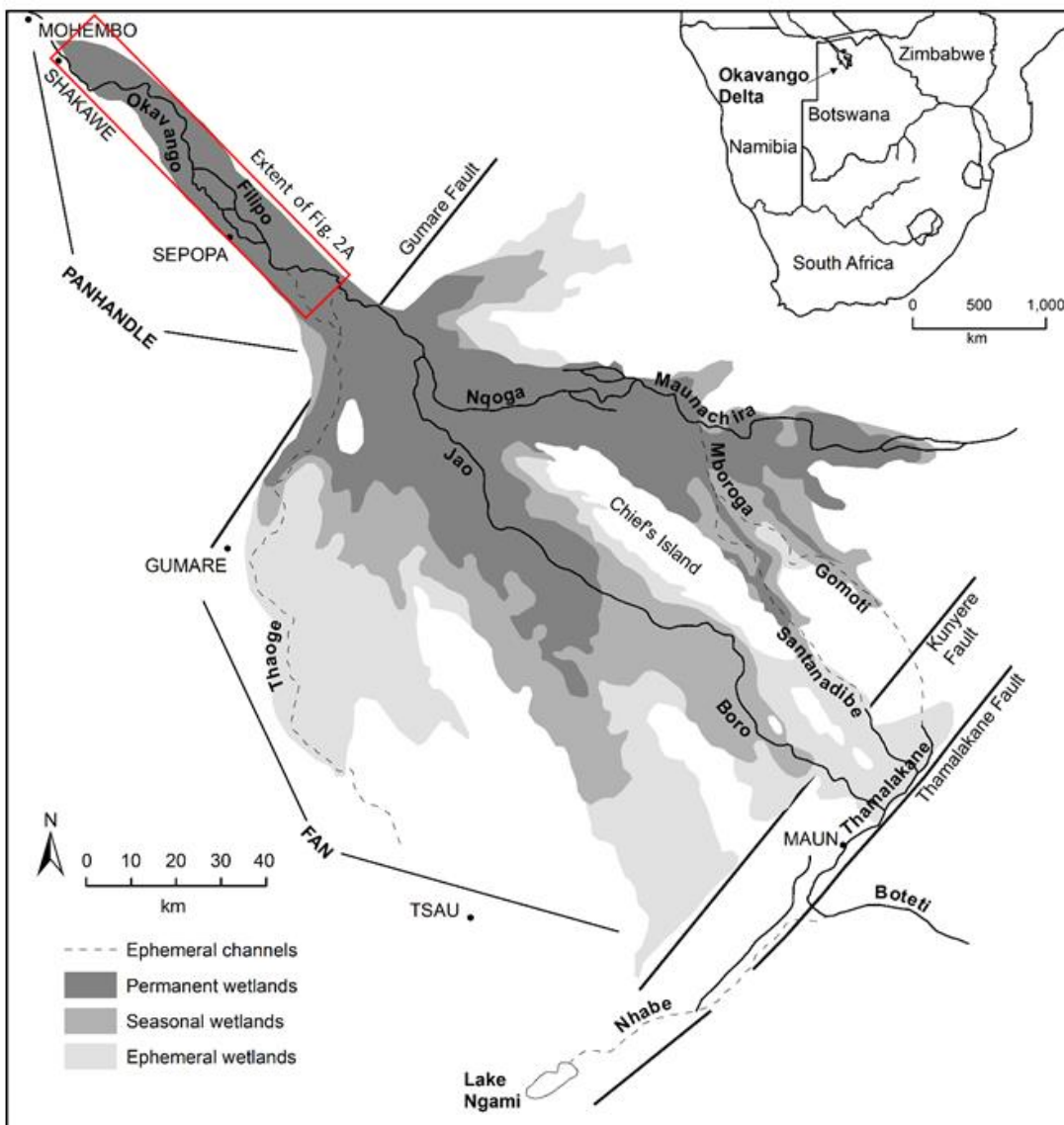
Figure 1. The Okavango Delta in Botswana.

The low-gradient, meandering channel of the Okavango River in the Panhandle experiences a significant reduction in size before dividing into the slightly steeper distributary reaches on the Fan (Tooth and McCarthy, 2004; McCarthy, 2013). The trunk stream has both regular and irregular meanders, and numerous scroll bars, cutoffs, point bars and palaeochannels. Bedload sediment transport greatly exceeds suspended-load sediment transport in the system, and dense vegetation (mainly *Cyperus papyrus* and *Phragmites spp.*) and peat form permeable organic-rich banks that stabilise and confine the channels but allow lateral water seepage into the surrounding wetlands (McCarthy, et al., 1991). Interactions between sediment deposition in and around channels, vegetation growth, fires, and island formation by chemical sedimentation create a mosaic of landforms with high geomorphological and biological diversity throughout the Delta (McCarthy, 2013). In the Panhandle, a prominent ~26 km (valley distance) anastomosing reach occurs where numerous channels split from and rejoin the Okavango trunk stream (Fig. 1). The oldest active secondary channel (Filipo) diverges from the Okavango upstream of younger channels that link the Okavango to the Filipo. These secondary channels incorporate older, abandoned channel segments. Smith et al. (1997) proposed that avulsions in the anastomosing reach of the Okavango Panhandle were initiated by base-level displacement due to local faulting. In contrast, avulsion in the unconfined reaches on the Fan is controlled by channel perching, which occurs as a result of rapid in-channel deposition of bedload material and heavy vegetation confinement (see McCarthy, et al., 1992; McCarthy, 2013). Thus, dense vegetation causes a reduction in flow velocity that promotes in-channel aggradation, with a series of positive feedback mechanisms – that is, further dissipation of flow, vegetation growth and encroachment in channels, and entrapment of floating aquatic vegetation and clastic sediments. Elevated water-surface levels in these perched channels compared with the surrounding wetlands lead to channel failure when water escapes through breaches in the vegetated margins, or along pre-existing hippopotamus trails, which become new channels (McCarthy et al., 1992). These new channels on the Fan are initially erosional, but over time both the new channel and adjacent wetlands aggrade until abandonment occurs and the cycle is repeated (McCarthy, et al., 1988).

This paper documents the internal mechanisms of channel adjustment in the Okavango River and its branches in the Panhandle region of the Okavango Delta using evidence collected from four field campaigns spanning 21 years (i.e. 1995, 2008 (2), 2016). This study is an extension of the Smith et al. (1997) dataset collected in 1995, with data from repeat surveys in 2008 and 2016. We quantify and assess the hydrological processes responsible for the transfer and deposition of bedload sediment that interact with vegetation to drive geomorphological changes in the Panhandle, including channel formation, branching, and termination. We discuss the role of avulsion and particularly channel failure in the development and evolution of a dynamic anastomosing reach in response to sustained flow and sediment load, and we discuss the role of avulsion in the Okavango in the context of avulsion in other dryland settings.

Methods

Data for this study were collected over four field campaigns between 1995 and 2016, using a range of field and desktop methods.

Channel mapping and morphometrics

Channel mapping in the Panhandle region of the Okavango Delta (Fig. 2A and 2B) was undertaken using standard methods, with centrelines, margins and other geomorphological features (e.g. point bars, scroll bars, cutoffs, palaeochannels) digitised manually from aerial photography and satellite imagery in ArcMap v10.3 (see Larkin et al. in prep. [Chapter 3]). All channel morphometric measurements were undertaken during field campaigns in September 1995, April and November 2008, and August 2016 at cross-sections located at channel bifurcation or return nodes in the anastomosing reach (see Smith et al. 1997). The cross-sections were situated on relatively straight reaches at a distance of 50-100 m from the bifurcation or return nodes (nodes A-F; Fig. 2C). Channel width and depth measurements were obtained using standard tape and pole techniques from tethered boats (see McCarthy et al. 1991).

Water depth profiles, velocity and discharge

Water depth profiles and velocity were measured at cross-sections (nodes A-F) in 1995, 2008 and 2016 to assess the distribution of flow in channels of the anastomosing reach and how they have changed over time. In September 1995 (see Smith et al. 1997), November 2008 and August 2016, water levels and discharges were measured during periods of declining or low flow (i.e. sub-bankfull flow) in the Panhandle approximately 4-7 months after peak annual discharge which occurs around April (Fig. 3). In contrast, water levels and discharges (and bedload transport rates) were measured during a period of high flow in the Panhandle in April 2008. Velocity was measured from tethered boats using vane-type current meters positioned successively at either 0.5 or 1 m depth intervals and at varying distances (up to 4 m intervals) across each channel (see McCarthy et al. 1991; Smith et al. 1997). Flow velocity and depth measurements were contoured and spatially integrated to obtain mean velocity (m s^{-1}) and channel cross-sectional area (m^2), together yielding discharge (m^3 s^{-1}) for each cross-section site (see Supplementary Figure 1 for 2016 cross-sections). As each node had three channel segments, two discharges were measured directly and the third calculated by difference. The accuracy of this method was confirmed by Smith et al. (1997), who showed that values calculated by difference were within 2 % of total measured discharge.
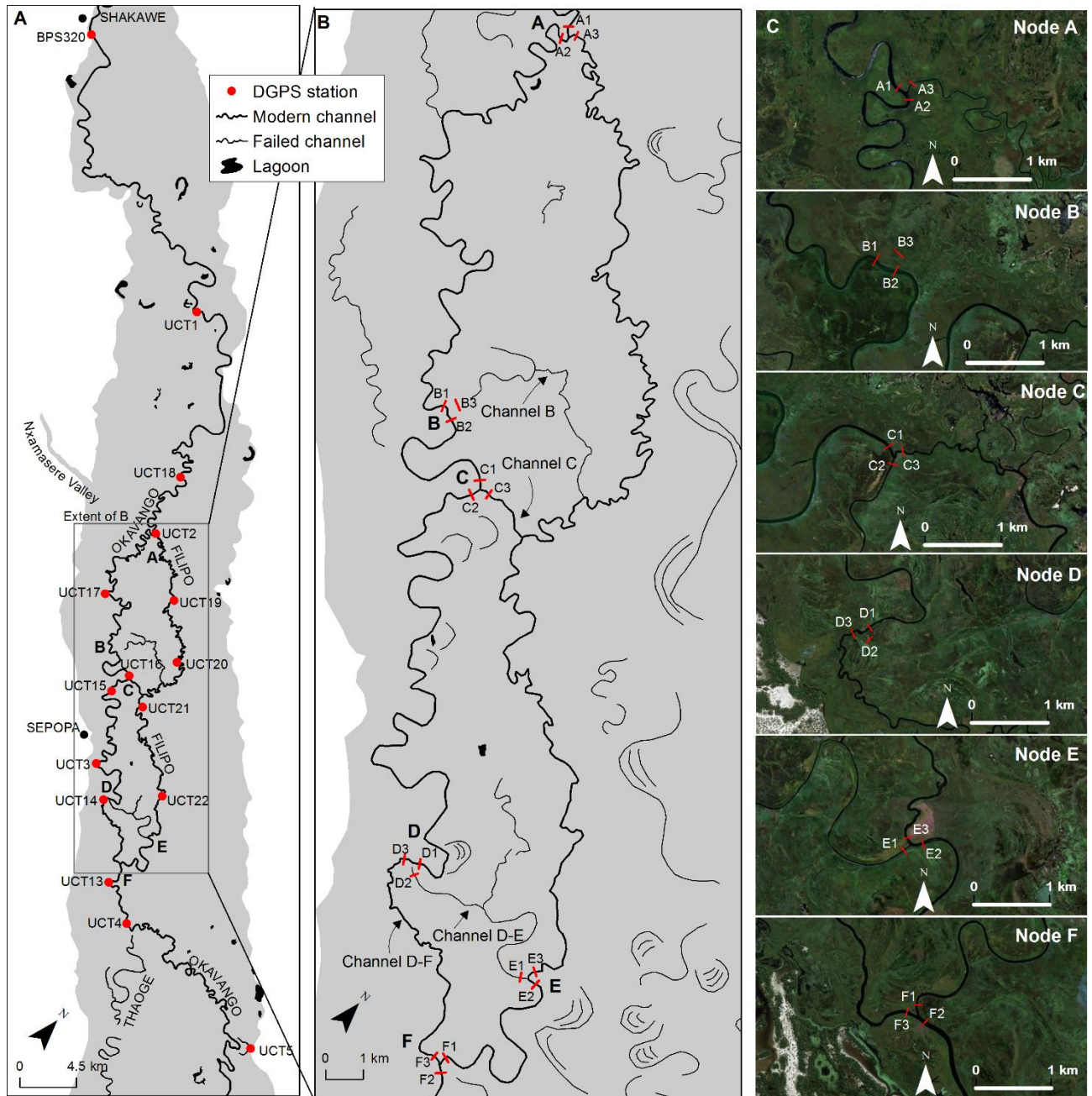
Figure 2. (A) The Okavango Panhandle with DGPS station locations where channel morphometrics, flow velocity and discharge and bedload transport rates were measured. Stations A, B, C, and D are at avulsion nodes (bifurcation points), while stations E and F are at convergent return junctions. All DGPS stations are in the same location as those reported in Smith et al. (1997). (B) The anastomosing reach of the Okavango Panhandle including locations of cross-sections where velocity and discharge were measured in 1995, 2008, and 2016. (C) Satellite images of nodes A-F.
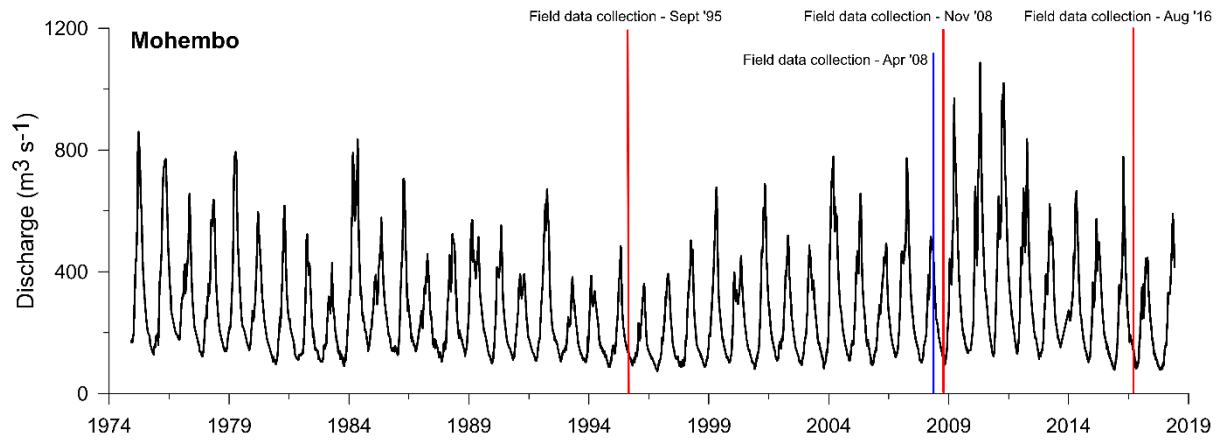
Figure 3. A 44-year time series of discharge at the Mohembo gauge on the Okavango River at the head of the Panhandle. Overlain in red are the three field campaigns when data was collected under waning or low flow (sub-bankfull) conditions. Overlain in blue is the field campaign when data was collected under high flow conditions. Data source: Okavango Research Institute (2018).

Bedload sediment transport

Bedload sediment transport rates (kg s^{-1}) were measured under declining flow conditions in September 1995 and under high flow conditions in April 2008, using Helley-Smith bedload samplers deployed in a uniform grid pattern. At each site, 24 to 72 individual measurements were taken to account for spatial variability and channel width (see McCarthy et al. 1991). The derivative equation of a linear regression for measured bedload transport and discharge for September 1995 and April 2008 was used to model bedload transport rates for November 2008 and August 2016 using discharge measurements from those later field campaigns (Supplementary Figure 2). Bedload transport is positively correlated with discharge (R = 0.89; Supplementary Fig. 2). Values have been normalised to September 1995 using multipliers in order to calculate proportional changes in bedload transport rates between different channels (i.e. 2008 bedload transport values multiplied by 0.8717, and 2016 bedload transport values multiplied by 0.7212, to normalise to values from Sept, 1995).

Water-surface elevation and channel slope

DGPS stations for water-surface elevation measurements were equivalent to those established in September 1995 by Smith et al. (1997) (Fig. 2; Supplementary Table 1). Repeat DGPS measurements were conducted in November 2008 using the same methods as Smith et al. (1997), as described by Merry et al. (1998), and again in August 2016 using slightly modified methods. Smith et al. (1997) established DGPS stations on elevated ground near active channels (usually abandoned termite mounds or small islands) and then surveyed to the waterline using a digital level. However, in 2016 none of the original benchmarks installed by Smith et al. (1997) could be physically located and so water-surface elevations were measured at the waterline as close as possible (usually within 50 m) to the coordinates of Smith et al. (1997). All stations were measured over a period of 7-10 days and individual observations lasted from 0.5 to 1 hour, and water level fluctuations were negligible during each field campaign. In 2016, each position was logged using a Trimble® GPS Pathfinder® ProXRT receiver and antenna. The

vertical distance between the antenna and the surface of the water was measured manually using a tape measure (±0.2 cm). Post-processed differential correction was performed in Pathfinder Office, resulting in a vertical precision typically within 5 cm, and all better than 10 cm. Channel slope estimates were derived using differences in elevation over distance between DGPS stations.

Results

Channel configuration

Channel configuration in the anastomosing reach and historical changes due to avulsion prior to 1995 are described in detail by Smith et al. (1997) and Larkin et al. (in prep) [i.e. Chapter 3]. In 1995, the anastomosing study reach had five channels with four bifurcation nodes (divergent avulsion points) and four return junctions (confluences) active. The Filipo and three other channels here referred to as 'B', 'C' and 'D-F', diverted from and ultimately rejoined the Okavango River (Fig. 2). The eastward diversion of the Filipo channel (at node A, formed before 1955) is located ~23 km upstream of its 1995 return junction (at node E). The eastward divergence points of channels B (at node B, formed before 1962) and C (at node C, formed circa 1995) from the Okavango towards the Filipo are a further ~10 and 12 km downvalley from the initial Filipo bifurcation, respectively (Fig. 2). Approximately 10 km further downvalley, channel D-F diverged westward from the Okavango (at node D, formed between 1962 and 1991) and rejoined the Okavango downstream (at node F), below the Filipo confluence in 1995 (at node E) (Fig. 2). Channel D-F created a shortcut for flow in the Okavango trunk stream between nodes D and E (here referred to as 'D-E'), a reduction of ~6 km in channel length (Fig. 2, Smith et al. 1997).

In 2008, the reach had four channels with two bifurcation nodes and four return junctions active. Channel D-F had widened and captured significant flow, leading to a complete avulsion and the abandonment of channel D-E which was engulfed by vegetation (abandonment complete by 2011; Larkin et al., in prep [Chapter 3]). The bifurcation point at node D was abandoned as channel D-F became the single dominant flow path bypassing in this segment, although some leakage from the wetlands returned to the Filipo at node E (Fig. 2). Similarly, the bifurcation point at node B had closed with vegetation by 2008 (abandonment complete by 2011), leading to the partial failure of channel B further downstream. The other segments of the Okavango, Filipo, and channel C all continued to carry flow between 1995 and 2008 (Fig. 2).

The trend of channel failure has continued to 2016, when the reach had three channels with two bifurcation nodes and three return junctions active. Channel B and its confluence with the Filipo were entirely abandoned by 2016, and flow capture by channel C had increased, leading to greater diversions from the Okavango to the Filipo in this segment. Due to the majority abandonment of channel D-E, the main confluence of the Okavango and Filipo presently occurs at node F. Channel pattern and planform have remained relatively stable in the remaining active channels (Larkin et al., in prep [Chapter 3]),

although there have been significant local changes in channel width, velocity and discharge, bedload transport, and slope, as described below.

Channel width

Measurements from the field campaigns show that channel width has changed between 1995, 2008 and 2016 in segments of the Okavango River, the Filipo channel, and the branches that connect (or shortcut) the Okavango and Filipo (Fig. 4; Table 1). At node A, channel width in the upper segment of the Okavango decreased overall by ~8 % and the upper Filipo decreased by ~43 %. At node B, channel B closed entirely with vegetation since 1995 (i.e. channel failure). At node C, Okavango channel width decreased by ~26 % and channel C increased in width by ~108 %. At node D, the Okavango decreased in width by ~21 %, while channel D-E closed entirely with vegetation since 1995 (i.e. channel failure) and channel D-F became enlarged (incomplete data). At node E, channel D-E decreased in width by ~44 % and the Filipo increased by ~18 %. At node F, the lower segment of channel D-F increased by ~10 % and, between 2008 and 2016, the Filipo decreased by ~11 % near the Okavango and Filipo junction .
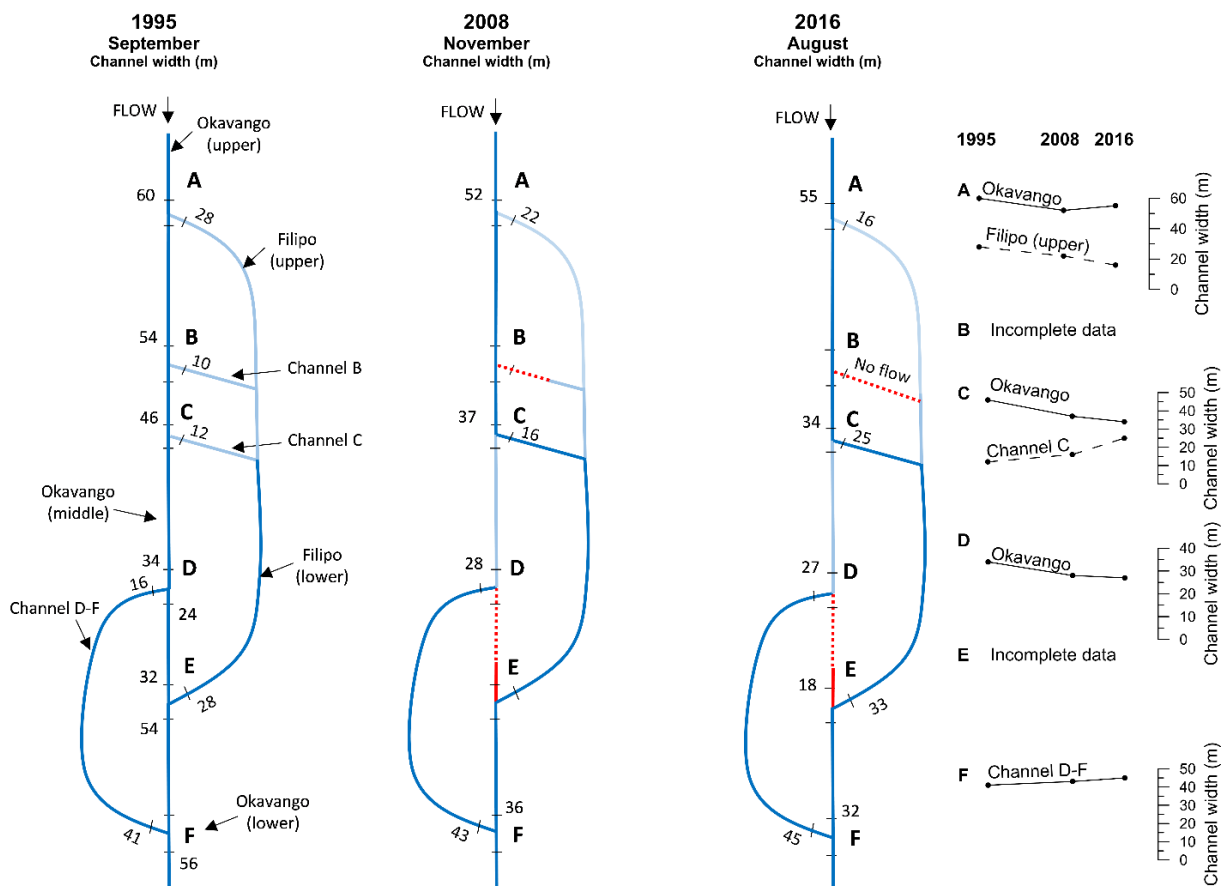
Figure 4. Schematic diagram of measured channel widths at channel junctions in the anastomosing reach of the Okavango River in the Panhandle for 1995, 2008, and 2016. A synthesis of change in channel width over time is presented at the right side of the figure. Dark blue lines are the dominant channels, light blue are secondary or failing channels, and red dashed lines are failed channels.

Table 1. Data for the field sites located around six DGPS stations (nodes A-F) in the anastomosing reach of the Okavango Panhandle. See Supplementary Table 2 for channel depth and velocity data.

DGPS station	Node	Node type[a]	Site	Description	Width (m)			Δ width (%)	Discharge (m³ s⁻¹)			Δ discharge (%)	Bedload transport (kg s⁻¹)			Δ bedload (%)	Channel slope (m m⁻¹)			Δ slope (%)
					1995	2008	2016	Width	1995	2008[c]	2016[c]	Discharge	1995	2008[c]	2016[c]	Bedload	1995	2008	2016	Slope
UCT2	A	Bif	A1	Oka. U/S	60	52	55	-8	106.80	106.80	106.80	0.0	1.45	1.45	1.45	0.0	0.0000966	0.0000597	0.0000812	-15.9
			A2	Oka. D/S	-	-	-	-	79.80[d]	86.36[d]	87.26[d]	9.4	1.09[d]	1.45[d]	1.45[d]	33.0	-	-	-	-
			A3	Filipo	28	22	16	-43	27.00	20.44	19.54	-27.6	0.36	0.00	0.00	-100.0	0.000143	0.0001274	0.0000952	-33.4
-	B	Bif	B1	Oka. U/S	54	-	-	-	87.90	-	-	-	1.55	-	-	-	0.0000907	0.0001053	0.0000995	9.7
			B2	Oka. D/S	-	-	-	-	78.0[d]	-	-	-	1.48[d]	-	-	-	-	-	-	-
			B3	Channel B	10	-	-	-	9.90	N/A	N/A	-	0.07	-	-	-	-	-	-	-
UCT16	C	Bif	C1	Oka. U/S	46	37	34	-26	76.10	89.74	86.44	13.6	1.32	1.13	1.08	-18.0	0.000106	0.0000695	0.0001311	23.8
			C2	Oka. D/S	-	-	-	-	55.10[d]	43.30[d]	36.70[d]	-33.4	1.12	0.82[d]	0.66[d]	-40.9	-	-	-	-
			C3	Channel C	12	16	25	108	21.00	46.44	49.74	136.8	0.20	0.31	0.42	110.5	0.000317	0.0001972	0.000158	-50.0
UCT14	D	Bif	D1	Oka U/S	34	28	27	-21	52.10	40.12	37.21	-28.6	0.73	0.19	0.20	-73.3	0.0000834	0.0000987	0.000098	17.5
			D2	Oka. D/S	24	-	-	-	23.10	N/A	N/A	-	0.26	-	-	-	-	-	-	-
			D3	Channel D-F	16	-	-	-	30.00	-	37.21[d]	24.0	0.36	-	-	-	-	-	-	-
-	E	Ret	E1	Channel D-E	32	-	18	-44	25.60	-	12.86	-49.8	0.18	-	0.00	-	-	-	-	-
			E2	Filipo D/S	54	-	-	-	86.30	-	85.58[d]	-0.8	0.74	-	0.84	12.9	-	-	-	-
			E3	Filipo U/S	28	-	33	18	60.70	-	72.72	19.8	0.36	-	0.84[d]	132.1	0.0000689	0.0000963	0.0001119	62.4
UCT13[b]	F	Ret	F1	Channel E-F	-	36	32	-11	74.90[d]	83.49	72.10	-3.7	1.07	1.01	0.82	-22.6	-	-	-	-
			F2	Oka. D/S	56	-	-	-	110.30	124.11[d]	127.17[d]	15.3	1.13	1.20[d]	1.34[d]	18.7	-	-	-	-
			F3	Channel D-F	41	43	45	10	35.4	40.6	55.1	55.6	0.07	0.20	0.52	695.7	0.000113	0.000976	0.0000397	-64.9

[a] Bif = bifurcation; Ret = return.
[b] DGPS station located downstream from node.
[c] Data normalised to 1995.
[d] Discharge calculated by difference.
- no data.
N/A discharge could not be measured.

Discharge and flow distribution

Discharge and flow distribution have changed between 1995, 2008 and 2016 in the study reach (Fig. 5; Table 1). At node A, discharge in the Filipo decreased by ~28 % while discharge increased by ~9 % in the Okavango. Flow ceased in channel B at node B. Downstream at node C, flow in the Okavango increased by ~14 %, while below the bifurcation, flow in the Okavango decreased by ~33 % and increased in channel C by ~137 %. At node D, flow in the Okavango decreased by ~29 %, while channel D-E ceased to flow and channel D-F increased by ~24 %. At node E, flow out of channel D-E decreased by ~50 % and the Filipo increased by ~20 %. At node F, flow in channel D-F increased by ~56 % and decreased in the Filipo by ~4 %. During all years measured, discharge at the downstream end of the anastomosing reach has exceeded discharge at the upstream end, which has been attributed to flows returning to channels from wetlands through leakage during the declining phase of the annual flood cycle (Smith et al., 1997). Nonetheless, flow out of the anastomosing reach below the confluence of the Okavango and Filipo increased by ~15 % between 1995 and 2016, despite less channels being active in 2016.
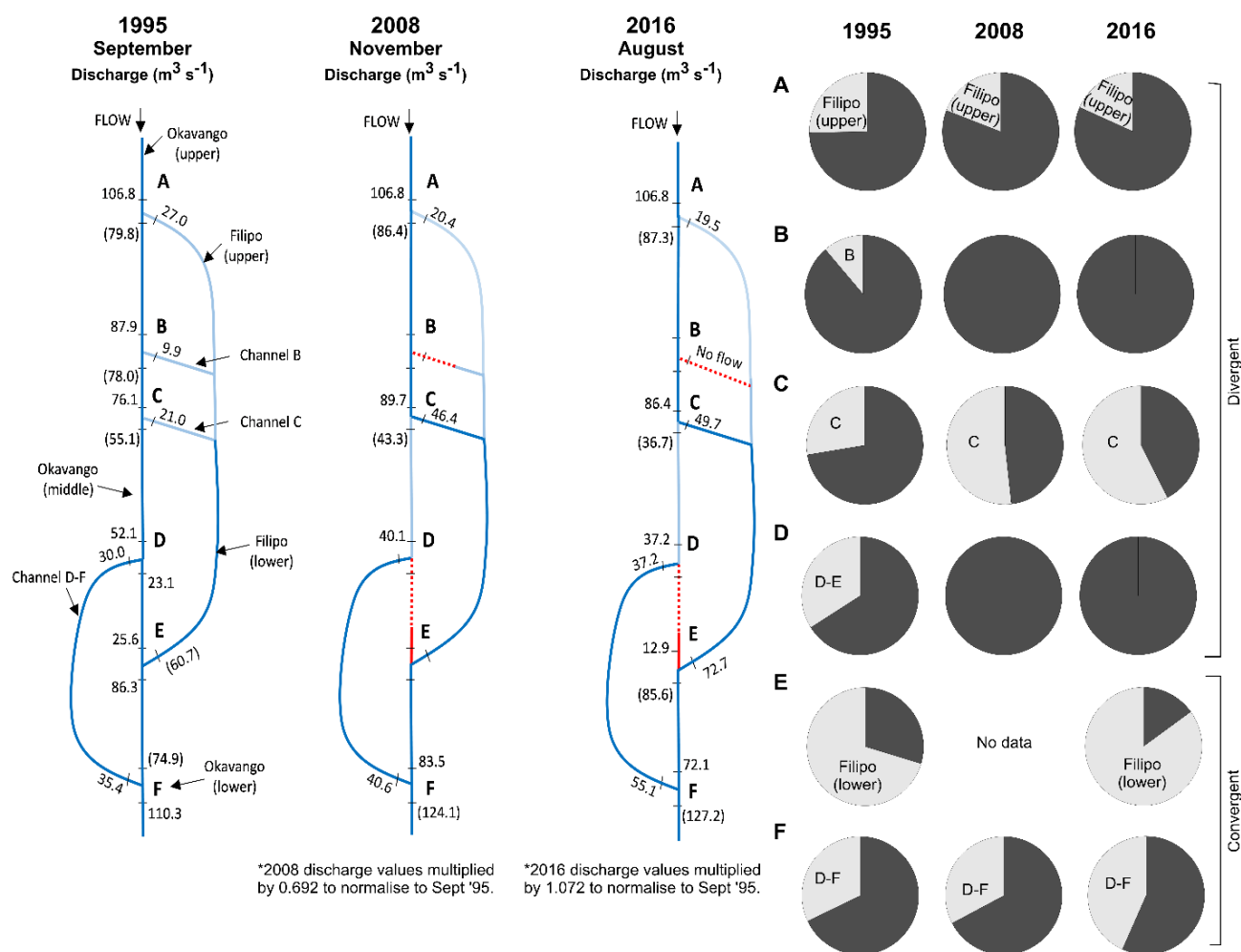
Figure 5. Schematic diagram of measured and estimated discharge values for channels in the anastomosing reach of the Okavango River in the Panhandle for 1995, 2008, and 2016. Values in brackets have been calculated by difference/addition of the other two diverging/converging branches, respectively. Dark blue lines are the dominant channels, light blue are secondary or failing channels, and red dashed lines are failed channels. Values have been normalised to September 1995 in order to calculate proportional changes in water balance between different

channels, which are represented by the pie charts at the right of the figure. The pie charts represent the proportional balance of flow (both at divergent and convergent junctions) between the Okavango main stem (dark shading) and the avulsive channels (light grey shading; labelled Filipo (upper), B, C, D-E, Filipo (lower), and D-F).

Bedload sediment transport

Bedload sediment transport has changed between 1995, 2008 and 2016 in the study reach (Fig. 6; Table 1). At node A, bedload transport in the Okavango downstream of the bifurcation increased by ~33 % and ceased in the Filipo. Bedload transport also ceased in channel B at node B. Downstream at node C, bedload transport in the Okavango upstream of the bifurcation decreased by ~18 %, while below the bifurcation bedload transport in the Okavango decreased by ~41 % and increased in channel C by ~111 %. At node D, bedload transport in the Okavango decreased by ~73 %, while channel D-E ceased to transport bedload. At node E, bedload from channel D-E ceased and increased in the Filipo by ~132 %. At node F, bedload transport in channel D-F increased by ~696 % (disproportionately high increase in sediment transport rate due to very low bedload transport rate in 1995) and decreased in the Filipo by ~23 %. Bedload transport out of the anastomosing reach below the confluence of the Okavango and Filipo increased by ~19 %, although the sediment transport rate at the downstream end of the reach is still lower than the rate at the upstream end of the reach indicating overall sediment sequestration. In 1995, when the anastomosing reach had five active channels, bedload transport at the reach scale declined overall by ~22 % (Fig. 6). In 2008, when four channels were active, bedload transport rate at the reach scale declined by ~17 % (Fig. 6). And in 2016, when three anastomosing channels were active, bedload transport rates at the reach scale declined by ~7.5 % (Fig. 6).
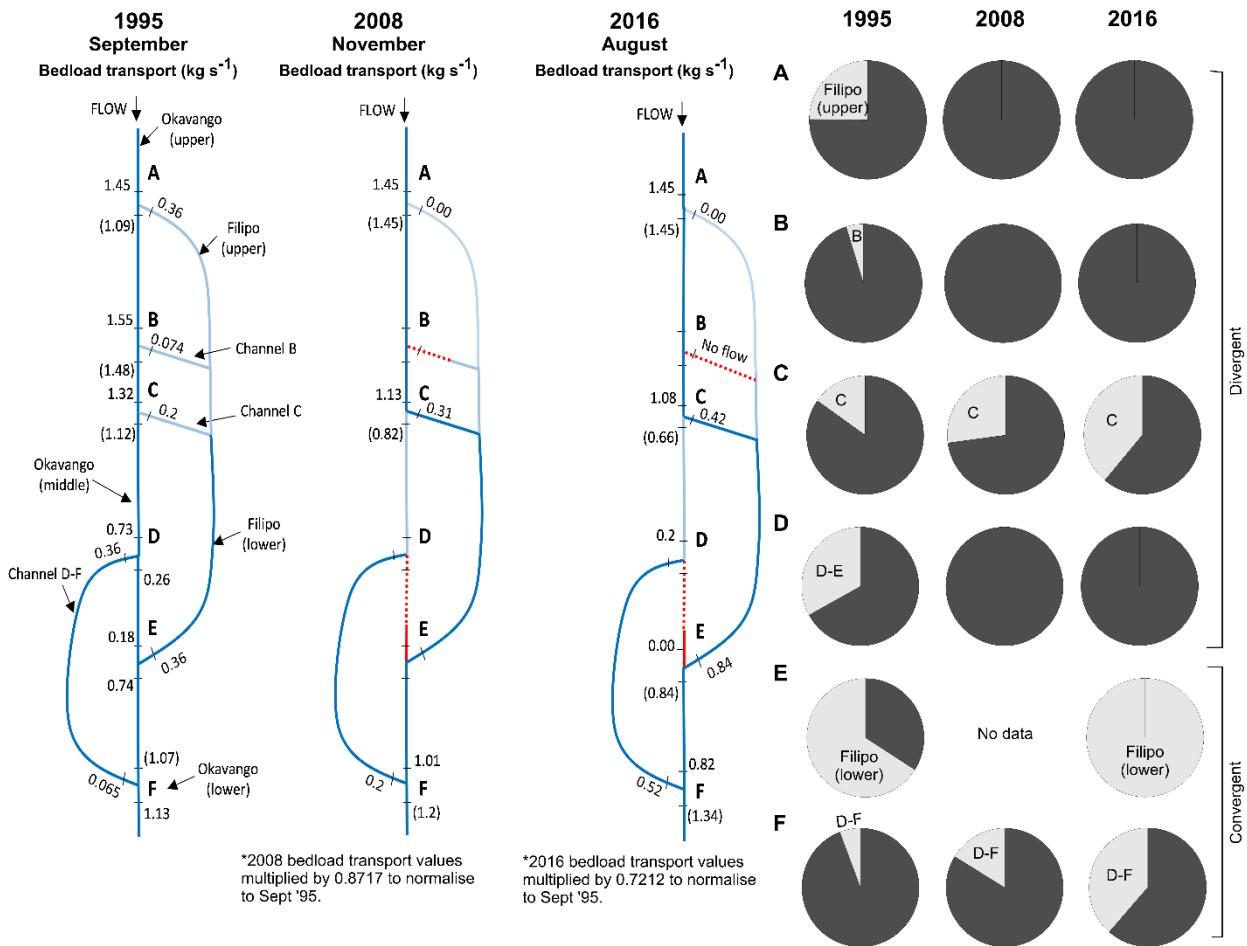
Figure 6. Schematic diagram of measured and modelled bedload transport rate values for channels of the anastomosing reach of the Okavango in the Panhandle for 1995, 2008 and 2016. Dark blue lines are the dominant channels, light blue are secondary or failing channels, and red dashed lines are failed channels. Values have been normalised to September 1995 in order to calculate proportional changes in bedload transport rates between different channels which is represented in the pie charts at the right side of the figure. Bedload transport rates for November 2008 and August 2016 were modelled using the relationship between measured discharge and measured bedload transport rates undertaken in September 1995 and April 2008 (see Supplementary Fig. 2). The pie charts represent the proportional balance of flow (both at divergent and convergent junctions) between the Okavango main stem (dark shading) and the avulsive channels (light grey shading; labelled Filipo (upper), B, C, D-E, Filipo (lower), and D-F).

Water-surface elevations and channel slope

In 1995, significant differences in water-surface elevation existed at parallel downvalley and downstream positions in each channel (Fig. 7). The greatest cross-valley water-surface elevation difference occurred in 1995 when the water surface elevation of the Filipo channel was ~112 cm lower than the Okavango River at an equivalent point downvalley, which occurred in the middle segment of the Filipo (between UCT16 and UCT21, near node C; Smith et al. 1997). In 2008, the Filipo again had lower water-surface elevations than the Okavango, although the maximum difference had decreased to ~70 cm. In 2016, the entire length of the Filipo channel had equivalent water-surface elevations as the Okavango, demonstrating a significant reduction in the hydraulic gradient between the Filipo and Okavango channels in this reach. However, the channel gradient of the upper Filipo and channel C is still

steeper than the main Okavango channel (Fig. 8). The trends are the same for downstream channel distance, although the differences in water-surface elevations are slightly more pronounced. The Filipo channel is slightly straighter than the Okavango and therefore has a slightly steeper channel course over the anastomosing reach (Fig. 7B, D, and F).

Differences between water-surface elevations at paired sites provide estimates of channel slope around the avulsion nodes in the study reach (Fig. 8; Table 1). At node A, channel slope in the Okavango decreased by ~16 % and decreased in the Filipo by ~33 %. A change in slope was not measured at node B where channel B had failed, although slope must be significantly reduced since the channel is infilled with vegetation and sediment. At node C, slope in the Okavango increased by ~24 % and decreased in channel C by ~50 %. At node D, slope in the Okavango increased by ~18 % and decreased in channel D-F by ~65 %, while channel D-E suffered the same fate as channel B and became infilled with vegetation and sediment. At node E, slope increased in the Filipo by ~62 %.
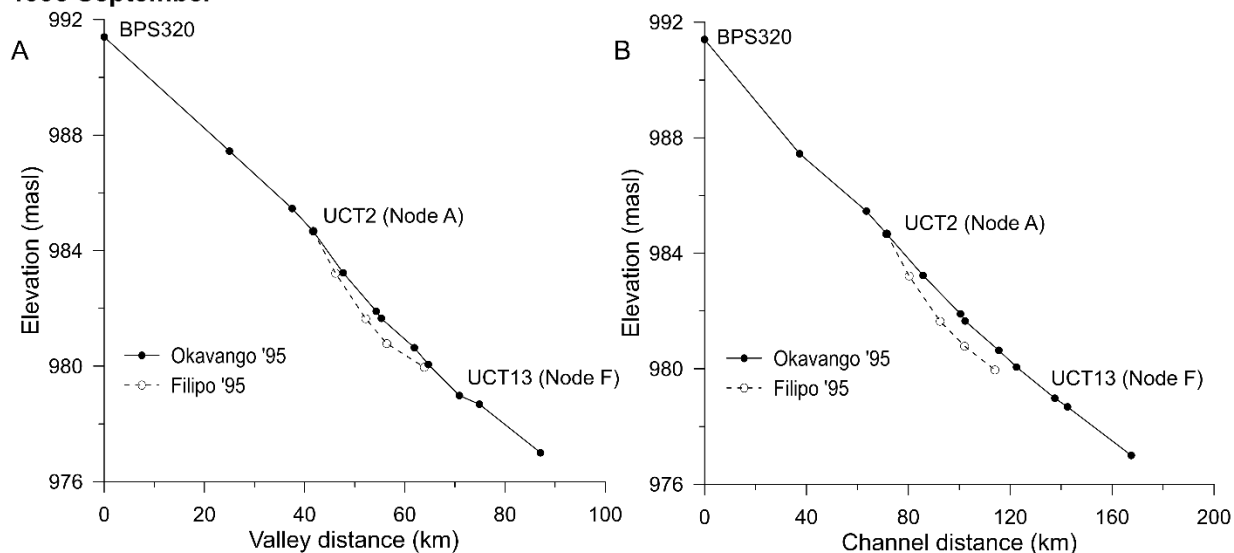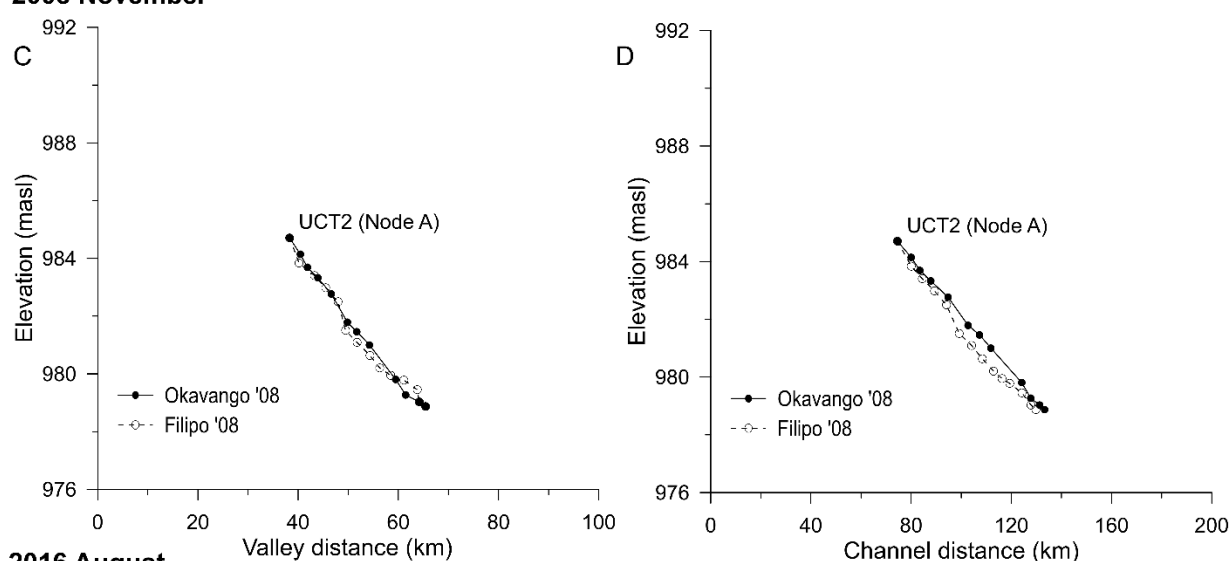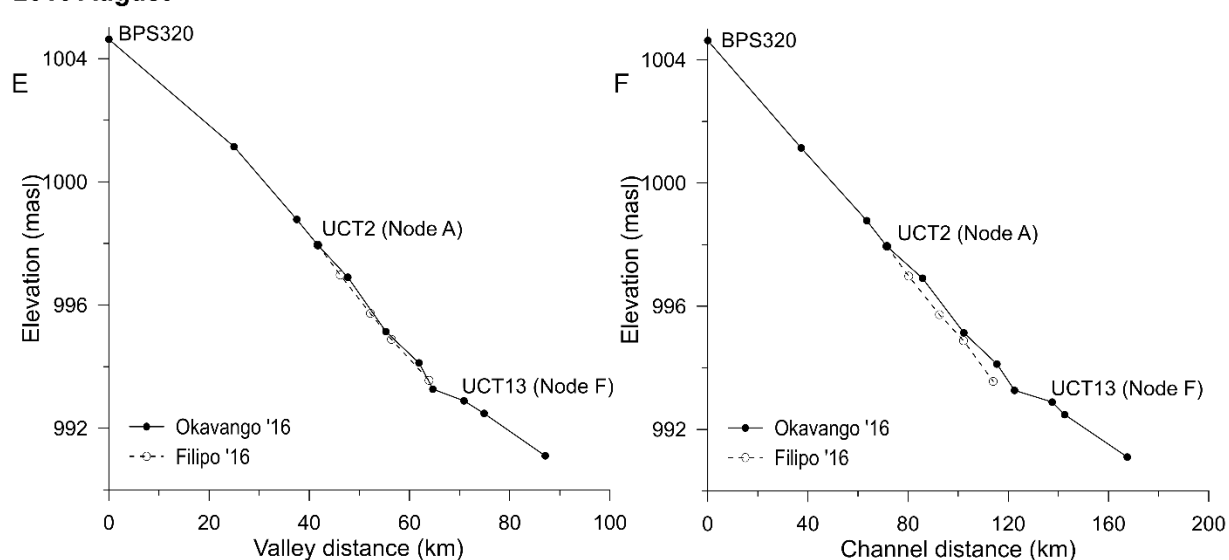
Figure 7. Water-surface elevations of the Okavango River and Filipo channel from the Botswana-Namibia border and through the anastomosing reach in the Panhandle; A) over valley distance in 1995, B) over channel distance in 1995, C) over valley distance in 2008, D) over channel distance in 2008, E) over valley distance in 2016, and F) over channel distance in 2016. Three DGPS sites are labelled with their code on each profile, and nodes A and F are included in brackets for context.
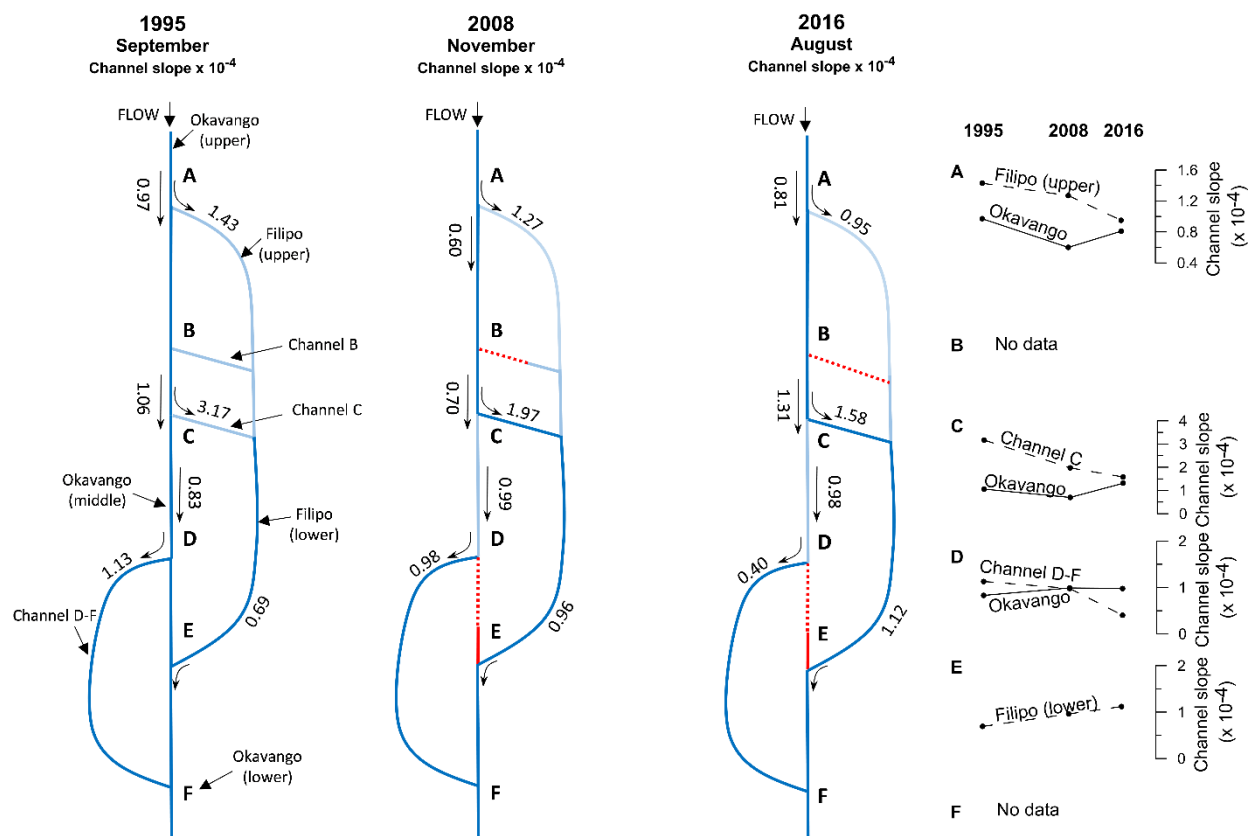
Figure 8. Water-surface gradients of the main Okavango channel and diverging channels. In general, the slopes of divergent channels exceed the slope of the trunk stream. Dark blue lines are the dominant channels, light blue are secondary or failing channels, and red dashed lines are failed channels.

Interpretation

In the historical period leading up to 1995, the Filipo channel, from its first offtake point to its junction with the Okavango ~23 km downvalley, was the predominant branch of the anastomosing reach in the Panhandle. The Filipo diverted ~25 % of total flow entering the reach and, after drawing additional flow from channels B and C, accounted for ~50 % of total flow exiting the reach. Our findings show that from 1995-2016, the upper segment of the Filipo (at node A) contracted with significant declines in channel width (~43 %), discharge (~28 %), bedload transport (100 %) and water-surface slope (~33 %) (Figs. 4, 5, 6, 8). At its first offtake the Filipo has become 12 m narrower (an average narrowing rate of 0.57 m a^{-1}) due to encroachment of dense vegetation (papyrus and phragmites) and it now diverts ~18 % of total flow entering the reach. The upper segment of the Okavango running parallel to the Filipo has maintained its morphology due to relatively minor changes in discharge and bedload, although it has become deeper (Supplementary Table 1). A reduction in the hydraulic gradient between the Okavango and the Filipo is likely a key contributing factor for the progressive failure of the upper Filipo channel.

Conversely, the lower segment of the Filipo (at node E) expanded in the period 1995-2016, with increases in channel width (~18 %; expansion rate of 0.24 m a^{-1}), discharge (~20 %), bedload (132 %) and

slope (~62 %). The significant fluvial enhancement of the lower Filipo is due to flow capture from the middle Okavango, particularly attributed to the rapid expansion of channel C (at node C) that diverted ~28 % of flow from the Okavango in 1995, and eventually captured ~58 % of flow in 2016. Channel C increased markedly in width (~108 %; expansion rate ~0.62 m a^{-1}), discharge (~137 %; flow capture rate ~1.37 m^3 s^{-1} a^{-1}) and bedload (~111 %; bedload capture rate ~0.01 kg s^{-1} a^{-1}) and experienced a decline in water-surface slope (~50 %), the latter possibly due to grading or planation of the bed along its length. Nevertheless, channel C maintains a significant hydraulic advantage over the Okavango in the equivalent position downstream, as does the lower Filipo (Fig. 8). Enlargement of the lower Filipo occurred despite the failure of channels B and D-E that previously connected the Okavango to the Filipo upstream and downstream of channel C, respectively. Channel B closed entirely with vegetation (at node B) leading to termination of channelised flow and bedload transport, hence channel failure, soon after 1995. Channel D-E had a similar fate, becoming blocked by stands of phragmites and clumps of floating papyrus (at node D) and suffering dramatic declines in discharge (~50 %) and bedload (100 %) along its length and at the return junction with the Filipo (at node E).

Due to flow capture by, and enlargement of, channel C and the lower Filipo, the middle Okavango (downstream of node C and at node D) experienced significant channel contraction and a decline in fluvial efficiency, as shown by decreases in width (~26 and 21 %), discharge (~33 and 29 %), and bedload (~41 and 73 %), despite increases in slope (~24 and 18 %) from 1995-2016. This reach has particularly prominent intrusions of hippo grass (*Vossia cuspidata*) along the channel margins. However, channel D-F (at node F), a branch of the Okavango that forms a bypass to channel D-E, increased in width (~10 %), discharge (~56 %) and bedload transport (~696 %). Increases in discharge (~15 %) and bedload (~19 %) were also measured at the end of the anastomosing reach below the confluence of the Okavango and Filipo. Enhanced end-of-reach discharge is attributed to channel enlargement, steepening and reduced sinuosity in key segments upstream, possibly related to upstream-retreating knickpoints (e.g. channel D-F), that together promote through- and return-flow from the surrounding wetlands during the declining phase of the annual flood (Smith et al., 1997). Indeed, leakage from the wetlands surrounding the active and failed channels is vitally important for downstream flow, as seen at the return junction of D-E where flow is maintained into the Filipo despite the head of channel D-E being blocked by vegetation.

If the trend of rapid channel contraction in the upper segment of the Filipo continues, this reach will become susceptible to abandonment and will either fail (as channel B and D-E have done) leaving a single thread Okavango channel at this position, or the Okavango here will become primed for a second round of avulsion. Indeed, in 2016, the downstream end of the upper Filipo (i.e. upstream of the junction with channel C) became blocked by floating vegetation (Chapter 3). A similar fate awaits the middle segment of the Okavango, which has also contracted significantly since 1995. If both these key segments were to be abandoned without subsequent new channel formation by avulsion, then a single channelised flow path would develop through the upper Okavango, into channel C and then the lower

Filipo, returning to the Okavango downstream at node F. At the current rates of channel expansion and contraction, and without significant external forcing on the hydrology or geomorphology, this scenario of a future single-thread Okavango is highly likely. The anastomosing study reach has already lost two active channels, two bifurcation nodes and one return junction due to consolidation of flow in the Okavango, Filipo and channel C since 1995, which equates to a net loss of at least ~15 km of channel length throughout the reach. The current anastomosing pattern is therefore likely to be a transitional state as channel C and the lower Filipo overtake segments of the Okavango in this part of the Panhandle, which is consistent with the concluding predictions made by Smith et al. (1997). If this interpretation is correct, this example of 'transitional anastomosis' will contrast with the long-term 'stable anastomosis' that characterises some other dryland rivers and wetlands, especially in Australia (e.g. Knighton and Nanson, 1993; Huang and Nanson, 2000; 2007; Huang et al., 2004).

Water-surface elevations are also an important indicator of bed level grading and system equilibration in the anastomosing reach of the Okavango in the Panhandle. The Filipo, which in 1995 had a noticeably lower water-surface level than the Okavango in its middle reaches, has raised to an equivalent elevation as the Okavango (Fig. 7). This is attributed to a combination of sediment dispersal and aggradation in segments of both the Filipo and the Okavango, as well as excision and channel deepening in other segments. Bed grading and equilibration at a common base-level is related to declining fluvial efficiency and reduced sediment transport in the anastomosing reach. A strong positive correlation exists between discharge and bedload sediment transport (Supplementary Fig. 2), and bedload transport is severely inhibited and tends to cease when discharge falls below a threshold of ~20 m^3 s^{-1}. This is the case for channels B and D-E which have suffered from channel failure, while the upper Filipo sits at this threshold and, as such, does not transport bedload and appears to be progressively being abandoned, particularly at its downstream end (i.e. just upstream of the channel C junction) which became blocked by vegetation prior to 2016. The cause-effect relationships between declining channel size, discharge, sediment transport, low channel slope and channel initiation and abandonment therefore define the mechanisms of avulsion and channel failure in this system. Avulsion may occur through flow diversion into a new channel or the reconnection of a nearby palaeochannel, or excision of the existing channel due to knickpoint retreat which may revive a failing channel. New channels form quickly and relatively easily due to the presence of numerous hippopotami trails and abandoned channel traces and lagoons that provide a 'path of least resistance' away from the aggrading channel. Only a small proportion of these new channels are more efficient than the existing channel, and subsequently few survive to become incorporated in the main channel. Channel failure is characterised by precipitous declines in discharge and bedload sediment transport, leading to a positive feedback cycle of vegetation growth and sediment accumulation within the failing channel. Eventually the failing channels cease to function as conduits for sediment and are abandoned.

Discussion

Extrinsic or intrinsic forcing of Okavango River avulsion?

A combination of extrinsic forces and intrinsic processes affect avulsion in the Okavango Panhandle, but these are difficult to disentangle. Based on DGPS measurements of water surface elevations, Smith et al. (1997) argued that anastomosis in the Panhandle is a result of down-faulting of a graben which displaced local base-level and initiated avulsion. In this scenario, extrinsic, neotectonic movement is responsible for accelerated in-channel sedimentation creating hydraulically advantageous gradients away from the trunk stream and the formation of the Filipo and other avulsive channels (i.e. B, C, and D-F). If avulsion has been triggered by neotectonic movement, then the system will continue to aggrade to fill the accommodation space made by down-faulting and will eventually re-organise into a single, stable channel. In the absence of further extrinsic, neotectonic disturbance, the Okavango River will likely not be characterised by avulsion in this part of the Panhandle. Water surface elevation data from 2008 and 2016 do not, however, conclusively indicate the presence of faulting, and Smith et al. (1997) note that surface expression of the apparent faulting in aerial imagery is subtle to non-existent.

Alternatively, based on the additional two decades of monitoring/measurement, we propose that avulsion and anastomosis in the Okavango Panhandle is driven by intrinsic processes and thresholds related to downstream declines in discharge and in-channel blockages due to sedimentation and vegetation. In this scenario, avulsion is a cyclic process within the natural range of variability of the modern Okavango River, whereby progressive downstream declines in discharge exceed an energy threshold promoting enhanced bed accumulation in channels confined by dense vegetation. The trapping of sediment in the channels leads to perched channels with superelevated water surface levels relative to the surrounding wetlands. The vegetation-confined channels cannot adjust their planform or their slope easily (e.g. by straightening) under modern hydrological conditions. Given the downstream declines in discharge (Larkin et al., in prep [Chapter 3]), and the inability of the Okavango to adjust its channel planform to improve sediment transport efficiency, it is most likely that avulsion occurs to bypass particularly inefficient reaches. Supporting this interpretation is the fact that the avulsion of the Nqoga from the Thaoge, which occurred only ~4 km downstream from the anastomosing reach, has been driven by these same intrinsic processes related to in-channel sedimentation (McCarthy et al., 1992; McCarthy, 2013). Despite a 21-year record of field measurements of channel width, discharge, bedload transport rate, and water surface elevations, it is not possible to definitively conclude whether the fundamental drivers of avulsion in the anastomosing reach of the Panhandle are intrinsic processes or extrinsic forcing. Nevertheless, evidence for bed aggradation as the main mechanism leading to avulsion in other parts of the Okavango Delta and our interpretations support the hypothesis that avulsion in the Panhandle is an intrinsically-driven process related to threshold responses without needing to invoke neotectonic activity as the key driver. The key mechanisms of avulsion and channel failure are related to in-channel sedimentation, hydraulic gradients, and vegetation encroachment.

Mechanisms of avulsion and channel failure in the Okavango Panhandle

Avulsion is characteristic of many single- and multi-channelled dryland rivers around the world and it is widely accepted that avulsion is unlikely to occur in the absence of a hydraulic advantage for a new channel (Jones and Schumm, 1999). In the Okavango, intrinsic hydraulic inefficiency and thresholds of bedload sediment transport related to downstream declines in discharge serve to promote in-channel sedimentation and to elevate bed and water levels in aggrading channels. Measured and modelled bedload transport rates demonstrate that sediment sequestration occurs in the anastomosing reach in the Panhandle (e.g. in 1995 bedload transport rates declined from ~1.45 kg s^{-1} at node A to ~1.13 kg s^{-1} at node F; Fig. 6). Fluvial adjustments that might typically occur to improve downstream sediment transport capacity, such as channel straightening (Nanson and Huang, 2017), cannot readily be made in the vegetation-confined channels of the Panhandle. For instance, there was no discernible lateral channel migration in the 54 years between 1962 and 2016 in the anastomosing reach (Larkin et al., in prep [Chapter 3]), meaning that sediment cannot be stored in lateral point bar or scroll bar deposits and therefore must remain within the channels.

The mechanisms of avulsion and channel failure in the Okavango Panhandle operate as follows. Bedload sediment is trapped within increasingly inefficient channels, raising bed and surface water elevations relative to the surrounding wetlands. This serves to reduce the slope of the existing channels (Fig. 9). Dense vegetation and peat that make up much of the permeable channel banks trap fine sediment from suspension, promoting subtle alluvial ridge growth and creating local increases in cross-floodplain gradient; that is, an increase of the potential avulsion course slope. The net effect is an increase in the ratio of the potential avulsion course slope to the existing channel course slope, which primes the system for avulsion. The threshold of channel width where avulsive behaviour becomes characteristic of the Okavango River appears to be ~50-60 m. With hydraulically advantageous gradients away from the channel, flows exploit and enlarge the ubiquitous hippopotami trails or other weaknesses in the banks to form new channels leading to the lower-lying part of the floodplain (Larkin et al., in prep [Chapter 3]). The new channels evolve and enlarge due to upstream knickpoint retreat, which serves to excavate sediment and to join irregular sinuous segments to less sinuous remnants of palaeochannels. Diversion of water and sediment to the new channel reduces flow downstream in the original, less efficient, channel, which is encroached upon by vegetation (i.e. *Vossia cuspidata, Cyperus papyrus,* and *Phragmites* spp.). When discharge in a channel declines to <20 m^3 s^{-1}, they are no longer able to transport bedload sediment and are destined to fail and become blocked by vegetation. In some cases, floating clumps of papyrus have blocked channels before they have crossed the low-flow threshold. The influence of vegetation on channels of the Okavango cannot be overstated (Ellery et al., 2003); the channels face a constant struggle against vigorously-growing aquatic vegetation and a positive feedback occurs where intrusive vegetation slows flow velocity encouraging sedimentation and further vegetation growth (McCarthy et al., 1992). Such a feedback probably explains why the middle Okavango River near

Sepopa continues its trajectory towards channel failure despite the water surface elevations becoming equivalent in the Okavango and Filipo since 1995.
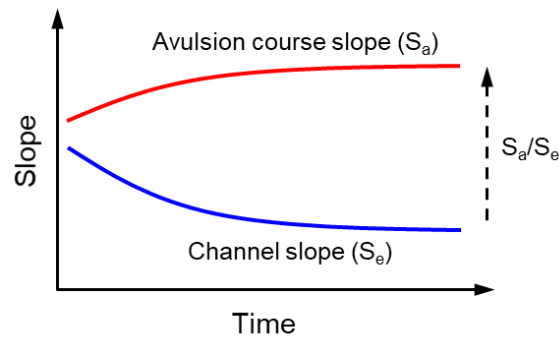
Figure 9. Conceptual diagram highlighting the relationship between declining slope of the existing channel (S_e) and concomitant increase in the slope of the potential avulsion course (S_a). Source: modified from Jones and Schumm (1999).

This is a similar process to avulsion in the unconfined reaches on the Okavango Fan, which is also controlled by channel perching that occurs as a result of rapid in-channel deposition of bedload sediment, vegetation confinement, and hydraulically advantageous flows away from the channel (see McCarthy, et al., 1992; McCarthy, 2013). However, the unconfined nature of the Fan means that newly formed channels rarely re-join with the trunk channel, as occurs in the Panhandle. Channels on the Fan begin to fail at their distal downstream end which can be characterised by rapid rates of in-channel aggradation (>5 cm a^{-1}) leading to backfilling of the failing channel. The upstream progression of channel failure along the major channels of the Fan is accompanied by formation of another channel on the topographically lower floodplain, and the resulting changes to flooding patterns over thousands of square kilometres of wetlands can be dramatic, as has been documented over the historical period (see McCarthy et al., 1992 and Larkin et al., in prep [Chapter 3] for summaries).

These mechanisms of avulsion have similarities to intrinsically-driven avulsions of the Tshwane and Klip rivers in northern and eastern South Africa, respectively. The Tshwane and Klip rivers maintain a single channel but are characterised by periodic, reach-scale avulsion leading to the abandonment of an inefficient reach (Tooth et al., 2007; Larkin et al., 2017). In the Tshwane River, high rates of sedimentation within, and adjacent to, the channel creates hydraulically-advantageous cross-floodplain gradients, and increasing sinuosity reduces the efficiency of sediment transport (Larkin et al., 2017). A new channel is formed by incision on the floodplain and the former channel is quickly infilled and abandoned. The mechanism of avulsion on the Klip River is similar, although much lower sedimentation rates mean that avulsion occurs much less frequently than on the Tshwane (Tooth et al., 2007).

Although channel flanking vegetation plays a much more prominent role, and the transitional anastomosing state persists longer in the Okavango River, the Tshwane and Klip rivers provide examples of single-thread, dryland rivers which periodically avulse in response to intrinsic thresholds related to sediment transport efficiency and hydraulic gradients.

The overall effect of avulsion in the Okavango Panhandle, Tshwane and Klip rivers is to locally maintain or maximise fluvial efficiency, by abandoning inefficient reaches. In contrast, similar mechanisms of channel avulsion in other settings do not always lead to channel maintenance and these rivers are characterised by channel breakdown in wetlands. For example, many low-energy, dryland rivers in Australia are characterised by channel breakdown and wetland formation in their middle and lower reaches, and the most well studied is the Macquarie River in eastern Australia. Dramatic downstream declines in discharge and stream power promote contraction of the Macquarie River and sedimentation both within and adjacent to the channel (Ralph and Hesse, 2010). Development of an alluvial ridge promotes hydraulically advantageous gradients away from the trunk stream which are exploited by newly formed channels through incision. However, persistent downstream declines in discharge and repeated avulsions that divert water from the trunk stream result in channel termination when channelised flow can no longer be maintained (Ralph and Hesse, 2010). In this case, the mechanisms of avulsion are similar to the Okavango, Tshwane, and Klip rivers (i.e. channel inefficiency, aggradation, and hydraulic gradients), but avulsion is ultimately unable to improve flow and sediment transport efficiency substantially enough to prevent the cessation of channelised flow and sediment transport. This highlights the complexity of avulsion in different settings.

Maximum flow efficiency, avulsion and anastomosis

Intrinsic processes and thresholds are responsible for adjustments made to a rivers shape or planform in order to maximise flow and sediment transport efficiency. Flow efficiency can be defined as the ratio of sediment transported to the stream power expended (Huang and Nanson, 2000). In low-energy settings, adjustments that maximise flow and sediment transport efficiency include increasing channel slope in the form of straightening, adjusting channel width/depth ratio, and/or the formation of multiple, narrower channels (e.g. ridge-form anastomosis, Tooth and Nanson, 1999). Where channel slope cannot be adjusted (e.g. a channel is already straight or dense riparian vegetation precludes lateral adjustment), adjusting channel form (i.e. width/depth ratio) or increasing the number of channels provides the potential to increase, or maintain, sediment flux by maximising flow velocity. Hydraulically, a narrower channel section that is relatively deep (i.e. low width/depth ratio) will transport more sediment per unit of stream power due to the concentration of flows and enhanced velocity (Nanson and Huang, 1999; 2017). For example, analysis of anabranching rivers in central Australia such as the Marshall and Plenty Rivers (Nanson and Huang, 2017) and Magela Creek (Jansen and Nanson, 2004) showed that the anabranching channels exhibit greater sediment transport capacity than a single, large channel.

In the Okavango, however, net accumulation of sediment occurs through the anastomosing reach, but sediment transfer out of the reach improves when less channels are active. This suggests improved sediment transport capacity with fewer channels and/or reduced total length of channels. It is possible that the dense riparian vegetation that retards lateral migration and reduces flow velocity at the channel margins has a greater impact on sediment transport capacity when multiple channels exist by forming a greater proportion of the total wetted perimeter of the channels. This argument is supported by the width/depth threshold which defines channel behaviour in the Okavango determined by Tooth and McCarthy (2004). Channels with a width/depth ratio of <10 are unable to laterally migrate, and presumably have lower sediment transport rates, due to the proportionally higher influence of sidewall vegetative roughness at the channel boundaries (Tooth and McCarthy, 2004). Our findings do not support the idea of the Okavango River in the Panhandle being characterised by stable anastomosis which occurs on some other large dryland rivers (e.g. Cooper Creek, Nanson and Knighton, 1996). Although, it should be noted that the multi-channelled planform of the Okavango River in the Panhandle has persisted throughout the historical period, and it is possible that the multiple, rapidly-forming though short-lived channels result in an essentially multi-channelled planform over the medium-long term. Nevertheless, our data suggest that the current channel pattern of anastomosis in the Panhandle is transitional, and a single channel will likely rationalise as the remaining channels fail (i.e. upper Filipo, middle Okavango). While the multi-channelled planform in the Okavango Panhandle does not improve flow efficiency or persist as a stable channel pattern in the way that it does in many other dryland rivers, the process of avulsion ultimately improves flow efficiency by gradually abandoning inefficient, failing channels.

Conclusion

The avulsion process in the Okavango Panhandle is complex and somewhat chaotic, with numerous channels forming and failing in response to in-channel sedimentation and hydraulic gradients. Hydro-geomorphological changes documented over 21 years highlight the fundamental mechanisms of avulsion and channel failure that dominate this system, and highlight the transitional nature of anastomosis in this system. Understanding mechanisms and thresholds of avulsion are critical for river and wetland management, as avulsive systems redistribute water and sediment in ways that have dramatic impacts on ecological processes, habitat diversity, riverside communities and resource use (Smith et al., 1989; Slingerland and Smith, 2004; Ralph et al., 2016). Assessing the natural range of variability (i.e. types and rates of key processes) of large, and internationally important rivers such as the Okavango improves our ability to forecast future trajectories of change brought about by intrinsic threshold responses and/or climate and land use changes in these critical systems.

Acknowledgements

References

Aqrawi AAM, 2001. Stratigraphic signatures of climatic change during the Holocene evolution of the Tigris-Euphrates delta, lower Mesopotamia. Global and Planetary Change, 28, 267-283.

Berendsen HJA, and Stouthamer E, 2002. Paleogeographic evolution and avulsion history of the Holocene Rhine-Meuse delta, The Netherlands. Netherlands Journal of Geosciences, 81(1), 97-112.

Bowler JM, 1967. Quaternary chronology of Goulburn valley sediments and their correlation in southeastern Australia. Journal of the Geological Society of Australia, 14(2), 287–292.

Bridge JS, Leeder MR, 1979. A simulation model of alluvial stratigraphy. Sedimentology, 26(5), 617-644.

Bryant M, Falk P, Paola C, 1995. Experimental study of avulsion frequency and rate of deposition. Geology, 23(4), 365-368.

Donselaar ME, Cuevas Gozalo MC, and Moyano S, 2013. Avulsion processes at the terminus of low-gradient semi-arid fluvial systems: Lessons from the Rio Colorado, Altiplano endorheic basin, Bolivia. Sedimentary Geology 283, 1–14.

Ellery WN, McCarthy TS, Smith ND, and Hall B, 2003. Vegetation, hydrology, and sedimentation patterns on the major distributary system of the Okavango Fan, Botswana. Wetlands 23, 357–375.

Fryirs KA, Ralph TJ, Larkin ZT, Tooth S, Humphries M, McCarthy T, Hesse PP, and Mosimanyana E, 2018. A nested hierarchical perspective to enhance interpretations and communication in fluvial geomorphology for use in water resources management: Lessons from the Okavango Delta, Botswana. Geographical Journal 184, 192–207.

Giosan L, Clift PD, Macklin MG, Fuller DQ, Constantinescu S, Durcan JA, Stevens T, Duller GAT, Tabrez AR, Gangal K, Adhikari R, Alizai A, Filip F, VanLaningham S, and Syvitski JPM, 2012. Fluvial landscapes of the Harappan civilization. Proceedings of the National Academy of Sciences 109, 1688–1694.

Gumbricht T, McCarthy TS, and Merry CL, 2001. The topography of the Okavango Delta, Botswana, and its tectonic and sedimentological implications. South African Journal of Geology, 104(3), pp.243-264.

Huang HQ, Chang HH, and Nanson GC, 2004. Minimum energy as the general form of critical flow and maximum flow efficiency and for explaining variations in river channel pattern. Water Resources Research 40, 1–13.

Huang HQ, and Nanson GC, 2000. Hydraulic geometry and maximum flow efficiency as products of the principle of least action. Earth Surface Processes and Landforms 25, 1–16.

Huang HQ, and Nanson GC, 2007. Why some alluvial rivers develop an anabranching pattern. Water Resources Research, 43(7), 1–12.

Huang HQ, and Nanson GC, 2008. Least action principle, equilibrium states, iterative adjustment and the stability of alluvial channels. Earth Surface Processes and Landforms, 33, 923–942.

Jacobberger PA, 1987. Geomorphology of the upper Inland Niger Delta. Journal of Arid Environments, 13, 95-112.

Jain V, and Sinha R, 2004. Fluvial dynamics of an anabranching river system in Himalayan foreland basin, Baghmati river, north Bihar plains, India. Geomorphology, 60(1-2), 147-170.

Jansen JD, and Nanson GC, 2004. Anabranching and maximum flow efficiency in Magela Creek, northern Australia. Water Resources Research, 40(4), 1–12.

Jones L, and Schumm S, 1999. Causes of avulsion: an overview. In: Smith, N.D., Rogers, J. (Eds.), Fluvial Sedimentology VI, International Association of Sedimentologists, Special Publication No. 28. Blackwell Scientific Publications, Oxford, pp. 171–178

Knighton AD, and Nanson GC, 1993. Anastomosis and the continuum of channel pattern. Earth Surface Processes and Landforms, 18, 613-625.

Larkin ZT, Ralph TJ, Tooth S., Duller GAT, and Fryirs KA, in prep. River response to Holocene hydroclimatic change in the OKavanago Panhandle, Botswana.

Larkin ZT, Tooth S, Ralph TJ, Duller GAT, McCarthy T, Keen-Zebert A, and Humphries MS, 2017. Timescales, mechanisms, and controls of incisional avulsions in floodplain wetlands: Insights from the Tshwane River, semiarid South Africa. Geomorphology 283, 158–172.

Li J, Bristow CS, Luthi SM, and Donselaar ME, 2015. Dryland anabranching river morphodynamics: Rio Capilla, Salar de Uyuni, Bolivia. Geomorphology 250, 282–297.

Makaske B, Smith DG, and Berendsen HJA, 2002. Avulsions, channel evolution and floodplain sedimentation rates of the anastomosing upper Columbia River, British Columbia, Canada. Sedimentology, 49, 1049-1071.

McCarthy TS, Ellery WN, and Bloem A, 1998. Some observations on the geomorphological impact of hippopotamus (Hippopotamus amphibius L.) in the Okavango Delta, Botswana. African Journal of Ecology 36, 44–56.

McCarthy TS, Ellery WN, and Stanistreet IG, 1992. Avulsion mechanisms on the Okavango fan, Botswana: the control of a fluvial system by vegetation. Sedimentology, 39, 779-795.

Morozova GS, 2005. A review of Holocene avulsions of the Tigris and Euphrates Rivers and possible effects on the evolution of civilizations in Lower Mesopotamia. Geoarchaeology: An International Journal, 20(4), 401-423.

McCarthy TS, 2013. The Okavango Delta and its place in the geomorphological evolution of southern Africa. South African Journal of Geology 116, 3–54.

McCarthy TS, Stanistreet IG, Cairncross B, Ellery WN, Ellery K, Oelofse R, and Grobicki TSA, 1988. Incremental aggradation on the Okavango Delta-fan, Botswana. Geomorphology, 1(3), pp.267-278.

McCarthy TS, Ellery WN, and Stanistreet IG, 1992. Avulsion mechanisms on the Okavango fan, Botswana: the control of a fluvial system by vegetation. Sedimentology 39, 779–795.

McCarthy TS, Stanistreet IG, and Cairncross B, 1991. The sedimentary dynamics of active fluvial channels on the Okavango fan, Botswana. Sedimentology, 38, 471-487.

Merry CL, Heister H, Barry M, Ellery WN, McCarthy TS, Rüther H, and Sternberg H, 1998. GPS heighting in Okavango Delta. Journal of Surveying Engineering, 124, 145-155.

Miller JR, 1991. Development of anastomosing channels in south-central Indiana. Geomorphology, 4(3-4), 221-229.

Nanson GC and Huang HQ, 1999. Anabranching rivers: divided efficiency leading to fluvial diversity. In: Varieties of fluvial form, 7, pp.477-494.

Nanson GC, and Huang HQ, 2017. Self-adjustment in rivers: Evidence for least action as the primary control of alluvial-channel form and process. Earth Surface Processes and Landforms, 42(4), 575–594.

Nanson GC, and Huang HQ, 2018. A philosophy of rivers: Equilibrium states, channel evolution, teleomatic change and least action principle. Geomorphology, 302, 3–19.

Nanson GC, and Knighton AD, 1996. Anabranching rivers: their cause, character and classification. Earth Surface Processes and Landforms, 21, 217-239.

Okavango Research Institute, 2018. Okavango Delta Monitoring and Forecasting. URL: http://www.okavangodata.ub.bw/ori/monitoring/water/index.php Date last accessed: 4/09/2018.

Phillips JD, 2012. Log-jams and avulsions in the San Antonio River Delta, Texas. Earth Surface Processes and Landforms 37, 936–950.

Polvi LE, and Wohl E, 2013. Biotic Drivers of Stream Planform. BioScience 63, 439–452.

Ralph TJ, and Hesse PP, 2010. Downstream hydrogeomorphic changes along the Macquarie River, southeastern Australia, leading to channel breakdown and floodplain wetlands. Geomorphology 118, 48–64.

Ralph TJ, Hesse PP, and Kobayashi T, 2016. Wandering wetlands: spatial patterns of historical channel and floodplain change in the Ramsar-listed Macquarie Marshes, Australia. Marine and Freshwater Research 67, 782–802.

Schumann RR, 1989. Morphology of Red Creek, Wyoming, an arid-region anastomosing channel system. Earth Surface Processes and Landforms, 14, 277-288.

Schumm SA, 1968. River adjustment to altered hydrologic regimen - Murrumbidgee River and palaeochannels, Australia. United States Geological Survey Professional Paper, 598, 1-65.

Slingerland R, and Smith ND, 2004. River Avulsions and Their Deposits. Annual Review of Earth and Planetary Sciences, 32, 257–285.

Smith ND, Cross TA, Dufficy JP, and Clough SR, 1989. Anatomy of an avulsion. Sedimentology, 36, 1-23.

Smith ND, McCarthy TS, Ellery WN, Merry CL, and Rüther H, 1997. Avulsion and anastomosis in the panhandle region of the Okavango Fan, Botswana. Geomorphology 20, 49–65.

Smith DG, and Pearce CM, 2002. Ice jam-caused fluvial gullies and scour holes on northern river flood plains. Geomorphology 42, 85–95.

Stevaux JC, and Souza IA, 2004. Floodplain construction in an anastomosed river. Quaternary International, 114, 55-65.

Stouthamer E, and Berendsen HJA, 2007. Avulsion: The relative roles of autogenic and allogenic processes. Sedimentary Geology 198, 309–325.

Toonen WHJ, van Asselen S, Stouthamer E, and Smith ND, 2016. Depositional development of the Muskeg Lake crevasse splay in the Cumberland Marshes (Canada), 41, 117-129.

Tooth S, 2000. Downstream changes in dryland river channels: the Northern Plains of arid central Australia. Geomorphology, 34, 33-54.

Tooth S, and McCarthy TS, 2004. Controls on the transition from meandering to straight channels in the wetlands of the Okavango Delta, Botswana. Earth Surface Processes and Landforms 29, 1627–1649.

Tooth S, and Nanson GC, 1999. Anabranching rivers on the Northern Plains of arid central Australia. Geomorphology, 29, 211-233.

Tooth S, Rodnight H, Duller GAT, McCarthy TS, Marren PM, and Brandt D, 2007. Chronology and controls of avulsion along a mixed bedrock-alluvial river. Bulletin of the Geological Society of America 119, 452–461.

Supplementary Material
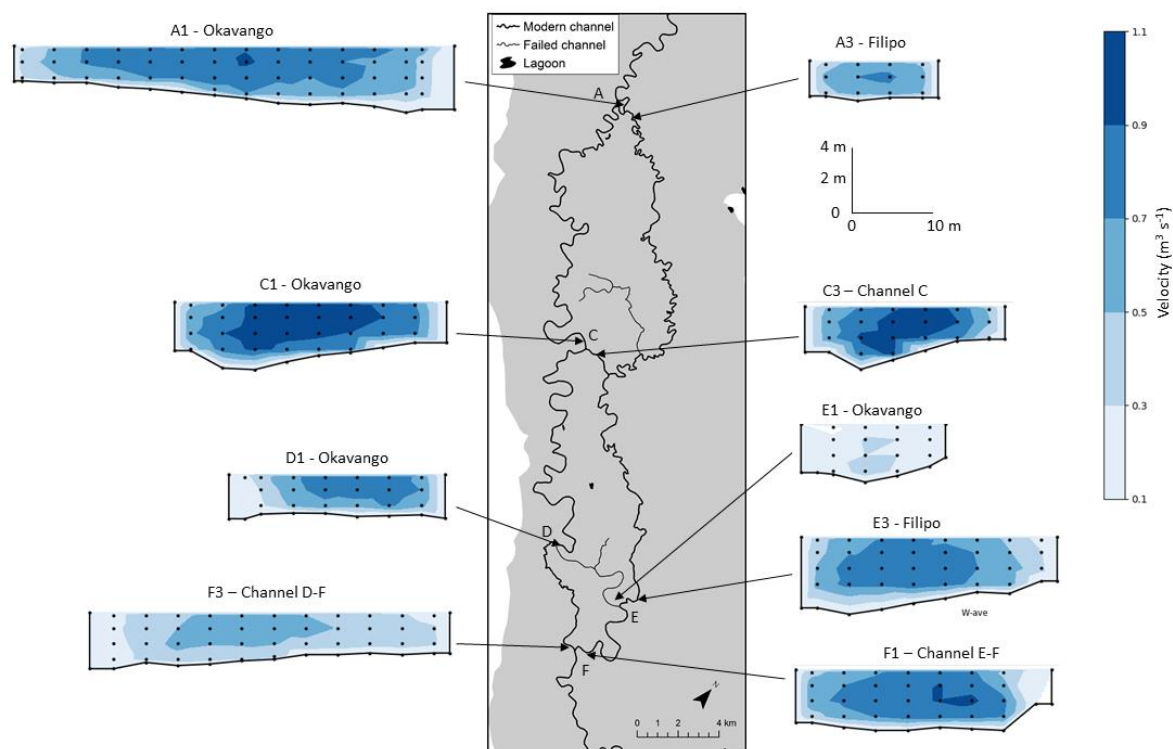
Supplementary Figure 1. Water depth-velocity sampling points and spatially integrated contour profiles for nine cross-sections in the anastomosing reach of the Okavango River in the Panhandle, measured in August 2016.
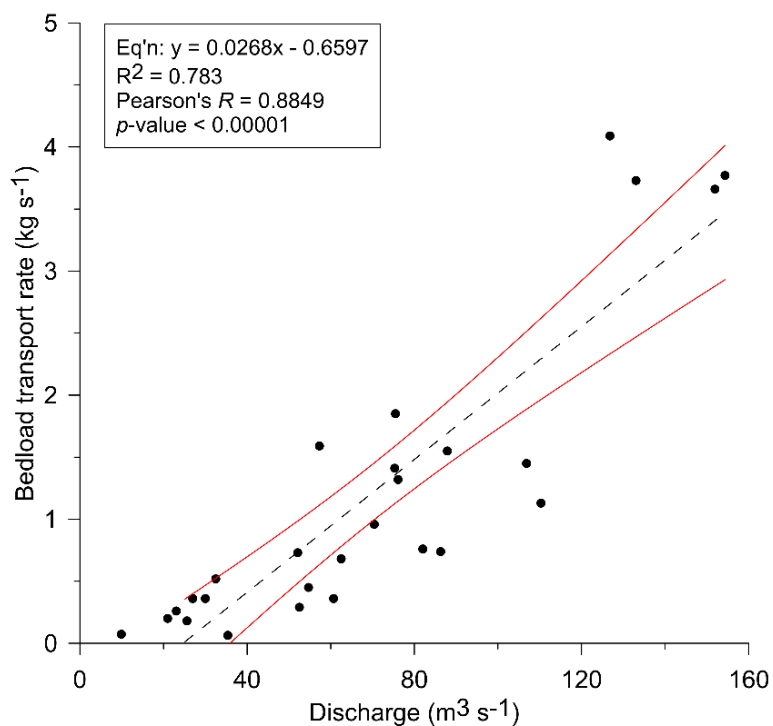
Supplementary Figure 2. Measured discharge and bedload transport from September 1995 and April 2008. The derivative equation was used to model bedload transport rates for November 2008 and August 2016 using discharge values measured in those field campaigns. Red lines indicate the 95 % confidence intervals.

Supplementary Table 1. Coordinates of the DGPS stations in the Okavango Panhandle.

DGPS station	Channel	Latitude	Longitude
BPS320	Okavango	18.360347160S	21.846303837E
UCT1	Okavango	18.457098754S	22.034561130E
UCT2	Filipo	18.594131522S	22.118595302E
UCT3	Okavango	18.744468580S	22.196842627E
UCT4	Okavango	18.814902775S	22.289434296E
UCT5	Okavango	18.822027439S	22.414752660E
UCT13	Okavango	18.801610454S	22.260317161E
UCT14	Okavango	18.760256180S	22.218057460E
UCT15	Okavango	18.698873537S	22.170473970E
UCT16	Okavango	18.682198193S	22.172539890E
UCT17	Okavango	18.648721898S	22.120502826E
UCT18	Okavango	18.552390494S	22.104857933E
UCT19	Filipo	18.620973989S	22.160363357E
UCT20	Filipo	18.652287748S	22.191486578E
UCT21	Filipo	18.692557188S	22.194601579E
UCT22	Filipo	18.726421463S	22.245504267E

Supplementary Table 2. Depth and velocity data measured at cross section sites at avulsion nodes A-F.

Cross-section site	Depth (m)			Velocity (m s^{-1})		
	1995	2008	2016	1995	2008	2016
A1	3.05	3.62	4.2	0.58	0.486	0.57
A2	-	-	-	-	-	-
A3	2.03	2.65	2.5	0.48	0.337	0.49
B1	2.66	-	-	0.61	-	-
B2	-	-	-	-	-	-
B3	2.39	-	-	0.41	-	-
C1	2.72	3.02	4.3	0.61	0.75	0.7
C2	-	-	-	-	-	-
C3	3.38	3.68	4	0.52	0.815	0.64
D1	2.75	2.38	2.85	0.56	0.523	0.49
D2	2.09	-	-	0.46	-	-
D3	3.28	-	-	0.57	-	-
E1	2.1	-	3.7	0.38	-	0.21
E2	3.25	-	-	0.49	-	-
E3	4.48	-	4.9	0.48	-	0.53
F1	-	3.06	3.9	-	0.67	0.59
F2	3.61	-	-	0.55	-	-
F3	3.35	2.6	3.6	0.26	0.332	0.38

CHAPTER 5

Threshold responses of dryland rivers to future global hydroclimatic change

Larkin Z.T.[1]*, Ralph T.J.[1], Tooth S.[2,3], Fryirs K.[1], Carthey A.J.R.[4]^

[1]Department of Environmental Sciences, Macquarie University, North Ryde, NSW, Australia

[2]Department of Geography and Earth Sciences, Aberystwyth University, Aberystwyth, UK

[3]School of Geosciences, University of the Witwatersrand, Johannesburg, South Africa

[4]Department of Biological Sciences, Macquarie University, North Ryde, NSW, Australia

(zacchary.larkin@hdr.mq.edu.au*, tim.ralph@mq.edu.au, set@aber.ac.uk, kirstie.fryirs@mq.edu.au, alexandra.carthey@mq.edu.au)

*Corresponding author

^ See Table 1.1 in chapter 1 for author contributions.

Abstract

Rivers provide crucial ecosystem services in water-stressed drylands. Dryland rivers are geomorphologically diverse, ranging from through-going, single channels to discontinuous, multi-channelled systems, yet we have limited understanding of their sensitivity to future hydroclimatic changes. Here, we characterise for the first time the geomorphology of dryland rivers with catchments across a humid to arid gradient covering >1,800,000 km^2 of continental eastern Australia. Statistical separation of five specific river types and quantification of their present-day catchment hydroclimates enables identification of potential thresholds of change. Projected aridity increases across eastern Australia by 2070 (RCP4.5) will result in ~80% of the dryland rivers crossing a threshold from one type to another, thereby undergoing major geomorphological changes. The most dramatic cases will see currently through-going rivers (e.g. Murrumbidgee, Macintyre) experience step changes towards greater discontinuity, characterised by pronounced downstream declines in channel size and local termination. Our approach and findings are applicable to the analysis of other dryland rivers globally where hydroclimate is the principal driver of change. Early identification of dryland river responses to future hydroclimatic change has far-reaching implications for the approximately 2 billion people that live in drylands and rely on riverine ecosystem services.

Main text

Rivers are lifelines in climatically variable and water-stressed drylands, the dry subhumid through hyperarid environments that cover 40-50% of the Earth's land surface and host ~28% of the world's population (1, 2). Dryland rivers are fundamentally important for human populations, providing a

plethora of provisioning, regulating, supporting and cultural ecosystem services (3, 1). Yet dryland rivers exist in marginal environments and are threatened by declines in water availability due to climate change and human impacts (4, 5). Rivers are not static conduits of water, sediment and nutrients, but adjust dynamically to a suite of internal and external drivers. Among various external drivers (e.g. tectonic activity, sea level fluctuations, climate), research has shown that late Quaternary hydroclimatic changes have driven substantial geomorphological changes to many dryland rivers globally (e.g. 6-9). To date, however, assessment of the potential likelihood and pathways of geomorphological changes in dryland rivers due to future hydroclimate changes have not been considered in any rigorous or systematic fashion (10-11). Analyses of future changes have tended to focus on dryland hydrology, such as surface water availability or river flow regimes (e.g. 5, 12-14), rather than the implications of these changes for river physical structure and behaviour (e.g. number of channels, sinuosity, lateral stability, landform assemblages). This is a critical knowledge gap, as dryland river geomorphology provides the physical template atop which complex ecosystems and anthropogenic land uses operate and intersect (15), thereby defining the range and quality of ecosystem service delivery.

In drylands, a continuum of river types extends from relatively high-energy rivers that maintain a single, continuous channel downstream, to lower energy, declining or discontinuous rivers that undergo various forms of channel breakdown, including disintegration into networks of multiple, smaller channels and/or termination on unchannelled plains termed floodouts (cf. 16; Fig. 1). In some instances, channel breakdown is associated with extensive floodplain wetlands (e.g. 17) that provide ecosystem services in these water-stressed settings (e.g. wildlife habitat, water filtration and supply). Previous research has suggested that this continuum of river types may be related to hydroclimatic gradients, with greater aridity leading to a greater propensity for channel breakdown (18-19). To refine these concepts and identify globally relevant thresholds of change in dryland rivers, we characterise for the first time the geomorphology of rivers draining >1,800,000 km^2 of continental eastern Australia, and establish the hydroclimatic conditions under which different river types persist. First, we categorise Australian dryland rivers into five types using a suite of geomorphological characteristics. Second, we establish the distinct hydrological characteristics of these river types using streamflow gauge data and correlate these characteristics with catchment aridity. Third, by establishing robust and significant relationships between modern dryland river types, hydrology and catchment aridity, we define envelopes of aridity index (AI) values for each river type. Fourth, we use downscaled global climate model projections to project future hydroclimatic changes. Where projections suggest a catchment will shift outside of the envelope of aridity defined by modern climatic data, we anticipate the trajectory of geomorphological change for that river and identify the geomorphological thresholds that may be crossed. This approach provides a conceptually sound, quantitatively-tested method for broader, continental and global studies of dryland river sensitivity to hydroclimatic changes. Early identification of dryland river responses to such changes will have far-reaching implications for the assessment of future changes to dryland river ecosystem service delivery.

Diversity of Australian dryland rivers

Much of continental eastern Australia is characterised by large catchments that host perennial, intermittent or ephemeral rivers and associated wetlands. These catchments are located in a post orogenic, intracratonic setting, where denudation rates and river sediment loads are low compared to global averages. Beyond the headwaters, many rivers follow lengthy courses across piedmonts and lowland plains where bedrock outcrop is less common, few substantial tributary inputs are received, and alluvial river styles dominate (20). While Australian dryland rivers display a range of alluvial styles (e.g. single channel versus multiple channel), with many also undergoing downstream morphological changes, we have defined five geomorphological types represented in the middle to lower reaches of Australian dryland rivers (Fig. 1, Supplementary Fig. 1). Two overarching categories are recognised: rivers with through-going channels to their catchment outlet (e.g. a lake or another river) and rivers with discontinuous channels (e.g. characterised by zones where channels lose definition or where channels terminate). Further differentiation is achieved by defining dominant river planform (sinuous, non-sinuous) and pattern (meandering, straight, anabranching/anastomosing, distributary), the nature of downstream decline in channel size after leaving valley (bedrock) confinement (maintaining, declining, or terminating), and the presence/absence and type of wetlands (Supplementary Table 1 and methods). The five types are: Type 1 – through-going, sinuous channels that maintain size downstream; Type 2 – through-going, sinuous channels that decline in size downstream; Type 3 – through-going to discontinuous, sinuous channels that decline in size downstream; Type 4 – discontinuous, non-sinuous channels that that decline in size downstream; Type 5 – discontinuous, non-sinuous channels that decline in size downstream and terminate (e.g. at a floodout) (Fig 1).
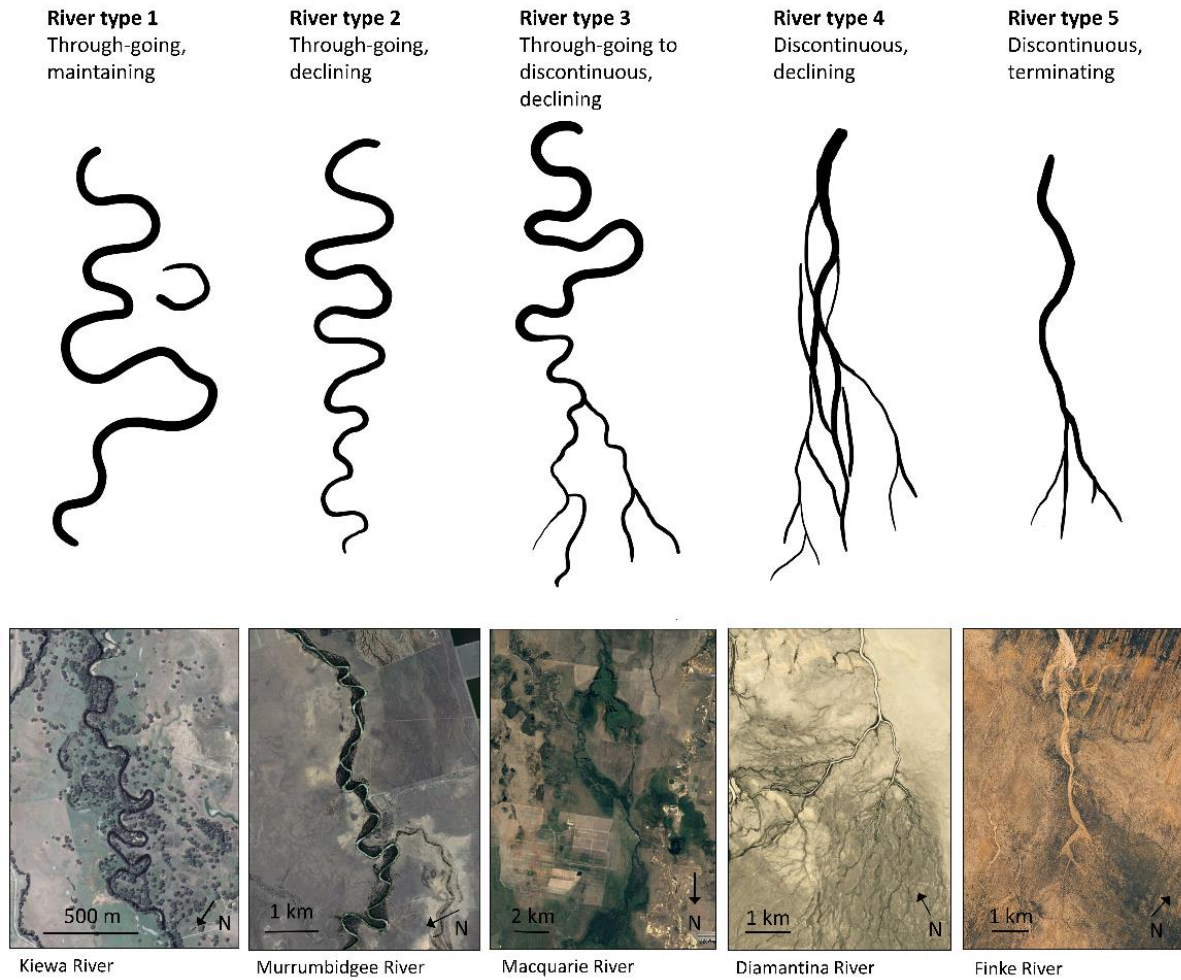
Figure 1. Schematic of the five dryland river types defined in this study, with satellite images of typical examples from various Australian rivers (Google Earth, 2017). Flow direction is from top to bottom in all diagrams and images.

Climatic gradient in continental eastern Australia

Approximately 78% of the Australian continent is classified as dryland (21), and across the eastern half of the continent, there is a pronounced aridity gradient from humid (AI >0.65), through dry subhumid (AI 0.65-0.5) and semiarid (AI 0.5-0.2), to arid (AI 0.2-0.05) (Fig. 2). Pronounced periods of above- and below-average rainfall combine to also make Australian hydroclimates (including river flow regimes) some of the most variable in the world (22-26), a characteristic that persists despite the presence of dams and associated flow regulation in many catchments. In this tectonically stable setting, and in reaches where rivers are free from bedrock influence, these hydroclimatic variations are a key driver of channel-floodplain geomorphology and river response. The relationship between climate, hydrology, and geomorphology is complex but may be expressed through various metrics including mean and peak runoff, flow variability, and stream power. Stream power is a function of river discharge and slope, and represents the energy exerted by water on the bed and banks of a river (27). It is widely used as a quantitative measure of the potential for flow to initiate channel adjustment through erosion or deposition (28-29).
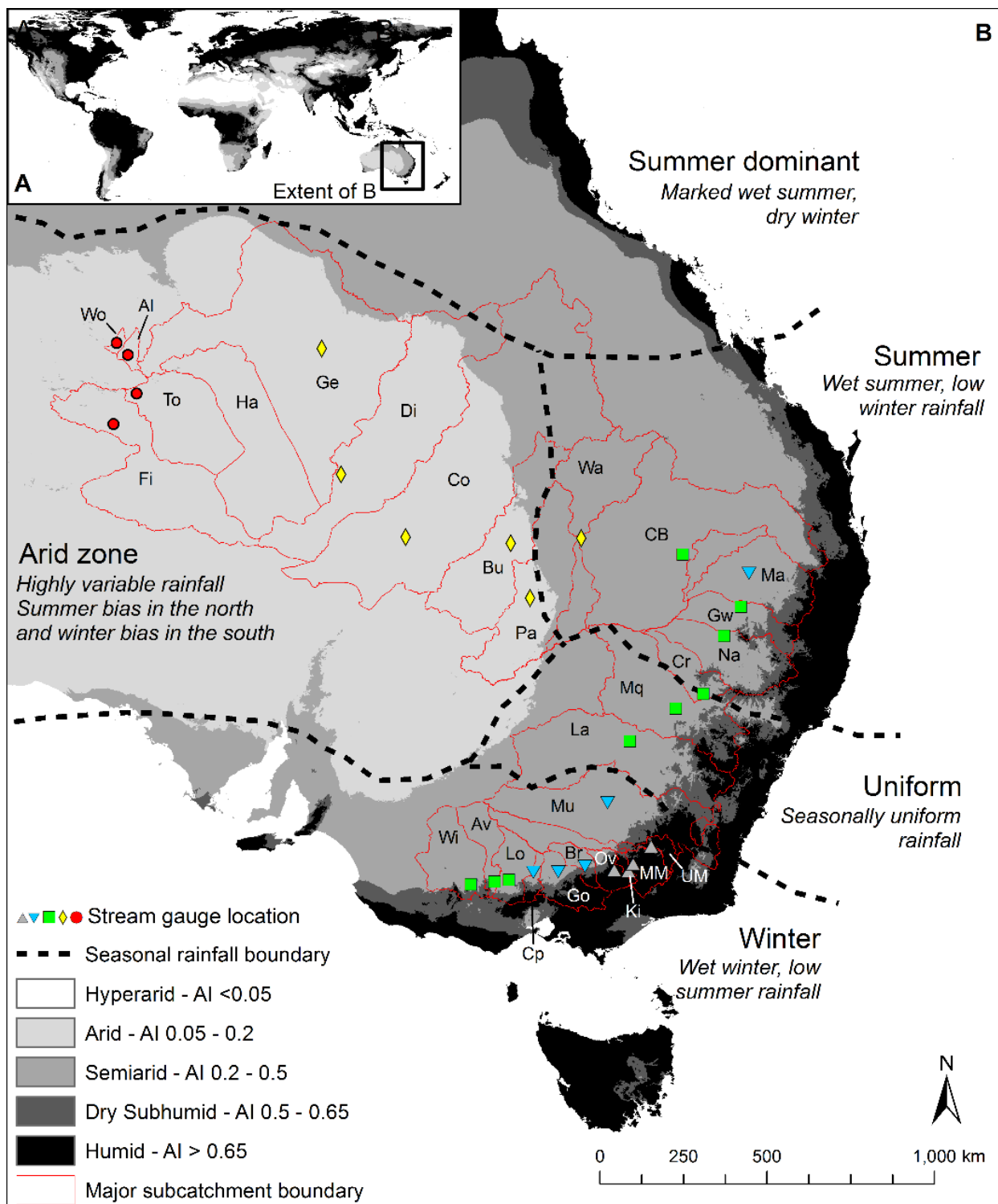
Figure 2. Global aridity index [AI] = annual precipitation [PPT]/annual potential evapotranspiration [PET] for (A) the world and (B) central and southeastern Australia. AI data sourced from a publicly available dataset (30). Drylands have AI <0.65 (31). There are currently no hyperarid regions on the Australian continent. In B), seasonal rainfall boundaries are marked by dashed black lines and are adapted from the Australian Bureau of Meteorology's climate classification data. Stream gauges were selected nearest to the end of bedrock confinement in each sub-catchment and symbols represent different river types: open black triangles are Type 1; inverted blue triangles are Type 2; green squares are Type 3; yellow diamonds are Type 4; and red circles are Type 5 (see Fig. 1). Study catchments are labelled as follows: Ki – Kiewa, MM – Mitta Mitta, Ov – Ovens and UM – Upper Murray (open black triangles); Br – Broken, Cp – Campaspe, Go – Goulburn, Ma – Macintyre and Mu – Murrumbidgee (inverted blue triangles); Av – Avoca, CB – Condamine-Balonne, Cr – Castlereagh, Gw – Gwydir, La – Lachlan, Lo – Loddon, Mq – Macquarie, Na – Namoi and Wi – Wimmera (green squares); Bu – Bulloo, Co – Cooper Creek, Di – Diamantina, Ge – Georgina, Pa – Paroo and Wa – Warrego (yellow diamonds); Al – Allungra Creek, Fi – Finke, Ha – Hay, To – Todd and Wo – Woodforde (red circles). Note there is no useable gauge in the Hay catchment.

Hydroclimatic controls on Australian dryland river geomorphology

To examine the links between hydroclimate and geomorphology, the five river types (Fig. 1; Table S1) have been subjected to pairwise analysis of similarities (ANOSIM) of key variables (Fig. 3; Supplementary Table 3 and Supplementary Table 4). AI is the variable that best defines significant differences between river types (except for Types 4 and 5; one-way ANOVAs, see Supplementary Fig. 1). Through-going, maintaining rivers (Type 1) occur in catchments where ~65-87% of the total catchment area is classed as humid and mean catchment AI is 0.8-1.0 (Fig. 3; Supplementary Fig. 2). Through-going, declining rivers (Type 2) occur in catchments where ~7-48% of total catchment area is classed as humid and mean catchment AI is 0.45-0.78. Through-going to discontinuous, declining rivers (Type 3) occur in catchments where ~0.2-8% of the total catchment area is classed as humid and mean catchment AI is 0.3-0.46. Discontinuous, declining rivers (Type 4) have no catchment area that is humid or even dry subhumid and mean catchment AI is 0.14-0.28. Discontinuous, terminating rivers (Type 5) occur in catchments that are typically 100% arid and mean catchment AI is 0.10-0.17 (Fig. 3; Supplementary Fig. 2).
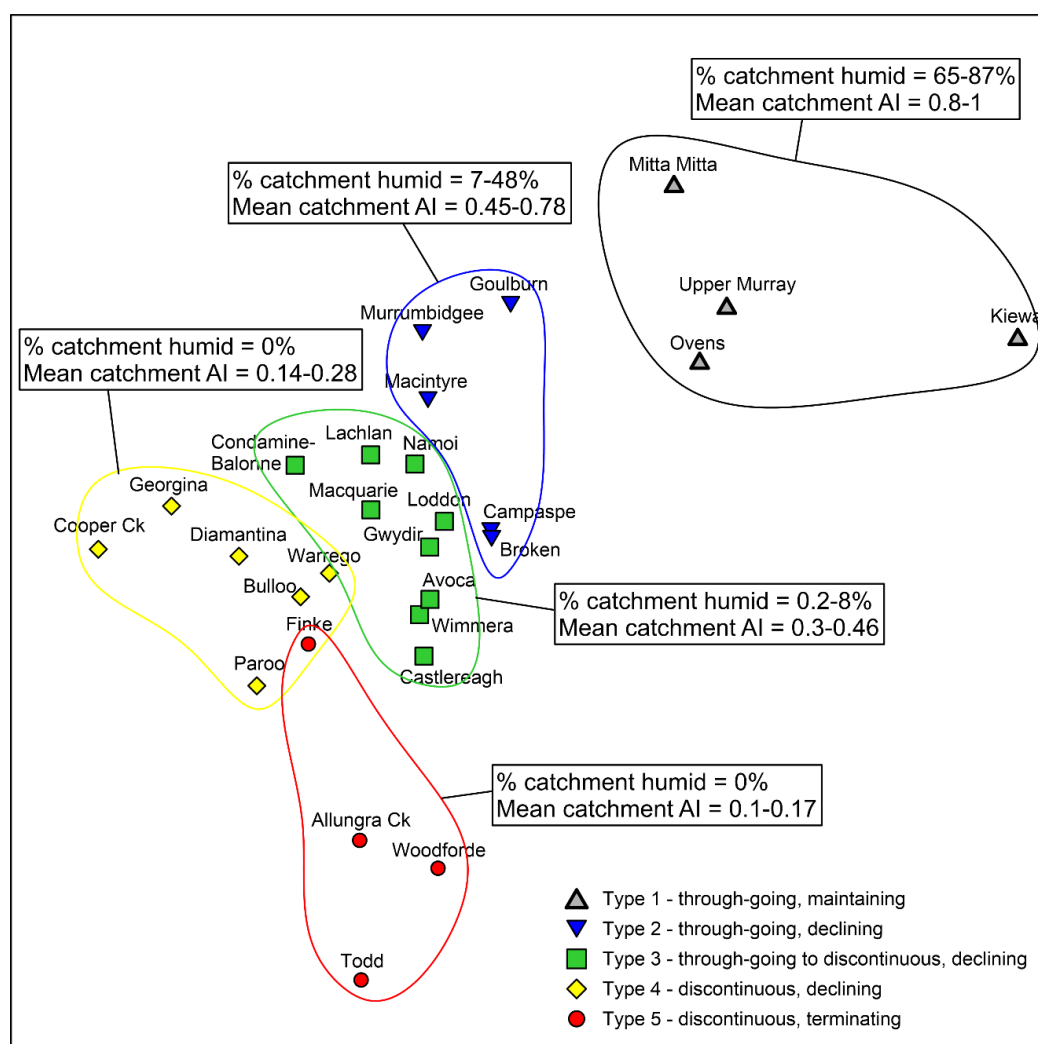
Figure 3. Non-parametric multidimensional scaling (MDS) resemblance matrix visualising the level of similarity between each river type based on key geomorphological and hydroclimatic variables (see methods; Supplementary Table 1). Each river type is significantly different from one another (pairwise ANOSIM $p < 0.05$; see

Supplementary Table 3 and Supplementary Table 4). Each point represents a different river and points closer together are more similar to one another based on the measured variables, and points further apart are more dissimilar. Pairwise ANOSIM analysis shows that each river type is statistically different from one another ($p < 0.05$; see Supplementary Table 3 and Supplementary Table 4). Annotations summarise the percentage of catchment area classed as humid for each river type, and the envelopes of mean catchment AI values for each river type.

The links between catchment aridity and key hydrologic variables (including river flow metrics) have been established in previous research (e.g. 22-26) but the distinct trends and clusters that emerge from this analysis demonstrate comprehensively, for the first time, the level of control that hydroclimate exerts on the geomorphology of these Australian dryland rivers. There is a strong and significant positive correlation between AI and mean annual runoff (Pearson's $R = 0.79$, p = 0.00001), and all river types are significantly different except for Types 4 and 5 (pairwise ANOSIM, p<0.05; Fig. 4A). There is a significant positive correlation between AI and mean peak annual runoff (Pearson's $R = 0.59$, p = 0.004), and all river types are significantly different except for Types 2 and 3 (pairwise ANOSIM, p<0.05; Fig. 4B). There is a strong and significant positive correlation between AI and bankfull gross stream power (Pearson's $R = 0.78$, p = 0.001; Fig. 4C). There is a strong and significant negative correlation between AI and coefficient of annual flow (CV_{af}; Pearson's $R = -0.78$, p = 0.00001), and all river types are significantly different except for Types 2 and 3 (pairwise ANOSIM, p<0.05; Fig. 4D).

Overall, catchments with a mean AI classed as humid or dry subhumid have greater mean annual runoff (>40 mm a^{-1}) and stream power (>900 W m^{-1}), lower flow variability (CV_{af} <0.9), and support through-going river types (most Types 1 and 2). Catchments with a mean AI classed as semiarid or arid have lower mean annual runoff (<55 mm a^{-1}) and gross stream power (<760 W m^{-1}), greater flow variability (CV_{af} >0.8), and tend to be characterised by discontinuous river types (most Type 3 rivers, and Types 4 and 5; Fig. 4). These thresholds define the hydroclimatic conditions that are responsible for channel (dis)continuity in these dryland rivers (i.e. through-going vs. discontinuous). There is also an intrinsic, but poorly defined, channel termination threshold (type 5 rivers have mean annual peak runoff of <2mm) causing Type 4 and 5 rivers to break down into unchannelised wetlands or floodouts.
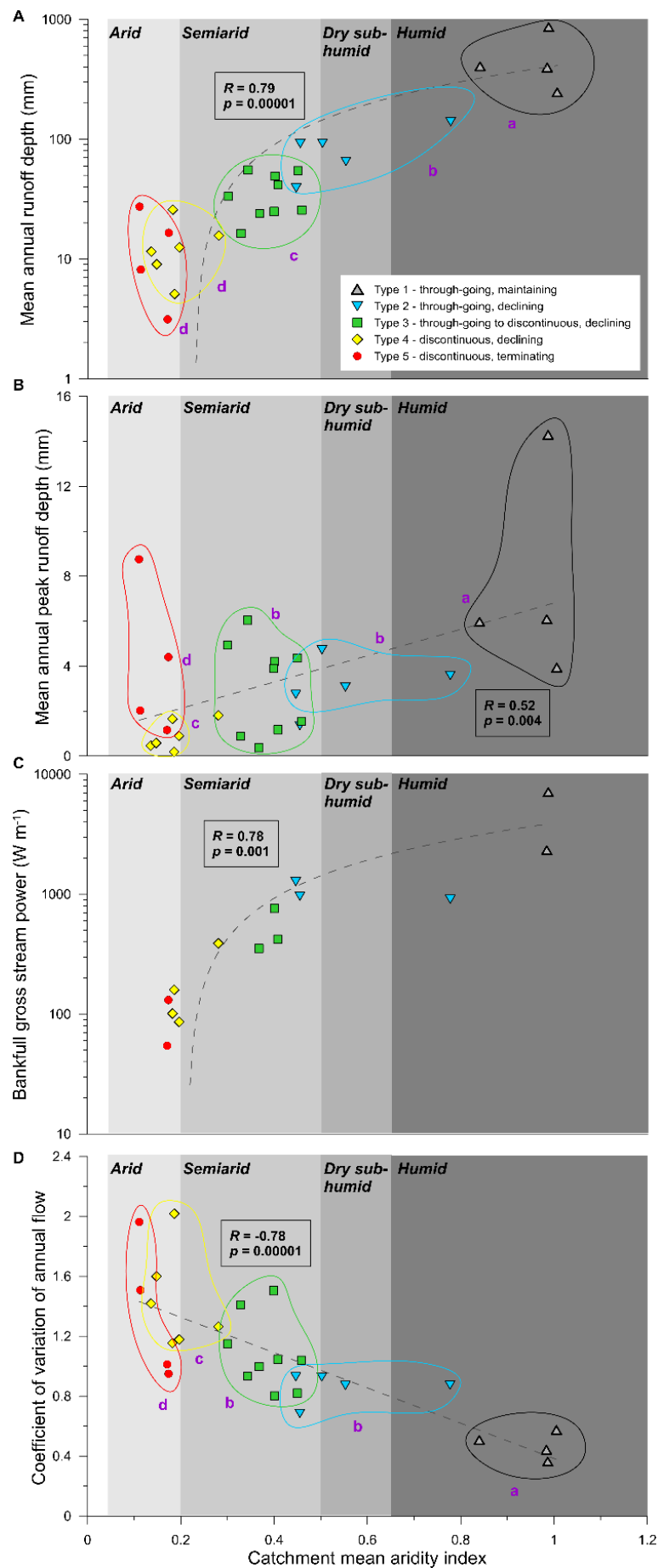
Figure 4. Catchment mean AI plotted against various hydrologic and hydraulic parameters. Pearson's correlation coefficient (*R*) indicates the strength of the linear association between the variables (note that the log-scale for A and C makes the regressions appear curved). The p-value (*p*) indicates the statistical significance of the linear

correlation between the variables. Lowercase purple letters indicate the results of a pairwise ANOSIM; groups sharing the same letter are not significantly different. (A) mean annual runoff depth (mm) at stream gauge locations nearest to the end of bedrock confinement in each sub-catchment (see Fig. 2 for gauge locations); (B) mean annual peak runoff depth (mm); (C) bankfull gross stream power (estimated using bankfull discharge estimates from gauged cross sections and ratings tables). In this case, there are insufficient gauge data to confidently estimate bankfull stream power for all rivers, meaning statistical analysis across river types cannot be undertaken; (D) CV_{af}.

These findings highlight the key influence of hydroclimatic conditions on river types across a continuum, manifested in differences in river planform, pattern and downstream channel (dis)continuity. Many Australian dryland rivers, especially Types 2, 3, 4 and 5, are characterised by downstream declines in bankfull discharge (Supplementary Fig. 1), which result from flow transmission losses associated with floodwave attenuation, evapotranspiration, or groundwater recharge (32-34). Downstream declines in bankfull discharge are commonly associated with downstream decreases in channel slope, which collectively result in downstream decreases in stream power and sediment transport capacity, thus promoting sediment deposition. These changes may lead to a contraction of channel width and/or to channel avulsion, the process of channel relocation on a floodplain (e.g. 35). Avulsion can form new channels that may supersede the original trunk channel in single-channel rivers, or create new channels that operate in parallel with the trunk channel in multi-channelled rivers. In more arid settings, however, there is a threshold beyond which stream power becomes too low to maintain sediment transport in a defined channel. Hence, channel breakdown occurs, leading to unchannelised wetlands (Types 3 and 4) and/or floodouts without significant wetlands (Type 5), particularly where there are barriers to flow resulting from aeolian or alluvial deposits, or minor bedrock outcrop (16).

Recognition of these links between hydroclimates and dryland river geomorphology allows each of the five river types to be defined within a range of catchment AI values. Establishing these AI envelopes allows us to identify which rivers exist close to a threshold between different river types, and then use climate projections to forecast future trajectories of change for rivers subject to changing hydroclimatic conditions.

Climate change projections and impacts on Australian dryland rivers

Previous studies investigating future hydrological changes to inland Australian rivers have predicted lower stream flows resulting from warming and altered precipitation patterns (36-39). Decreases in runoff in southern Australia have been projected with a high confidence, resulting from both reductions in winter rainfall and increased temperatures (39). These projected runoff decreases in southern Australia accord with our projections of increased future aridity in continental eastern Australia for 2070 (see Supplementary Fig. 3) under representative concentration pathway 4.5 (RCP4.5; cf. 40). RCP4.5 is a relatively moderate climate change pathway and was chosen to understand which rivers are the most sensitive to conservative scenarios of future climate change. Interestingly, our modelling of future

aridity under RCP8.5 suggests very similar changes in aridity over the Australian continent (Supplementary Fig. 3), likely due to increased projected rainfall across parts of northern and central Australia under RCP8.5, as well as higher projected temperatures, relative to RCP4.5, resulting in a similar net projected change in AI for both scenarios. Since contemporary levels of catchment aridity are closely correlated with mean and peak annual runoff, stream power, and flow variability (Fig. 4), and different hydroclimatic conditions are associated with distinct river types, we can assess how Australian dryland rivers may respond to projected hydroclimatic changes related to aridity indices. Given the magnitude of rainfall reductions and evapotranspiration increases projected for much of the Australian continent under RCP4.5 (Supplementary Fig. 3), many catchments will likely experience substantial aridification (Fig. 5; Supplementary Fig. 3). Particularly sensitive rivers are those that are close to a threshold of change between different river types and that therefore may be subject to significant geomorphological adjustments under these future climate conditions.

Indeed, of the 29 rivers analysed in this study, 23 (~80%) are projected to cross a threshold to another river type due to future catchment aridification and associated changes in hydrological conditions under RCP4.5 (Fig. 5). The largest magnitude changes are likely to affect the currently through-going, maintaining rivers (Type 1) with headwaters in the Australian southeastern highlands. These highlands are projected to have some of the most severe reductions in rainfall (see Supplementary Fig. 3), likely as a result of a projected upward trend in the southern annular mode which shifts the average track of the southern hemisphere westerlies further south, reducing winter rainfall over southern Australia (41). All four Type 1 rivers are projected to change to through-going, declining rivers (Type 2). Reduced runoff and stream power will likely lead to sediment deposition and downstream declines in channel size (Fig. 5). Although the Kiewa, Mitta Mitta, Upper Murray and Ovens rivers (Type 1) occupy only a small proportion of the Murray-Darling Basin (3.8%), they currently supply a disproportionately large amount of discharge (>33%) to the basin. Therefore, reductions in mean annual runoff and downstream declines in flow will have major impacts for water users and ecosystem services in this basin, which is Australia's most important agricultural region.

The most dramatic change in river morphology is from a through-going, declining river (Type 2) to a more discontinuous river (Types 3 and 4). Under RCP4.5, the currently through-going, declining Campaspe, Broken, Macintyre, and Murrumbidgee rivers (Type 2) are projected to have significantly reduced discharges and stream powers and more highly variable flow regimes, thereby becoming discontinuous rivers more characterised by channel breakdown and unchannelised wetlands (Types 3 and 4). A change in river structure and function of this magnitude will decrease hydrological and sediment connectivity, with profound and lasting impacts on water and sediment distribution, ecosystem dynamics, and ecosystem services in systems that are currently heavily used for irrigated agriculture and grazing. These changes are potentially irreversible and will increase the likelihood of

ecosystem collapse in these marginal environments (c.f. 42). This will likely exacerbate existing high tensions surrounding water use and storage in inland Australia (43-44).

Nearly all of the currently through-going to discontinuous (Type 3) rivers except the Gwydir and Namoi are projected to become Type 4 rivers with discontinuous, declining channels (Fig. 5). Catchment aridification may also impact inundation regimes in semi-permanent and intermittent floodplain wetlands associated with these rivers, likely inducing a change to more ephemeral floodplain wetlands, or semi-permanent in-channel waterholes. Potential reductions in discharge and flow frequency will be particularly profound for wetlands of national and international ecological importance (e.g. Ramsar wetlands) such as the Macquarie Marshes, Gwydir wetlands, Narran Lake wetlands, and the Great Cumbung Swamp on the lower Lachlan River. Except for the Warrego River (Fig. 5), further declines in flow may result in many of these rivers even transitioning into discontinuous, terminating rivers (Type 5) with few or no significant wetlands.

Discontinuous, terminating rivers (Type 5) are projected to experience even more arid hydroclimatic conditions, most likely with even greater flow variability than at present. While there are currently no Australian dryland rivers that are characterised by the levels of aridity projected for the Hay, Todd, and Finke catchments (Fig. 5), increased flow variability may impact severely on the health of the well-developed riparian vegetation assemblages that are such a critical influence on channel process and form in these rivers (20). There are no hyperarid regions currently on the Australian continent, but reference to other hyperarid areas around the world (e.g. central Sahara Desert), may provide an indication of what can expected for the small regions of Australia projected to experience hyperarid conditions by the second half of this century (e.g. lack of bankline-stabilising vegetation; Supplementary Fig. 3).

In summary, greater aridification of the Australian continent is projected for the second half of this century under both moderate (RCP4.5) and business-as-usual (RCP8.5) scenarios (Supplementary Fig. 3). The influence of this enhanced aridification on the hydrology, physical structure, and biogeomorphic function of Australian dryland rivers is likely to be dramatic but, until now, has not been considered in any rigorous or systematic manner. Our approach is a quantitively-tested form of ergodic reasoning with powerful uses for understanding river response to future climate change.

Catchment AI envelope for each river type based on modern catchments.
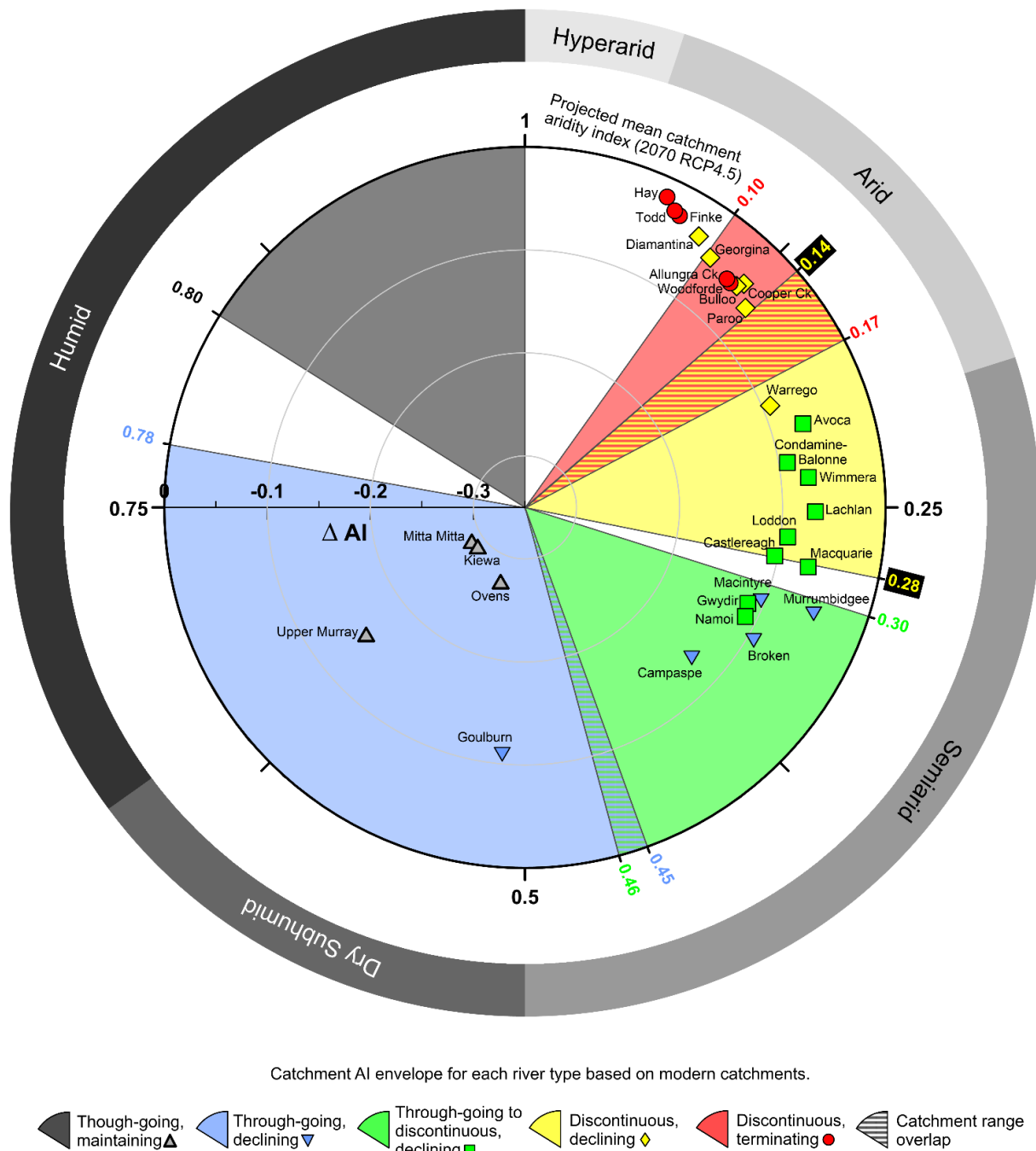
Figure 5. Polar plot displaying the projected catchment AI value for each catchment (angle axis) and the raw change in AI value for each river projected for 2070 RCP4.5 (radius axis). Note that rivers closest to the centre of the plot have the largest projected Δ AI. Coloured segments represent the envelope of AI values assigned to each river type based on modern catchment characteristics. Future catchment AI and Δ AI values are plotted over the top of these catchment envelopes. Catchment symbols represent the modern river type and those that are a different colour to the underlying segment are rivers projected to change river type by 2070 RCP4.5.

Implications for river response in drylands globally

Our findings demonstrate that even under a relatively conservative future emissions scenario (RCP4.5), projected aridification and associated changes to hydrological conditions across continental eastern Australia are likely to lead to significant geomorphological thresholds being crossed this century. The vast majority of rivers included in this study were highly sensitive to hydroclimatic change.

While Australia possesses a number of distinctive river styles (e.g. 20), the novel approach outlined in this study can be used to assess the geomorphic sensitivity of dryland rivers globally, especially where hydroclimatic factors are the key drivers of river response. Many parts of dryland Africa, South and North America, and central and western Asia are generally projected to experience declines in surface water availability and river flow in coming decades (13-14, 45-49). As such, rivers in these regions may also respond to hydroclimatic change by transitioning from through-going to more discontinuous river types. For instance, despite varying degrees of bedrock control, river morphology in southern Africa varies across strong hydroclimatic gradients, with through-going, maintaining rivers more common in subhumid catchments, and through-going and declining or discontinuous and/or terminating rivers more common in semiarid and arid catchments (18-19). In drylands where there is a higher degree of tectonic and bedrock influence on valley confinement and river morphology (e.g. the Mediterranean and parts of the Middle East), the influence of hydroclimatic drivers on river adjustment may manifest in different ways to those outlined here. For example, in steep, confined river valleys, dryland rivers may respond mainly by altering the magnitude of cut and fill cycles rather than by undergoing any pronounced changes in channel continuity (20). In these settings, our approach will still be valid, although different weightings for the suite of controlling conditions and new thresholds will need to be identified for different river types.

Forecasting the sensitivity of dryland river geomorphology to climate-driven hydrological changes is critical due to the importance of geomorphology for the range and quality of ecosystem services in these marginal environments (1). Dryland rivers sustain many unique and threatened ecosystems and help support the livelihoods of approximately 2 billion people who live in the world's drylands (1-2). Given heightened concern over the likelihood of a global average temperature rise of >1.5 °C by the end of the century, major changes to hydroclimates and river geomorphology are likely to occur within a few generations. Our approach to forecasting likely geomorphological changes in dryland rivers provides a key tool to identify thresholds of river response in otherwise poorly monitored systems, and may provide advance warning of such changes to inform water resource development, adaptation, and management strategies.

References

1. Millennium Ecosystem Assessment (MEA) *Ecosystems and Human Well-being: Wetlands and Water* (World Resources Institute: Washington, DC, 2005).

2. Van der Esch S. et al. *Exploring future changes in land use and land condition and the impacts on food, water, climate change and biodiversity: Scenarios for the Global Land Outlook.* (PBL Netherlands Environmental Assessment Agency, The Hague, 2017).

3. Costanza, R. et al. The value of the world's ecosystem services and natural capital. *Nature* **387,** 253–260 (1998).

4. Pekel, J.-F., Cottam, A., Gorelick, N., & Belward, A.S. High-resolution mapping of global surface water and its long-term changes. *Nature* **540,** 418–422 (2016).

5. Rodell, M. et al. Emerging trends in global freshwater availability. *Nature* **557,** 651-659 (2018).

6. Schumm, S.A. *The Fluvial System*. (Wiley, New York, 1977).

7. Nanson, G.C. and Tooth, S., 1999. Arid-zone rivers as indicators of climate change, In: *Palaeoenvironmental Reconstructions in Arid Lands* (Balkema, Rotterdam, 1999, pp.175-216).

8. Woodward, J.C., Williams, M.A.J., Garzanti, E., Macklin, & M.G., Marriner, N. From source to sink: Exploring the Quaternary history of the Nile. *Quat. Sci. Rev.* **130,** 3–8 (2015).

9. Hesse, P.P. et al. Palaeohydrology of lowland rivers in the Murray-Darling Basin, Australia. *Quat. Sci. Rev.*, **200,** 85-105 (2018).

10. Lane, S.N. 21st century climate change: Where has all the geomorphology gone? *Earth Surf. Process. Landforms* **38,** 106–110 (2013).

11. Fryirs, K.A. River sensitivity: A lost foundation concept in fluvial geomorphology. *Earth Surf. Process. Landforms* **42(1),** 55-70. (2017).

12. Nijssen, B., O'Donnell, G.M., Hamlet, A.F., & Lettenmaier, D.P. Hydrologic sensitivity of global rivers to climate change. *Clim. Change* **50,** 143–175 (2001).

13. Milly, P.C.D., Dunne, K.A., & Vecchia, A. V., Global pattern of trends in streamflow and water availability in a changing climate. *Nature* **438,** 347–350 (2005).

14. De Wit, M. and Stankiewicz, J. Changes in surface water supply across Africa with predicted climate change. *Science* **311,** 1917-1921 (2006).

15. Brierley, G.J. & Fryirs, K.A. Eds. 2008. *River Futures: An Integrative Scientific Approach to River Repair* (Island Press, Washington DC, 2008).

16. Tooth, S. 1999. Floodouts in central Australia. In: Miller, A.J., Gupta, Ž.A. Eds., *Varieties of Fluvial Form* (Wiley, Chichester, pp. 219–247, 1999).

17. Tooth, S. & McCarthy, T.S., Wetlands in drylands: geomorphological and sedimentological characteristics, with emphasis on examples from southern Africa. *Prog. Phys. Geogr.* **31,** 3–41 (2007).

18. Grenfell, S.E., Grenfell, M.C., Rowntree, K.M., & Ellery, W.N. Fluvial connectivity and climate: A comparison of channel pattern and process in two climatically contrasting fluvial sedimentary systems in South Africa. *Geomorphology* **205,** 142–154 (2014).

19. Larkin, Z.T., Ralph, T.J., Tooth, S., & McCarthy, T.S., The interplay between extrinsic and intrinsic controls in determining floodplain wetland characteristics in the South African drylands. *Earth Surf. Process. Landforms* **42,** 1092–1109 (2017).

20. Tooth S. & Nanson G.C. Distinctiveness and diversity of arid zone river systems. In: *Arid Zone Geomorphology: Process, Form and Change in Drylands*, Thomas D.S.G. Ed., 3rd edn. (John Wiley & Sons: Chichester; 269–300, 2011).

21. Peel M.C., Finlayson B.L., & McMahon T.A. Updated world map of the Köppen-Geiger climate classification. Hydrology and Earth System Sciences Discussions, European Geosciences Union, 4 (2), pp.439-473 (2007).

22. McMahon, T.A., Finlayson, B.L., Haines, A., & Srikanthan, R., 1987. Runoff variability: a global perspective, In: The Influence of Climatic Change and Climatic Variability on the Hydrologic Regime and Water Resources, IAHS Publ., **168,** 3-12 (1987).

23. McMahon, T.A., Peel, M.C., Vogel, R.M., & Pegram, G.G.S. Global streamflows - Part 3: Country and climate zone characteristics. *J. Hydrol.* **347,** 272–291 (2007).

24. McMahon, T.A., Murphy, R.E., Peel, M.C., Costelloe, J.F., & Chiew, F.H.S. Understanding the surface hydrology of the Lake Eyre Basin: Part 2-Streamflow. *J. Arid Environ.* **72,** 1869–1886 (2008).

25. Verdon, D.C., Wyatt, A.M., Kiem, A.S., & Franks, S.W. Multidecadal variability of rainfall and streamflow: Eastern Australia. *Water Resour. Res.* **40,** 1–8 (2004).

26. Peel, M.C., McMahon, T.A., & Finlayson, B.L., Continental differences in the variability of annual runoff-update and reassessment. *J. Hydrol.* **295,** 185–197 (2004).

27. Brierley G.J. & Fryirs K.A. *Geomorphology and River Management: Applications of the River Styles Framework* (Blackwell Publications: Oxford; 398, 2005).

28. Chang, H.H. Minimum stream power and river channel patterns. *J. Hydrol.* **41,** 303–327 (1979).

29. Yochum, S.E., Sholtes, J.S., Scott, J.A., & Bledsoe, B.P. Stream power framework for predicting geomorphic change: The 2013 Colorado Front Range flood. *Geomorphology* **292,** 178–192 (2017).

30. Trabucco, A., Zomer, R.J., 2009. Global Aridity Index (Global-Aridity) and Global Potential Evapo-Transpiration (Global-PET) Geospatial Database., in: Information, C.C.f.S. (Ed.), Published online, available from the CGIAR-CSI GeoPortal at: http://www.csi.cgiar.org.

31. United Nations Environment Programme (UNEP). *World Atlas of Desertification* (Edward Arnold: London; 15–45, 1992).

32. Knighton, A.D. & Nanson, G.C. Flow transmission along an arid zone anastomosing river, Cooper Creek, Australia. *Hydrol. Process.* **8(2),** 137-154 (1994).

33. Ralph, T.J. & Hesse, P.P. Downstream hydrogeomorphic changes along the Macquarie River, southeastern Australia, leading to channel breakdown and floodplain wetlands. *Geomorphology* **118,** 48–64 (2010).

34. Pietsch, T.J. & Nanson, G.C. Bankfull hydraulic geometry; the role of in-channel vegetation and downstream declining discharges in the anabranching and distributary channels of the Gwydir distributive fluvial system, southeastern Australia. *Geomorphology* **129,** 152–165 (2011).

35. Slingerland, R. & Smith, N.D., River avulsions and their deposits. *Annu. Rev. Earth Planet. Sci* **32,** 257–285 (2004).

36. Hughes, L. Climate change and Australia: Trends, projections and impacts. *Austral Ecol.* **28,** 423–443 (2003).

37. Chiew, F.H.S. & McMahon, T.A. Modelling the impacts of climate change on Australian streamflow. *Hydrol. Process.* **16,** 1235–1245 (2002).

38. Chiew, F.H.S., Young, W.J., Cai, W., & Teng, J. Current drought and future hydroclimate projections in southeast Australia and implications for water resources management. *Stoch. Environ. Res. Risk Assess.* **25,** 601–612 (2011).

39. CSIRO and Bureau of Meteorology (BoM). Projections: Atmosphere and the land, Climate Change in Australia Information for Australia's Natural Resource Management Regions: Technical Report, 2015.

40. van Vuuren, et al. The representative concentration pathways: An overview. *Clim. Change* **109,** 5–31 (2011).

41. Shi, G., Ribbe, J., Cai, W., Cowan, T., & Nin, E. An interpretation of Australian rainfall projections. *Geophys. Res. Lett.* **35,** 1–6 (2008).

42. Harris, R.M.B., et al. Biological responses to the press and pulse of climate trends and extreme events. *Nat. Clim. Chang.* **8,** 579–587 (2018).

43. Kingsford, R.T. Ecological impacts of dams, water diversions and river management on floodplain wetlands in Australia. *Austral Ecol.* **25,** 109–127 (2000).

44. Connell, D. & Grafton, R.Q. Water reform in the Murray-Darling Basin. *Water Resour. Res.* **47(4),** 1–9 (2011).

45. Nash, L.L. & Gleick, P.H. Sensitivity of streamflow in the Colorado Basin to climatic changes. *J. Hydrol.* **125,** 221–241 (1991).

46. Shongwe, M.E., et al. Projected Changes in Mean and Extreme Precipitation in Africa under Global Warming. Part I: Southern Africa. *J. Clim.* **22,** 3819–3837 (2009).

47. Schewe, J. et al. Multimodel assessment of water scarcity under climate change. *Proc. Natl. Acad. Sci. U.S.A.* **111(9),** 3245-3250. (2013).

48. Seager, R. et al. Projections of declining surface-water availability for the southwestern United States. *Nat. Clim. Chang.* **3,** 482–486 (2013).

49. IPCC, 2014. Climate Change 2014: Synthesis Report. Contribution of Working Groups I, II and III to the Fifth Assessment Report of the Intergovernmental Panel on Climate Change, IPCC.

Acknowledgements

Author contributions

Z.L. and T.R. conceived the paper and developed the approach to assessing dryland river sensitivity to climate change. S.T., K.F. and A.C. helped to refine the approach and develop the paper. Z.L. collated all data and conducted the preliminary data analyses and modelling. Z.L. and T.R. designed all figures, and Z.L. drafted all figures and the initial text. A.C. assisted with statistical analyses. All authors provided feedback and edited drafts of figures and text, and all authors approved the final version of the paper.

Competing interests

The authors declare no competing interests.

Data availability

Modern aridity index data are publicly available from Trabucco and Zomer's (2009) Global Aridity Index (Global-Aridity) and Global Potential Evapo-Transpiration (Global-PET) Geospatial Database., in: Information, C.C.f.S. (Ed.), Published online, available from the CGIAR-CSI GeoPortal at: http://www.csi.cgiar.org. Downscaled global climate model projection data are publicly available from WorldClim – Global Climate data at: www.worldclim.org/. The data that support the findings of this paper are available from the corresponding author upon reasonable request.

Methods

River types

Large river catchments in continental eastern Australia straddle different climate zones from humid through to arid (Fig. 2). The rivers included in this study in some cases have humid upper reaches, but all have drylands (subhumid through arid climates) covering between 10 and 100% of their catchment areas. A framework was developed to categorise river types based on their geomorphological characteristics. The rivers analysed were the Kiewa, Mitta Mitta, Ovens, Upper Murray, Broken, Campaspe, Goulburn, Macintyre, Murrumbidgee, Avoca, Condamine-Balonne, Castlereagh, Gwydir, Lachlan, Loddon, Macquarie, Namoi, Wimmera, Bulloo, Cooper Creek, Diamantina, Georgina, Paroo, Warrego, Allungra Creek, Finke, Hay, Todd, and Woodforde. Although dryland river types fall along a continuum (50-51), we use five geomorphological characteristics to define five dryland river types (Fig.

1, Supplementary Table 1) as derived using Google Earth satellite imagery and a 30 m Shuttle Radar Topography Mission (SRTM) digital elevation model (DEM):

1. longitudinal continuity of channels (through-going, discontinuous);
2. nature of reduction in channel width downstream of the end of major bedrock confinement (maintaining, declining, terminating);
3. dominant river planform (sinuous, non-sinuous),
4. dominant river pattern (single-thread (meandering, straight), multi-thread (anabranching, anastomosing, distributary));
5. presence/absence of wetlands, and where present, type of wetlands (e.g. permanent, intermittent, ephemeral).

Supplementary Table 1. Geomorphological measures used to differentiate the five dryland river types.

Channel continuity		Dominant river planform	Dominant river pattern	Wetlands (presence/ absence, type)	River type
Through-going	Maintaining	sinuous	meandering or anabranching/anastomosing	permanent wetlands	Type 1 – through-going, maintaining
	Declining			permanent and intermittent wetlands	Type 2 – through-going, declining
Discontinuous			meandering/straight, anabranching/anastomosing, or distributary		Type 3 – through-going to discontinuous, declining
		non-sinuous		intermittent and ephemeral wetlands	Type 4 – discontinuous, declining
	Terminating		straight, anabranching/anastomosing, or distributary, with trunk channel terminating in a floodout (unchannelled plain)	no significant wetlands	Type 5 – discontinuous, terminating

Aridity, hydrology and hydraulics

Aridity has been expressed as mean annual precipitation (MAP) divided by potential mean annual evapotranspiration (MAE; 52). Aridity index (AI) data were sourced from the datasets compiled by Trabucco and Zomer (2009, 53), available from the Consultative Group for International Agriculture Research Consortium for Spatial Information (CGIAR-CSI) GeoPortal (http://www.csi.cgiar.org). Hydrology data were sourced from the New South Wales Department of Primary Industries Office of Water, the Victorian Department of Environment, Land, Water and Planning Water Measurement Information System, the Queensland Government Water Monitoring Information Portal, and the

Northern Territory Water Resources Data and Information Centre. Gauges were chosen as near as possible to the end of bedrock confinement on each river (i.e. usually in the transition from the upper to middle reaches) and each had at least 30 years of continuous flow records, except for the Finke River and Allungra Creek gauges that had 13 and 16 years of flow records, respectively (Supplementary Table 2). It should also be noted that the Hay River does not have a suitable gauge and was not included in hydrological analysis, but was included for catchment aridity analyses.

Supplementary Table 2. Stream gauges that provided the flow data used in this study (see Fig. 2).

River	Gauge name	Gauge number	Period of gauge record	Number of years
Mitta Mitta	Tallandoon	401204	1934 – 2017	83
Kiewa	Mongan's Bridge	402203	1955 – 2017	62
Upper Murray	Jingellic	401201	1900 – 2017	117
Ovens	Myrtleford	403210	1961 – 2017	56
Goulburn	Murchison	405200	1900 – 2017	117
Campaspe	Barnadown	406201	1978 – 2017	39
Broken	Casey's Weir	404242	1972 – 2017	45
Murrumbidgee	Narrandera	410005	1914 – 2017	103
Macintyre	Boggabilla	416002	1900 – 2017	117
Lachlan	Condobolin	412006	1900 – 2017	117
Macquarie	Baroona	421127	1986 – 2017	31
Gwydir	Pallamallawa	418001	1900 – 2017	117
Namoi	Mollee	419039	1965 – 2017	52
Loddon	Laanecoorie	407203	1900 – 2017	117
Wimmera	Eversley	415207	1963 – 2017	54
Condamine-Balonne	St George	422201F	1971 – 2017	46
Avoca	Archdale Junction	408206	1987 – 2017	30
Castlereagh	Mendooran	420004	1953 – 2010	57
Warrego	Wyandra	423206A	1967 - 2017	50
Paroo	Willara Crossing	424002	1975 – 2017	42
Cooper Creek	Nappa Merrie	003103A	1965 – 2017	52
Bulloo	Autumnvale	011202A	1967 – 2017	50
Diamantina	Birdsville	A0020101	1966 – 2017	51
Georgina	Roxborough Downs	001203A	1967 – 2017	50
Finke	Finke RS Crossing	G0050116	2004 – 2017	13
Todd	Heavitree Gap	G0060126	1973 – 2017	44
Woodforde	Arden Soak	G0280010	1975 – 2017	42
Allungra Creek	Allungra Waterhole	G0280004	2001 – 2017	16

Hydrological variables were calculated from these flow records using standard methods. Mean annual runoff was calculated by dividing mean annual discharge (megalitres; ML) by catchment area (km^2). Mean annual peak runoff was calculated by dividing mean annual peak discharge (ML) by catchment area (km^2). Coefficient of variation of annual flow (CV_{af}) was calculated by dividing the standard deviation of mean annual discharge by mean annual discharge. Hydraulic variables were calculated from a combination of hydrological data derived from these flow records and topographic (i.e. slope) data derived from 3-5 km transects along the floodplain at each gauge location using a 30 m SRTM DEM. Gross bankfull stream power is the product of bankfull discharge ($m^3\,s^{-1}$), channel slope (m m^{-1}), and the

specific weight of water-sediment mixture (given the low suspended loads of most Australian rivers, this was assumed constant at 9800 kg m^{-2} s^{-2}). The relationships between aridity and specific hydrological variables (annual runoff depth [annual discharge normalised for catchment area] and coefficient of variation of annual flow) were then analysed using basic linear regressions.

Climate data and future climate projections

ArcMap v.10.2 software was used for catchment scale analyses of AI, precipitation, and future climate model outputs. Gridded modern AI data was clipped to each study subcatchment and the proportional aridity was calculated with exported cell counts of each unique AI value in the sub-catchment (cells equivalent to ~1 km by ~1 km). Weighted mean catchment AI was also calculated from this output.

To derive future precipitation and potential evapotranspiration, we used outputs from 16 downscaled global climate models (GCMs) that were part of the Intergovernmental Panel on Climate Change's (IPCC) Fifth Coupled Model Intercomparison Project (CMIP5, 54). These models are BCC-CSM1-1, CCSM4, CNRM-CM5, GFDL-CM3, GISS-E2-R, HadGEM2-AO, HadGEM2-CC, HadGEM2-ES, INMCM4, IPSL-CM5A-LR, MIROC-ESM-CHEM, MIROC-ESM, MIROC5, MPI-ESM-LR, MRI-CGCM3, and NorESM1-M. The outputs used were from model runs assuming Representative Concentration Pathway (RCP) 4.5. The relatively conservative RCP4.5 was chosen to understand which dryland river catchments were most sensitive to even relatively moderate scenarios of future climate change. Future aridity under RCP8.5 was also modelled to understand the difference between scenarios (see Supplementary Fig. 3). Due to projected increases in rainfall over parts of northern and central Australia under RCP8.5 relative to RCP4.5 (Supplementary Fig. 3), projected net change in AI over the Australian continent is very similar for both RCP4.5 and RCP8.5. RCPs are named according to the radiative forcing of greenhouse gases expected for 2100 depending on various scales of emissions reductions (RCP2.6, 4.5, 6, 8.5) (55). RCP4.5 is a relatively moderate future pathway in which emissions peak around 2040 and then decline with a radiative forcing of 4.5 W m^{-2} above pre-industrial values by 2100 (55). Future projected precipitation is an output from the CMIP5 models. Mean annual temperature (Tmean) and annual temperature range (Trange) were the outputs used in conjunction with solar radiation (RA) to model future potential evapotranspiration using the Hargreaves-Samani equation (Equation (1); 56-59). The Hargreaves-Samani equation was used to calculate the modern AI used in this study (53) and was therefore also for the future projections. It has been shown to perform nearly as well as the common FAO Penman method but requires substantially less parametrisation with more readily available data (58). Future projected precipitation was then divided by modelled future potential evapotranspiration to provide future AI values across Australia.

$$\text{Equation (1) } PET = 0.0023RA(Tmean + 17.8)Trange^{0.5}$$

Multivariate analysis of variables associated with river types

The five river types were compared across 10 hydrological and geomorphological variables (Supplementary Table 3) using a multivariate approach in Primer v6 (60). Data for 11 variables was collected (Supplementary Table 3; Supplementary Fig. 1), however bankfull gross stream power was not included in statistical tests due to inadequate data. ANOSIM (analysis of similarity) and pairwise tests among all combinations of river types were performed on a resemblance matrix based on Euclidean distances, and based on 9999 permutations. R statistics were calculated for each pairwise comparison, where R values closer to 1 indicate greater differences between two compared groups (60). Significance was determined where $p<0.05$ (Supplementary Table 4). Non-parametric multidimensional scaling (nMDS) plots were constructed based on the resemblance matrix to visually represent the similarity among rivers, where each point on the figure represents a single river, points closer together are more similar to one another on the measured variables, and points further apart are more dissimilar. One-way ANOVAs were also performed to determine the difference between river types for each variable. Tukey's honest significant difference (HSD) test determined which groups were significantly different from one another at $p < 0.05$. Results are presented in extended data (Supplementary Fig. 1).

Supplementary Table 3. Variables used in ANOSIM and their units. Geomorphological measures were calculated using Google Earth satellite imagery and a 30 m SRTM DEM. (Note: * not used in statistical analysis).

Variable	Units
Catchment area	km^2
Average slope of alluvial plain	$m\ m^{-1}$
Average sinuosity (channel distance/ valley distance)	Dimensionless
Proportional net change in channel width 50 km downstream of confinement	(%/50 km downstream of bedrock confinement)
Mean annual runoff depth	mm
Mean annual peak runoff depth	mm
Coefficient of variability of annual flow (std. dev./mean	%
Mean annual gross stream power	$W\ m^{-1}$
*Bankfull gross stream power	$W\ m^{-1}$
Mean catchment AI (mean annual precipitation/potential annual evapotranspiration)	Dimensionless
Median catchment AI (mean annual precipitation/potential annual evapotranspiration)	Dimensionless

References

50. Tooth S, Nanson GC. 2011. Distinctiveness and diversity of arid zone river systems. In Arid Zone Geomorphology: Process, Form and Change in Drylands, Thomas DSG (ed), third edn. John Wiley & Sons: Chichester; 269–300.

51. Tooth, S., 2013. Dryland Fluvial Environments: Assessing Distinctiveness and Diversity from a Global Perspective, Treatise on Geomorphology.

52. United Nations Environment Programme (UNEP). 1992. World Atlas of Desertification. Edward Arnold: London; 15–45.

53. Trabucco, A., Zomer, R.J., 2009. Global Aridity Index (Global-Aridity) and Global Potential Evapo-Transpiration (Global-PET) Geospatial Database., in: Information, C.C.f.S. (Ed.), Published online, available from the CGIAR-CSI GeoPortal at: http://www.csi.cgiar.org.

54. Hijmans, R.J., Cameron, S.E., Parra, J.L., Jones, G., Jarvis, A., 2005. Very high resolution interpolated climate surfaces for global land areas 25, 1965–1978.

55. van Vuuren, D.P., Edmonds, J., Kainuma, M., Riahi, K., Thomson, A., Hibbard, K., Hurtt, G.C., Kram, T., Krey, V., Lamarque, J.F., Masui, T., Meinshausen, M., Nakicenovic, N., Smith, S.J., Rose, S.K., 2011. The representative concentration pathways: An overview. Clim. Change 109, 5–31.

56. Hargreaves, G.H., Samani, Z.A., 1982. Estimating potential evapotranspiration. Journal of the Irrigation and Drainage Division – ASCE 108 (3), 225–230.

57. Hargreaves, G.H., Samani, Z.A., 1985. Reference crop evapotranspiration from temperature. Appl. Eng. Agric. 1 (2), 96–99.

58. Hargreaves, G.H., Allen, R.G., 2003. History and evaluation of Hargreaves evapotranspiration equation. J. Irrig. Drain. Eng. 129, 53–63. doi:10.1061/(ASCE)0733-9437(2003)129:1(53)

59. Heydari, M.M., Tajamoli, A., Ghoreishi, S.H., Darbe-Esfahani, M.K., Gilasi, H., 2015. Evaluation and calibration of Blaney–Criddle equation for estimating reference evapotranspiration in semiarid and arid regions. Environ. Earth Sci. 74, 4053–4063.

60. Clarke, K.R., and Gorley, R.N., 2006. PRIMER v6: User Manual/Tutorial. PRIMER-E: Plymouth

Supplementary Information
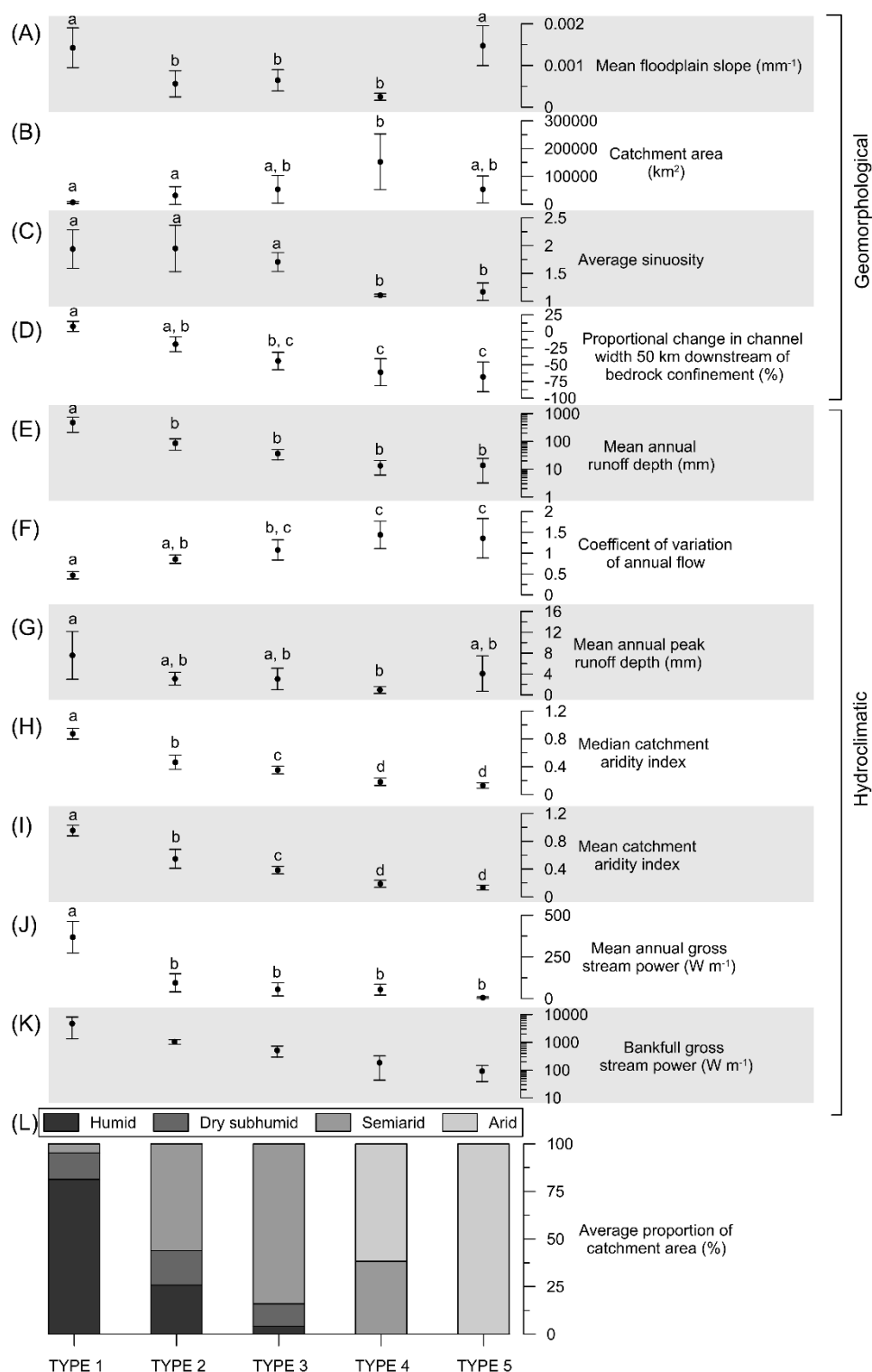
Supplementary Figure 1. Comparison of the five river types based on 11 geomorphological and hydroclimatic variables. Plots show mean plus error bars representing one standard deviation (Type 1, n = 4; Type 2, n = 5; Type 3, n = 9; Type 4, n = 6; Type 5, n = 4). One-Way ANOVAs were performed to identify statistically significant differences between river types for each variable. Points sharing the same letter are not significantly different according to Tukey's honest significant difference (HSD) test. (A) No systematic trend between floodplain slope and river type. (B) No systematic trend between catchment area and river type, although Types 1 and 2 tend to have smaller catchments. (C) Significant differences between sinuosity and river type, with Types 1, 2, and 3 having significantly higher sinuosity than Types 4 and 5. (D) Negative correlation between rate of downstream change in channel size and river type. (E) Negative correlation between mean annual runoff depth and river type, although the only significant difference is between Type 1 and the other types. (F) Positive correlation between CV_{af} and river type, albeit with substantial overlap between types. (G) Weak negative correlation between mean annual

peak runoff and river type. (H) Significant differences between river types explained by median catchment Aridity Index (AI), except for Types 4 and 5. (I) Significant differences between river types explained by mean catchment AI. Catchment aridity is the best variable to differentiate river types, except for Types 4 and 5. (J) Negative correlation between mean annual gross stream power (measured at gauge nearest to the end of bedrock confinement) and river types. (K) Negative correlation between bankfull gross stream power (measured at gauge nearest to the end of bedrock confinement) and river type, although there is not enough gauge data available to perform one-way ANOVAs. (L) Average proportion of catchment in each climate zone for each of the five river types demonstrates the progressive increase in the overall level of catchment aridity from Type 1 to Type 5.

Supplementary Table 4. One-way Analysis of Similarity (ANOSIM) pairwise test statistics.

River types	R statistic	Significance (P-value)
1, 2	0.781	0.008
1, 3	0.971	0.001
1, 4	0.996	0.005
1, 5	1.000	0.029
2, 3	0.350	0.008
2, 4	0.899	0.002
2, 5	0.956	0.008
3, 4	0.659	0.0004
3, 5	0.787	0.001
4, 5	0.548	0.010
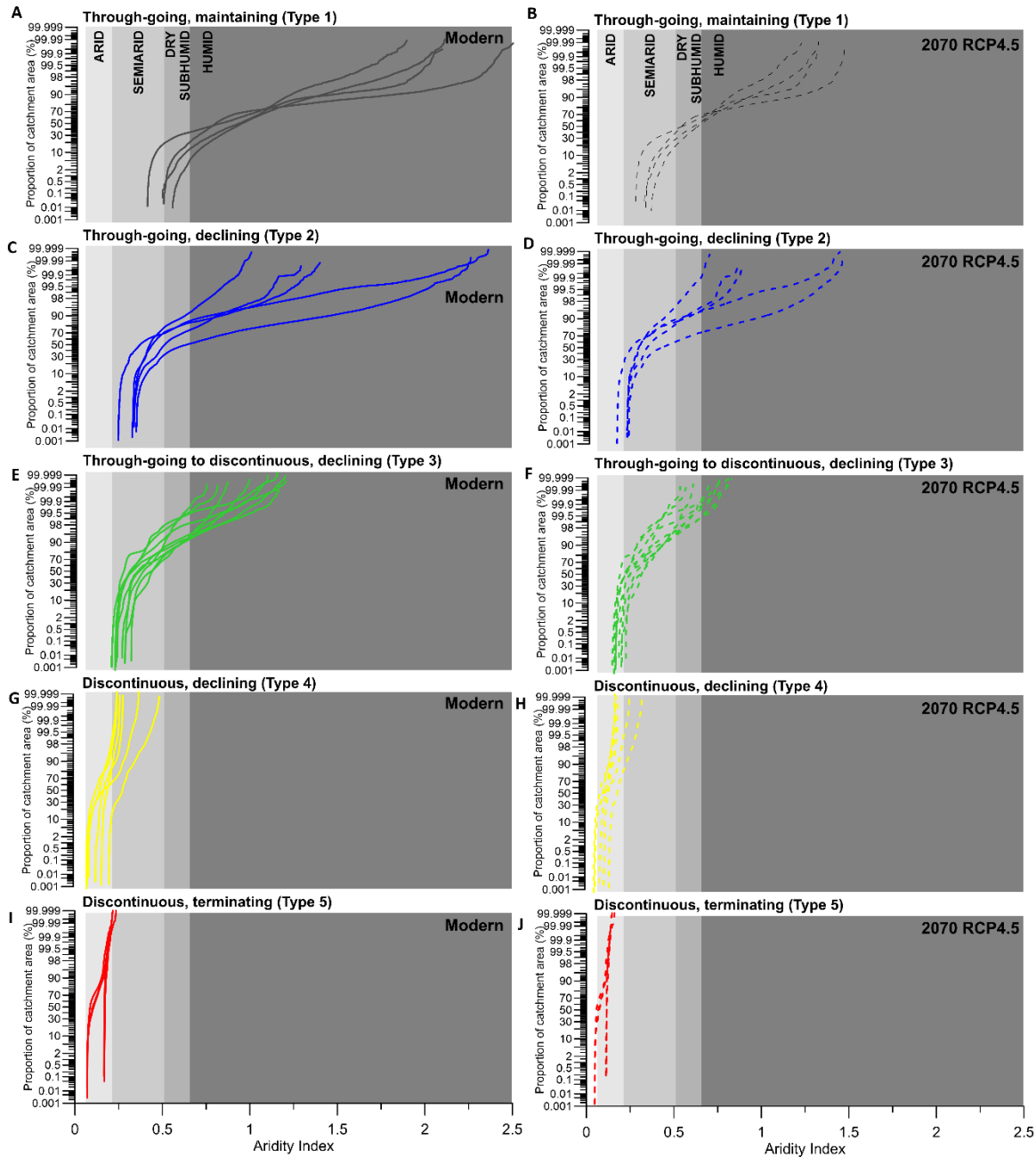
Supplementary Figure 2. The proportions of the catchments of the five river types in different climate zones, as defined by the Aridity Index (AI). Through-going maintaining (Type 1) and through-going, declining rivers (Type 2) have higher proportions of their catchment in humid regions. Through-going to discontinuous, declining rivers (Type 3) have much smaller proportions of their catchments in humid regions with discontinuous, declining (Type 4) and discontinuous, terminating (Type 5) rivers having entirely semiarid or arid catchments. These graphs are plotted with a probability y-axis (upper 10% and lower 10% plotted on log scale) to accentuate the differences between river types for the most humid 10% of each catchment.

A Modern PPT (1960 - 1990)

B 2070 RCP4.5 ΔPPT

C 2070 RCP8.5 ΔPPT

3800 mm

130 mm

>-200mm | -125mm - -75mm | -25mm - -10mm | +10mm - +25mm | +75mm - +125mm
-200mm - -125mm | -75mm - -25mm | -10mm - +10mm | +25mm - +75mm | +125mm - +200mm

D Modern AI (1960 - 1990)

E 2070 RCP4.5 AI

F 2070 RCP8.5 AI

Hyperarid - AI < 0.05   Arid - AI 0.05 - 0.2   Semiarid - AI 0.2 - 0.5   Dry Subhumid - AI 0.5 - 0.65   Humid - AI > 0.65
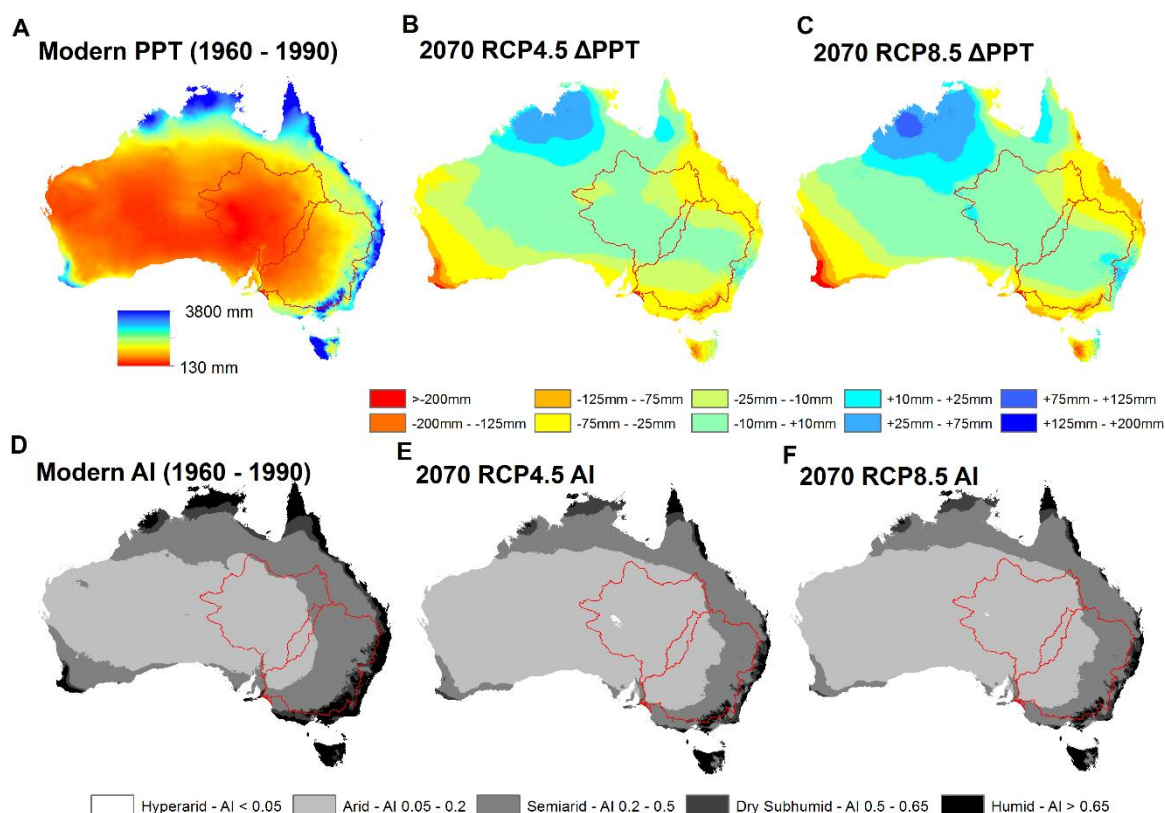
Supplementary Figure 3. (A) Modern distribution of annual precipitation (PPT, mm a^{-1}) across the Australian continent. (B) Average projected change in precipitation (PPT, mm a^{-1}) in 2070 using outputs from 14 IPCC CMIP5 GCMs under RCP 4.5. (C) Average projected change in precipitation (PPT, mm a^{-1}) in 2070 using outputs from 14 IPCC CMIP5 GCMs under RCP 8.5. (D) Modern Aridity Index (AI) across the Australian continent. (E) Projected (2070 RCP4.5) AI values across the Australian continent. (F) Projected (2070 RCP8.5) AI values across the Australian continent. The Murray-Darling, Bulloo, and Lake Eyre catchment boundaries (the main focus of this study) are marked in red.

CHAPTER 6

Discussion

6.1 Thesis synthesis

This thesis has explored the overarching controls on, and processes of, dryland river geomorphic responses to Holocene hydroclimatic change. Evidence from the Warrego and Okavango rivers demonstrates how profound morphological changes have occurred over recent millennia, leading to radically different river character and behaviour. In the Warrego, a large, sinuous meandering channel adjusted primarily by lateral channel migration during the mid Holocene (until ~4.7 ka). In contrast, the modern river is a much smaller, straight, multichanelled system which has dramatic downstream declines in discharge, numerous distributary channels, and experiences channel breakdown (Chapter 2). Similarly, lateral migration was the key process of river adjustment in the Okavango in the mid Holocene (until ~3.5 ka), while avulsion is now the key driver of channel adjustment, where much smaller channels fail and new channels form over annual to decadal timescales (Chapters 3 and 4). For Australian rivers in general, analysis of river morphology and channel discontinuity across a pronounced hydroclimatic gradient in central and eastern Australia has highlighted the role of climate in defining fluvial geomorphology and the likely future impacts of climate change (Chapters 5).

This discussion chapter is structured around the three key questions that guided this research (Table 6.1). First, to complement and expand on the empirical records presented in this thesis, Holocene fluvial records from drylands around the world will be assessed to understand how dryland rivers have responded to past hydroclimatic change (Section 6.2). Second, fundamental intrinsic processes of channel adjustment that define the natural range of variability of dryland rivers will be discussed in the context of extrinsic forcing. These forces can change the boundary parameters of a fluvial system, ultimately resulting in a change to a river's character and behaviour (Section 6.3). Third, given the high geomorphological sensitivity of the Warrego and Okavango rivers (and other dryland rivers around the world) to hydroclimatic changes, the implications of future climate change for dryland river geomorphology is considered in the context of the uncertainty surrounding such forecasting (Section 6.4).

Table 6.1. Relationship between the overarching research questions, thesis aims, research approach and the chapters of this thesis associated with each.

Research questions	Thesis objectives	Research approach	Associated chapters
How have dryland rivers responded to climate-driven hydrological change in the *past*?	1) Determine the timing of Holocene phases of enhanced fluvial activity in the Warrego and Okavango catchments. 2) Reconstruct the character and behaviour of the palaeo-Warrego and palaeo-Okavango.	- Sample large palaeochannels for optically stimulated luminescence dating. - Use modern width:discharge relationships to quantify the palaeohydrology of the Holocene Warrego and Okavango rivers and contrast with modern river hydrology. - Review literature to determine hydroclimatic drivers of Holocene river change.	Chapters 2 & 3
What processes define the natural range of variability of *modern* dryland rivers?	3) Define the character and behaviour of the modern Warrego and Okavango rivers and compare and contrast the modern river styles with the palaeo rivers. 4) Quantify patterns and mechanisms of key drivers of fluvial change, namely channel avulsion and failure in the Okavango River.	- Use detailed field surveys and mapping (historical aerial photos and satellite imagery) to quantify morphometric and hydraulic variables. - Measure discharge and water surface elevations and compare data from 1995, 2008 and 2016 to accurately track avulsion of the Okavango River. - Determine the mechanics of channel avulsion and failure in the Okavango River.	Chapters 3 & 4
How will dryland rivers respond to *future* hydroclimatic change?	5) Use global climate model projection data to assess future Australian dryland river response to climate change.	- Categorise Australian dryland rivers based on their geomorphology. - Statistically assess the differences between river types based on hydrological, climatic and geomorphological variables. - Define extrinsic aridity thresholds between river types. - Model future continental aridity for 2070 using global climate model outputs to predict which rivers are likely to cross these extrinsic thresholds.	Chapter 5

6.2 Global dryland river response to Holocene climate change

This thesis has presented new Holocene fluvial records from the Warrego and Okavango rivers showing that both of these catchments experienced significantly higher discharge during the mid Holocene and mid-late Holocene, and that hydroclimatic changes triggered dramatic step-changes in the character and behaviour of both rivers (Chapters 2 and 3). Such dramatic changes to fluvial systems in the Holocene have not been particularly well documented, and while highly constrained Holocene fluvial records from drylands are relatively scarce, there is emerging evidence that declines in fluvial activity have occurred in drylands on most continents since the mid Holocene (Table 6.2 and references therein). Compilation of published Holocene fluvial records from drylands suggest that, by and large, many systems were characterised by enhanced fluvial activity (e.g. large channels, higher discharges, more laterally active) during the mid Holocene and have shifted to lower energy conditions (e.g. smaller channels and

discharges, less laterally active) in the late Holocene (Table 6.2). The exact timing of this common morphological transition varies globally, which is to be expected given the thresholds and lags inherent in fluvial adjustment, the limitations of fluvial chronologies (e.g. resolution, amount of available material for dating), and the considerable complexities of climatic teleconnections and non-linearity of climate feedbacks in the ocean and atmosphere. However, with the notable exception of the North American southwest, the overwhelming pattern indicates a late Holocene quiescence of fluvial activity in drylands around the world (Table 6.2). This global pattern of mid-late Holocene decline in dryland fluvial activity appears to have been driven by changes to the Intertropical Convergence Zone (ITCZ) and the El Niño-Southern Oscillation (ENSO), which were discussed in the context of eastern Australia and southern Africa in Chapters 2 and 3, respectively.

Until now, this broad synchroneity of Holocene fluvial activity across the world's drylands has not been considered rigorously. Hence, taking a regional perspective, the following section of this discussion highlights the significance of the Warrego and Okavango Holocene records and synthesises key aspects of the changing character and behaviour of dryland rivers during the Holocene and their predominant hydroclimatic drivers.

Table 6.2. Summary of key Holocene dryland fluvial records from Africa, Australia, Asia, South America, and North America.

Continent (countries)	River system	Physiographic description of catchment	Climatic controls on rainfall/runoff	Mid Holocene fluvial characteristics	Late Holocene/ modern fluvial characteristics	Timing of transition	References
Africa (Angola, Botswana, Namibia)	Okavango River	Endorheic basin with low gradient headwater catchments extending north into the Angolan highlands. Catchment mantled by aeolian Kalahari sand. Okavango Delta occupies a large half graben related to the East African Rift System.	Monsoonal rainfall during the austral summer months over headwater catchments Angolan highlands. Atlantic and Indian Ocean sourced rainfall related to the Congo Air Boundary. Annual flood peak reaches the Okavango Delta during the austral winter months, which is the dry season.	Relatively large (120-160 m wide) meandering channel with rapid lateral migration rate (~6-9 m a^{-1}).	Relatively small (30-90 m) channel with very slow lateral migration rate during the historical period, but is characterised by periodic channel avulsion.	Uncertain but after ~3.5 ka	*This thesis;* Tooth et al. (in prep)
Africa (Algeria, Mali, Mauritania, Morocco)	Tamanrasett River	Rising in the Haggar and Atlas mountains, the palaeo-Tamanrasett flows westwards to the Atlantic Ocean.	Boreal summer rainfall related to the movement of the ITCZ. Very little rainfall under modern climate.	Unknown. However, active fluvial system was transporting sediment to the ocean.	Inactive fluvial system buried by aeolian sedimentation.	Uncertain but after ~6.5 ka	Skonieczny et al. (2015)
Africa (Libya)	Kufrah River	Rising in the Tibesti mountains, flowing north into the Mediterranean Sea.	Boreal summer rainfall related to the movement of the ITCZ. Very little rainfall under modern climate.	Unknown.	Inactive fluvial system buried by aeolian sedimentation.	Uncertain (no dating) but thought to be after the mid Holocene	Paillou et al. (2009; 2012)

Table 6.2. *Continued.*

Continent (countries)	River system	Physiographic description of catchment	Climatic controls on rainfall/runoff	Mid Holocene fluvial characteristics	Late Holocene/ modern fluvial characteristics	Timing of transition	References
Africa (Tanzania, Uganda, Ethiopia, Sudan, Egypt)	Nile River	Second largest basin on Earth, rising in Ugandan and Ethiopian highlands and flowing north through the 'Desert Nile' alluvial reaches of the Sahara Desert.	ITCZ rainfall during much of the year over the tropical Ugandan headwaters provides year round base flow which is enhanced by boreal summer monsoonal rainfall over the Ethiopian highlands.	Anabranching channel with higher discharge than present. Numerous wadis reactivated in the contemporary 'Desert Nile' contributed substantial amounts of water and sediment to the Nile.	Channel network contraction resulted in a single active channel that was narrower than in the mid Holocene. 'Desert Nile' wadis are inactive.	~4.5 ka	Woodward et al., (2015a, b)
Australia	Warrego River	Inland draining river in eastern Australia (tributary of the Barwon-Darling) with upland headwater catchments on the western slopes of the Great Dividing Range.	Rainfall and runoff are intermittent and mostly occur during the austral summer months related to localised convective thunderstorms or the southward penetration of monsoonal troughs.	Large, high-energy anabranching and meandering river. Laterally active channel with a well-developed meander belt and alluvial ridge.	Low sinuosity, laterally stable channel declining significantly in size downstream with numerous ephemeral distributary channels. Distributary channels break down into intermittent floodplain wetlands while waterholes along the main channel represent the only permanent surface water in the catchment.	After ~4.7 ka	*This thesis*

Table 6.2. *Continued.*

Continent (countries)	River system	Physiographic description of catchment	Climatic controls on rainfall/runoff	Mid Holocene fluvial characteristics	Late Holocene/ modern fluvial characteristics	Timing of transition	References
Australia	Macquarie River	Inland draining river in eastern Australia (tributary of the Barwon-Darling) with upland headwater catchments on the western slopes of the Great Dividing Range.	Annual rainfall is largely uniform with a slight summer seasonality. Most rain falls over headwater catchments in the Great Dividing Range. High interannual variability of runoff often well correlated with the El Niño-Southern Oscillation (ENSO).	Relatively large (~100 m wide) meandering, through-going channel that maintained a channelised course to its trunk stream, the Barwon River.	Small (~20-30 m wide) channel which declines dramatically in size downstream, and breaks down into a large system of unchannelised floodplain wetlands.	~5.6 ka	Yonge and Hesse 2009; Ralph and Hesse (2010); Hesse et al. (2018a, b)
Australia	Gwydir River	Inland draining river in eastern Australia (tributary Barwon-Darling) with upland headwater catchments on the western slopes of the Great Dividing Range.	Annual rainfall is largely uniform with a slight summer seasonality. Most rain falls over headwater catchments in the Great Dividing Range. High interannual variability of runoff often well correlated with the ENSO.	Mid Holocene fluvial characteristics are not well understood, but it is thought that prior to the transition to the modern system, the Gwydir would have been characterised by a single large channel.	Relatively small channel which declines dramatically in size downstream, forming several distributary channels and a series of floodouts associated with extensive floodplain wetlands.	Uncertain but thought to be mid Holocene (by ~5 ka)	Pietsch and Nanson (2011); Pietsch et al. (2013)

Table 6.2. *Continued.*

Continent (countries)	River system	Physiographic description of catchment	Climatic controls on rainfall/runoff	Mid Holocene fluvial characteristics	Late Holocene/ modern fluvial characteristics	Timing of transition	References
Australia	Hale River	Inland draining river in the Lake Eyre basin in central Australia. In its lower reaches the river is impeded by aeolian dunes of the Simpson Desert.	Rainfall and runoff amounts are generally low and highly variable. Runoff is generally generated by localised convective thunderstorms during the Austral summer months or related to monsoonal troughs/ex-tropical cyclones that penetrate far enough south over the Australian continent.	The mid-Holocene Hale River was characterised by a series of very large floods that reworked and redeposited aeolian dunes of the northern Simpson Desert.	Ephemeral channel that does not significantly rework aeolian dunes and terminates in the dunefield.	~4 ka	Tooth et al. (2017)
Australia	Finke River	Inland draining river in the Lake Eyre basin in central Australia. In its lower reaches the river is impeded by aeolian dunes of the Simpson Desert.	Rainfall and runoff amounts are generally low and highly variable. Runoff is generally generated by localised convective thunderstorms during the Austral summer months or related to monsoonal troughs/ex-tropical cyclones that penetrate far enough south over the Australian continent.	Actively laterally migrating with relatively high rates of floodplain formation by vertical accretion. This mid Holocene period is also correlated with a hiatus in dune-building.	Ephemeral channel characterised by channel infilling and slow rates of vertical accretion and floodplain development.	~5 ka	Nanson et al. (1995)

Table 6.2. *Continued.*

Continent (countries)	River system	Physiographic description of catchment	Climatic controls on rainfall/runoff	Mid Holocene fluvial characteristics	Late Holocene/ modern fluvial characteristics	Timing of transition	References
Asia (Pakistan)	Indus River	Rising in the Himalaya, the Indus River has steep headwater catchments and a large alluvial megafan on its lower reaches before it discharges in the Arabian Sea.	High glaciated Himalayan catchments transmit seasonal snow melt to the lower arid reaches. These seasonal flows are augmented by monsoonal rainfall during the boreal summer months.	High energy, distributive river with relatively high sedimentation rates building a large alluvial ridge.	More laterally stable channel with lower discharge, lower sedimentation rates and much less frequent channel avulsion. Decline in the monsoon decreased the sediment load to discharge ratio to a degree that promoted channel incision and increased lateral stability.	~4 ka	Gibling et al. (2005); Giosan et al. (2012)
Asia (India)	Mahi River	Headwater catchments in the Vindhyachal mountain range of western India provide the majority of the discharge for the river which, in its lower reaches, traverses semiarid plains where it is confined by Pleistocene terraces.	The catchment receives monsoonal rainfall during the boreal summer months. Streamflow is seasonal with peak flows during the monsoon season and low flows during the boreal winter months. Snow melt does not contribute to annual flows.	Large (~1,000 m wide), relatively low sinuosity (~1.04) braided channel, with a high width:depth ratio (~71).	Smaller (~210 m wide) meandering channel with a lower width:depth ratio (~42) that is confined within the mid Holocene macro channel.	Uncertain but reportedly a gradual decline in fluvial activity from ~5 ka	Sridhar (2007)

166

Table 6.2. *Continued.*

Continent (countries)	River system	Physiographic description of catchment	Climatic controls on rainfall/runoff	Mid Holocene fluvial characteristics	Late Holocene/ modern fluvial characteristics	Timing of transition	References
Asia (China)	Shiyang River	Rising in the North Qilian mountains, northeast of the Tibetan Plateau, the Shiyang River flows northeast across alluvial plains before dissipating in a terminal floodout.	The headwater catchments receive rainfall during boreal summer months related to the eastern China Monsoon, which is responsible for the bulk of the runoff within the system. The lower reaches are cold and dry.	Meandering and aggrading river with large floodplain.	Aridification ~4.8 ka triggered a series of periods of incision. Channel much more laterally stable confined by terraces, and not characterised by net aggradation.	~4.8 ka	Gao et al. (2016)
South America (Argentina)	Pastos Chicos River	Catchment located in a tectonic depression, rising on the eastern slopes of the Taire mountain range (3000-4500 masl), draining onto an alluvial plain containing playa lakes towards its trunk stream, the Coranzuli River.	Low amounts of annual rainfall occur during the austral summer months largely due to the South American Monsoon.	Perennial meandering river supporting adjacent floodplain wetlands.	Incised, straight channel reworking mid channel and lateral bars during relatively infrequent flows.	Between 6 and 4.2 ka	Tchilinguirian et al. (2014)
North America (United States of America, Mexico)	Santa Cruz and San Pedro rivers	Rising in the mountains of northern Mexico/southern Arizona, the Santa Cruz and San Pedro rivers flow north in partly confined valleys to their trunk stream, the Gila River.	Summer monsoon rainfall responsible for most flooding in the Santa Cruz and San Pedro rivers. Rainfall is strongly correlated with ENSO, being wetter during El Niño periods.	Relatively quiescent period of fluvial activity with a distinct hiatus in arroyo cutting which is thought to be linked to prevailing La Niña conditions.	Significant increase in frequency and magnitude of arroyo cutting as wetter conditions return.	~4 ka	Waters and Haynes (2001)

6.2.1 Significance of the Holocene Warrego and Okavango records

Palaeoenvironmental research in the drylands of Australia and southern Africa has a long history, and has illuminated the complex late Quaternary evolution of rivers, lakes and deserts in both regions (e.g. Du Toit, 1926, 1933; Bowler, 1967, 1976, 1986; Bowler et al., 1976; Nanson et al., 1992; Magee and Miller, 1998; Meadows, 2001; Burrough and Thomas, 2008, 2013; Fitzsimmons et al., 2013). The Holocene records from the Warrego and Okavango rivers presented in this thesis contribute a fundamental insight into Holocene hydroclimatic drivers and dynamics, as well as highlighting the type of river response and high geomorphological sensitivity of two large dryland rivers to relatively modest hydroclimatic changes, in eastern Australia and southern Africa, respectively.

By isolating tropical hydroclimatic drivers, the Warrego record allows us to disentangle northern, tropical sources of moisture from southern, extratropical sources of moisture responsible for enhanced runoff, which has proved difficult for some previous studies (e.g. Cohen et al., 2012, 2015). The Warrego River is largely isolated from the influence of the mid-latitude westerlies that bring seasonal winter rain to southern Australia, meaning that the hydroclimatic drivers of change in the catchment can be more tightly defined. The mechanisms responsible for enhanced runoff during the mid Holocene in the Warrego catchment also differ to those proposed for earlier periods in the late Quaternary. During the last glacial maximum (LGM) in southeastern Australia, enhanced runoff efficiency and large palaeochannel formation and maintenance is thought to be a result of temperature-mediated controls on discharge rather than regional-scale increases in precipitation (Reinfelds et al., 2014; Hesse et al., 2018a, b). These controls include a larger and longer-lasting seasonal snowpack, enhanced orographic rainfall (i.e. low temperatures extending to lower altitude), feedbacks between CO_2 and vegetation, reduced evapotranspiration or a combination of these factors (Hesse et al., 2018a). Although global temperatures were slightly higher during the early-mid Holocene, the magnitude of this thermal maximum varied regionally and cannot account for enhanced runoff in eastern Australia alone (Petit et al., 1999; Braconnot et al., 2012). Rather, global- and regional-scale changes to tropical atmospheric circulation and associated teleconnections were responsible for enhanced rainfall, and hence enhanced runoff and higher energy river behaviour in the Warrego catchment during the mid Holocene, and also responsible for the subsequent decline in the late Holocene (Chapter 2). The behaviour of the Warrego River under mid Holocene conditions may provide an analogue for other periods in the late Quaternary, where a large fluvial response occurs with relatively moderate temperature forcing. For example, during Marine Isotope Stage 3 (MIS3), very large channels persisted in catchments throughout the Murray-Darling Basin (Hesse et al., 2018a, b), although these cannot be explained by temperature forcing alone, as has been suggested for large palaeochannels during the LGM. This strongly suggests that changes in catchment precipitation can have disproportionately large effects on runoff amount and discharge in Australian dryland rivers.

The Warrego record supports other dryland fluvial records in Australia, such as the palaeochannel record from the Macquarie River (Hesse et al., 2018a, b), that indicate the mid Holocene was characterised by larger, high-energy rivers, and that modern fluvial systems in the Australian drylands are likely to have evolved to their present forms in the late Holocene (Chapter 2). The data presented in Chapter 2 highlight that the Holocene was characterised by more profound river changes in eastern Australian drylands than perhaps previously acknowledged, as much more attention has been given to palaeochannels dating from MIS5 through MIS2, compared to the Holocene (MIS1) (Kemp and Spooner, 2007; Page et al., 2009; Mueller et al., 2018). As mentioned in Chapter 1, geoproxy records used to understand past climates have, understandably, focussed on periods of more dramatic hydroclimatic change. The Warrego and Macquarie river records indicate that increased attention should be placed on the Holocene evolution of Australia's dryland rivers, as these records provide an indication of the response of dryland rivers to hydroclimatic change under interglacial boundary conditions that are relatively similar to today. This has implications for improving our understanding of river response to future climate change.

The Okavango record supports the spatial dichotomy that seems to appear in palaeoenvironmental records from the central and northern Kalahari Desert, whereby increased mid Holocene monsoonal rainfall over Angolan headwater catchments transmitted a 'wetter' signal (i.e. large palaeochannels and permanent lakes) into the locally drier central and northern Kalahari (Chapter 3; Burrough and Thomas, 2013). The complexity of palaeoenvironmental records in the southern African drylands reflects an inherently complicated relationship between hydroclimatic drivers such as the ITCZ, the CAB, winter westerlies in the southern regions, and the relative importance of Indian or Atlantic Ocean sourced moisture. The Okavango record provides a chronologically-constrained 'missing link' between enhanced rainfall in the Angolan highlands during the mid Holocene and the most recent highstand in the Mababe Depression (Burrough and Thomas, 2008; Dupont et al., 2008; Tierney et al., 2011; Chapter 3). Geoproxy records from the central Kalahari have largely been extrapolated from palaeolake shorelines or dunes, while fluvial records have been mostly unexplored (Thomas et al., 2000; Burrough et al., 2007, 2012; Burrough and Thomas, 2008, 2013; Riedel et al., 2014). Fluvial records in the central and northern Kalahari Desert should be further exploited to improve palaeoclimatic interpretations, particularly given the spatial complexity and apparent contradictions that appear in the palaeo-record. For example, the Okavango, Kwando, and Zambezi river floodplains have preserved countless palaeochannels that would help to illuminate late Quaternary hydroclimatic and fluvial dynamics in the northern Kalahari. In addition to contributing to the understanding of Holocene hydroclimatic dynamics, the Okavango fluvial record allows us to narrow the uncertainty surrounding how the Okavango River will respond to future hydroclimatic change (Chapter 3). Given projected declines in streamflow in the Okavango catchment (Andersson et al., 2006; Shongwe et al., 2009), a large, rapidly laterally migrating channel will not develop, but avulsion dynamics may reduce the reliability of channels for communities and tourist lodges as channels contract and come closer to the threshold of failure (Chapters 3 and 4).

6.2.2 Holocene changes to the Intertropical Convergence Zone (ITCZ)

6.2.2.1 Northern Africa and enhanced mid-Holocene fluvial activity

During the Holocene African Humid Period (AHP; ~11–5.5 ka), the currently hyperarid Sahara Desert received high amounts of rain (up to 10 times the present day) and supported diverse vegetation, permanent lakes and rivers, and human populations (Tierney et al., 2017). The ITCZ and its associated monsoonal rainfall shifted further north than its modern extent during the early-mid Holocene due to orbital forcing which increased northern hemisphere summer insolation (Singarayer and Burrough, 2015; Tierney et al., 2017). Modelling suggests that dust and vegetation feedbacks enhanced the northward penetration of the ITCZ and associated monsoonal rainfall to ~31° N, when orbital forcing alone would have shifted it northward to ~16° N (Pausata et al., 2016; Tierney et al., 2017). Proxies such as marine and lake cores (Singarayer and Burrough, 2015; Shanahan et al., 2015; Collins et al., 2017) indicate that the so-called 'Green Sahara' terminated abruptly at ~5.5 ka, which is intriguing given that orbital forces only changed gradually. It is thought that a combination of high-latitude forcing and vegetation feedbacks were responsible for this non-linear response to gradual orbital forcing (Collins et al., 2017). Rapid North Atlantic Ocean cooling around 6–5 ka slowed down the Atlantic Meridional Overturning Circulation (AMOC), which resulted in southward expansion of the polar vortex and cold anomalies in the mid-latitudes, reducing monsoonal precipitation (Collins et al., 2017). This likely triggered vegetation and local water balance feedbacks whereby decreased soil moisture and decreased vegetation and wetland/lake extent reduced the penetration of the monsoon, accelerating the aridification of northern Africa at ~5.5 ka (Collins et al., 2011; 2017; Tierney et al., 2017).

These oceanic-atmospheric changes impacted river hydrology and geomorphology. The Nile River today sources the majority of its runoff from humid headwaters in the equatorial highlands of eastern Africa. During the latest AHP, however, countless desert wadis were activated in the lower Nile valley which contributed substantial amounts of water and sediment to the river (Woodward et al., 2015a, b). The early-mid Holocene Nile had an anabranching planform and transported higher discharge than present (Woodward et al., 2015a, b). As monsoonal rains over northern Africa retreated to more or less their modern extent ~5.5 ka, the Nile channel network contracted and became a single, narrower channel (Woodward et al., 2015a, b). High resolution mapping of the Sahara Desert has also revealed large palaeodrainage systems that likely were last active during the early-mid Holocene (e.g. Tamanrasett River valley, Skonieczny et al., 2015, and the Kufrah River, Paillou et al., 2009; 2012). At the end of the AHP, these catchments were gradually buried by aeolian sediments and rendered completely inactive (Skonieczny et al., 2015). Overall, this evidence from northern Africa shows that enhanced fluvial activity was coincident with that in the Okavango in the mid Holocene, although enhanced fluvial activity in the Okavango persisted until ~3.5 ka.

6.2.2.2 Asia and enhanced mid-Holocene fluvial activity

With a more northerly ITCZ, the mid Holocene also saw increased rainfall associated with the Indian monsoon, and fluvial records from the Indus and Mahi rivers in Pakistan and India, respectively, reflect higher discharges and higher energy conditions during this period (Jain and Tandon, 2003; Gibling et al., 2005; Sridhar, 2007; Giosan et al., 2012). During the mid Holocene, the Indus River was a high-energy, distributary fluvial system with rapid sedimentation rates and relatively frequent avulsions (Giosan et al., 2012). As the monsoon declined ~5 ka, the Indus River became more laterally stable with lower sedimentation rates. Lower sediment load resulted in channel incision, further reducing lateral instability through channel migration or avulsion (Giosan et al., 2012). The Mahi River in western India also underwent significant changes as a result of the mid-late Holocene decline of the Indian monsoon. During the mid Holocene the Mahi River was a very wide (~1000 m), high-energy, braided river (Sridhar, 2007). By contrast, the late Holocene Mahi River is a significantly narrower (~200 m), lower energy, meandering channel confined within the mid Holocene macro-channel. The timing of this change in river character and behaviour is uncertain but is thought to have occurred gradually since ~5 ka (Sridhar, 2007). Similarly, aggradation and incision cycles in rivers of the Northern Hill Range in western India suggest enhanced fluvial activity during the early-mid Holocene and subsequent decline in the late Holocene, although these records are complicated somewhat by tectonics (Bhattacharya et al., 2013; Prizomwala et al., in press). The Shiyang River in western China has also undergone pronounced change in river behaviour after aridification that began ~4.8 ka (Gao et al., 2016). The mid Holocene Shiyang River was a meandering and aggrading river with a large floodplain, but aridification at ~4.8 ka triggered a series of incisional periods, and the modern channel is much more laterally stable and is not characterised by aggradation (Gao et al., 2016).

6.2.3 Holocene changes to the El Niño-Southern Oscillation (ENSO)

6.2.3.1 Western South America and enhanced mid-Holocene fluvial activity

While drylands in Africa and Asia are largely affected by monsoonal changes brought about by fluctuation of the ITCZ, drylands in Australia, western South America and North America are generally more directly affected by changes to the ENSO. ENSO is a tropical climate mode in the Pacific Ocean which is responsible for interannual climatic variability in numerous regions around the world (Goosse et al., 2010). Easterly equatorial trade winds driven by zonal pressure differences form the surface component of the Pacific Walker circulation. Deep convection over the Western Pacific Warm Pool (WPWP) is compensated by subsidence over the eastern Pacific, where oceanic upwelling maintains a shallow thermocline and relatively cool sea surface temperatures (SST). Variations in the strength of the easterly trade winds and variations in the SST gradient across the Pacific Ocean drive various ENSO teleconnections. El Niño conditions occur when trade winds weaken and the eastern Pacific Ocean is relatively warmer than normal shifting the zone of deep convection to the central and eastern Pacific. This results in drier than normal conditions over Australia, Indonesia, and the central western Andes,

and wetter than normal conditions in coastal South America, and southwest North America. Stronger easterly trade winds increase the size of the WPWP and increase convection over the western Pacific while increasing upwelling in the eastern Pacific, and this phase is known as La Niña (Grootemaat, 2008; Goosse et al., 2010). La Niña conditions are associated with wetter than normal conditions over Australia, Indonesia and the central western Andes, and drier than normal conditions in coastal South America and southwest North America (Grootemaat, 2008; Goosse et al., 2010).

The central western Andes host unique high-altitude drylands in the rain shadow of the main Andes mountain range. Wetter conditions in the central western Andes during the mid Holocene have been linked to La Niña conditions in the Pacific Ocean (Carré et al., 2012). The Pastos Chicos River in the arid highlands of northwestern Argentina experienced relatively wet conditions during the early-mid Holocene from ~9–6 ka with a perennial, meandering channel which supported peat formation and adjacent floodplain wetlands (Tchilinguirian et al., 2014). From ~6–4.2 ka, aridification of the catchment reduced the abundance of wetland plant species and triggered channel incision as the water table fell and sediments became more prone to erosion. The modern Pastos Chicos River is a laterally stable, low-sinuosity channel which adjusts mainly by reworking in-channel bars during relatively infrequent flows (Tchilinguirian et al., 2014). Fluvial records from western South America are not particularly well-documented, but evidence does suggest wetter conditions and increased fluvial activity during the early-mid Holocene, and a decline in the mid-late Holocene. The mean La Niña state of the Pacific Ocean during the early-mid Holocene was likely responsible for this pattern of Holocene fluvial change in the central western Andes (Carré et al., 2012).

6.2.3.2 Southwest North America and reduced mid-Holocene fluvial activity

Rivers in the drylands of southwestern North America experienced an approximately anti-phase pattern of Holocene hydroclimatic change compared to many other drylands. The mid Holocene was a period of warm but dry conditions in the southwestern drylands of North America, thought to be associated with the prevailing La Niña state of the Pacific Ocean (Waters and Haynes, 2001; Borejsza and Frederick, 2010). Cooler and wetter conditions emerged ~5–4 ka with increased frequency of large-scale flooding, likely due to the increase in the frequency and intensity of El Niño events since ~5 ka (Ely, 1997; Bacon et al., 2010). The fluvial response to this Holocene climate change was slightly different to other drylands as bedrock-confined reaches of rivers in the North American southwest are characterised by cut and fill cycles rather than the lateral planform adjustments made by large, laterally unconfined rivers that tend to be more widespread in some other drylands. Cutting of arroyos (incised river channels) typically occurs during wetter periods when high magnitude flooding enhances the likelihood of significant erosion (Waters and Haynes, 2001; Harden et al., 2010). The Santa Cruz and San Pedro rivers were characterised by arroyo cutting in the early Holocene and, more frequently, in the late Holocene since ~4 ka (Waters and Haynes, 2001). In the mid Holocene there was a hiatus in arroyo cutting due to a lack of large magnitude floods capable of incising channels (Waters and Haynes, 2001). In the Casas

Grandes River of northern Mexico fluvial responses to Holocene climate change appear to have been relatively muted, but the mid Holocene was a period of widespread soil formation thought to be due to the prevailing warmer and drier conditions (Nordt, 2003). Arroyo formation can also be driven by intrinsic thresholds related to stream power, so disentangling extrinsic drivers in fluvial systems that record intrinsically-driven, cyclic processes can be difficult. Nevertheless, the flood chronologies (Ely, 1997; Bacon et al., 2010) and evidence from arroyos (Waters and Haynes, 2001; Nordt, 2003) indicate that rivers in the southwestern North American drylands experienced relatively lower energy, drier conditions during the mid Holocene and progressively wetter and higher energy conditions in the late Holocene. The review of Holocene flooding by Harden et al. (2010), notes that fluvial dynamics in the North American southwest were highly complex with bedrock rivers recording more frequent flooding in the mid-late Holocene correlating periods of increased precipitation in the late Holocene. However, alluvial river records have more flood units dated to the early-mid Holocene. This is likely due to the differences in selective preservation with alluvial reaches not often preserving the largest floods, but highlights the complexity of the Holocene fluvial record in southwest North America (Harden et al., 2010). The apparently conflicting, out-of-phase records from southwestern North America and eastern Australia strengthen the interpretation of ENSO dynamics being responsible for the spatial variation in Holocene fluvial records in these regions. The proposed La Niña-dominated mid Holocene and El Niño-dominated late Holocene pattern is reflected in the regionally-specific responses to these climatic conditions.

6.2.4 Summary of Holocene dryland fluvial change

Unlike more dramatic periods of late Quaternary hydroclimate change, such as changes associated with emergence from the LGM, the Holocene hydroclimate changes responsible for these various river responses were relatively modest and regional in scale, but nonetheless had significant impacts on the character and behaviour of dryland rivers around the world. Although the precise forms and processes of river response to Holocene climate change have varied significantly (Table 6.2), the pronounced changes suggest that in many settings, dryland rivers have been highly sensitive to these hydroclimatic changes. To understand further just how dryland rivers respond to changing hydroclimatic conditions and how this sensitivity may vary of space and time, it is important to consider the intrinsic processes responsible for ongoing adjustment in a river and how the processes operating within this natural range of variability are affected by extrinsic, hydroclimatic forcing. This consideration forms the subject of Section 6.3.

6.3 Intrinsic processes and extrinsic forcing – evolution of fluvial systems in the Warrego and Okavango catchments

River character and behaviour are products of the interactions between intrinsic processes and extrinsic forces (Schumm, 1977). Intrinsic processes (including geomorphic thresholds, lags, and feedbacks) define the natural range of variability of a system and are responsible for channel long profile, planform and cross-sectional adjustment (Schumm, 1973, 1979). The crossing of extrinsic geomorphic thresholds, however, may shift the available energy parameters of a system, thereby implementing a new set of intrinsic processes that will attempt to maintain or maximise flow efficiency and stability (Schumm, 1973, 1979; Nanson and Huang, 2017, 2018). This manifests in changes to a river's character and behaviour. Given its control over the amount of discharge transported by a river (McMahon, 1979; McMahon et al. 1987; 2007; 2008), climate is a particularly important extrinsic force that can dramatically change the available energy in a river. Over late Quaternary timescales, in the absence of tectonics, and where valley slope is relatively constant, increases or decreases in runoff tend to result in increases or decreases in the stream power of a river, respectively. Accordingly, this will influence the suite of intrinsic processes that occur within a river. In time, this determines whether energy must be expended or conserved to maintain flow efficiency and whether nonequilibrium responses, such as channel breakdown, become characteristic of the system.

As shown in Chapters 2 and 3 and summarised in Figure 6.1, as a result of Holocene hydroclimatic changes, the Warrego and Okavango rivers have undergone dramatic reductions in channel size, discharge and stream power as well as changes in river behaviour. The mid Holocene Warrego River was a large, meandering river that actively laterally migrated. Unit stream power in the Burrenbilla palaeochannel was ~10.2 Wm^{-2} (95 % CI between ~3.2 and 32.3 $W\,m^{-2}$), declining to ~8.3 $W\,m^{-2}$ (95 % CI between ~2.7 and 25 $W\,m^{-2}$) in the Coongoola channel after Burrenbilla failed (Fig. 6.1). Sometime after ~4.7 ka, as a result of climate-driven hydrological declines in the catchment, unit stream power declined substantially to the modern values of between ~1.3 and 2.7 $W\,m^{-2}$ at the equivalent position downstream. This suggests that the threshold of stream power between a continuous, meandering channel and a discontinuous, straight, anastomosing or distributary river is ~3 $W\,m^{-2}$ in this particular setting (Fig. 6.1). Dropping below this threshold resulted in a step-change in both the character and behaviour of the Warrego River. The Warrego River had a significant deficit of energy meaning that a meandering, energy-consuming channel could not be maintained. Instead, energy-enhancing anabranching channels (Nanson and Huang, 1999; Jansen and Nanson, 2004; Huang and Nanson, 2007) formed in some reaches. In other reaches, pronounced and persistent downstream declines in discharge and stream power induced nonequilibrium channel responses forming distributary channels characterised by eventual channel breakdown and formation of floodplain wetlands.

Stream power in the Okavango did not decline as markedly as the Warrego between the mid Holocene and late Holocene. Unit stream power was between ~2.7 and 3.4 $W\,m^{-2}$ (declining slightly downstream)

in the mid Holocene when the Okavango was a large, rapidly migrating channel, and declined to between ~1.7 and 2.5 W m^{-2} in the late Holocene when the channel became more laterally stable and more characterised by periodic avulsion (Fig. 6.1). It is possible that channel shape is more important in the unusual, vegetation-controlled channels of the Okavango (Tooth and McCarthy, 2004). Tooth and McCarthy (2004) argue that Okavango channels with a width/depth ratio of <10 will not migrate laterally as vegetative roughness along the banks affects a larger proportion of the wet perimeter of modern channels, stifling lateral channel migration (Tooth and McCarthy, 2004). The Ngarange-Ntsanyana palaeochannel had a width/depth ratio of >31, while the modern system has width/depth ratios between ~6–14, which means that lateral migration is either slow or non-existent (Chapters 3 and 4). Given downstream flow declines, this results in sediment accumulating within the channel banks, elevating the channel bed relative to the surrounding swamps and priming the river for periodic avulsion to a lower elevation course. Evidence from the ongoing avulsion of the Filipo channel suggests that the new channel will have a partly inherited planform based on exploited hippopotami trails and abandoned channel segments, rather than a planform closely adjusted for maximum flow efficiency (Chapter 4). It will likely take a long time for the Filipo to develop a regularly meandering planform given prohibitively low lateral migration rates under modern conditions.

As noted in Section 6.3, the magnitude of mid-late Holocene climate change globally was relatively modest relative to other periods of climate change in the late Quaternary. Nonetheless, it triggered profound changes in the character and behaviour of both the Okavango and Warrego rivers, as well as many other dryland rivers around the world. This suggests that some dryland rivers are particularly sensitive to climate-driven hydrological change and begs the question "how might dryland rivers respond to future hydroclimatic changes?" Fluvial geomorphology has, until now, rarely been considered in previous studies of the impact of future climate change on dryland rivers (Chapter 5), but it is critical to understand as the geomorphology of a river fundamentally underpins ecosystem structure and function, and human land use. This consideration forms the basis of Section 6.4.
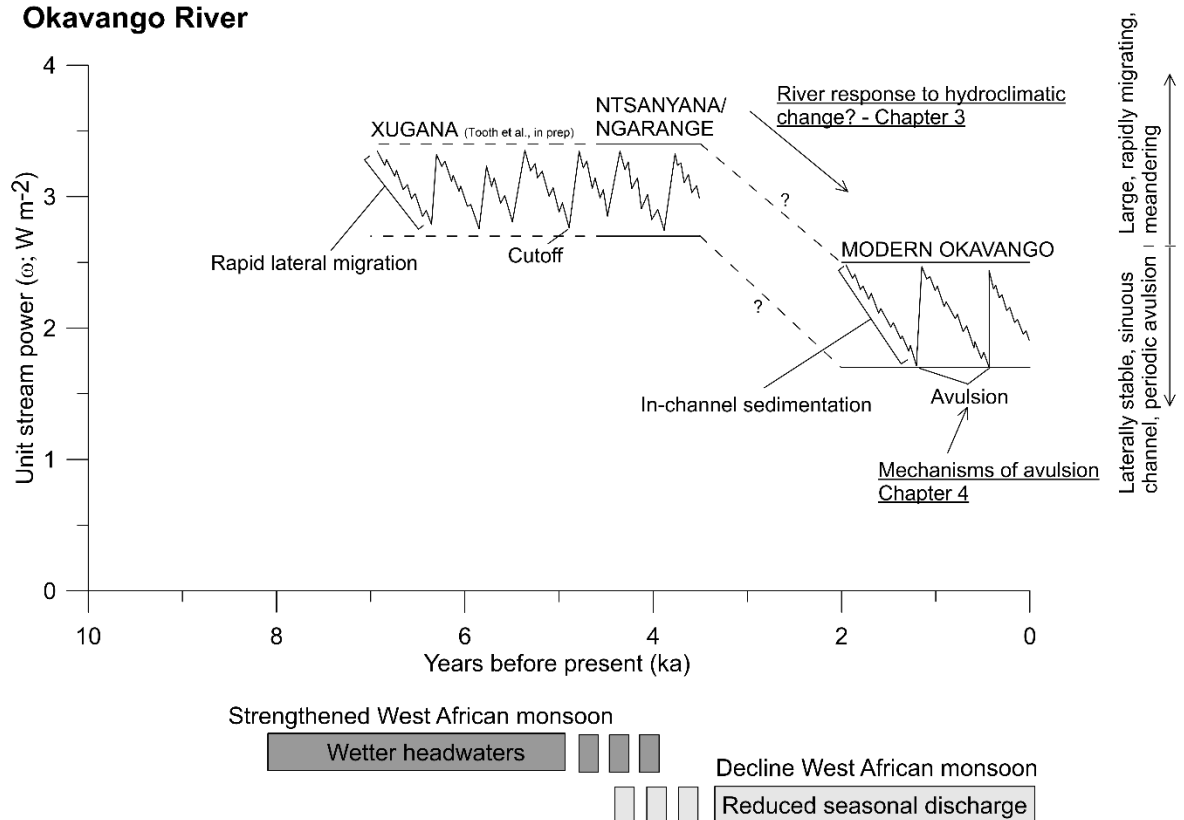
Warrego River
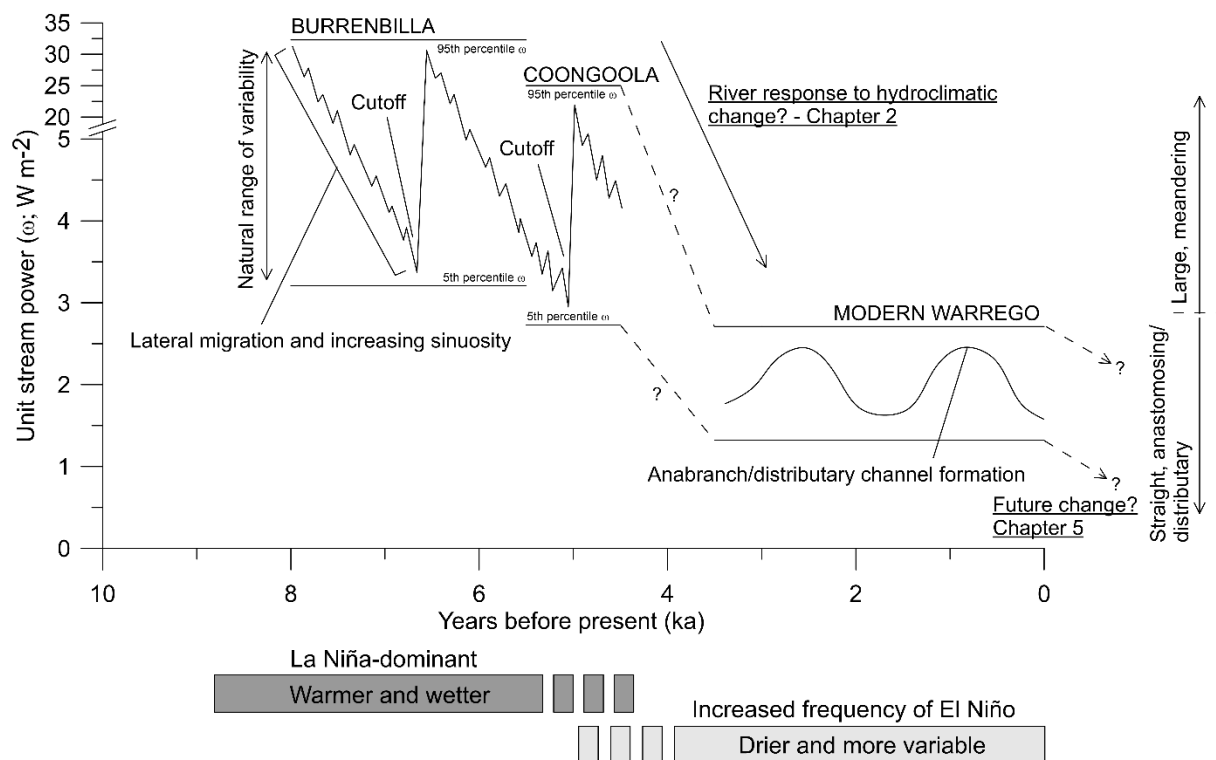
Okavango River

Figure 6.1. River evolution schematic for the Warrego and Okavango rivers (cf. river evolution diagram in Fryirs et al., 2012). Underlined labels represent the different aspects of this research addressed by each of the four key chapters in this thesis.

6.4 The future for dryland rivers

Most global climate models project increased aridity and/or climatic variability for the world's drylands (Arnell, 1999; Greve and Seneviratne, 1999; Feng and Fu, 2013; Schewe et al., 2014; Seager et al., 2013; Cook et al., 2014; Fu and Feng, 2014; IPCC, 2014; CSIRO and BoM, 2015; Gosling and Arnell, 2016). Our understanding of the potential impacts of increased aridity on dryland rivers is growing but is typically limited to analyses of hydrological responses (i.e. changes to surface water availability and flow regimes; e.g. Nijssen et al., 2001; Milly et al., 2005; de Wit and Stankiewicz, 2006; Rodell et al., 2018). While this is a critically important aspect of change, such hydrological changes typically have closely associated geomorphological impacts that are largely unconsidered, and these that may have profound and lasting impacts on the >2 billion people that live in drylands and rely on the ecosystem services provided by dryland rivers (MEA, 2005; Van der Esch, 2017). Understanding how increases in aridity will influence the character and behaviour of rivers is difficult, but Chapter 5 of this thesis addresses this issue by quantifying thresholds of catchment aridity that define Australian dryland river character and behaviour. Most Australian dryland rivers in central and eastern Australia are projected to undergo some form of geomorphological change due to catchment aridification towards the end of this century, in the form of increased likelihood of river discontinuity, flow disconnection and channel breakdown.

Beyond Australia, we know that climate change impacts in the coming decades and centuries will affect the hydrological characteristics of many other dryland rivers around the world, most likely in the form of aridification (Nijssen et al., 2001; Milly et al., 2005; de Wit and Stankiewicz, 2006; Rodell et al., 2018). It is also clear that, owing to population growth, demand for water will continue to increase into the future (Arnell, 1999; Cai and Rosegrant, 2002; Rosegrant and Cai, 2002), which will be particularly important in dryland regions already characterised by water scarcity. This projected conflict of increasing demand for a declining resource is alarming and, given the sensitivity of many dryland rivers to climatic and hydrological change, highlights that further research is required to fully understand how dryland rivers will respond to these pressures (Fig. 6.2). Considerable uncertainty surrounds the magnitude (as opposed to the direction) and variability of future changes to precipitation and evapotranspiration, and for the sensitivity and complex response of dryland fluvial systems to such future changes. Chapter 5 demonstrated that many Australian dryland rivers appear to be highly sensitive to future increases in aridity, and a similar approach applied in drylands around the world would improve our assessment of the relative sensitivity of other dryland rivers globally to future climate changes (Fig. 6.2). Some of the most economically and environmentally important rivers in the world flow through dryland regions, including the Nile, Niger, and Rio Negro, so improving our understanding of their likely future trajectories is critical (Fig. 6.2). Another uncertain aspect of the geomorphological response of dryland rivers to climate change relates to timeframes of change. It is uncertain at this stage by how much the geomorphological change in dryland rivers will lag the relatively rapid climatic and hydrological changes. In relatively low-energy, slowly adjusting systems, change may

occur relatively slowly and lag hydroclimatic changes by further decades. However, the exceedance of thresholds may induce faster step-change responses in dryland rivers, so it is important to continue to attempt to improve our understanding of the likely timescales of future change.
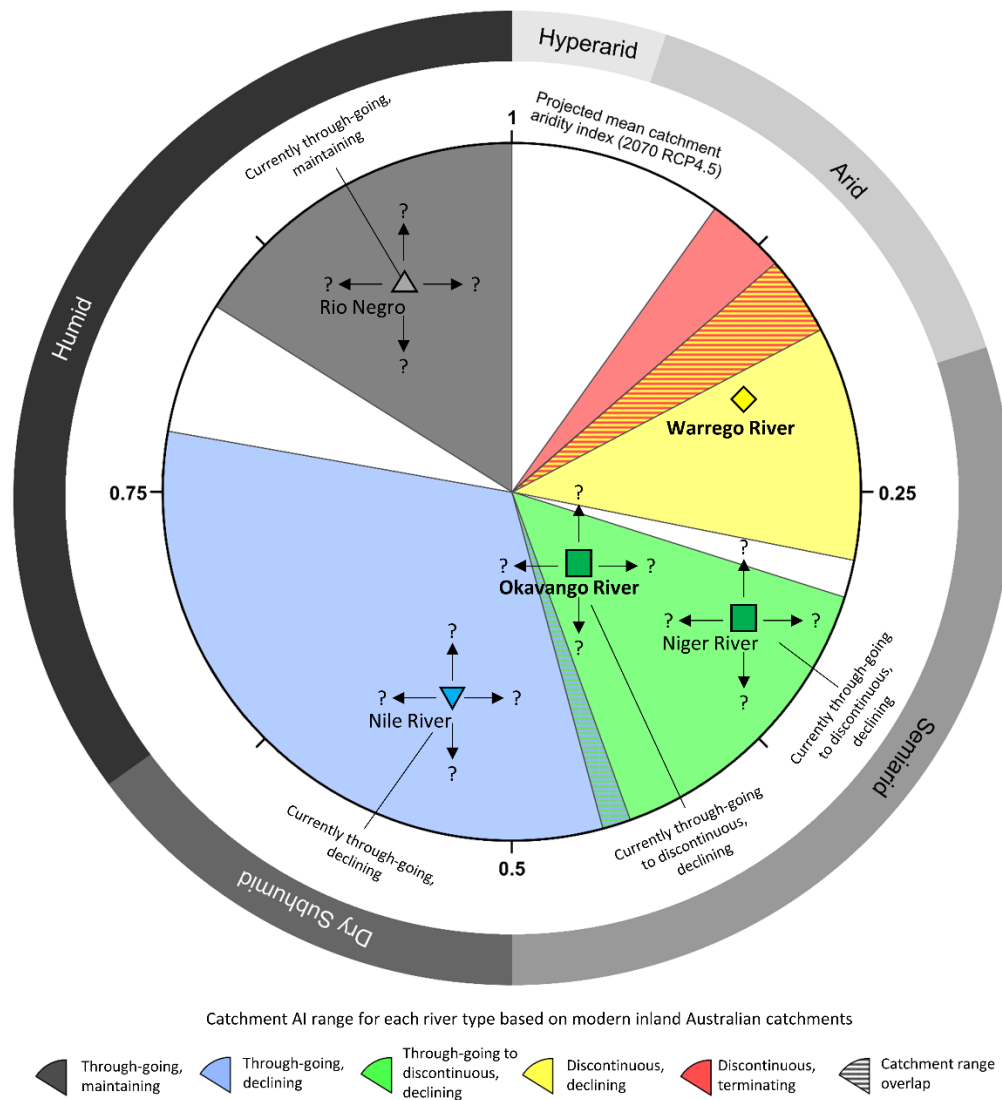
Figure 6.2. Conceptual figure depicting four large dryland rivers from different parts of the world. Rivers depicted are the currently through-going, maintaining Rio Negro, Argentina, the through-going, declining Nile River, Egypt, and the through-going to discontinuous, declining Okavango River, Botswana and Niger River, Mali. In Chapter 5, it was projected that the Warrego River would not cross a threshold to another river type. It is uncertain whether the other large, and regionally very important, rivers depicted in this figure are likely to cross extrinsic geomorphic thresholds with future hydroclimatic change. The approach outlined in Chapter 5 could help to estimate the trajectories of change for these and other dryland rivers around the world.

There is also uncertainty surrounding the role of human activities in exacerbating or mediating the impacts of climate change on dryland river hydrology and geomorphology. On one hand, improvements in water use efficiency in dryland regions may increase the viability of some agricultural practices even in progressively more arid regions. On the other hand, increasing demand for, and increased scarcity of, water may outweigh any improvements made to water use efficiency, especially given a burgeoning

human population and aspirations to raise living standards, including improved access to clean water (UN, 2018). Ultimately, the uncertainties surrounding the response of dryland rivers to future climate change are considerable, but this thesis has made a substantial contribution by beginning to narrow the margin of uncertainty and improve our understanding of the potential future trajectories of change in Australian rivers particularly, and other dryland rivers more generally, by contextualising modern rivers in relation to their Holocene evolution (Chapters 2, 3 and 4) and defining extrinsic thresholds that define river character and behaviour (Chapter 5).

6.5 Conclusions

Research undertaken explicitly to understand the past, present, and future geomorphological sensitivity of dryland rivers to climate change is relatively scarce, but this thesis has made a significant and novel contribution to address this imbalance. Palaeofluvial studies are generally undertaken from the perspective of exploiting geoproxies such as palaeochannels to reconstruct past hydroclimates (Hesse et al., 2018a; Mueller et al., 2018). This is a critical line of investigation in its own right but does not necessarily help us to understand the thresholds defining how rivers respond to such hydroclimate changes. More research focussed specifically on defining thresholds of river character and behaviour is needed to improve our understanding of the relative sensitivity/insensitivity of dryland rivers to hydroclimatic change. This will help to develop a more spatially and temporally extensive understanding of dryland river response that, in an era of rapid environmental change, may have important practical implications.

In general, the geomorphological impacts of future climate change on dryland rivers so far have been little considered. Hydrological modelling has focussed on the projected changes to hydrological regimes, which is a critical part of improving our understanding of the impacts of climate change (e.g. Nijssen et al., 2001; Milly et al., 2005; de Wit and Stankiewicz, 2006; Rodell et al., 2018), but more emphasis needs to be placed on understanding how rivers will adjust geomorphologically to these changing catchment hydrological conditions. Such information is critical because the geomorphological response of rivers can dramatically change ecosystem structure and function, as well as patterns of land use. With refinement, the approach developed in Chapter 5 may help to incorporate changes to the physical structure and functioning of rivers more routinely into future analyses of the impacts of climate change. As our understanding of the response of dryland rivers to past, present and future hydroclimatic changes improves, management strategies can begin to be developed that allow ecosystems, communities, agricultural practices, and infrastructure to adapt to the potentially very dramatic 21st century transformations in the character and behaviour of dryland rivers around the world.

References

Andersson L, Wilk J, Todd MC, Hughes DA, Earle A, Kniveton D, Layberry R, and Savenije HHG, 2006. Impact of climate change and development scenarios on flow patterns in the Okavango River. Journal of Hydrology 331, 43–57.

Arnell NW, 1999. Climate change and global water resources. Global Environmental Change, 31–49.

Bacon SN, McDonald E V., Caldwell TG, and Dalldorf GK, 2010. Timing and distribution of alluvial fan sedimentation in response to strengthening of late Holocene ENSO variability in the Sonoran Desert, southwestern Arizona, USA. Quaternary Research 73, 425–438.

Bhattacharya F, Rastogi BK, Ngangom M, Thakkar MG, and Patel RC, 2013. Late Quaternary climate and seismicity in the Katrol hill range, Kachchh, western India. Journal of Asian Earth Sciences 73, 114–120.

Borejsza A, and Frederick CD, 2010. Fluvial response to Holocene climate change in low-order streams of central Mexico. Journal of Quaternary Science 25, 762–781.

Bowler JM, 1967. Quaternary chronology of Goulburn valley sediments and their correlation in southeastern Australia. J. Geol. Soc. Aust. 14, 287–292.

Bowler JM, 1976. Aridity in Australia: Age, origins and expression in aeolian landforms and sediments. Earth Science Reviews 12, 279–310.

Bowler JM, 1986. Spatial variability and hydrologic evolution of Australian lake basins: Analogue for pleistocene hydrologic change and evaporite formation. Palaeogeography Palaeoclimatology Palaeoecology 54, 21–41.

Bowler J, Hope G, Jennings J, Singh G, and Walker D, 1976. Late Quaternary Climates of Australia and New Guinea. Quaternary Research, 6(3), 359-394.

Braconnot P, Luan Y, Brewer S, and Zheng W, 2012. Impact of Earth's orbit and freshwater fluxes on Holocene climate mean seasonal cycle and ENSO characteristics. Climate Dynamics 38, 1081–1092.

Burrough SL, and Thomas DSG, 2008. Late Quaternary lake-level fluctuations in the Mababe Depression: Middle Kalahari palaeolakes and the role of Zambezi inflows. Quaternary Research 69, 388–403.

Burrough SL, and Thomas DSG, 2013. Central southern Africa at the time of the African Humid Period: A new analysis of Holocene palaeoenvironmental and palaeoclimate data. Quaternary Science Reviews 80, 29–46.

Burrough SL, Thomas DSG, Shaw PA, and Bailey RM, 2007. Multiphase Quaternary highstands at Lake Ngami, Kalahari, northern Botswana. Palaeogeography, Palaeoclimatology, Palaeoecology 253, 280–299.

Burrough SL, Thomas DSG, Bailey RM, and Davies L, 2012. From landform to process: Morphology and formation of lake-bed barchan dunes, Makgadikgadi, Botswana. Geomorphology 161–162, 1–14.

Cai X, and Rosegrant MW, 2002. Global Water Demand and Supply Projections: Part 1. A Modeling Approach. Water International 27, 159–169.

Carré M, Azzoug M, Bentaleb I, Chase BM, Fontugne M, Jackson D, Ledru MP, Maldonado A, Sachs JP, and Schauer AJ, 2012. Mid-Holocene mean climate in the south eastern Pacific and its influence on South America. Quaternary International 253, 55–66.

Cohen TJ, Jansen JD, Gliganic LA, Larsen JR, Nanson GC, May JH, Jones BG, and Price DM, 2015. Hydrological transformation coincided with megafaunal extinction in central Australia. Geology, 43(3), 195–198.

Cohen TJ, Nanson GC, Jansen JD, Jones BG, Jacobs Z, Larsen JR, May JH, Treble P, Price DM, Smith AM, 2012. Late Quaternary mega-lakes fed by the northern and southern river systems of central Australia: Varying moisture sources and increased continental aridity. Palaeogeography, Palaeoclimatology, Palaeoecology, 356–357, 89–108.

Collins JA, Prange M, Caley T, Gimeno L, Beckmann B, Mulitza S, Skonieczny C, Roche D, and Schefuß E, 2017. Rapid termination of the African Humid Period triggered by northern high-latitude cooling. Nature Communications 8(1372), 1-11.

Collins JA, Schefuß E, Heslop D, Mulitza S, Prange M, Zabel M, Tjallingii R, Dokken TM, Huang E, MacKensen A, Schulz M, Tian J, Zarriess M, and Wefer G, 2011. Interhemispheric symmetry of the tropical African rainbelt over the past 23,000 years. Nature Geoscience 4, 42–45.

Cook BI, Smerdon JE, Seager R, and Coats S, 2014. Global warming and 21st century drying. Climate Dynamics, 43(9-10), 2607-2627.

CSIRO and Bureau of Meteorology (BoM), 2015. Projections: Atmosphere and the land, Climate Change in Australia Information for Australia's Natural Resource Management Regions: Technical Report.

De Wit M and Stankiewicz J, 2006. Changes in surface water supply across Africa with predicted climate change. Science 311, 1917-1921.

Dupont LM, Behling H, and Kim J-H, 2008. Thirty thousand years of vegetation development and climate change in Angola (Ocean Drilling Program Site 1078). Climate of the Past 4, 107–124.

Du Toit, AL, 1926. The Geology of South Africa. Oliver and Boyd, Edinburgh. Second edition, 463pp.

Du Toit, AL, 1933. Crustal movement as a factor in the geographical evolution of South Africa. South African Journal of Science, 16, 3-20.

Ely LL, 1997. Response of extreme floods in the southwestern United States to climatic variations in the late Holocene. Geomorphology 19, 175–201.

Feng S, and Fu Q, 2013. Expansion of global drylands under a warming climate. Atmospheric Chemistry and Physics, 13(19), 10081–10094.

Fitzsimmons KE, Cohen TJ, Hesse PP, Jansen J, Nanson GC, May JH, Barrows TT, Haberlah D, Hilgers A, Kelly T, Larsen J, Lomax J, and Treble, P, 2013. Late Quaternary palaeoenvironmental change in the Australian drylands. Quaternary Science Reviews, 74, 78–96.

Fryirs K, Brierley GJ, and Erskine WD, 2012. Use of ergodic reasoning to reconstruct the historical range of variability and evolutionary trajectory of rivers. Earth Surface Processes and Landforms, 37(7), 763–773.

Fu Q and Feng S, 2014. Responses of terrestrial aridity to global warming. Journal of Geophysical Research: Atmospheres, 119(13), 1–13.

Gao H, Li Z, Pan B, Liu F, and Liu X, 2016. Fluvial responses to late Quaternary climate change in the Shiyang River drainage system, western China. Geomorphology 258, 82–94.

Gibling MR, Tandon SK, Sinha R, and Jain M, 2005. Discontinuity-Bounded Alluvial Sequences of the Southern Gangetic Plains, India: Aggradation and Degradation in Response to Monsoonal Strength. Journal of Sedimentary Research 75, 369–385.

Giosan L, Clift PD, Macklin MG, Fuller DQ, Constantinescu S, Durcan JA, Stevens T, Duller GAT, Tabrez AR, Gangal K, Adhikari R, Alizai A, Filip F, VanLaningham S, and Syvitski JPM, 2012. Fluvial landscapes of the Harappan civilization. Proceedings of the National Academy of Sciences 109, 1688–1694.

Goosse H., P.Y. Barriat, W. Lefebvre, M.F. Loutre and V. Zunz, (2010). Introduction to climate dynamics and climate modelling. Online textbook available at http://www.climate.be/textbook.

Gosling SN, and Arnell NW, 2016. A global assessment of the impact of climate change on water scarcity. Climatic Change, 134(3), 371–385.

Greve P, and Seneviratne SI, 1999. Assessment of future changes in water availability and aridity. Geophysical Research Letters, 42, 5493–5499.

Grootemaat GD, 2008. The relationship of flooding in Australian dryland rivers to synoptic weather patterns, El Niño southern oscillation, sea surface temperatures and rainfall distribution, unpubl. PhD thesis, University of Wollongong.

Harden T, Macklin MG, and Baker VR, 2010. Holocene flood histories in south-western USA. Earth Surface Processes and Landforms 35, 707–716.

Hesse PP, Williams R, Ralph TJ, Fryirs KA, Larkin ZT, Westaway KE, and Farebrother W, 2018a. Palaeohydrology of lowland rivers in the Murray-Darling Basin, Australia. Quaternary Science Reviews, 200, 85–105.

Hesse PP, Williams R, Ralph TJ, Larkin ZT, Fryirs KA, Westaway KE, and Yonge D, 2018. Dramatic reduction in size of the lowland Macquarie River in response to Late Quaternary climate-driven hydrologic change. Quaternary Research, 90(2), 360–379.

Huang HQ, and Nanson GC, 2007. Why some alluvial rivers develop an anabranching pattern. Water Resources Research, 43(7), 1–12.

IPCC, 2014. Climate Change 2014: Synthesis Report. Contribution of Working Groups I, II and III to the Fifth Assessment Report of the Intergovernmental Panel on Climate Change [Core Writing Team, R.K. Pachauri and L.A. Meyer (eds.)]. IPCC, Geneva, Switzerland, 151 pp.

Jain M, and Tandon SK, 2003. Fluvial response to Late Quaternary climate changes, western India. Quaternary Science Reviews 22, 2223–2235.

Jansen JD, & Nanson GC, 2004. Anabranching and maximum flow efficiency in Magela Creek, northern Australia. Water Resources Research, 40(4), 1–12.

Kemp J, and Spooner NA, 2007. Evidence for regionally wet conditions before the LGM in southeast Australia: OSL ages from a large palaeochannel in the Lachlan Valley. Journal of Quaternary Science 22, 423–427.

Magee JW, and Miller GH, 1998. Lake Eyre palaeohydrology from 60 ka to the present: Beach ridges and glacial maximum aridity. Palaeogeography, Palaeoclimatology, Palaeoecology 144, 307–329.

McMahon TA, 1979. Hydrologic characteristics of arid zones. Pages 105-123 In: The hydrology of areas of low precipitation. Canberra (Australia): International Association of Hydrologic Scientists. Publication no. 128.

McMahon TA, Finlayson BL, Haines A, and Srikanthan R, 1987. Runoff variability: a global perspective. IASH-AISH, 168, pp.3-11.

McMahon TA, Peel MC, Vogel RM, and Pegram GGS, 2007. Global streamflows - Part 3: Country and climate zone characteristics. Journal of Hydrology 347, 272–291.

McMahon TA, Murphy RE, Peel MC, Costelloe JF, and Chiew FHS, 2008. Understanding the surface hydrology of the Lake Eyre Basin: Part 2-Streamflow. Journal of Arid Environments 72, 1869–1886.

Meadows ME, 2001. The role of Quaternary environmental change in the evolution of landscapes: case studies from southern Africa. Catena, 42, 39–57.

Millennium Ecosystem Assessment (MEA). 2005. Ecosystems and Human Well-being: Wetlands and Water. World Resources Institute: Washington, DC.

Milly PCD, Dunne KA, and Vecchia AV, 2005. Global pattern of trends in streamflow and water availability in a changing climate. Nature, 438(7066), 347–350.

Mueller D, Jacobs Z, Cohen TJ, Price DM, Reinfelds IV, and Shulmeister J, 2018. Revisiting an arid LGM using fluvial archives: a luminescence chronology for palaeochannels of the Murrumbidgee River, south-eastern Australia. Journal of Quaternary Science, 33(7), pp.777-793.

Nanson GC, Chen XY, and Price DM, 1995. Aeolian and fluvial evidence of changing climate and wind patterns during the past 100 ka in the western Simpson Desert, Australia. Palaeogeography, Palaeoclimatology, Palaeoecology, 113(1), 87–102.

Nanson GC and Huang HQ, 1999. Anabranching rivers: divided efficiency leading to fluvial diversity. In: Varieties of fluvial form, 7, pp.477-494.

Nanson GC, and Huang HQ, 2017. Self-adjustment in rivers: Evidence for least action as the primary control of alluvial-channel form and process. Earth Surface Processes and Landforms, 42(4), 575–594.

Nanson GC, and Huang HQ, 2018. A philosophy of rivers: Equilibrium states, channel evolution, teleomatic change and least action principle. Geomorphology, 302, 3–19.

Nanson CG, Price DM, and Short SA, 1992. Wetting and drying of Australia over the past 300,000 years. Geology, 20, 791–794.

Nijssen B, O'Donnell GM, Hamlet AF, and Lettenmaier DP, 2001. Hydrologic sensitivity of global rivers to climate change. Climatic Change, 50(1–2), 143–175.

Nordt L, 2003. Late Quaternary fluvial landscape evolution in desert grasslands of northern Chihuahua, Mexico. Bulletin of the Geological Society of America 115, 596–606.

Page KJ, Kemp J, and Nanson GC, 2009. Late Quaternary evolution of Riverine Plain paleochannels, southeastern Australia. Australian Journal of Earth Sciences, 56, S19–S33.

Paillou P, Schuster M, Tooth S, Farr T, Rosenqvist A, Lopez S, and Malezieux JM, 2009. Mapping of a major paleodrainage system in eastern Libya using orbital imaging radar: The Kufrah River. Earth Planetary Science Letters 277, 327–333.

Paillou P, Tooth S, andLopez S, 2012. The Kufrah paleodrainage system in Libya: A past connection to the Mediterranean Sea? Comptes Rendus - Geoscience 344, 406–414.

Pausata FSR, Messori G, and Zhang Q, 2016. Impacts of dust reduction on the northward expansion of the African monsoon during the Green Sahara period. Earth and Planetary Science Letters 434, 298–307.

Petit RJ, Raynaud D, Basile I, Chappellaz J, Ritz C, Delmotte M, Legrand M, Lorius C, and Pe L, 1999. Climate and atmospheric history of the past 420,000 years from the Vostok ice core, Antarctica. Nature, 399, 429–413.

Pietsch TJ, and Nanson GC, 2011. Bankfull hydraulic geometry; the role of in-channel vegetation and downstream declining discharges in the anabranching and distributary channels of the Gwydir distributive fluvial system, southeastern Australia. Geomorphology 129, 152–165.

Pietsch TJ, Nanson GC, and Olley JM, 2013. Late Quaternary changes in flow-regime on the Gwydir distributive fluvial system, southeastern Australia. Quaternary Science Reviews 69, 168–180.

Prizomwala SP, Yadav G, Solanki T, Das A, Chauhan G, and Makwana N, (in press). Style and stages of valley fill aggradation-incision cycles in the Northern Hill Range, Kachchh, Western India. Quaternary International.

Ralph TJ, and Hesse PP, 2010. Downstream hydrogeomorphic changes along the Macquarie River, southeastern Australia, leading to channel breakdown and floodplain wetlands. Geomorphology, 118(1–2), 48–64.

Reinfelds I, Swanson E, Cohen T, Larsen J, and Nolan A, 2014. Hydrospatial assessment of streamflow yields and effects of climate change: Snowy Mountains, Australia. Journal of Hydrology 512, 206–220.

Riedel F, Henderson ACG, Heußner KU, Kaufmann G, Kossler A, Leipe C, Shemang E, and Taft L, 2014. Dynamics of a Kalahari long-lived mega-lake system: hydromorphological and limnological changes in the Makgadikgadi Basin (Botswana) during the terminal 50 ka. Hydrobiologia 739, 25–53.

Rodell M, Famiglietti JS, Wiese DN, Reager JT, Beaudoing HK, Landerer FW, and Lo M-H, 2018. Emerging trends in global freshwater availability. Nature, 557, pp. 651-659.

Rosegrant MW, and Cai X, 2002. Global Water Demand and Supply Projections: Part 2. Results and Prospects to 2025. Water International 27, 170–182.

Schewe J, Heinke J, Gerten D, Haddeland I, Arnell NW, Clark DB, Dankers R, Eisner S, Fekete BM, Colón-González FJ and Gosling SN, 2014. Multimodel assessment of water scarcity under climate change. Proceedings of the National Academy of Sciences, 111(9), pp.3245-3250.

Shanahan TM, Mckay NP, Hughen KA, Overpeck JT, Otto-Bliesner B, Heil CW, King J, Scholz CA, and Peck J, 2015. The time-transgressive termination of the African humid period. Nature Geoscience 8, 140–144.

Shongwe ME, van Oldenborgh GJ, van den Hurk BJJM, de Boer B, Coelho CAS, and van Aalst MK, 2009. Projected Changes in Mean and Extreme Precipitation in Africa under Global Warming. Part I: Southern Africa. Journal of Climate 22, 3819–3837.

Schumm SA, 1973. Geomorphic thresholds and the complex response of drainage systems. In Fluvial Geomorphology, Morisawa M (ed). State University of New York: Binghampton, NY; 299–310.

Schumm SA., 1977. The fluvial system (Vol. 338). New York: Wiley.

Schumm SA, 1979. Geomorphic thresholds: the concept and its applications. Transactions of the Institute of British Geographers 4:485–515.

Seager R, Ting M, Li C, Naik N, Cook B, Nakamura J, and Liu H, 2013. Projections of declining surface-water availability for the southwestern United States. Nature Climate Change, 3(5), 482–486.

Singarayer JS, and Burrough SL, 2015. Interhemispheric dynamics of the African rainbelt during the late Quaternary. Quaternary Science Reviews 124, 48–67.

Skonieczny C, Paillou P, Bory A, Bayon G, Biscara L, Crosta X, Eynaud F, Eacute BM, Revel M, Aleman N, Barusseau JP, Vernet R, Lopez S, and Grousset F, 2015. African humid periods triggered the reactivation of a large river system in Western Sahara. Nature Communications 6, 1–6.

Sridhar A, 2007. Mid–late Holocene hydrological changes in the Mahi River, arid western India. Geomorphology 88, 285–297.

Tchilinguirian P, Morales MR, Oxman B, Lupo LC, Olivera DE, and Yacobaccio HD, 2014. Early to Middle Holocene transition in the Pastos Chicos record, dry Puna of Argentina. Quaternary International 330, 171–182.

Tierney JE, Pausata FSR, and De Menocal PB, 2017. Rainfall regimes of the Green Sahara. Science Advances 3, 1–10.

Tierney JE, Russell JM, Sinninghe Damsté JS, Huang Y, and Verschuren D, 2011. Late Quaternary behavior of the East African monsoon and the importance of the Congo Air Boundary. Quaternary Science Reviews 30, 798–807.

Thomas DSG, O'Connor PW, Bateman MD, Shaw PA, Stokes S, and Nash DJ, 2000. Dune activity as a record of late Quaternary aridity in the Northern Kalahari: New evidence from northern Namibia interpreted in the context of regional arid and humid chronologies. Palaeogeography, Palaeoclimatology, Palaeoecology 156, 243–259.

Tooth S, Craddock RA, Durcan J, Maxwell T, and Wilson Purdy S, 2017. Late Quaternary aeolian-fluvial interactions in arid central Australia: implications for models of dryland river floodplain and linear dune development, Annual Conference Programme and Abstract, British Society for Geomorphology Annual Meeting, University of Hull, 4-6 September 2017, p.55.

Tooth S, McCarthy TS, Duller GAT, Assine ML, Wolski P, and Coetzee G, In prep. Significantly enhanced mid Holocene fluvial activity in a globally-important, arid-zone wetland: the Okavango Delta, Botswana.

Tooth S, and McCarthy TS, 2004. Controls on the transition from meandering to straight channels in the wetlands of the Okavango Delta, Botswana. Earth Surface Processes and Landforms, 29(13), 1627–1649.

United Nations (UN), 2018. The Sustainable Development Goals Report. New York. Available from: https://unstats.un.org/sdgs/files/report/2018/TheSustainableDevelopmentGoalsReport2018-EN.pdf

Van der Esch S, ten Brink B, Stehfest E, Bakkenes M, Sewell A, Bouwman A, Meijer J, Westhoek H and van den Berg, M., 2017. Exploring future changes in land use and land condition and the impacts on food, water, climate change and biodiversity: Scenarios for the Global Land Outlook. PBL Netherlands Environmental Assessment Agency, The Hague.

Waters MR, and Haynes CV, 2001. Late Quaternary arroyo formation and climate change in the American Southwest. Geology 29, 399–402.

Woodward JC, Williams MAJ, Garzanti E, Macklin MG, and Marriner N, 2015a. From source to sink: Exploring the Quaternary history of the Nile. Quaternary Science Reviews 130, 3–8.

Woodward J, Macklin M, Fielding L, Millar I, Spencer N, Welsby D, and Williams M, 2015b. Shifting sediment sources in the world's longest river: A strontium isotope record for the Holocene Nile. Quaternary Science Reviews 130, 124–140.

Yonge D, and Hesse PP, 2009. Geomorphic environments, drainage breakdown, and channel and floodplain evolution on the lower Macquarie River, central-western New South Wales. Australian Journal of Earth Sciences 56, 35–53.

APPENDICES

APPENDIX 1 – Hesse et al. (2018a)

Palaeohydrology of lowland rivers in the Murray-Darling Basin, Australia

APPENDIX 2 – Hesse et al. (2018b)

Dramatic reduction in size of the lowland Macquarie River in response to Late Quaternary climate-driven hydrologic change

APPENDIX 3 – Fryirs et al. (2018)

A nested hierarchical perspective to enhance interpretations and communication in fluvial geomorphology for use in water resources management: Lessons from the Okavango Delta, Botswana

APPENDIX 1

Palaeohydrology of lowland rivers in the Murray-Darling Basin, Australia

Paul P. Hesse[*], Rory Williams, Timothy J. Ralph, Kirstie A. Fryirs, Zacchary T. Larkin, Kira E. Westaway, Will Farebrother

Department of Environmental Sciences, Macquarie University, Sydney, NSW, 2039, Australia

ABSTRACT

This study derives a new function describing the relationship of channel bankfull discharge (Q_{bf}) to channel width in modern rivers of the Murray-Darling Basin (MDB) of southeastern Australia and applies this to dated palaeochannels of seven rivers to quantify late Quaternary discharge history in this important basin. All rivers show high MIS3 and MIS2 Q_{bf}, declining in the Holocene. The Q_{bf} of modern MDB rivers is correlated with total catchment precipitation but comparison with palaeochannel Q_{bf} estimates shows that while enhanced runoff efficiency is necessary to account for much larger late Pleistocene palaeochannels, either lower or higher precipitation rates could have prevailed. A strong association between relative palaeo- Q_{bf} enhancement and temperature suggests a temperature-mediated mechanism controlling river discharge, such as the fraction of precipitation stored as snow and thawing in spring, the enhancement of orographic rainfall, or CO_2 feedbacks with vegetation cover. Significantly enhanced MIS3 Q_{bf} requires an additional mechanism, such as increased rainfall. These findings are consistent with others that increased moisture availability was associated with past colder climates, although this was not necessarily the result of enhanced precipitation.

© 2018 Elsevier Ltd. All rights reserved.

1. Introduction

Understanding the hydrological response to climate change is of fundamental concern to both future and palaeoclimate studies. Yet there is a tension between modern data and modelling analyses linking colder temperatures with lower values of aridity or drought indices, and a widespread view in the palaeoclimate community that colder climates, such as during the last glacial maximum (LGM), were more arid (Scheff et al., 2017). Recent studies have explored both what is meant by terms such as aridity, drier and wetter in relation to palaeoclimate proxies and our interpretation of those proxies (Prentice et al., 2017; Scheff et al., 2017). One such proxy, with a history of conflicting climatic interpretation, is palaeochannels. In many lowlands they appear to offer one of the few, and most promising, insights into past hydrology and climate.

The palaeochannels of the Murray-Darling Basin (MDB) have long been used as a proxy for late Quaternary climate change in southeastern Australia (e.g.Bowler, 1978a; Nanson et al., 1992; Page et al., 2009). Much effort has gone into examining the geomorphology and chronology of the palaeochannels of these river systems, with early work concentrating on the southern Riverine Plains of the Murray and Goulburn Rivers (Pels, 1964; Bowler, 1967) and Murrumbidgee River (Butler, 1950, 1958; Langford-Smith, 1960; Schumm, 1968). The first generation of luminescence dating (using thermoluminescence – TL) was also conducted on these rivers (Page et al., 1991, 1996) replacing an earlier scant radiocarbon chronology plagued by contaminated ages. The Murrumbidgee TL chronology (Page et al., 1996) has provided the template for interpretation of the hydrology and chronology of subsequent investigations. More recent studies have examined the Darling (Bowler et al., 1978; Lawrie et al., 2012), Macquarie (Watkins and Meakin, 1996; Hesse et al., 2018), Lachlan (Kemp and Rhodes, 2010, 2017), Namoi (Young et al., 2002; Wray, 2009) and Gwydir (Pietsch et al., 2013) rivers (Fig. 1), and revised the Murrumbidgee chronology (Mueller et al., 2018), extending the geographic and climatic range of investigations into the northern MDB and applying optically stimulated luminescence (OSL) dating.

Despite some general agreement that palaeochannels in marine

* Corresponding author.

E-mail addresses: paul.hesse@mq.edu.au (P.P. Hesse), rory.williams@mq.edu.au (R. Williams), tim.ralph@mq.edu.au (T.J. Ralph), kirstie.fryirs@mq.edu.au (K.A. Fryirs), zacchary.larkin@mq.edu.au (Z.T. Larkin), kira.westaway@mq.edu.au (K.E. Westaway), willfarebro@gmail.com (W. Farebrother).
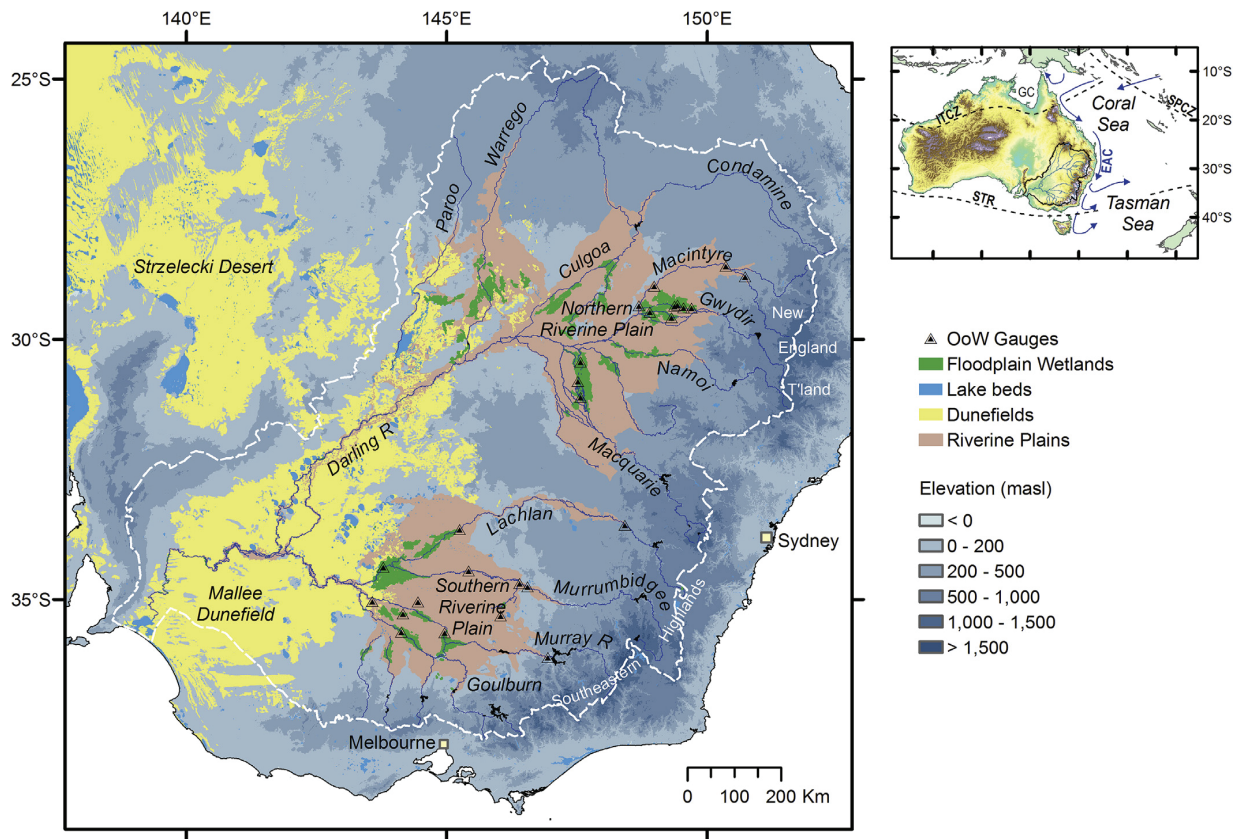
Fig. 1. Murray-Darling Basin (dashed white line) topography and drainage. Topography from Geoscience Australia Globalmap (2001). Areas of riverine plains (pink), floodplain wetlands (green) and dunefields (yellow) interpreted from ESRI background satellite imagery and Australian airborne radiometric mosaic (Geoscience Australia). NSW Office of Water gauge sites used to derive discharge equations shown by triangles. The index map shows the East Australian Current (EAC) and average January positions of the inter-tropical convergence zone (ITCZ), South Pacific Convergence Zone (SPCZ) and sub-tropical ridge (STR). GC — Gulf of Carpentaria. (For interpretation of the references to colour in this figure legend, the reader is referred to the Web version of this article.)

oxygen isotope stage (MIS) 5, 3 and 2 were larger than the modern MDB rivers, there are still areas of uncertainty. For example, it is not clear what conditions contributed to the elevated bankfull discharges of the last glacial cycle. Proxy evidence suggests the last glacial maximum (LGM) climate of southeastern Australia was up to 9 °C colder than the pre-industrial modern era (Galloway, 1965; Miller et al., 1997; Barrows et al., 2002). Consequently, the alpine tree line was much lower (Sweller and Martin, 2001; Kershaw et al., 2007) and fluctuated with hemispheric temperature change. However, treelessness at lower altitudes has also been attributed to lower precipitation (Dodson and Wright, 1989) and the effects of lower atmospheric carbon dioxide (Hesse et al., 2003). Some lakes were full or enlarged at the LGM and this has been attributed to either lower catchment evapotranspiration (Page et al., 1994) or high precipitation (Shulmeister et al., 2016) resulting in a positive moisture balance. However, the LGM was also a time of dry lakes in central Australia (Magee and Miller, 1998) and 'mega-lakes' existed at times during MIS5 and 3. Enhanced dust fluxes were experienced during the LGM (Hesse, 1994; Petherick et al., 2008; Fitzsimmons et al., 2013) and dune building has been found to have been greater at the LGM (Fitzsimmons et al., 2007, 2013; Hesse, 2016) in the Strzelecki Desert of central Australia and the Mallee Dunefield of the western MDB. There is thus a mixed picture of the nature of southeastern Australian environmental conditions at the LGM and earlier: some indicators of wetness, relating to runoff, strong

evidence for much colder conditions, and some evidence indicative of aridity.

1.1. Palaeochannels and palaeohydrology of Murray-Darling Basin rivers

Previous studies have contributed to development of a regional framework of palaeochannel formation, palaeodischarge and associated fluvial activity over the last glacial cycle (Page et al., 2009). Following Bowler (1978b), this framework identified 'phases' of fluvial activity, each with multiple channels of characteristic planform and size ('complexes' in the terminology of Bowler, 1978; 'systems' in the terminology of Page et al., 1996). In each study, palaeochannel systems were identified and dated with a range of techniques and sampling densities.

Vast differences in the size of the palaeochannels relative to their modern fluvial counterparts have been interpreted as recording past episodes of greater bankfull discharge (Langford-Smith, 1959; Schumm, 1968). Schumm (1968) was the first to attempt a quantification of the palaeo bankfull discharges, applying Manning's equation to reconstructed channel dimensions and slope, and assumed roughness. For the 'ancestral' Gum Creek phase cutoff at Tombullen on the Murrumbidgee he derived a bankfull discharge around five times greater than the modern river. Bowler (1978) applied Dury's (1976) empirical equations relating bankfull

discharge to meander wavelength, channel bed width and cross-sectional area but noted large discrepancies between gauged and predicted discharges for modern rivers. Nevertheless, Bowler (1978) estimated palaeodischarges two to four times greater than those of the modern Goulburn River. The Coocalla palaeochannel of the Gwydir River in the northern MDB had the largest discharge, relative to its modern equivalent, up to 100 times greater (Pietsch et al., 2013). Many studies have derived bankfull discharge estimates from palaeochannels across the MDB, using either Manning's equation (Page and Nanson, 1996), Dury's equation (Young et al., 2002; Wray, 2009), Limerinos' equation (Kemp and Rhodes, 2010) or more than one approach (Kemp and Rhodes, 2010; Pietsch et al., 2013). The data used to make these estimates have come from both subsurface investigation of paleaochannel width and depth and the interpretation of surficial palaeochannel width and meander wavelength from imagery.

Explanations for the larger palaeochannels and greater fluvial bankfull discharges during much of the last glacial cycle have included:

1. A colder climate, creating larger seasonal snow packs, particularly over the upper parts of the southern catchments, leading to high seasonal (spring-summer) channel-forming discharges (Langford-Smith, 1959, 1960; Bowler, 1978b; Page et al., 1996, 2009; Kemp and Spooner, 2007; Reinfelds et al., 2014). This mechanism has been proposed by proponents of both a wetter (pluvial) LGM (Langford-Smith, 1959, 1960), and lower LGM precipitation (Kemp and Rhodes, 2010) following the modelling of Galloway (1965). Schumm (1968) proposed that the MIS5 and MIS3 'prior streams' carried larger floods than the modern Murrumbidgee but had lower overall discharge, reflecting a drier climate

2. Periglacial activity in the southeastern highlands (Bowler, 1978b; Page et al., 1996), but not the New England Tablelands in the north (Bowler et al., 1978), contributing to enhanced sediment loads and aggradational fluvial phases

3. A lower alpine tree line and reduced vegetation cover through much of the highlands (Sweller and Martin, 2001; Kershaw et al., 2007) reducing transpiration and increasing the run-off efficiency (Bowler, 1978b; Ogden et al., 2001; Page et al., 2009)

4. Higher rainfall (Nanson et al., 2008; Pietsch and Nanson, 2011) derived from the Coral Sea and East Australian Current, enhanced by low sea levels trapping a pool of warm water against the northeast Australian coast. This mechanism is distinct from enhancement of the Australian monsoon, proposed for northern and central Australia (e.g.Magee et al., 2004)

5. Enhanced run-off (through any of the mechanisms listed above), leading to greater connectivity through the catchment, providing increased discharge and sediment supply, and development of single-thread laterally migrating channels (Kemp and Rhodes, 2010) distinct from the tendency to form multiple distributary channels in some modern rivers (Pietsch et al., 2013). The reverse trend (multiple-channels to single-thread) has also been ascribed to the Murrumbidgee catchment (Langford-Smith, 1960; Pels, 1969) as a consequence of decreasing sediment load in the Holocene.

In this study we aim to test several of these alternative (and sometimes conflicting) explanations by examining older and new palaeochannel archives from both northern and southern parts of the MDB, using a common approach to reconstruction of palaeochannel hydrology and the best available chronologies. We will use modern catchment climate and hydrological data to examine the climatic drivers of river bankfull discharge. We will compare the timing of hydrological changes between catchments and compare them with proposed independent controls such as temperature. We will compare the responses in northern and southern catchments to detect the applicability of explanations relying on latitudinal gradients in temperature and moisture sources.

1.2. Palaeohydrological reconstruction

A key element involved in developing palaeohydrology estimates involves choosing an approach to relate channel dimensions to river discharge. Most palaeodischarge equations are based on the understanding that channel form is created by bankfull discharge (Church, 1992). Wharton (1995) collated 25 regional discharge equations relating to channel metrics (mostly bankfull width) and showed that they are as varied as the regions from which they are derived. Non-measured parameters must explain the differences between the region-specific equations. Therefore, either more parameters must be included in a general equation that covers geographically diverse rivers or regionally appropriate equations should be applied.

The two main equation types used are (1) *hydraulic* (e.g. Manning's), using channel size and shape, slope and roughness, and (2) *regime* (e.g. Dury, 1976), which are derived by correlating simple channel parameters with known discharges. Dury (1976) derived a series of regression equations that identify the relationship between measurable channel parameters (bed width, depth, cross-sectional area, meander wavelength) and discharge for a range of rivers. The benefit of this approach is that the equations are relatively simple and the necessary data may be obtained from remote sensing (Borisova et al., 2006). Notwithstanding criticisms of this approach (Williams, 1978; Pickup and Rieger, 1979), in this paper we have developed a new regime equation for the MDB rivers, following Dury's approach, because it is most applicable to the palaeochannels preserved on the surface of the riverine plains.

In this paper we develop novel palaeodischarge reconstructions using an empirical channel width-discharge relationship derived from modern MDB gauge data, which we applied to all dated palaeochannels of lowland rivers in the MDB. Kemp and Rhodes (2010) observed that much of the data used to derive Dury's (1976) equations are from humid, mid-latitude regions in North America, Europe and Siberia. They concluded that their use outside their empirical range to estimate the highly variable and often longitudinally diminishing flows of inland Australia was problematic (Knighton, 1998; Kemp, 2005). Bowler (1978b) noted internal discrepancies between discharge estimates using three of Dury's equations and significant deviations from modern gauge data.

2. Murray-Darling Basin

The MDB extends across more than one million square kilometres of the southeastern interior of Australia (Fig. 1). The MDB encompasses a range of seasonal rainfall distributions with the northern catchments receiving proportionally more summer rainfall and the southern catchments more winter rainfall (Fig. 2). Climates range from arid in the west through to humid in the east (Fig. 2). Precipitation is highest on the highlands in the east, especially the southeastern alpine region, resulting from orographic lifting of winter frontal systems within the westerly wind system. Large (long return-period) floods are commonly associated with deep troughs extending from the inter-tropical convergence zone (ITCZ) in northern Australia during the summer months (Fig. 1).

The highlands in the east and southeast are drained through relatively steep, confined valleys before debouching on to broad, low-slope distributive fluvial systems (DFS), large alluvial forms with radiating channel patterns (Weissmann et al., 2010). These
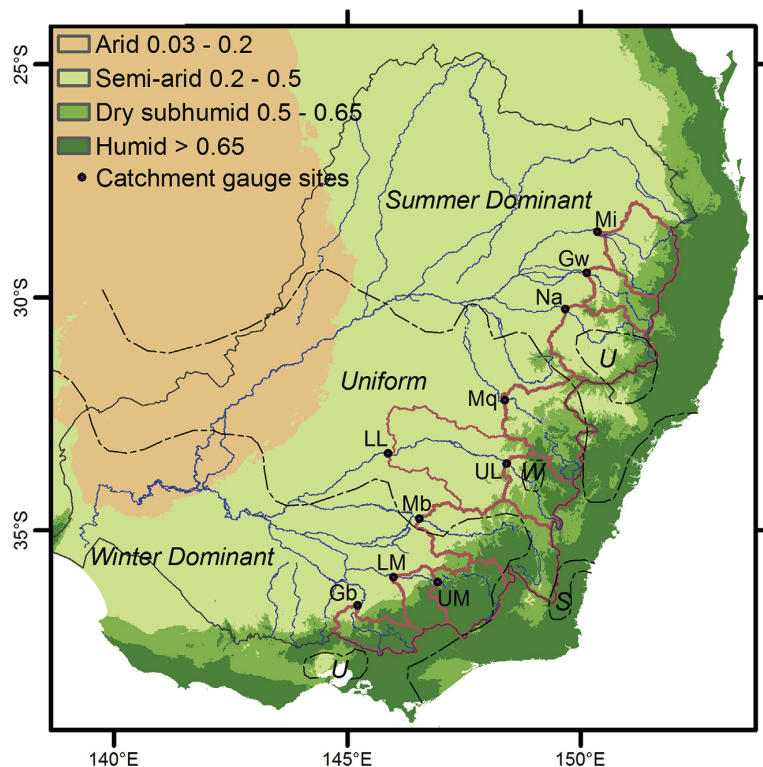
Fig. 2. Rainfall effectiveness and seasonality. Aridity index (shaded) is the ratio of mean annual precipitation to mean annual potential evapotranspiration (Trabucco and Zomer, 2009). Rainfall seasonality (ratio of Nov–Apr to May–Oct precipitation) from Bureau of Meteorology data, based on 1900–1999 period. Catchments for major MDB rivers outlined in red and gauges used to determine catchment runoff indicated by dots (Table 2). Mi – Macintyre, Gw – Gwydir, Na – Namoi, Mq – Macquarie, UL – Upper Lachlan, LL – Lower Lachlan, Mb – Murrumbidgee, UM – Upper Murray, LM – Lower Murray, Gb – Goulburn. (For interpretation of the references to colour in this figure legend, the reader is referred to the Web version of this article.)

riverine plains of the Murray and Darling basins (south and north, respectively; Fig. 1) preserve a shallow sequence of Neogene and Quaternary alluvial sediments (Watkins and Meakin, 1996; Kingham, 1998). Low rates of subsidence and deposition (Brown and Stephenson, 1991) create the ideal environment for preservation of a series of Quaternary palaeochannels visible on the surface of the plains.

Most DFS rivers within the MDB are losing streams (their discharge declines downstream) (Fig. 3) because of transmission losses and an absence of tributary inputs. Consequently, sediment load also decreases and is deposited on floodplains or in-channel (Olive et al., 1994). Several rivers in the MDB suffer such dramatic loss of flow that they have become disconnected, or are approaching disconnection, from the trunk stream (e.g. Gwydir, Paroo, Macquarie, Lachlan, Loddon) (Figs. 1, 4 and 5). Some of these channels also break down, losing continuity, and flood out (Tooth, 1999), forming extensive floodplain wetlands which dissipate flow and sediment load (Yonge and Hesse, 2009; Ralph and Hesse, 2010b).

3. Methods

3.1. Palaeochannel mapping and morphometrics

To standardise palaeo-discharge estimates across the MDB, previously mapped and dated palaeochannels were remeasured for this study. A 5m LiDAR (Light Detection and Ranging) DEM
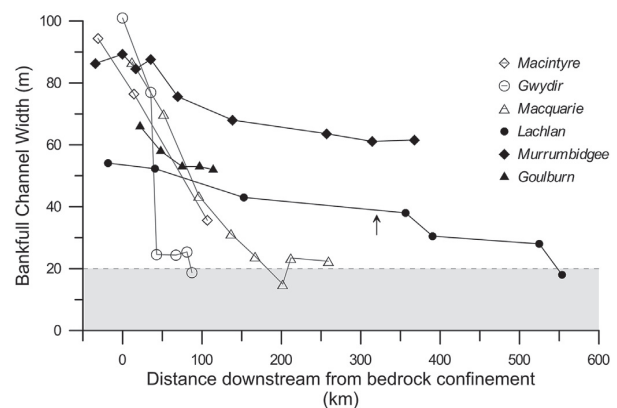
Fig. 3. Downstream trends in channel width of Murray-Darling Basin DFS rivers (data measured from satellite imagery). Northern MDB rivers are indicated by open symbols and southern MDB rivers by solid symbols. The horizontal dashed line and shaded area indicate the proposed threshold below which channels are observed to break down and form floodplain wetlands. Arrow indicates location of second point of confinement at the head of the Lachlan DFS.

(digital elevation model) is available for the NSW portion of the MDB (NSW Government Spatial Services) and, in the Macquarie River system, a 1 m LiDAR DEM (NSW Office of Environment and Heritage) was used to measure palaeochannel dimensions.

Fig. 4. Northern Riverine Plain of the Murray-Darling Basin. Dated palaeochannel sites from previous work are indicated by dots and selected palaeochannels by blue lines. Shaded topography is the same as for Fig. 1. DFS areas (pink), floodplain wetlands (green), dunefields and palaeochannels were interpreted from Esri background satellite imagery. QOB — Quombothoo palaeochannel, BIB — Bibbijibbery, BBB — Billybingbone, MIL — Milmiland, MDD — Mundadoo, MC — Marra Creek (Hesse et al., 2018); CS — Central System (Young et al., 2002); BUN — Bunnor, GI — Gingham, CO — Coocalla, MM — Mia, KK — Kookabunna, KA — Kamilaroi (Pietsch et al., 2013). (For interpretation of the references to colour in this figure legend, the reader is referred to the Web version of this article.)

Outside NSW (Goulburn River and a portion of the Murray River plains) the highest available resolution satellite TM imagery in Google Earth and ESRI background imagery in ArcGIS was used to map and measure palaeochannels. All measurements were based on the dated reach of each palaeochannel. Palaeochannel mapping across the MDB has previously been approached at the scale of individual catchments. This may lead to variation in individual interpretation of geomorphic forms or the use of inconsistent definitions (e.g. bank-full level (Wharton, 1995) between studies and catchments.

Bankfull width (W_{bf}) was measured at meander inflection points from topographic profiles extracted from the LiDAR DEM. Mean reach bankfull width was calculated from up to nine individual measurements along a reach, depending on preservation. Meander wavelength (L) was calculated by measuring the distance between inflection points along the reach over up to nine wavelengths.

3.2. Palaeochannel ages

We derived palaeochannel ages from meta-analysis of published luminescence ages and new OSL ages from a new site on the Yanco palaeochannel of the Murrumbidgee River (Supplementary Data). We derived probability density functions (PDFs) of ages from each palaeochannel to determine median (50th percentile) age, 5th and 95th percentile ages. We therefore estimated independent ages for each dated palaeochannel which may have been ascribed to a broader 'phase' of fluvial activity. Most palaeochannels are dated by 1—3, exceptionally 7, ages. In all cases (except the Gulgo palaeochannel of the Lachlan, below) we used only ages from fluvial sediments and not the related source-bordering sand dunes. This compilation therefore includes some palaeochannel systems dated by thermoluminescence (TL) and some dated by single grain (SG) —OSL, or other OSL methods. There is only limited evidence to support the equivalence of both methods: Banerjee et al. (2002)
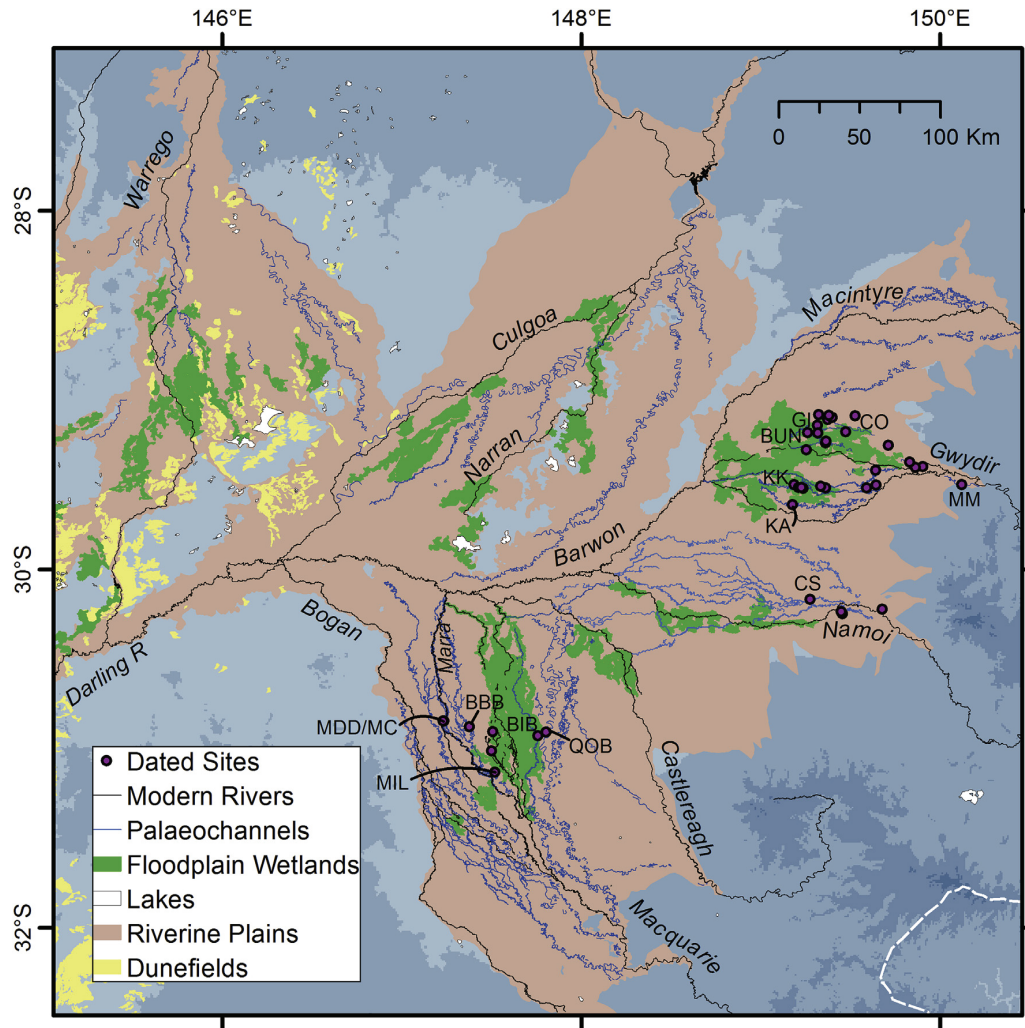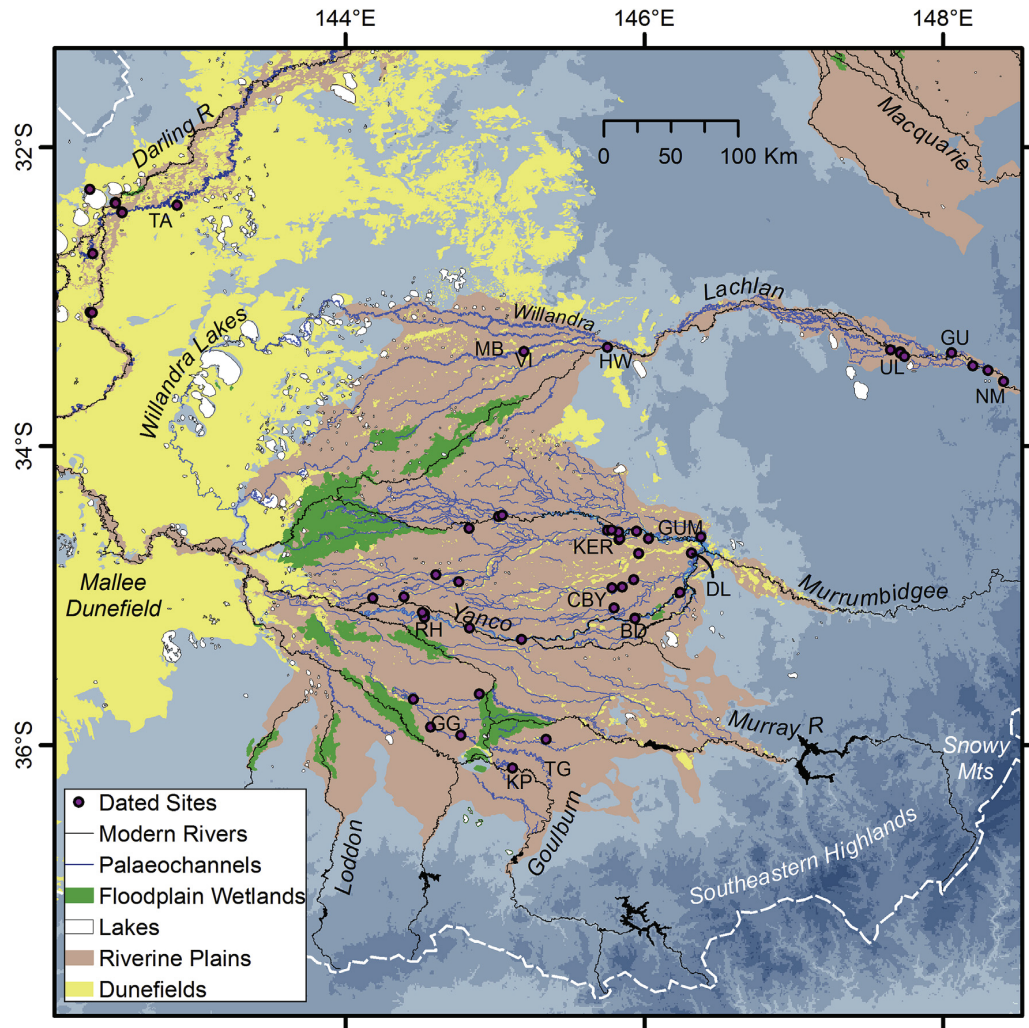
Fig. 5. Southern Riverine Plain of the Murray-Darling Basin. Dated palaeochannel sites from previous work are indicated by dots and selected palaeochannels by blue lines. Shaded topography is the same as for Fig. 1. DFS areas (pink), floodplain wetlands (green), dunefields (yellow) and palaeochannels (blue lines) were interpreted from Esri background satellite imagery. KP — Kotupna, TG — Tallygaroopna, GG — Green Gully, CBY — Coleambally, KER — Kerarbury, GUM — Gum Creek, NM — Nanima, GU — Gulgo, UL — Ulguetherie, HW — Hunthawang, VI — Viela, MB — Middle Billabong; DL — Dry Lake, BD — Bundure, RH — Rhyola; TA — Talyawalka Creek. (For interpretation of the references to colour in this figure legend, the reader is referred to the Web version of this article.)

used single-aliquot OSL (mean age) to date samples from three palaeochannel systems (Yanco, Kerarbury and Coleambally) identified by Page et al. (1996). The reported ages are similar to the TL ages but no sampling locations were reported or direct comparisons with TL ages provided. The single OSL age from the Yanco system (Banerjee et al., 2002) (9.4 ± 0.8 ka) is younger than TL age estimates from three locations (13.6–18.2 ka) (Page et al., 1996) but overlap at 2σ (Supplementary data). Our new SG-OSL age from a different site on the Yanco palaeochannel (Supplementary data) agrees closely with the TL ages and is somewhat older (15 ± 2 ka) than the single-aliquot OSL age of Banerjee et al. (2002). A new study (Mueller et al., 2018) applied both single grain (SG)—OSL and TL dating methods to Yanco and Gum Creek system sediments. Overall they found that the SG-OSL central age model (CAM) ages to be somewhat younger than the TL ages, but with some overlap. Their new TL ages, however, were significantly older than previously published TL ages for the same palaeochannels (Page et al.,

1996).

Gwydir palaeochannel SG-OSL ages (Pietsch et al., 2013) that can be associated with a particular palaeochannel trace have been selected. The modern river system ('Gwydir') has been identified by several ages younger than 5 ka (Pietsch et al., 2013), however these have not been associated with channels distinct from the extant rivers and so are not treated here as a palaeochannel system. Several TL ages for palaeochannels of the Namoi or nearby streams (Young et al., 2002) are not clearly related to surface palaeochannel traces. Only ages from the Central System at Pian Ck (Young et al., 2002) can be reliably extrapolated to nearby and downstream palaeochannel reaches (Wray, 2009).

New SG-OSL minimum age model (MAM) ages of Macquarie palaeochannels (Hesse et al., 2018) date six large and longitudinally continuous palaeochannels on the surface of the Macquarie DFS as well as late Holocene precursors of the modern river. These ages are used in preference to earlier TL (Watkins,

1992; Watkins and Meakin, 1996) and single-aliquot OSL (Yonge and Hesse, 2009) ages because the distribution of palaeodoses supports a minimum age model approach (Hesse et al., 2018) and because several of the TL ages come from unknown contexts or only shallow depths (Watkins, 1992; Watkins and Meakin, 1996).

Palaeochannel ages (single aliquot regenerative (SAR) OSL) of the Lachlan River come from the mid-Lachlan valley (Kemp and Spooner, 2007; Kemp and Rhodes, 2010), which is a wide alluvial plain bounded by bedrock hills with a complex network of palaeochannel traces, and palaeochannels near the head of the DFS (Kemp et al., 2017). Only one, saturated, age of Gulgo palaeochannels has been reported and one age of a source-bordering sand dune associated with a Gulgo system palaeochannel (Kemp and Rhodes, 2010). We have used the dune age to characterise the age of the Gulgo system. We have taken the median age of all Ulgutherie phase ages from around Bedgerebong for the nearby Ulgutherie Creek palaeochannel of that system. We used only the OSL ages of the Nanima palaeochannel system, although they cover the range of the additional ^{14}C age determinations of this system (Kemp and Rhodes, 2010).

TL ages of Murrumbidgee palaeochannels (Page et al., 1996) have been used but applied to individual palaeochannel traces, rather than grouped for entire palaeochannel phases. We excluded all dune ages because some are clearly younger than their associated palaeochannel ages (Page et al., 1996). We have used the SG-OSL ages of the Tombullen Reach (Gum Ck) and Yanco palaeochannels (Mueller et al., 2018). We have also made SG-OSL age estimates of bedload sediment and source-bordering sand dune at the Dry Lake site on the upper reach of Yanco Creek (Supplementary data).

There is a small number of TL ages from the inter-related Goulburn and Murray River palaeochannels upstream and downstream of the Cadell Fault block. We used the ages reported by Page et al. (1996) which were revised from an earlier paper (Page et al., 1991). We average all 'pre-Cadell' ages and applied the median age to the Tallygaroopna palaeochannel of the Goulburn River. A single TL age (Page et al., 1996) on fluvial sediment has been applied to two separate palaeochannel reaches associated with the Kotupna phase of the Goulburn River (Bowler, 1978b).

Several palaeochannels of the mid-Darling River have been dated by SAR OSL (Lawrie et al., 2012), including the Talyawalka Creek − Anabranch palaeochannel thought to be related to the Acres Billabong palaeochannel (upstream) previously dated by ^{14}C (Bowler et al., 1978).

3.3. Discharge equations

Empirical relationships were derived from observed bankfull discharge and associated contemporary channel parameters of the MDB. Bankfull discharge (Q_{bf}), as opposed to a flood recurrence interval, was used as it provides a consistent discharge measurement at maximum stream power, whether or not the river's flow has been modified or regulated over the period of record. Likewise, bankfull width (W_{bf}) has been used, rather than bed width (Dury, 1976), because it can be measured on both modern and palaeochannels from surface features.

The New South Wales Office of Water maintains a real-time and historical water monitoring database (http://realtimedata.water.nsw.gov.au/water.stmppbm=SURFACE_WATER&rs3&rskm.url; Pinneena 10.2) for many of the alluvial rivers of the MDB. The bankfull level at each site was determined from cross-sections and converted to bankfull discharge from the ratings table. Monitoring stations were selected for inclusion only when they contained all the relevant data and where the bankfull level could be estimated with confidence (Table 1). Channel bankfull width was also measured from the LiDAR DEM or ESRI background imagery in ArcGIS. Where there was more than ~10% difference between the NSW Office of Water site width and the reach average width determined from the satellite imagery the site was also rejected.

3.4. Catchment climate and hydrology

For this analysis, gauges at the lowest point of bedrock confinement of large MDB tributaries were identified (Table 2) and used to define catchment areas. These sites included all major tributaries to the trunk stream as it entered the DFS. In some cases gauges are sited to monitor flows for distribution to users (e.g. Willandra Weir, Yarrawonga Weir) and are not suitable for analysis of bankfull discharge however total catchment discharge has been reported (http://realtimedata.water.nsw.gov.au). The large Lachlan catchment was divided into the upper catchment, above Nanami, which feeds the broad alluvial mid-Lachlan valley and its palaeochannels, and the lower catchment (from Nanami to Willandra Weir) covering the remaining catchment area contributing to the DFS. The upper Murray (to Doctors Point, near Albury) captures all flows from the Murray, Mitta Mitta, and Keiwa rivers, while the 'lower' Murray catchment between Doctors Point and Yarrawonga Weir includes the Ovens River catchment.

All of these catchments are regulated to some extent, have reservoirs, and some have irrigation off-takes. The Murrumbidgee and Upper Murray receive flows from the Snowy River via the Snowy Mountains Hydroelectricity Scheme (0.38×10^6 ML/yr and 0.46×10^6 ML/yr respectively; Snowyhydro.com.au 3/9/17). Therefore, to some extent flood (or peak) discharges should not be regarded as faithful to natural flow conditions and reported Murrumbidgee and Upper Murray mean annual flows (Q_r) are higher than natural.

Gridded (0.05°) mean (1961−1990) annual precipitation data was downloaded from the Bureau of Meteorology (http://www.bom.gov.au/jsp/ncc/climate_averages/rainfall/IDCraingrids.jsp). SRTM 1 s DEM elevation data was sourced from Geoscience Australia (http://www.ga.gov.au) and clipped for each catchment, from which hypsometric curves were derived. Aridity index (P/PE) data for each catchment was integrated from available gridded data sets (Trabucco and Zomer, 2009).

4. Results

4.1. Palaeochannel dimensions and ages

The bankfull width and meander wavelength of dated palaeochannels from the Northern Riverine Plain (Fig. 4) and Southern Riverine Plain (Fig. 5) of the MDB show a very large range of sizes (Table 3). While the largest dated palaeochannel is the upper Waddi Arm of the Kerarbury system on the Murrumbidgee DFS (mean reach width 817 m) the largest palaeochannels relative to the closest reach of the modern river course are located on the Macquarie DFS (Quombothoo, 12 times wider than the modern river) and Gwydir (Coocalla, 14 times wider). Because the DFS rivers decrease in size downstream (Fig. 3) it is most informative to consider each of the palaeochannels relative to their position on the DFS (Fig. 6). In this context, the Waddi and Yanco palaeochannels are notable for their extraordinary width relative to the modern Murrumbidgee River (Fig. 6a and Supplementary data). All the Murrumbidgee palaeochannels were larger than the modern river at comparable distances across the DFS. The rate of decline of width of the Waddi and Yanco palaeochannels was much greater than for the modern river and more similar to the modern northern MDB rivers (Fig. 3).

Table 1
Office of Water (OoW) Gauge sites and channel dimensions.

NSW Office of Water site name	Latitude	Longitude	Elevation (masl)	OoW Depth (m)	OoW W_{bf}[a] (m)	W_{bf} at Gauge RS[b] (m)	Reach Mean W_{bf} RS (m)	Mean reach L (m)	Mean reach A (m)	Rating Table Q_{bf}[c] ML/day	Rating Table Q_{bf} m³/sec
Murray @ Doctors Pnt	−36.1123	146.9399	148	6.0	100	128	107.6	885	401	38600	447
Murray R @ Barham	−35.6298	144.1245	71	6.8	86	107	92.9	590	263	26400	306
Edward R @ Toonalook	−35.6428	144.9596	86	3.4	55	52	56.5	590	371	3070	36
Wakool @ Stoney Xing	−35.0376	143.5702	54	9.3	80	77	75.2	842	460	22400	259
Niemur R Barh-Mln Rd	−35.2739	144.1595	68	11.2	52	54	46.8	556	218	20100	233
M/Bidgee Narrandera	−34.7554	146.5489	138	9.6	90	79	89.3	914	529	52200	604
M/Bidgee D/S Yanco Weir	−34.6953	146.4007	139	7.6	77	76	84.6	903	388	22100	256
M/Bidgee @ Carrathool	−34.4493	145.4174	106	9.3	64	70	68	690	209	36100	418
M/Bidgee D/S Redbank	−34.3798	143.7817	67	7.1	62	71	61.1	664	353	10100	117
Billabong Cocketgedong	−35.3142	146.0355	116	1.4	29	30	28	186	89	1800	21
Billabong @ Darlot	−35.0442	144.4464	72	4.2	28	33	34.4	490	228	3640	42
Lachlan R @ Nanami	−33.5739	148.4181	249	9.7	50	63	54.1	963	193	24500	284
Lachlan @ Whealbah	−33.6544	145.2488	116	5.4	36	38	30.5	248	172	4400	51
Macquarie @Oxley Stn	−31.1175	147.5695	158	3.5	18	16	24	225	144	2000	23
Macquarie @Pillicawarrina	−30.8072	147.5149	141	2.5	28	18	23.45	242	83	1300	15
Macquarie @ Carinda Rd	−30.4347	147.5696	126	2.0	26	10	22.4	224	44	934	11
Gwydir @ Brageen Crossing	−29.3973	149.5465		4.1	31	25	24.4	417	47	4950	57
Gwydir @ Allambie Br	−29.3449	149.4307	175	5.1	20	26	25.4	350	51	3470	40
Gwydir @ Millewa	−29.3627	149.3736	172	2.1	13	22	18.7	350	51	522	6.0
Mehi D/S Gundare Regulator	−29.5888	149.315	192	3.5	33	36	28.5	198		3340	39
Mehi River @ Bronte	−29.4773	148.9023	146	3.2	30	39	35.3	190	146	3270	38
Gingham Channel @ Teralba	−29.3995	149.6991	193	3.6	30	25	25.4	291		5210	60
Macintyre @ Holdfast	−28.7997	150.7296	277	6.0	100	83	94.4	1356	521	54400	630
Macintyre @ Boggabilla	−28.5916	150.3615	237	7.8	77	129	76.5	1583		31200	361
Barwon R @ Mungindi	−28.9762	148.9848	153	3.0	52	71	48.8	419	152	7820	91
Barwon @ Mogil Mogil	−29.353	148.6885	140	5.9	50	62	45.4	801	239	8680	101

[a] Bankfull width.
[b] Measured from remote sensing imagery.
[c] Bankfull discharge.

Table 2
River Gauges used in analysis of catchment hydrology and climate.

Catchment	Gauge	Q_{bf}	Q_t[a]	Note
Macintyre (Mi)	Boggabilla	Y	1895–2017	
Gwydir (Gw)	Pallamallawa	Y	1892–2017	
Namoi (Na)	Mollee	Y	1965–2017	
Macquarie (Mq)	Baroona	Y	1986–2017	
Lachlan − lower (LL)	u/s Willandra Weir	N	1941–2017	
Lachlan − upper (UL)	Nanami	Y	1958–2017	d/s Belubula R
Lachlan − total (TL)	u/s Willandra Weir	N	1941–2017	
Murrumbidgee (Mb)	Narrandera	Y	1891–2017	
Murray − lower (LM)	d/s Yarrawonga Weir	N	1938–2017	d/s Ovens R
Murray − upper (UM)	Doctors Point	Y	1929–2017	d/s Keiwa R
Murray − total (TM)	d/s Yarrawonga Weir	N	1938–2017	
Goulburn (Gb)	Murchison	Y	1881–1956	

[a] Q_t is the mean annual flow, covering the stated interval. The same interval is also used to generate the ratings table used to derive Q_{bf}.

Table 3
Palaeochannel ages, dimensions and predicted bankfull discharges.

River System	Palaeochannel (system)	Distance D/S from confinement (km)	Median Age (ka)	Age 5th percentile (ka)	Age 95th percentile (ka)	Mean Reach Width (m)	predicted Q$_{bf}$ (m3s-1)[e]	Q$_{bf}$ 5th percentile	Q$_{bf}$ 95th percentile	Modern Comparison Width (m)	Modern Comparison Q$_{bf}$ (m3s-1)	PC/Modern Width ratio	PC/Modern Q$_{bf}$ ratio
Gwydir	Challucum (Bunnor)	35	61.5	50.5	72.5	203	2813	849	9322	63	207	3.2	13.6
	Bunnor (Bunnor)	65	58.4	48.2	68.6	190	2425	741	7941	24	24	7.9	101.1
	Mia (Coocalla)	−5	39.3	34.2	44.4	303	6904	1922	24791	85	401	3.6	17.2
	Coocalla (Coocalla)	54	35.7	30.9	41	340[d]	8937	2426	32923	24	24	14.2	372.4
	Gingham (Coocalla)	68	38.3	32.2	44.5	162	1697	532	5406	24	24	6.8	70.7
	Kamilaroi (Kamilaroi)	56	17.1	15.4	18.7	161	1673	526	5327	24	24	6.7	69.7
	Kookabunna (Kamilaroi)	84	17.9	15.1	20.9	126	966	315	2965	25	27	5.0	35.8
Namoi	Eastern	66				91	466	158	1377	32	45	2.8	10.4
	Central (Carrabear)	88	12.4[a]	9.6	15.2	52	130	46	371	34	51	1.5	2.6
	Cubbaroo (Carrabear)	95	12.4[a]	9.6	15.2	72	276	95	799	34	51	2.1	5.4
	Coolibah (Carrabear)	110	12.4[a]	9.6	15.2	71	176	72	195	34	51	2.1	3.4
	Myall Camp	55				47	106	37	302	32	45	1.5	2.4
Macquarie	Quombothoo	186	53.9	38.8	65.7	284	5970	1686	21145	24	22	12.1	271.4
	Bibijijbbery	184	34.1	27.1	41.2	125	949	309	2910	24	22	5.3	43.1
	Billybingbone	196	20.1	17.7	26.1	92	477	161	1412	24	22	3.9	21.7
	Milmiland	164	21.7	19	24.3	114	772	255	2339	24	24	4.8	32.8
	Mundadoo	210	5.6	4.8	6.4	86	410	140	1207	24	22	3.7	18.7
	Marra	210	2	1.7	2.4	31	42	15	120	24	22	1.3	1.9
	Terminus	180	3.4	0.5	5.6	22	19	7	57	24	24	0.9	0.8
	Willie	193	1.2	0.6	5.8	15	8	3	25	24	22	0.6	0.4
Lachlan	Sandhills (Gulgo)	41	66.6[b]	58.5	74.7	193	2512	765	8247	53	139	3.6	18.1
	Half Moon Lagoon (Ulgutherie)	41	24.2	17.7	33.1	231	3758	1107	12761	53	139	4.4	27.0
	Ulgutherie Ck (Ulgutherie)	87	24.2	17.7	33.1	123	915	299	2800	52	135	2.4	6.8
	Nanima	0	3.1	1.6	5.4	49	116	41	332	54	145	0.9	0.8
	Viela (Middle Billabong)	383	18.3	14.1	22.2	114	772	255	2339	37	62	3.1	12.5
	Hunthawang (Middle Billabong)	326	16.1	11.5	20.3	65	219	76	631	43	87	1.5	2.5
	Lachlan @ Hunthawang	326	6.4	4.9	9.3	56	157	55	449	43	87	1.3	1.8
Murrumbidgee	Bundure Arm (Coleambally)	85	100	85.2	114.8	141	1243	399	3877	76	307	1.9	4.0
	Yamma Arm (Coleambally)	102	85.1	72.9	97.5	189	2397	733	7840	76	307	2.5	7.8
	Booroorban (Kerarbury)	191	59.8	45.2	69.2	120	866	284	2641	64	209	1.9	4.1
	Romani Arm (Kerarbury)	196	47.8	37.8	57.8	143	1283	410	4010	64	209	2.2	6.1
	Waddi Arm U (Kerarbury)	120	45.9	39.6	52.1	817[d]	63753	13871	293022	68	242	12.0	263.4
	Waddi Arm L (Kerarbury)	248	37.5	30.45	47.9	568[d]	28229	6767	117761	64	209	8.9	135.1
	McGrath Arm (Kerarbury)	58	37.8	20.8	54.7	145	1323	423	4145	68	242	2.1	5.5
	(Hay Arm) Kerarbury	196	46.8	41.8	51.7	186	2313	709	7542	64	209	2.9	11.1
	Tabratong Arm (Gum Ck)	151	24.7	20.05	29.3	168	1841	574	5901	68	242	2.5	7.6
	Carrathool Arm (Gum Ck)	149	29.4	21.8	36.9	210	3035	910	10120	68	242	3.1	12.5
	Oolambeyan Arm (Gum Ck)	122	29.8	25	34.5	369	10737	2861	40300	68	242	5.4	44.4
	Tombullen Reach (Gum Ck)	48	33.8	30.15	38.25	195	2571	782	8457	88	428	2.2	6.0
	Dry Lake Reach (Yanco U)	22	22.5	14.2	26.5	572	28675	6863	119840	85	396	6.7	72.4
	Thurrowa Reach (Yanco M)	133	22.5	14.2	26.5	468	18289	4604	72661	85	396	5.5	46.2
	Wanganella Reach (Yanco L)	280	22.5	14.2	26.5	337	8762	2383	32211	68	242	5.0	36.2
	Rhyola Reach (Yanco L)	296	22.5	14.2	26.5	243	4210	1227	14438	61	191	4.0	22.0
Murray	Strathmerton	164	90.1	83	97.1	309	7214	2000	26014	68		4.5	
	Deniliquin	203	94.2	80.2	108.1	211	3068	919	10238	68		3.1	
	Green Gully U	203	93.9	85.3	102.4	195	2571	782	8457	68		2.9	
	Green Gully L (incl. Goulburn)	234	93.9	85.3	102.4	509	22080	5443	89557	93	306	5.5	72.2
	Thule Lagoon (incl. Goulburn)	257	65.1	59.1	71	402	13011	3397	49820	93	306	4.3	42.5
Goulburn	Tallygaroopna	65	91.1[c]	62.6	103.7	100	576	193	1717	53	139	1.9	4.1
	Kotupna	103	34.4	27.8	40.9	121	882.3	289	2694	53	139	2.3	6.3
	Kotupna	113	34.4	27.8	40.9	195	2571	782	8457	52	133	3.8	19.3
	Goulburn @ Green Gully	156	95.3	84.9	105.7	227	3614	1068	12229	74	226	4.4	16.0
Darling	Menindee Fm		84.9	61.9	108.1						289		

Table 3 (continued)

River System	Palaeochannel (system)	Distance D/S from confinement (km)	Median Age (ka)	Age 5th percentile (ka)	Age 95th percentile (ka)	Mean Reach Width (m)	predicted Q_{bf} (m3s-1)[e]	Q_{bf} 5th percentile	Q_{bf} 95th percentile	Modern Comparison Width (m)	Modern Comparison Q_{bf} (m3s-1)	PC/Modern Width ratio	PC/ Modern Q_{bf} ratio
	Menindee Fm @ Menindee		46.2	32.9	57.6	255	4690	1354	16244	74	289	3.4	16.2
	Relict Talyawalka –Anabranch @ Larloona (Coonambidgal 3)		27.8	22.2	36.1	92	477	161	1412	74	289	1.2	1.7
	Talyawalka-Anabranch @Appin (Coonambidgal 2)		19.5	16	23.5	161	1673	526	5327	74	289	2.2	5.8
	Talyawalka – Anabranch @Cuthero (Coonambidgal 2)		19.5	16	23.5	161	1673	526	5327	74	289	2.2	5.8
	Darling @ Chalky Well (Coonambidgal 1)		7.4	6.4	8.4					74	289		
	Darling @ Menindee (Coonambidgal 1)		3.2	1.5	4.3	65	219	76	631	74	289	4.0	0.8

[a] Ages extrapolated from Pian Ck bridge pit (Young et al., 2002).
[b] Age of the Gulgo source-bordering dune at Sandhills (Kemp and Rhodes, 2010).
[c] Median age of all pre-Cadell channel ages reported in Page et al. (1996).
[d] Infilled and mounded channels.
[e] Prediction based on equation (1) (text) using channel bankfull width.

All MIS3 and MIS2 palaeochannels of the Macquarie DFS were much larger than the modern river and larger than their modern Murrumbidgee equivalents (Fig. 6b). This is also true for the Gwydir DFS palaeochannels (Fig. 6c) and the Pleistocene Lachlan palaeochannels (Fig. 6d). With limited preservation, it is not possible to determine the size of the Quombothoo palaeochannel of the Macquarie DFS close to the head of the DFS. The variability in width of palaeochannels of similar age may represent real variability in successive channels of a single-thread river, variability of size of multiple anabranches which were active synchronously (within dating uncertainties), or reduction of channel size during or following abandonment (Stannard, 1961; Page and Nanson, 1996).

4.2. Palaeo-discharge estimates using a regime equation specific to lowland rivers of the MDB

Discharge and channel dimensions of 26 contemporary channel locations on the riverine plains of the MDB were used to derive an empirical regime equation for lowland rivers in the MDB (Table 1). The range of Q_{bf} covered two orders of magnitude from 630 m³s⁻¹ at Holdfast on the Macintyre River to 6 m³s⁻¹ on the Gwydir River at Millewa (one of many channels on the Gwydir DFS and 87 km downstream from the point of loss of confinement). Between these is a spread of values skewed to the lower end (Table 1).

Bankfull width (W_{bf}) and meander wavelength (L) were explored, following Dury (1976), for relationships with Q_{bf}. There is a strong relationship between W_{bf} and L for the modern rivers ($r^2 = 0.62$; $p < 0.0001$) (Fig. 7a), similar to that found by Dury (1976) and covering the middle of the range of values for rivers measured by Dury. Surprisingly, since bankfull width was measured here (c.f. bed width measured by Dury, 1976), for a given wavelength, the MDB rivers have lower width than found by Dury (1976), suggesting that there are characteristics of the climate, hydrology and/or catchment topography which lead to a different characteristic channel geometry compared with the rivers measured by Dury. Therefore, we chose to derive empirical regime equations for the MDB, rather than to rely on Dury's equations.

The relationship between W_{bf} and L (Fig. 7a) suggests that all the rivers considered here are, in a sense, scaled versions of the same fundamental planform. This holds even though the rivers cover a range of width:depth ratios from less than 5 to around 20 (Fig. 7b). Notably, there is no pattern of width:depth ratio according to channel size.

A regression analysis was undertaken using data from the contemporary channels to identify a relationship between measurable channel/catchment parameters and discharge. Stepwise regression showed mean bankfull width, alone, to be the best predictor of bankfull discharge (Fig. 7c):

$$\log_{10} Q_{bf} = 2.2412 \log_{10} W_{bf}^{1.7224} \tag{1}$$

$r^2 = 86.7\%$ $p = {<}0.0001$

Where Q_{bf} is bankfull discharge and W_{bf} is mean bankfull width for the reach.

This log regression has a better distribution of residuals and variance than a regression of non-log transformed data, produces realistic discharge estimates (non-negative) for small channels, and narrower 95% prediction intervals for larger discharges.

An additional regression analysis was undertaken using meander wavelength to estimate channel discharge (Fig. 7d). The relationship of discharge to wavelength is much weaker, with a
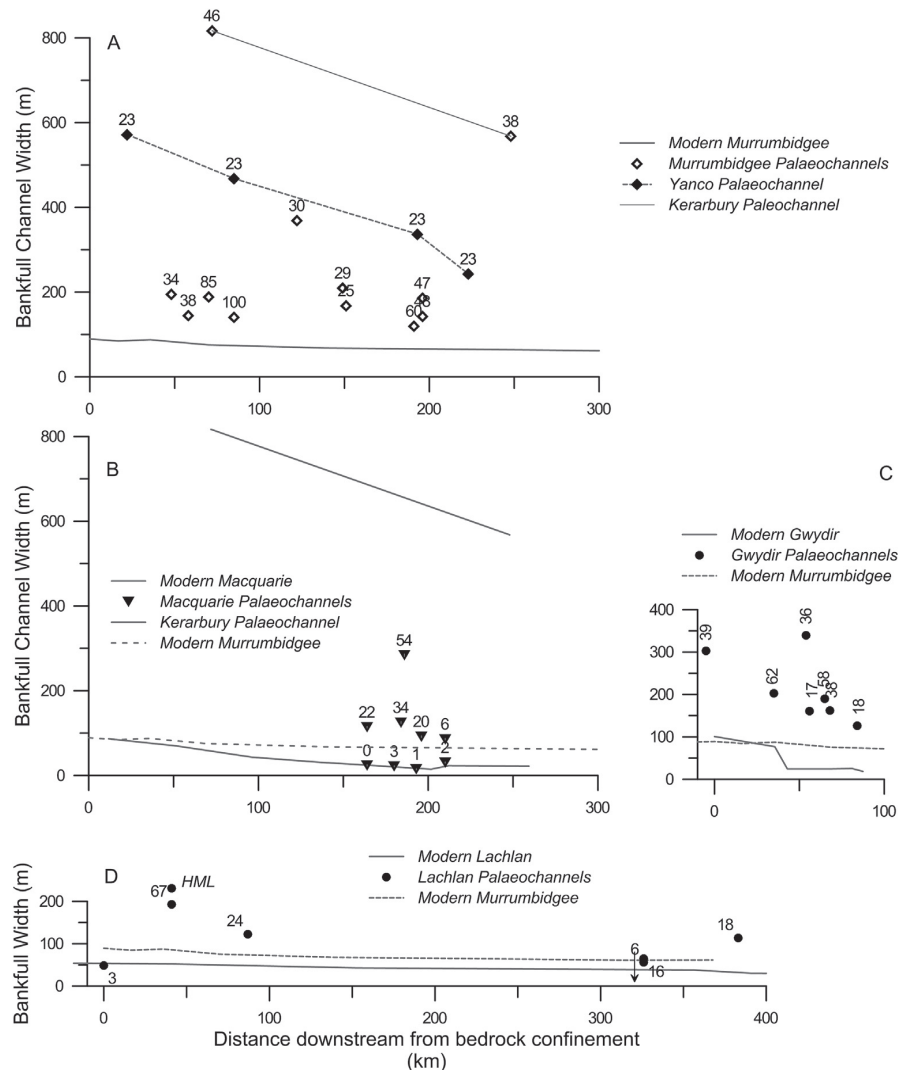
Fig. 6. Downstream changes in mean reach width for palaeochannels of MDB rivers. (a) Murrumbidgee River palaeochannels. Median ages (ka) for palaeochannels are shown by labels. Modern river shown for comparison. (b) Macquarie River and its palaeochannels compared with the Murrumbidgee River (dashed line) and the Waddi Arm (Kerarbury) palaeochannel of the Murrumbidgee River. (c) Gwydir River and palaeochannels and (d) Lachlan River and palaeochannels. Arrow indicates location of second point of confinement at the head of the Lachlan DFS. The undated Half Moon Lagoon (HML) (mapped as Ulgutherie by Kemp and Rhodes, 2010) is also included for comparison.

coefficient of determination (R^2) of 71% compared to the log transformed width-discharge value of 87%. When predicting discharge (within two standard deviations) using wavelength, the uncertainties are much larger than the log-transformed width equation.

4.3. Palaeo-discharge estimates

Palaeodischarge estimates derived for the MDB palaeochannels (Table 3) range from 42 m^3s^{-1} for Marra Creek palaeochannel on the Macquarie DFS to 63753 m^3s^{-1} for the upper Waddi Arm palaeochannel on the Murrumbidgee. These estimates carry large uncertainties, especially so at the upper end where the extrapolation from the modern observations is greatest.

Compared with the modern bankfull discharges, the largest of the MDB palaeochannels carried 263 times (upper Waddi Arm,

Murrumbidgee), 372 times (Coocalla, Gwydir) and 270 times (Quombothoo, Macquarie) the Q_{bf} of the modern river at an equivalent point on the DFS.

4.4. Catchment climate and hydrology

To understand the determinants of channel Q_{bf}, we undertook an analysis of modern channels, catchment precipitation, runoff and topography. Unexpectedly, there is no relationship between Q_{bf} and mean annual flow (Q_t) (Fig. 8a). Likewise, there is no clear relationship between Q_{bf} and the peak annual discharge (Fig. 8b) (although this measure is the most likely to be have been altered by river regulation). However, there is a strong relationship between Q_{bf} and total catchment precipitation (P_t) (km^3/yr) ($r^2 = 0.77$) (Fig. 8c), for all catchments with the exception of the Gwydir, which has significantly higher Q_{bf} for its precipitation amount than other
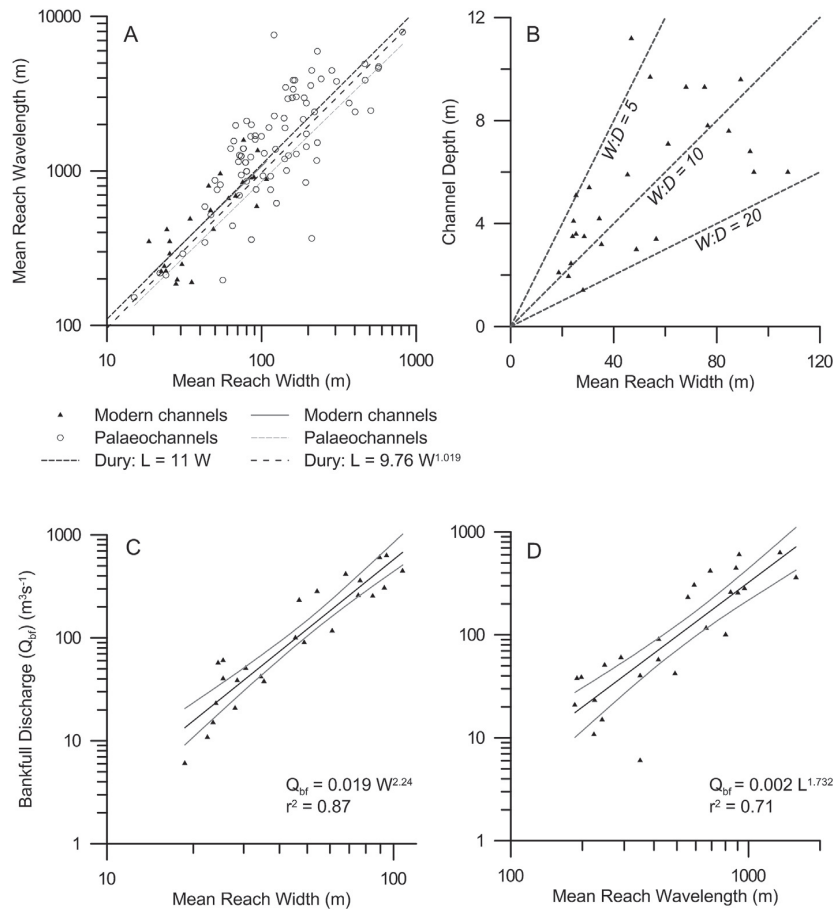
Fig. 7. (a) Channel wavelength versus bankfull width for all MDB modern and palaeochannel reaches used in this study. The regression of Dury (1976) between wavelength and bed width ($L = 9.76\ W^{1.109}$), and it's simplification ($L = 11\ W$) have also been added. (b) W_{bf} versus channel depth for modern gauging sites. Dashed lines show a range of width:depth ratios. (c) Regression between bankfull width and discharge used from NSW Office of Water gauging stations used to predict discharge, with 95% confidence intervals shown. (d) Regression between mean wavelength and bankfull discharge, with 95% confidence intervals shown.

rivers. Q_{bf} also scales with catchment size (with the exception of the Gwydir), which is to be expected because total precipitation is integrated over the entire catchment area.

The relationship (for rivers other than the Gwydir) is therefore:

$$Q_{bf} = a + b.\int P_r.A_c \qquad (2)$$

Where a and b are constants, $\int P_r$ is the integrated precipitation rate (mm/yr) over the catchment area (A_c). The term $\int P_r.A_c$ is also referred to as P_t (total catchment precipitation). The coefficient b describes the ratio of Q_{bf} to P_t and is the 'runoff factor of Q_{bf}' (R_{Qbf}).

The exceptional Q_{bf} of the Gwydir at Pallamallawa is consistent with the high Q_{bf} of the Gwydir at Yarraman Bridge (the next suitable gauge downstream). In most respects the Gwydir catchment is similar to other catchments (e.g. P_r, runoff factor (Q_t/P_t), elevation, hypsometry). It is possible that the channel is not in equilibrium with the discharge regime of the catchment. Historical channel avulsion, thick overbank sedimentation and high volumes of large wood downstream of Yarraman Bridge (also possibly underfit), attributed to historical catchment clearance (Erskine et al., 2012), leave open the possibility of historical channel modification of the Gwydir upstream of the modern wetlands.

The rate of contraction of channels on the DFSs (measured over approximately 100 km from the head of the DFS) (Fig. 8d) shows an inverse relationship with the ratio of Q_{bf}/Q_t (both measures converted to units of km^3/yr), used as an index of flow variability. The Gwydir, with by far the highest rate of channel contraction (Fig. 3), conforms to the pattern of high rates of channel contraction for all northern MDB rivers which have high bankfull discharge relative to their average annual discharge.

Precipitation rate in the MDB catchments is influenced by elevation, following the strong orographic nature of rainfall in these subtropical latitudes. This is strongest for maximum P_r, which is correlated with maximum elevation in all catchments (Fig. 9b). However median P_r has a more complex relationship with elevation, including a separate cluster formed by the Murray and Goulburn River catchments (Fig. 9b). In other words, there is another influence on precipitation which is not solely due to altitude but is related to latitude, such as temperature or zonal atmospheric circulation systems. The aridity index, defined as the ratio of precipitation to potential evapotranspiration (P/PE) follows a weak trend of increasing median values towards the south (Fig. 9c), somewhat different to the latitudinal pattern of median P_r which is relatively flat from the Macintyre to the Murrumbidgee but increases

markedly in the Murray and Goulburn catchments (Fig. 9a).

There are several feedbacks between precipitation and runoff. The average runoff depth (Q_t/A_c) is also correlated with the aridity index (P/PE) and also shows three clusters: Murray, Lachlan, all other catchments (Fig. 8e). The runoff factor (Q_t/P_t) also has a positive, non-linear relationship with median P/PE, such that the Murray and Goulburn catchments have a higher runoff factor, relative to P/PE, than other catchments (Fig. 8e).

5. Discussion

5.1. Size and age of MDB palaeochannels

Comparison of MDB palaeochannel ages (Fig. 10) shows only limited similarity in the timing between catchments. For example, only the Ulgutherie palaeochannel of the Lachlan and the Milmiland channel share a similar age probability distribution with the Yanco palaeochannel of the Murrumbidgee. The Kamilaroi palaeochannel of the Gwydir began after the Yanco and, on the basis of available ages, terminated earlier. The Darling and Macquarie rivers record active palaeochannels (Talyawalka-Anabranch, Billybingbone, respectively) slightly later than the Yanco at 20 ka. We found that there are similar mis-matches in timing between all palaeochannels of all the MDB river systems. The framework of temporally-correlated palaeochannel phases (Page et al., 2009; Pietsch et al., 2013) is not supported by the available luminescence dating.

It is highly likely that there are both sampling density and geomorphic factors contributing to the discrepancies in palaeochannel ages between river systems. The ever-increasing number of ages for different river systems has seen the blurring of previously reasonable groupings. Not all palaeochannels have been dated, often only the most obvious or most continuous, so we

should expect that additional dating will further change the age distribution. It is, therefore, unwise to place interpretations on gaps ('absence of evidence') while most palaeochannels are dated by only 1–3 age estimates and many more palaeochannels remain to be dated.

The lack of detectable synchroneity between even neighbouring catchments is also suggestive that external climate forcing is not responsible for the timing of the transition from one channel to another. Page et al. (1996) argued that shifts between aggradational and migrational phases of the Murrumbidgee palaeochannels were not convincingly tied to external climate shifts. Rather, the avulsion process which leads to the abandonment and formation of long channel reaches is likely to have had internal hydro-geomorphic forcings unique to each channel. Even the changes leading to the modern river systems, since the early Holocene, have not been synchronous between neighbouring catchments (Ogden et al., 2001). Nevertheless, the larger climate trends of the last glacial cycle may have exerted pressure on the size and planform of successive palaeochannels. In the Holocene, for example, all the river systems have trended towards smaller channels although each river system appears to have created new channels at different times in that transition.

This transition has seen different responses such that the Gwydir and Macquarie Rivers have reduced beyond an intrinsic threshold of discharge and sedimentation, similar to the process discussed by Ralph and Hesse (2010a) leading to channel breakdown, floodout and wetland formation, while the southern MDB rivers have generally remained continuous.

5.2. Palaeodischarge of lowland rivers in the Murray-Darling Basin

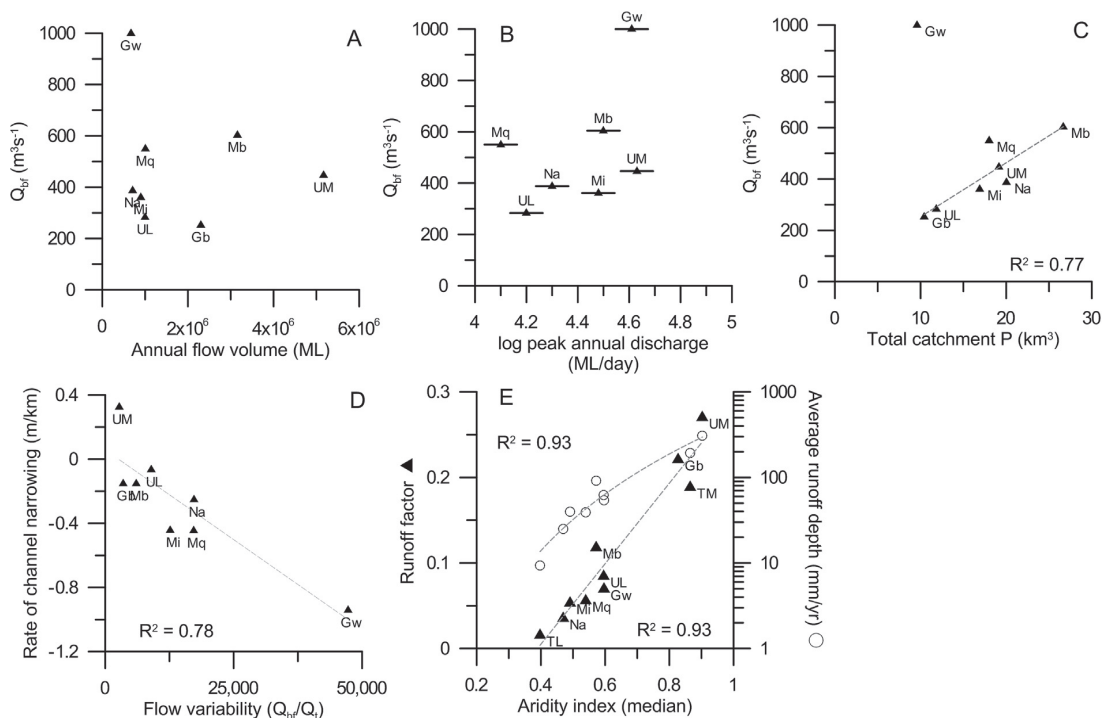We have found that modern MDB rivers with W:D ratios ranging

Fig. 8. Discharge of modern MDB rivers and explanatory environmental parameters. See Table 2 and Fig. 2 for location and definition of catchments. The regression in panel C does not include the Gwydir (Gw) catchment.
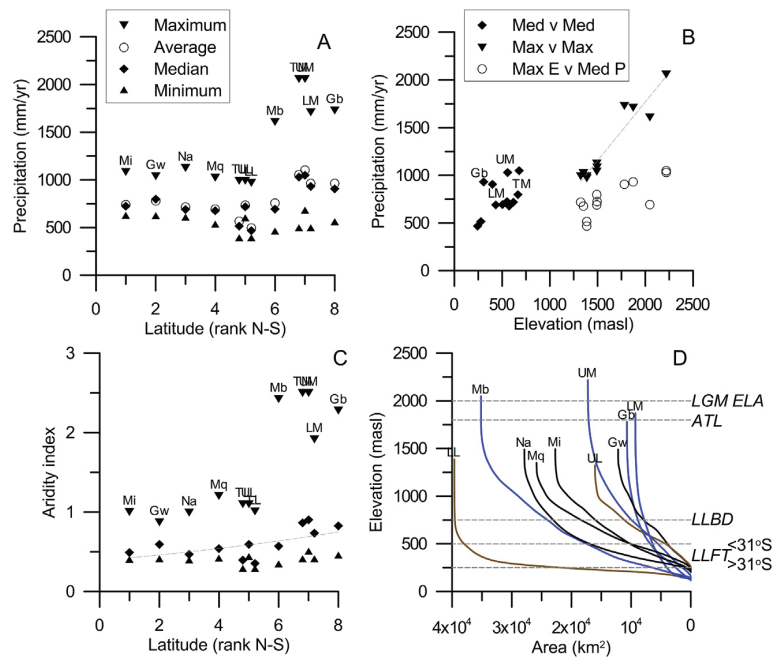
Fig. 9. Climate and topography of modern MDB catchments. Precipitation rate (mm/yr) (a, b) and aridity index (P/PE) (c) for MDB catchments, as shown in Fig. 2. (d) hypsometric curves for the same catchments with modern alpine tree line (ATL), LGM equilibrium line altitude (ELA), lower limit of periglacial block deposits (LLBD) and lower limit of freeze-thaw scree deposits (LLFT) shown (Slee and Shulmeister, 2015). Northern MDB catchments shown by blue lines, Lachlan catchment by brown lines, southern MDB catchments by black lines. (For interpretation of the references to colour in this figure legend, the reader is referred to the Web version of this article.)

from <5 up to 20 and with a range of sediment loads from purely suspended load to mixed load, conform to simple log-linear relationships between channel width and meander wavelength and between channel width or meander amplitude and bankfull discharge (Fig. 7). Dury (1976) observed that wavelength is a very conservative property of channels and it is possible that the broad scatter observed in the MDB channels reflects some degree of relict morphology. It is likely that the low discharge (and stream power) of these channels makes transformation of meander wavelength a very slow process compared to the adjustment of channel width.

Previous authors have noted the inaccuracies of the Dury regime equations when applied to MDB rivers (Bowler, 1978b). The regression relationship between channel width and bankfull discharge for modern MDB rivers developed here should redress those inaccuracies, but with high uncertainties. In addition, there is an inherent uncertainty in the extrapolation from the largest modern river (width ~ 100 m) to the largest palaeochannels (>200 m up to 817 m). However, Dury (1976) found single log-linear relationships (for slightly different parameters) extending to include channels, like the Amazon, much larger than any MDB palaeochannels. Therefore, we believe that it is reasonable to assume that our regression relationships are valid for channels five times or more wider than the largest MDB channel observed today.

The dated palaeochannels of the Macquarie River show a sequential decline in Q_{bf} but with two major step-like decreases (Fig. 11). The first was between the Quombothoo palaeochannel and the Bibbijibbery palaeochannel, 54–34 ka, while the second followed the Mundadoo channel before establishment of the modern channel configuration and characteristic floodplain wetlands of the Macquarie Marshes around 5.6–5.2 ka (Hesse et al., 2018). The Quombothoo palaeochannel (the largest visible on the surface of the Macquarie DFS) had a mean bankfull discharge around 270 times greater than the modern river (at Oxley). One of the factors

contributing to the very large difference in size between the Quombothoo palaeochannel and the modern Macquarie River (at Oxley) may be that the modern river decreases rapidly in size and discharge downstream from the point of loss of valley confinement (Fig. 3). It is possible, but undetermined, that the Quombothoo channel had a lower rate of channel decline.

Palaeodischarge estimates of the Gwydir palaeochannels from this study show similar trends to those of Pietsch et al. (2013) but are higher in magnitude in this study. This is the product both of the different regime equation we have developed and applied, and the channel width estimates derived from the LiDAR DEM. The Gwydir, which today declines rapidly in width on the DFS surface and floods out to form floodplain wetlands, was a much larger river system, further out on the DFS surface in MIS 4 and 2 but was largest in late-MIS3 (Fig. 11b). The timing of the transition to the modern regime is not well constrained by the available ages but was between the late MIS2 (19–16 ka) Coocalla system and the late Holocene (5–0 ka) (Pietsch et al., 2013).

Wray (2009) calculated discharges for the large late MIS2 (12.4 ka) Central/Coolibah/Cubbaroo system Namoi palaeochannels using Dury's (1976) wavelength equation, which resulted in higher estimated discharges compared to this study (Fig. 11b). We derived bankfull discharge values for other undated palaeochannels of the Namoi (Table 3) and they agree in relative terms with the values derived by Wray (2009). The largest palaeochannel, the undated Eastern System, had a mean bankfull discharge of 466 m³s⁻¹, compared with the equivalent modern Q_{bf} of 45 m³s⁻¹.

Together, these DFS rivers from the northern MDB show high discharge in MIS4, 3 and 2 with the highest discharges in mid to late MIS3 (Fig. 11b). All of these systems show a dramatic decline in discharge between MIS2 and the late Holocene but only in the Macquarie is the timing of this transition tightly constrained, to around 5.6–5.2 ka (Hesse et al., 2018).
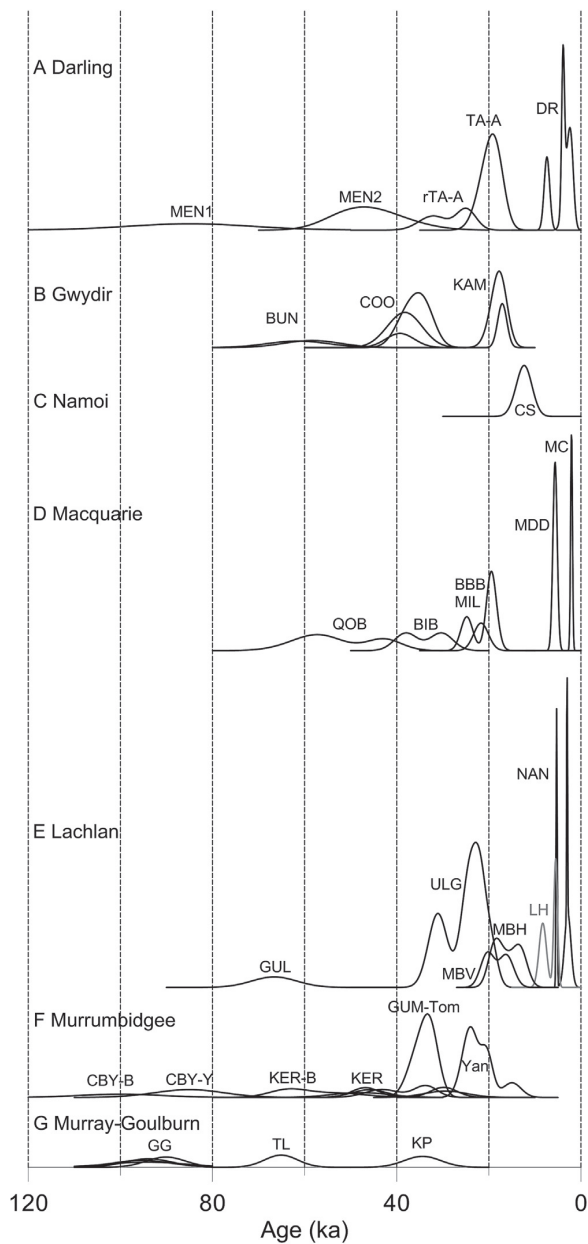
Fig. 10. Probability density functions of age estimates of MDB palaeochannels. The vertical axis (shown at the same scale for each series) represents the relative probability of an age estimate falling at a given time, with each age estimate normalised to an equal area. The height of each peak therefore depends on the uncertainty of each age estimate and the number of age estimates (and their overlap) for each palaeochannel. MEN — Menindee, rTA-A — relict Talyawalka-Anabranch, TA-A — Talyawalka-Anabranch; DR — Darling River; BUN — Bunnor (overlapping Bunnor, Challucum), COO — Coocalla (overlapping Coocalla, Gingham, Mia), KAM — Kamilaroi (overlapping Kamilaroi, Kookabunna); CS — Central System; QOB — Quombothoo, BIB — Bibbijibbery, BBB — Billybingbone, MIL — Milmiland, MDD — Mundadoo, MC — Marra Creek; GUL — Gulgo, ULG — Ulgutherie, NAN — Nanima, MBV — Middle Billabong at Viela, MBH — Middle Billabong at Hunthawang, LH — Lachlan at Hunthawang; CBY-B — Coleambally Bundure, CBY-Y — Coleambally Yamma, KER-B — Kerarbury Booroorban, KER — Kerarbury (overlapping Romani, Waddi, Hay), GUM-Tom — Gum Ck Tombullen, Yan — Yanco; GG — Green Gully/Tallygaroopna, TL — Thule Lagoon; KP — Kotupna.
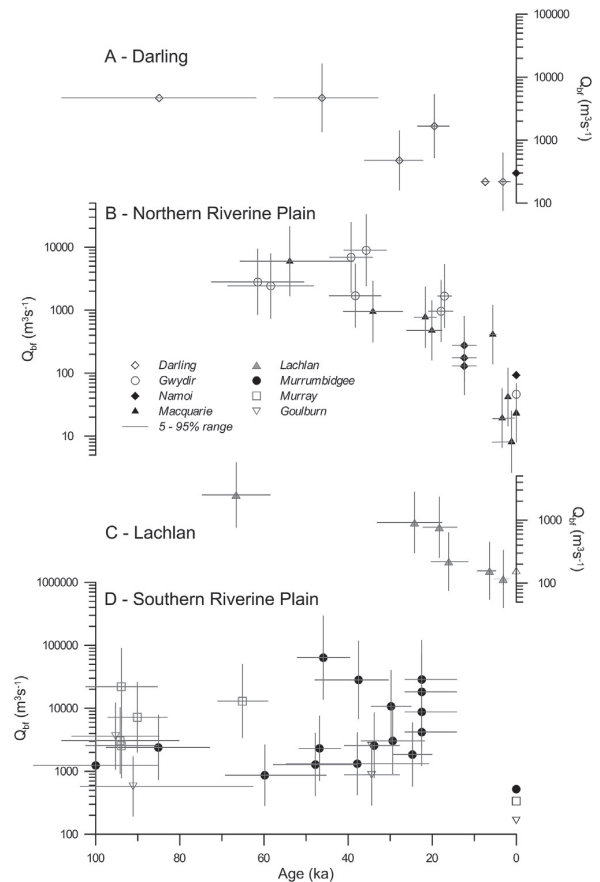

Fig. 11. Estimated bankfull palaeo-discharge plotted against palaeochannel age. A) mid Darling River, B) Macquarie, Gwydir and Namoi Rivers of the northern MDB, C) Lachlan River and, D) Murrumbidgee, Murray and Goulburn Rivers of the southern MDB. Regression equation (1) was used to calculate all palaeo-discharges. Modern discharges (right hand side) taken from nearest Office of Water gauging station. Errors for discharge are based on 95% prediction intervals.

On the mid-Lachlan River in the southern MDB, Gulgo (MIS4) and Ulgutherie (MIS2) palaeochannels were large, compared with the present, or the late Holocene Nanima palaeochannel (Fig. 11c). The 18.3 ka (median age) Middle Billabong palaeochannel at Viela was twice as wide as cutoffs identified by Kemp et al. (2017) as belonging to a later avulsion (median age 16.1 ka) of the upper Middle Billabong palaeochannel at Hunthawang, indistinguishable in width from the modern Lachlan River (6.4 ka) at the same site. Such a large channel reduction within the terminal Pleistocene would represent a very early and large response of the Lachlan to the Pleistocene-Holocene climate transition.

The largest Murrumbidgee palaeochannel was the upper Waddi Arm of the Kerarbury system (on average 817 m width) — 12 times the width of the nearby modern Murrumbidgee and with calculated discharge 263 times the modern river. Even the substantial MIS5 Coleambally, MIS3/2 Gum Creek and MIS2 Yanco palaeochannels, much larger than the modern river, were smaller than the early MIS3 Waddi (Fig. 11d). Our study reproduces the relative bankfull discharge levels between the largest channels of the Coleambally, Kerarbury and Gum Creek systems found by Page and Nanson (1996). However, our estimates of the palaeochannel palaeodischarges are much greater than the substantial estimates

of Page and Nanson (1996), largely because of the improved visibility of the palaeochannels in the LiDAR DEM. The rapid decline in width of the Waddi and Yanco palaeochannels downstream accounts for the much lower bankfull discharge of the lower reaches (Fig. 6). The large variability in size of Murrumbidgee palaeochannels, now clearly revealed by LiDAR, is partly a true reflection of the variability of the preserved palaeochannels which display many avulsions and distributaries, and may also be due to the reliance on single TL ages in many cases.

Some discharge estimates for Murray and Goulburn River palaeochannels are shown for comparison (Fig. 11d). However, the chronologies for each of these palaeochannels (established by TL) is very poor by comparison with the other river systems described above. The MIS5 (Page et al., 1991) Green Gully palaeochannel, formed by the combined flows of the Murray and Goulburn, was substantially larger than the combined modern rivers but the late MIS3 Kotupna palaeochannel of the Goulburn was larger than the Green Gully-equivalent Tallygaroopna palaeochannel.

The oldest (Menindee) and mid-Holocene deposits of the mid Darling River (Lawrie et al., 2012) are not associated with visible palaeochannels and are shown in Fig. 11a with discharges the same as the subsequent palaeochannel. There was a decline in discharge between mid-MIS3 and MIS2 and there was a further very large decrease in channel size between the MIS2 Talyawalka-Anabranch palaeochannel and the late Holocene (modern) Darling River (Lawrie et al., 2012).

5.3. Palaeohydrology of lowland rivers in the Murray-Darling Basin

Assuming that palaeochannels were single thread and the rate of channel size decrease with distance across the DFS was the same as today, we can speculate a little on past climate changes which may have been effective in increasing Q_{bf} (from Equation (2)). However, neither of those assumptions has been tested systematically for these MDB DFS palaeochannels. LiDAR-based mapping of the Macquarie DFS has confirmed that all the dated palaeochannels were single-channel rivers (Hesse et al., 2018) but we cannot be sure if this applies to other rivers. The published dated palaeochannel sites also span large longitudinal distances and so may be expected to vary, even if longitudinal rate of decline were constant. These caveats must be borne in mind in the following discussion, as well as interpretation of previous studies.

Catchment area and elevation can be assumed to have been constant on late Quaternary timescales. However, precipitation rates, their distribution (reflected in the integration $\int P_r$), a and b (from Equation (2)) are all possibly variable over time, affecting the Q_{bf} of MDB rivers. The result that Q_{bf} has a strong relationship with $\int P_r$ is convenient for interpreting palaeoclimatic changes because it suggests that many other variables which we expect to contribute to Q_{bf} (such as transmission losses within the catchment, losses to evapotranspiration, rainfall seasonality etc.) can be simplified. Principally, it seems most likely that increasing $\int P_r$ would have had a large impact on Q_{bf}.

In Fig. 12a reconstructed LGM palaeochannel Q_{bf} is plotted against P_t, applying the modern regression relationship between P_t and Q_{bf} to predict past P_t in the first instance. In this scenario, P_t (and hence P_r) many times greater than modern values would be necessary to account for the large palaeochannels, with no consistency between catchments. In the case of the Yanco palaeochannel, a twenty-fold increase in catchment P_t would be required to achieve the observed Q_{bf}. Assuming modern P_t. for the LGM palaeochannels in the MDB (Fig. 12b), all catchments would require higher values of coefficient b ($R_{Qbf} = Q_{bf}/P_t$) but, again, this would vary from catchment to catchment. If we assume double modern P_t

for the LGM channels then some catchments (e.g. Lower Lachlan) would require only low values of coefficient b, however if we assume half of modern P_t then all catchments would require higher values of b. From this analysis there is no clear decisive solution and LGM catchments may have experienced P_t lower or higher than today. However, within the range of expectable precipitation changes (±50% of modern), higher runoff factor of Q_{bf} would be necessary to achieve the large palaeochannels observed. This greater runoff factor of Q_{bf}, which is presently related to the rate of channel decline, is supported by the rapid declines in size of the Waddi and Yanco palaeochannels (Fig. 6), and has often been predicted because of many considerations, such as snowpack, lower PE, or reduced vegetation cover (Langford-Smith, 1959, 1960; Bowler, 1978b; Page et al., 1996, 2009; Kemp and Spooner, 2007; Reinfelds et al., 2014).

At 35 ka the palaeochannels are fewer and more scattered (Fig. 12c). The larger time window (allowing for age uncertainty) may contribute to the scatter. For the larger palaeochannels, higher P_t seems a likely requirement in addition to higher runoff efficiency. In this time window even smaller catchments had very large palaeochannels. At 50 ka the scatter is similarly great (Fig. 12d).

These scenarios cannot constrain past $\int P_r$ but they do point to higher runoff response to precipitation and the inability of precipitation change alone to account for the observed large palaeochannels. Under colder conditions at the LGM, PE would have been much lower than today, suggesting increased P/PE unless P was dramatically lower than today. Given the correlation between the runoff factor and P/PE (Fig. 8e) we may expect that any increase in $\int P_r$ would cause an additional increase in Q_{bf}. A higher value of b would have the effect of increasing Q_{bf} for all catchments, but particularly for the larger catchments: e.g. Murrumbidgee and Macquarie.

The principal proposed mechanism for higher past Q_{bf} in the MDB has related to LGM temperature reduction and the consequent effects on (1) the proportion of precipitation falling as snow, runoff seasonality, and peak runoff; (2) the impacts on the runoff factor and catchment connectivity; (3) sediment load enhanced by periglacial erosion; (4) and decreased vegetation cover. In the analysis of modern catchments undertaken here, temperature is only indirectly included: in PE, altitude and latitude as they affect P and runoff response. The simplest test of broad-scale temperature change as a control on Q_{bf} is a comparison of reconstructed Q_{bf} against the Antarctic (Vostok) ice-core proxy (deuterium) temperature record (Petit et al., 1999) and sea-surface temperature record from southern Australia (Lopes dos Santos et al., 2013). The inverted Vostok temperature record has been scaled arbitrarily to the Murrumbidgee palaeochannel record (Fig. 13). To overcome the influence of downstream channel decrease, to some degree, all palaeochannel width and Q_{bf} values are shown normalised to those of the nearest gauge site on the modern rivers.

There is a good correspondence between temperature and the relative change in Q_{bf} in the southern MDB catchments (Fig. 13a). We make the assumption that palaeochannels much below the temperature curve in this graph may have been one of multiple simultaneously active channels or that they formed in periods of reduced precipitation but we also note that our normalisation has not removed the effects of channel contraction completely (see four values for the Yanco palaeochannel). These arguments would be necessary to force agreement with many of the Murrumbidgee Gum Creek phase palaeochannels, which are all below the predicted values based on temperature. The very large MIS2 Yanco palaeochannel may be explicable in terms of the temperature effect alone but the even larger MIS3 Waddi palaeochannel was much larger than can be accounted for with the same fit.
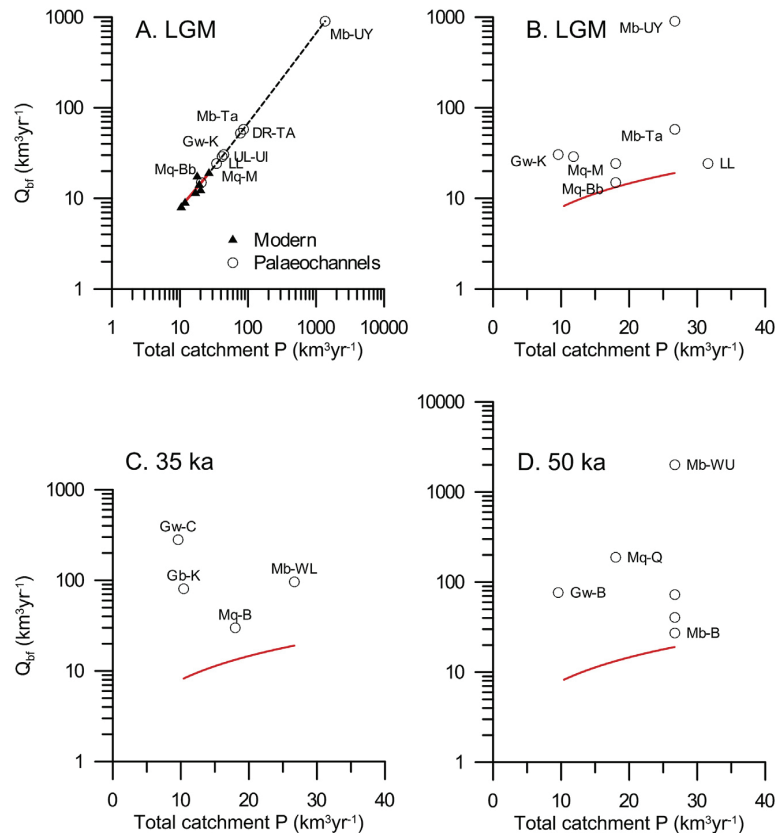
Fig. 12. (A) projected catchment P for LGM (22–20 ka) palaeochannels (within 2 sigma) (circles) based on the modern regression relationship and (B) assuming modern catchment P$_t$. The solid (red) line is the regression for modern channels (excluding the Gwydir) from Fig. 8c. Bankfull discharge expressed in units of km^3/yr, equivalent to P$_t$. (C) Palaeochannels (circles) dating to 35 ka (within 2 sigma), as for (B). (D) Palaeochannels (circles) dating to 50 ka (within 2 sigma), as for (B). Mq-Bb, Macquarie Bibbijibbery; Mq-M, Macquarie Milmiland; LL, Lower Lachlan Viela; UL-Ul, Upper Lachlan Ulgutherie; Gw-K, Gwydir Kookabunna; DR-TA, Darling River Talyawalka-Anabranch; Mb-Ta, Murrumbidgee Tabratong; Gw-C, Gwydir Coocalla; Gb-K, Goulburn Kotupna; Mq-B, Macquarie Bibbijibbery; Mb-WL, Murrumbidgee Waddi L; Gw-B, Gwydir Bunnor; Mq-Q, Macquarie Quombothoo; Mb-WU, Murrumbidgee Waddi U; Mb-B, Murrumbidgee Booroorban. (For interpretation of the references to colour in this figure legend, the reader is referred to the Web version of this article.)

In the northern MDB the relationship between relative Q$_{bf}$ and temperature (scaling taken from southern MDB) may also account for much of the decline in channel size from the LGM to the Holocene. However it does not account for either the large mid-Holocene Mundadoo palaeochannel (Macquarie) or large MIS3 palaeochannels (Gwydir and Macquarie) (Fig. 13b). A different temperature scaling would not improve the fit across the time series. Bayon et al. (2017) have used neodymium isotopes as a proxy of northern versus southern MDB sediment sources to the Murray River (Fig. 13c), arguing that more positive values relate to a greater relative input of northern MDB sediment and therefore higher erosion rates and higher flows. It is not easy to relate their findings to the palaeochannel record both because of the sparse nature of the palaeochannel record and the tendency for both regions to follow the same general trend.

The observed patterns confirm a prominent role for temperature change in determining discharge from these catchments. The palaeochannel records show that very high runoff was experienced in northern and southern MDB catchments, especially in MIS3, suggesting that an additional mechanism, such as precipitation enhancement, must have been widespread but they are not helpful in identifying the moisture source. Pietsch et al. (2013) argued for a northern (Coral Sea) source of moisture to the Gwydir catchment

and others have argued for increased advection of tropical moisture into southern Australia at times, including Heinrich stadials (Bayon et al., 2017; Fu et al., 2017; Treble et al., 2017) in response to southward movement of the ITCZ (McGee et al., 2014). However, within the limits of the available dating, the largest palaeochannels were not synchronous between catchments and not well correlated with Heinrich stadials, particularly HS1 when the effects have been proposed to have been greatest (McGee et al., 2014). Ellerton et al. (2017) have also argued for enhanced moisture to the LGM New England Tableland from the east. An eastern (Tasman Sea) source of moisture at the LGM (Ellerton et al., 2017), or other times, would have been moderated in the headwaters of the MDB catchments by the strong rainfall gradient across the highlands which, according to the distribution of periglacial slope deposits, persisted in the past (Slee and Shulmeister, 2015).

While the most likely source of moisture to the northern MDB in the past, as today, is the Coral Sea (Gimeno et al., 2010), sea surface temperature during MIS3 and 2 was marginally lower than during the Holocene in the Coral Sea (Lawrence and Herbert, 2005), and in the East Australian Current during MIS2 (Bostock et al., 2006). Therefore, rather than a simple dependence on SST (Pietsch et al. (2013), advection of moisture from northern Australia by more frequent, deeper, or more far-reaching troughs linked to the
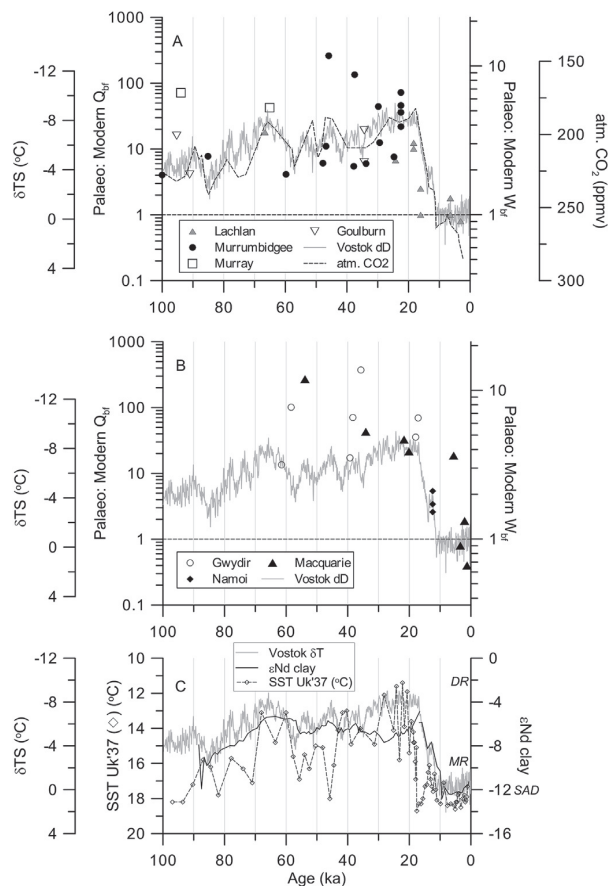
Fig. 13. Ratio of palaeochannel to modern river bankfull discharge for (A) the Southern Riverine Plain and (B) Northern Riverine Plain. The Vostok, East Antarctica, temperature record (δTS) (Petit et al., 1999) is shown, inverted, with colder temperatures towards the top, as well as the Vostok atmospheric carbon dioxide record (also inverted) (Fischer et al., 1999). (C) Southern Australia SST record (Lopes dos Santos et al., 2013) and εNd record of Darling River (DR), Murray River (MR) and South Australian dust (SAD) sediment contributions to the lower Murray River sediment deposited in the Great Australian Bight (Bayon et al., 2017). For clarity only median ages of each palaeochannel have been shown but age probabilities are the same as in Fig. 10 and 11.

summer monsoon may have occurred. This may have been favoured during intervals of high or intermediate sea-level (such as MIS3) when warm water was more extensive in the Gulf of Carpentaria and precluded by low sea levels during MIS2 (Torgersen et al., 1988). The very large Waddi, Coocalla and Quombothoo palaeochannels formed in early MIS3 (prior to 45 ka) when Lake Eyre and Lake Frome, in the monsoon-influenced zone of central Australia, reached their highest levels (Cohen et al., 2015). However, other very large palaeochannels formed up to 35 ka, when Lake Eyre had dried and Lake Frome had reduced substantially after monsoon-fed precipitation is thought to have decreased (Cohen et al., 2015).

Cohen and Nanson (2007) identified an early Holocene interval (10–4.5 ka), named the Nambucca Phase, in which fluvial deposition was in hiatus or absent from valleys in the highlands and along the coast of southeastern Australia. They interpreted this as a phase of enhanced flow causing widespread erosion. In our MDB synthesis, only the Mundadoo palaeochannel of the Macquarie River (5.6 ka), the Lachlan River at Hunthawang (6.4 ka) and the Darling River at Chalky Well (7.4 ka) (Table 3) fall within this interval and

only the Mundadoo was larger than the modern river. Enhanced discharges during this period, and high lake levels elsewhere in southeastern Australia around this time (Fitzsimmons and Barrows, 2010; Wilkins et al., 2013), cannot be explained by simple temperature forcing (Fig. 13). Modelling of the climate at 6 ka (Braconnot et al., 2012) (https://pmip3.lsce.ipsl.fr) shows small summer (DJF) temperature anomalies compared to present over Australia (<0.5 °C positive or negative depending on models). However, the same modelling did find higher summer (DJF) precipitation rates over northern Australia and the seas to the north of Australia, but not extending to the latitudes of the MDB.

From the simple comparison between palaeochannel size and atmospheric temperature it is not clear which mechanism(s) may have been most effective in enhancing Q_{bf} under lower air temperatures. As argued by Reinfelds et al. (2014), the effect of temperature on P, P/PE and Q are likely to have been widespread and large. Their model predicted a maximum three-fold increase in runoff factor if LGM temperatures are applied. The effects of snowpack accumulation and seasonal thaw are consistent with the patterns observed at the LGM. Although only a very small part of these catchments is alpine today or within the observed limits of periglacial block deposits (Fig. 9d) (Slee and Shulmeister, 2015), the disproportionate precipitation at these altitudes and higher runoff factor may have accentuated their contribution during MIS2 and the LGM.

Evidence of sparser, treeless vegetation in the southeastern highlands (Bowler et al., 1976), active dunes (Wasson, 1984) and increased dust addition to the desiccating Willandra Lakes (Bowler, 1978a) all contributed to the acceptance of an 'arid LGM' in Australia (Bowler, 1976). This model is also compatible with the scenario of high lake levels in closed basins at the LGM and the restricted extent of Australian glaciers under lower precipitation, while temperature and PE were also much lower (Galloway, 1965). While some of these lines of proxy evidence have been refined and corroborated (Nanson et al., 2003; Petherick et al., 2013), the interpretation of the MDB palaeochannels has always been controversial and remains, superficially, contradictory of the 'arid LGM' model.

Several new proxy records contribute to the obscurity of LGM climate interpretation. Lake levels at Little Llangothlin Lagoon (New England Tableland) were high in the LGM (Shulmeister et al., 2016) and local vegetation was a sub-alpine herbfield while rainforest vegetation persisted on the nearby escarpment (Ellerton et al., 2017). However in low altitude, southwestern Victoria, Lake Surprise experienced low lake levels during the LGM and high dust accumulation (Falster et al., 2018). In the presently semi-arid Flinders Ranges, speleothem growth records relatively wet conditions during the LGM, lasting until 15.8 ka (Treble et al., 2017). The oxygen isotopic record from emu eggshell in several sites in the arid zone suggest low summer moisture availability around the LGM but have different timing and duration (Miller et al., 2016). These interpretations are not easily reconcilable. To some extent they may represent the different sensitivities of different proxies and warn us that simple interpretations of palaeoclimate from proxy records is not possible.

Atmospheric carbon dioxide concentration has also fluctuated in the past, together with temperature fluctuations, (Fig. 13a). It has long been suspected that lower LGM atmospheric CO_2 concentration induced moisture stress (lower water use efficiency) in C3 plants, driving vegetation to less woody C3 and more herbaceous C4 plants (Jolly and Haxeltine, 1997; Woillez et al., 2011; Claussen et al., 2013; Shao et al., 2018). As a result, it may be that it was lower CO_2, not drier climate, which led to sparser, lower vegetation (Hesse et al., 2003) and possible increased runoff (Dosseto et al., 2010) in the headwaters of the MDB catchments. This may go

some way to resolving the contrast between 'dry' (more herbs and grasses, fewer trees) LGM vegetation and high runoff proxies (lakes and rivers). Prentice et al. (2017) developed a model to incorporate the effect of CO_2 on plants and LGM palaeoclimate reconstructions in Australia from pollen. They found that their model did induce higher moisture index (P/Eq (equilibrium evapotranspiration)), than without inclusion of the CO_2 effect, signifying generally 'wetter' conditions despite 'browner' vegetation, which might otherwise be interpreted as evidence of drier climate. Scheff et al. (2017) undertook a global analysis of pollen records and reached much the same conclusions as Prentice et al. (2017). Both studies failed to reproduce some aspects of the known temperature distribution in southeastern Australia but nevertheless point to a reconciliation of 'drier' vegetation with enhanced runoff. This is also compatible with enhanced dust flux from southeastern Australia at the LGM (Hesse, 2004; Fitzsimmons et al., 2013) as the result of sparser vegetation cover.

6. Conclusions

Our meta-analysis of the published ages of the dated palaeochannels shows that there are no clear clusters of ages common to all (or most) MDB rivers over the last 100 ka. Despite these differences in timing, there appear to be common trends in the size of the palaeochannels, suggesting an internal dynamic determining the timing of channel avulsion and formation in response to a common climate forcing trend.

MDB-specific discharge equations were developed using regression analysis of modern channel parameters and bankfull discharge values. The derived regime equation is similar to that of Dury (1976) but the empirical data shows somewhat narrower MDB channels, for a given bankfull discharge, than found by Dury.

MDB palaeochannels show an apparent correlation between Q_{bf} and hemispheric temperature (from Vostok ice core records). This suggests a strong temperature mediation of catchment runoff but additional mechanisms, such as higher runoff ratios, and enhanced precipitation in MIS 3 and early MIS1, are all necessary to explain the very large palaeochannels.

Based on modern climatic, hydrologic and geomorphic patterns, it is possible to conclude that much greater runoff effectiveness contributed to the enhanced LGM and MIS3 rivers. Under LGM conditions, either higher or lower precipitation rates may have resulted in higher bankfull discharge. However, both very high precipitation levels and the requirements for much higher runoff efficiency at lower precipitation levels may be unrealistic. During MIS3, both higher precipitation rates and higher runoff efficiency appear to be necessary to explain the very large palaeochannels observed.

These findings (higher runoff efficiency; temperature sensitivity) are consistent with a number of previously proposed mechanisms, such as the storage of precipitation in elevated parts of the catchment as ice or snow and seasonal release in delayed and enhanced floods, lower evapotranspiration, higher soil moisture, as well as with reduced vegetation cover, possibly because of feedbacks with atmospheric carbon dioxide levels.

Entering the late Holocene, the northern (Macquarie, Namoi and Gwydir) and southern catchments (Murray/Goulburn and Murrumbidgee) of the MDB showed very different responses. In response to greater discharge variability (higher Q_{bf}/Q_r) the flows of the Gwydir, Namoi and Macquarie Rivers have reduced in size and competence, leading to channel breakdown, floodout and wetland formation. While linked to the higher temperatures of the Holocene, this probably reflects a change in the nature of the subtropical summer moisture fluxes or their expansion southward in the Holocene.

Appendix A. Supplementary data

Supplementary data to this article can be found online at https://doi.org/10.1016/j.quascirev.2018.09.035.

References

Banerjee, D., Page, K., Lepper, K., 2002. Optical dating of palaeochannel deposits in the Riverine Plain, Southeastern Australia: testing the reliability of existing thermoluminescence dates. Radiat. Protect. Dosim. 101, 327—332.

Barrows, T.T., Stone, J.O., Fifield, L.K., Cresswell, R.G., 2002. The timing of the last glacial maximum in Australia. Quat. Sci. Rev. 21, 159—173.

Bayon, G., De Deckker, P., Magee, J.W., Germain, Y., Bermell, S., Tachikawa, K., Norman, M.D., 2017. Extensive wet episodes in Late Glacial Australia resulting from high-latitude forcings. Sci. Rep. 7, 44054. https://doi.org/10.1038/srep44054.

Borisova, O., Sidorchuk, A., Panin, A., 2006. Palaeohydrology of the Seim River basin, Mid-Russion Upland, based on palaeochannel morphology and palynological data. Catena 66, 53—73.

Bostock, H.C., Opdyke, B.N., Gagan, M.K., Kiss, A.E., Fifield, L.K., 2006. Glacial/interglacial changes in the East Australian current. Clim. Dynam. 26, 645—659.

Bowler, J.M., 1967. Quaternary chronology of Goulburn Valley sediments and their correlation in southeastern Australia. J. Geol. Soc. Aust. 14, 287—292.

Bowler, J.M., 1976. Aridity in Australia: age, origins and expressions in aeolian landforms and sediments. Earth Sci. Rev. 12, 279—310.

Bowler, J.M., Hope, G.S., Jennings, J.N., Singh, G., Walker, D., 1976. Late quaternary climates of Australia and new Guinea. Quat. Res. 6, 359—394.

Bowler, J.M., 1978a. Glacial age aeolian events at high and low altitudes: a Southern Hemisphere perspective. In: van Zinderen Bakker, E.M. (Ed.), Antarctic Glacial History and World Palaeoenvironments. Balkema, Rotterdam, pp. 149—172.

Bowler, J.M., 1978b. Quaternary climate and tectonics in the evolution of the riverine plain, southeastern Australia. In: Davies, J.L., Williams, M.A.J. (Eds.), Landform Evolution in Australasia. ANU Press, Canberra, pp. 70—112.

Bowler, J.M., Stockton, E., Walker, M.J., 1978. Quaternary stratigraphy of the Darling River near tilpa, New South Wales. Proc. Roy. Soc. Vic. 90, 79—88.

Braconnot, P., Harrison, S.P., Kageyama, M., Bartlein, P.J., Masson-Delmotte, V., Abe-Ouchi, A., Otto-Bliesner, B., Zhao, Y., 2012. Evaluation of climate models using palaeoclimatic data. Nat. Clim. Change 2, 417—424. https://doi.org/10.1038/NCLIMATE1456.

Brown, C.M., Stephenson, A.E., 1991. Geology of the Murray Basin, Southeastern Australia. Australian Government Publishing Service, Canberra.

Butler, B.E., 1950. A theory of prior streams as a causal factor of soil occurrence in the riverine plain of S.E. Australia. Aust. J. Agric. Res. 1, 231—252.

Butler, B.E., 1958. Depositional Systems of the Riverine Plain in Relation to Soils. CSIRO, Melbourne.

Church, M., 1992. Channel morphology and typology. In: Calow, P., Petts, G.E. (Eds.), The Rivers Handbook. Blackwell, Oxford, pp. 126—143.

Claussen, M., Selent, K., Brovkin, V., Raddatz, T., Gayler, V., 2013. Impact of CO2 and climate on Last Glacial Maximum vegetation - a factor separation. Biogeosciences 10, 3593—3604. https://doi.org/10.5194/bg-10-3593-2013.

Cohen, T.J., Nanson, G.C., 2007. Mind the gap: an absence of valley-fill deposits identifying the Holocene hypsithermal period of enhanced flow regime in southeastern Australia. Holocene 17, 411—418.

Cohen, T.J., Jansen, J.D., Gliganic, L.A., Larsen, J.R., Nanson, G.C., May, J.H., Jones, B.G., Price, D.M., 2015. Hydrological transformation coincided with megafaunal extinction in central Australia. Geology. https://doi.org/10.1130/G36346.1.

Dodson, J.R., Wright, R.V.S., 1989. Humid to arid to subhumid vegetation shift on pilliga sandstone, ulungra springs, New South Wales. Quat. Res. 32, 182—192.

Dosseto, A., Hesse, P., Maher, K., Fryirs, K., Turner, S.P., 2010. Climatic and vegetation control on sediment dynamics during the last glacial cycle. Geology 38, 395—398.

Dury, G.H., 1976. Discharge prediction, present and former, from channel dimensions. J. Hydrol. 30, 219—245.

Ellerton, D., Shulmeister, J., Woodward, C., Moss, P., 2017. Last Glacial Maximum and Last Glacial-Interglacial Transition pollen record from northern NSW, Australia: evidence for a humid late Last Glacial Maximum and dry deglaciation in parts of eastern Australia. J. Quat. Sci. 32, 717—728. https://doi.org/10.1002/jqs.2960.

Erskine, W.D., Saynor, M.J., Chalmers, A., Riley, S.J., 2012. Water, wind, wood and trees: Interactions, spatial variations, temporal dynamics, and their potential role in river rehabilitation. Geogr. Res. 50, 60—74. https://doi.org/10.1111/j.1745-

5871.2011.00731.x.

Falster, G., Tyler, J., Grant, K., Tibby, J., Turney, C.S.M., Lohr, S., Jacobsen, G., Kershaw, A.P., 2018. Millennial-scale variability in south-east Australian hydroclimate between 30,000 and 10,000 years ago. Quat. Sci. Rev. 192, 106—122. https://doi.org/10.1016/j.quascirev.2018.05.031.

Fischer, H., Wahlen, M., Smith, J., Mastroianni, D., Deck, B., 1999. Ice core records of atmospheric CO2 around the last three glacial terminations. Science 283, 1712—1714.

Fitzsimmons, K.E., Rhodes, E.J., Magee, J.W., Barrows, T.T., 2007. The timing of linear dune activity in the Strzelecki and Tirari Deserts, Australia. Quat. Sci. Rev. 26, 2598—2616.

Fitzsimmons, K.E., Barrows, T.T., 2010. Holocene hydrologic variability in temperate southeastern Australia: an example from lake George, New South Wales. Holocene 20, 585—597. https://doi.org/10.1177/0959683609356589.

Fitzsimmons, K.E., Cohen, T.J., Hesse, P.P., Jansen, J., Nanson, G.C., May, J.H., Barrows, T.T., Haberlah, D., Hilgers, A., Kelly, T., Larsen, J.R., Lomax, J., Treble, P., 2013. Late Quaternary paleonvironmental change in the Australian drylands: a synthesis. Quat. Sci. Rev. 74, 78—96.

Fu, X., Cohen, T.J., Arnold, L.J., 2017. Extending the record of lacustrine phases beyond the last interglacial for Lake Eyre in central Australia using luminescence dating. Quat. Sci. Rev. 162, 88—110. https://doi.org/10.1016/j.quascirev.2017.03.002.

Galloway, R.W., 1965. Late quaternary climates in Australia. J. Geol. 73, 603—618.

Gimeno, L., Drumond, A., Nieto, R., Trigo, R.M., Stohl, A., 2010. On the origin of continental precipitation. Geophys. Res. Lett. 37, L13804. https://doi.org/10.1029/2010gl043712.

Hesse, P., 2004. The Late Quaternary Record of Dust in Australia: Source Area Controls- Downstream Impacts, Wind-blown Dust Workshop- the Emission, Transport and Impacts of Wind-blown Dust from Soil Erosion: Modelling and Observation. CSIRO, Aspendale, Victoria, pp. 76—80.

Hesse, P.P., 1994. The record of continental dust from Australia in Tasman Sea Sediments. Quat. Sci. Rev. 13, 257—272.

Hesse, P.P., Humphreys, G.S., Selkirk, P.M., Adamson, D.A., Gore, D.B., Nobes, D.C., Price, D.M., Schwenninger, J.-L., Smith, B., Tulau, M., Hemmings, F., 2003. Late quaternary aeolian dunes on the presently humid blue Mountains, eastern Australia. Quat. Int. 108, 13—32.

Hesse, P.P., 2016. How do longitudinal dunes respond to climate forcing? Insights from 25 years of luminescence dating of the Australian desert dunefields. Quat. Int. 410, 11—29. https://doi.org/10.1016/j.quaint.2014.02.020.

Hesse, P.P., Williams, R., Ralph, T.J., Larkin, Z.T., Fryirs, K.A., Westaway, K.E., Yonge, D., 2018. Dramatic reduction in size of the lowland Macquarie River in response to Late Quaternary climate-driven hydrological change. Quat. Res. https://doi.org/10.1017/qua.2018.48 10.1017/qua.2018.48.

Jolly, D., Haxeltine, A., 1997. Effect of low glacial atmospheric CO$_2$ on tropical African montane vegetation. Science 276, 786—788.

Kemp, J., 2005. Mis-use of hydraulic geomtery to estimate palaeochannel disharges: sinuous late Pleistocene rivers in the Riverine Plain, SE Australia. The Fluvial System - Past and present dynamics and controls 33.

Kemp, J., Spooner, N.A., 2007. Evidence for regionally wet conditions before the LGM in southeast Australia: OSL ages from a large palaeochannel in the Lachlan Valley. J. Quat. Sci. 22, 423—427. https://doi.org/10.1002/jqs.1125.

Kemp, J., Rhodes, E.J., 2010. Episodic fluvial activity of inland rivers in southeastern Australia: palaeochannel systems and terraces of the Lachlan River. Quat. Sci. Rev. 29, 732—752.

Kemp, J., Pietsch, T.J., Gontz, A., Olley, J., 2017. Lacustrine-fluvial interactions in Australia's riverine plains. Quat. Sci. Rev. 166, 352—362. https://doi.org/10.1016/j.quascirev.2017.02.015.

Kershaw, A.P., McKenzie, G.M., Porch, N., Roberts, R.G., Brown, J., Heijnis, H., Orr, M.L., Jacobsen, G.E., Newall, P.R., 2007. A high-resolution record of vegetation and climate through the last glacial cycle from Caledonia Fen, southeastern highlads of Australia. J. Quat. Sci. 22, 481—500.

Kingham, R.A., 1998. Geology of the Murray-Darling Basin - Simplified Lithostratigraphic Groupings. Australian Geological Survey Organisation. Record, 1998/21.

Knighton, A.D., 1998. Fluvial Forms and Processes: a New Perspective. Arnold, London.

Langford-Smith, T., 1959. Deposition on the riverine plain of south-eastern Australia. Aust. J. Sci. 22, 73—74.

Langford-Smith, T., 1960. The dead river systems of the Murrumbidgee. Geogr. Rev. 50, 368—389.

Lawrence, K.T., Herbert, T.D., 2005. Late quaternary sea-surface temperatures in the western Coral Sea: implications for the growth of the Australian great barrier reef. Geology 33, 667—680. https://doi.org/10.1130/G21595.1.

Lawrie, K.C., Brodie, R.S., Tan, K.P.,D.,G., Magee, J., Clarke, J.D.A., Halas, L., Gow, L., Somerville, P., Apps, H.E., Smith, M.,N.B.,C., Abraham, J., Hostetler, S., Brodie, R.C., 2012. BHMAR Project: Geological and Hydrogeological Framework and Conceptual Model. Geoscience Australia Record. Geoscience Australia, Canberra, 2012/12.

Lopes dos Santos, R.A., Spooner, M., Barrows, T.T., de Deckker, P., Sinninghe Damste, J.S., Schouten, S., 2013. Comparison of organic (UK'37, TEXH86, LDI) and faunal proxies (foraminiferal assemblages) for reconstruction of late Quaternary sea surface temperature variability from offshore southeastern Australia. Paleoceanography 28, 377—387. https://doi.org/10.1002/palo.20035.

Magee, J.W., Miller, G.H., 1998. Lake Eyre palaeohydrology from 60 ka to the present: beach ridges and glacial maximum aridity. Palaeogeogr. Palaeoclimatol. Palaeoecol. 144, 307—329.

Magee, J.W., Miller, G.H., Spooner, N.A., Questiaux, D., 2004. Continuous 150 k.y. monsoon record from Lake Eyre, Australia: insolation-forcing implications and unexpected Holocene failure. Geology 32, 885—888.

McGee, D., Donohoe, A., Marshall, J., Ferreira, D., 2014. Changes in ITCZ location and cross-equatorial heat transport at the last glacial maximum, Heinrich stadial 1, and the mid-holocene. Earth Planet Sci. Lett. 390, 69—79. https://doi.org/10.1016/j.epsl.2013.12.043.

Miller, G.H., Magee, J.W., Jull, A.J.T., 1997. Low-latitude glacial cooling in the Southern Hemisphere from amino-acid racemization in emu eggshells. Nature 385, 241—244.

Miller, G.H., Fogel, M.L., Magee, J.W., Gagan, M.K., 2016. Disentangling the impacts of climate and human colonization on the flora and fauna of the Australian arid zone over the past 100 ka using stable istopes in avian eggshell. Quat. Sci. Rev. 151, 27—57. https://doi.org/10.1016/j.quascirev.2016.08.009.

Mueller, D., Jacobs, Z., Cohen, T.J., Price, D.M., Reinfelds, I., Shulmeister, J., 2018. Revisiting an arid LGM using fluvial archives: a luminescence chronology for palaeochannels of the Murrumbidgee River, south-eastern Australia. J. Quat. Sci. https://doi.org/10.1002/jqs.3059 10.1002/jqs.3059.

Nanson, G.C., Price, D.M., Short, S.A., 1992. Wetting and drying of Australia over the past 300 ka. Geology 20, 791—794.

Nanson, G.C., Cohen, T.J., Doyle, C.J., Price, D.M., 2003. Alluvial evidence of major Late-Quaternary climate and flow-regime changes on the coastal rivers of New South Wales. In: Gregory, K.J., Benito, G. (Eds.), Palaeohydrology: Understanding Global Change. John Wiley and Sons, Ltd, New York, pp. 233—258.

Nanson, G.C., Price, D.M., Jones, B.G., Maroulis, J.C., Coleman, M., Bowman, H., Cohen, T.J., Pietsch, T.J., Larsen, J.R., 2008. Alluvial evidence for major climate and flow regime changes during the middle and late Quaternary in eastern central Australia. Geomorphology 101, 109—129.

Ogden, R., Spooner, N.A., Reid, M., Head, J., 2001. Sediment dates with implications for the age of the conversion from palaeochannel to modern fluvial activity on the Murray River and tributaries. Quat. Int. 83—85, 195—210.

Olive, L.J., Olley, J., Murray, A.S., 1994. Spatial variation in suspended sediment transport in the Murrumbidgee River, New South Wales, Australia. In: Olive, L.J., Loughran, R.J., Kesby, J.A. (Eds.), Variability in Stream Erosion and Sediment Transport (Proceedings of the Canberra Symposium, December 1994) IAHS Publ. No. 224,1994. International Association of Hydrological Sciences, pp. 241—249.

Page, K., Dare-Edwards, A., Nanson, G., Price, D., 1994. Late quaternary evolution of lake urana, New South Wales, Australia. J. Quat. Sci. 9, 47—57.

Page, K., Nanson, G., Price, D., 1996. Chronology of Murrumbidgee River palaeochannels on the riverine plain, southeastern Australia. J. Quat. Sci. 11, 311—326.

Page, K.J., Nanson, G.C., Price, D.M., 1991. Thermoluminescence chronology of late Quaternary deposition on the Riverine Plain of south-eastern Australia. Aust. Geogr. 22, 14—23.

Page, K.J., Nanson, G.C., 1996. Stratigraphic architecture resulting from late quaternary evolution of the riverine plain, south-eastern Australia. Sedimentology 43, 927—945.

Page, K.J., Kemp, J., Nanson, G.C., 2009. Late quaternary evolution of riverine plain palaeochannels, southeastern Australia. Aust. J. Earth Sci. 56 (S1), S19—S33.

Pels, S., 1964. Quaternary sedimentation by prior streams on the Riverine Plain, south-west of Griffith, N.S.W. J. Proc. R. Soc. N. S. W. 97, 107—115.

Pels, S., 1969. Radio-carbon datings of ancestral river sediments on the Riverine Plain of southeastern Australia and their interpretation. J. Proc. R. Soc. N. S. W. 102, 189—195.

Petherick, L., McGowan, H., Moss, P., 2008. Climate variability during the Last Glacial Maximum in eastern Australia: evidence of two stadials? J. Quat. Sci. 23, 787—802. https://doi.org/10.1002/jqs.1186.

Petherick, L., Bostock, H.C., Cohen, T.J., Fitzsimmons, K.E., Tibby, J., Fletcher, M.-S., Moss, P., Reeves, J.M., Mooney, S., Barrows, T.T., Kemp, J., Jansen, J., Nanson, G., Dosseto, A., 2013. Climatic records over the past 30 ka from temperate Australia - a synthesis from the Oz-INTIMATE workgroup. Quat. Sci. Rev. 74.

Petit, J.R., Jouzel, J., Raynaud, D., Barkov, N.I., Barnola, J.M., Basile, I., Bender, M., Chappellaz, J., Davis, M., Delaygue, G., Delmotte, M., Kotlyakov, V.M., Legrand, M., Lipenkov, V.Y., Lorius, C., Pepin, L., Ritz, C., Saltzmann, E., Stievenard, M., 1999. Climate and atmospheric history of the past 420,000 years from the Vostok ice core, Antarctica. Nature 399, 429—436.

Pickup, G., Rieger, W.A., 1979. A conceptual model of the relationship between channel characteristics and discharge. Earth Surf. Process. 4, 37—42.

Pietsch, T.J., Nanson, G.C., 2011. Bankfull hydraulic geometry; the role of in-channel vegetation and downstream declining discharges in the anabranching and distributary channels of the Gwydir distributive fluvial system, southeastern Australia. Geomorphology 129, 152—165. https://doi.org/10.1016/j.geomorph.2011.01.021.

Pietsch, T.J., Nanson, G.C., Olley, J.M., 2013. Late Quaternary changes in flow-regime on the Gwydir distributive fluvial system, southeastern Australia. Quat. Sci. Rev. 69, 168—180.

Prentice, I.C., Cleator, S.F., Huang, Y.H., Harrison, S.P., Roulstone, I., 2017. Reconstructing ice-age palaeoclimates: quantifying low-CO2 effects on plants. Global Planet. Change 149, 166—176. https://doi.org/10.1016/j.gloplacha.2016.12.012.

Ralph, T.J., Hesse, P.P., 2010a. Downstream hydrogeomorphic changes along the Macquarie River, southeastern Australia, leading to channel breakdown and floodplain wetlands. Geomorphology 118, 48—64. https://doi.org/10.1016/j.geomorph.2009.12.007.

Ralph, T.J., Hesse, P.P., 2010b. Downstream hydrogeomorphic changes along the Macquarie River, southeastern Australia, leading to channel breakdown and

floodplain wetlands. Geomorphology 118, 48–64. https://doi.org/10.1016/j.geomorph.2009.12.007.

Reinfelds, I., Swanson, E., Cohen, T., Larsen, J.R., Nolan, A., 2014. Hydrospatial assessment of streamflow yields and effects of climate change: Snowy Mountains, Australia. J. Hydrol. 512, 206–220.

Scheff, J., Seager, R., Liu, H., Coats, S., 2017. Are glacials dry? Consequences for paleoclimatology and for greenhouse warming. J. Clim. 30, 6593–6609. https://doi.org/10.1175/JCLI-D-16-0854.1.

Schumm, S.A., 1968. River Adjustment to Altered Hydrologic Regimen - Murrumbidgee River and Paleochannels, Australia. US Geological Survey Professional Paper, vol. 598 (Washington).

Shao, Y., Anhauser, A., Ludwig, P., Schluter, P., Williams, E., 2018. Statistical reconstruction of global vegetation for the last glacial maximum. Global Planet. Change 168, 67–77. https://doi.org/10.1016/j.gloplacha.2018.06.002.

Shulmeister, J., Kemp, J., Fitzsimmons, K.E., Gontz, A., 2016. Wind regimes during the last glacial maximum and early Holocene: evidence from little Llangothlin Lagoon, new England Tableland, eastern Australia. Clim. Past 12, 1435–1444. https://doi.org/10.5194/cp-12-1435-2016.

Slee, A., Shulmeister, J., 2015. The distribution and climatic implications of periglacial landforms in eastern Australia. J. Quat. Sci. 30, 848–858. https://doi.org/10.1002/jqs.2823.

Stannard, M.E., 1961. Prior stream deposition. Aust. J. Sci. 24, 324–325.

Sweller, S., Martin, H.A., 2001. A 40,000 year vegetation history and climatic interpretations of burraga swamp, barrington tops, New South Wales. Quat. Int. 83–85, 233–244.

Tooth, S., 1999. Floodouts in Central Australia. In: Miller, A.J., Gupta, A. (Eds.), Varieties of Fluvial Form. John Wiley and Sons, pp. 219–247.

Torgersen, T., Luly, J.G., De Deckker, P., Jones, M.R., Searle, D.E., Chivas, A.R., Ullman, W.J., 1988. Late quaternary environments of the Gulf of Carpentaria, Australia. Palaeogeogr. Palaeoclimatol. Palaeoecol. 67, 245-226.

Trabucco, A., Zomer, R.J., 2009. Global aridity index (Global-Aridity) and global potential evapo-transpiration (Global-PET) geospatial database. In: Information, C.C.f.S. (Ed.), Published Online, Available from the CGIAR-CSI GeoPortal at. http://www.csi.cgiar.org.

Treble, P., Baker, A., Ayliffe, L., Cohen, T.J., Hellstrom, J.C., Gagan, M.K., Frisia, S.,

Drysdale, R.N., Griffiths, A.D., Borsato, A., 2017. Hydroclimate of the Last Glacial Maximum and deglaciation in southern Australia's arid margin interpreted from speleothem records (23-15 ka). Clim. Past 13, 667–687. https://doi.org/10.5194/cp-13-667-2017.

Wasson, R.J., 1984. Late Quaternary palaeoenvironments in the desert dunefields of Australia. In: Vogel, J.C. (Ed.), Late Cainozoic Palaeoclimates of the Southern Hemisphere. Balkema, Rotterdam, pp. 183–208.

Watkins, J., Meakin, N.S., 1996. Explanatory Notes- Nyngan and Walgett 1:250 000 Geological Sheets. Geological Society of New South Wales.

Watkins, J.J., 1992. Thermoluminescence dating of quaternary sediments from the nyngan - walgett area. Geological Survey of New South Wales, Quaterly Notes 89, 23–29.

Weissmann, G.S., Hartley, A.J., Nichols, G.J., Scuderi, L.A., Olson, M., Buehler, H., Banteah, R., 2010. Fluvial form in modern continental sedimentary basins: distributive fluvial systems. Geology 38, 39–42.

Wharton, G., 1995. The channel-geometry method: guidelines and applications. Earth Surf. Process. Landforms 20, 649–660.

Wilkins, D., Gouramanis, C., De Deckker, P., Fifield, L.K., Olley, J., 2013. Holocene lake-level fluctuations in lakes keilambete and Gnotuk, southwestern Victoria, Australia. Holocene 23, 784–795.

Williams, G.P., 1978. Bank-full dicharge of rivers. Water Resour. Res. 14, 1141–1154.

Woillez, M.-N., Kageyama, M., Krinner, G., de Noblet-Ducoudre, N., Viovy, N., Mancip, M., 2011. Impact of CO2 and climate on the Last Glacial Maximum vegetation: results from the ORCHIDEE/IPSL models. Clim. Past 7, 557–577. https://doi.org/10.5194/cp-7-557-2011.

Wray, R.A.L., 2009. Palaeochannels of the Namoi River floodplain, New South Wales, Australia: the use of multispectral landsat imagery to highlight a late quaternary change in fluvial regime. Aust. Geogr. 40, 29–49.

Yonge, D., Hesse, P.P., 2009. Geomorphic environments, drainage breakdown, and channel and floodplain evolution on the lower Macquarie River, central-western New South Wales. Aust. J. Earth Sci. 56, S35–S53. https://doi.org/10.1080/08120090902870780.

Young, R.W., Young, A.R.M., Price, D.M., Wray, R.A.L., 2002. Geomorphology of the Namoi alluvial plain, northwestern New South Wales. Aust. J. Earth Sci. 49, 509–523.

APPENDIX 2

Dramatic reduction in size of the lowland Macquarie River in response to Late Quaternary climate-driven hydrologic change

Paul P. Hesse*, Rory Williams, Timothy J. Ralph, Zacchary T. Larkin, Kirstie A. Fryirs, Kira E. Westaway, David Yonge
Department of Environmental Sciences, Macquarie University, Sydney, New South Wales 2109, Australia

Abstract

Palaeochannels of lowland rivers provide a means of investigating the sensitivity of river response to climate-driven hydrologic change. About 80 palaeochannels of the lower Macquarie River of southeastern Australia record the evolution of this distributive fluvial system. Six Macquarie palaeochannels were dated by single-grain optically stimulated luminescence. The largest of the palaeochannels (Quombothoo, median age 54 ka) was on average 284 m wide, 12 times wider than the modern river (24 m) and with 21 times greater meander wavelength. Palaeo-discharge then declined, resulting in a younger, narrower, group of palaeochannels, Bibbijibbery (125 m wide, 34 ka), Billybingbone (92 m, 20 ka), Milmiland (112 m, 22 ka), and Mundadoo (86 m, 5.6 ka). Yet these channels were still much larger than the modern river and were continuous downstream to the confluence with the Barwon-Darling River. At 5.5 ka, a further decrease in river discharge led to the formation of the narrow modern river, the ecologically important Macquarie Marshes, and Marra Creek palaeochannel (31 m, 2.1 ka) and diminished sediment delivery to the Barwon-Darling River as palaeo-discharge fell further. The hydrologic changes suggest precipitation was a driving forcing on catchment discharge in addition to a temperature-driven runoff response.

Keywords: Macquarie Marshes; Murray-Darling basin; Floodplain wetlands; Palaeohydrology; Holocene; Fluvial geomorphology

INTRODUCTION

Rivers respond dynamically to changes in climate and hydrology. Some rivers respond predictably through adjustments in sediment transport regime and channel morphology, while others experience less predictable changes through complex planform adjustments or threshold responses to hydrologic decline. One such marked change is the transition, either temporal or spatial, from a continuous, single-channelled planform to a multichannelled network or floodout (Tooth, 1999) form on an alluvial plain as part of a distributive fluvial system (DFS) (Hartley et al., 2010; Weissmann et al., 2010).

The recognition of large and morphologically diverse palaeochannels on the surface of the Murrumbidgee and Murray River alluvial plains (the Riverine Plain) of the Murray-Darling basin of southeastern Australia (Fig. 1) since the 1950s (Butler, 1950; Pels, 1964a, 1964b, 1966, 1969) led to research into past climate change and its hydrologic and geomorphological impacts on this continent (Bowler, 1967,

1975). Declining channel size and increasing sinuosity from the late Pleistocene to the Holocene was recognised in early studies (e.g., Schumm, 1968), but only with luminescence dating have the timing and relations to hemispheric and global phases of climate change been clarified (Nanson et al., 1992; Page et al., 1996). The developing framework recognises several distinct (temporally and morphologically) fluvial phases within the last glacial cycle; large, bedload-dominated palaeochannels in the late Pleistocene succeeded by smaller, mixed- or suspended-load channels in the Holocene (Page et al., 2009). However, despite the increasing geographical range of studies within the Murray-Darling basin (Young et al., 2002; Kemp and Rhodes, 2010; Pietsch et al., 2013) and advances in dating techniques, the reasons for the declining discharge remain speculative, and the timing of the Holocene transition remains unclear in many river systems (Ogden et al., 2001). Additional studies over a broad geographical range supported by palaeochannel dating are one way of testing and refining hypotheses about the causes and timing of these hydrologic and morphological changes.

The alluvial plain of the lower Macquarie River in the northern Murray-Darling basin preserves about 80 palaeochannels of highly variable size and morphology

*Corresponding author at: Department of Environmental Sciences, Macquarie University, Sydney, New South Wales 2109, Australia. E-mail address: paul.hesse@mq.edu.au (P.P. Hesse).

(Figs. 2 and 3). The plain is an example of a DFS, a large alluvial feature characterised by a radial, distributive channel pattern (Weissmann et al., 2010). The Macquarie DFS is notable for the breakdown of the modern river channel into complex floodouts (Tooth, 1999). These floodouts form the Macquarie Marshes (Yonge and Hesse, 2009; Ralph and Hesse, 2010), one of the largest inland wetlands in Australia and a wetland of international importance recognised under the Ramsar Convention for the protection of migratory waterbirds. Similar floodouts and wetlands are found in other Murray-Darling basin DFS rivers like the Gwydir, Lachlan, Loddon, and several others (Fig. 1). This channel breakdown leads to partial hydrologic disconnection from the receiving trunk streams, the Darling and Murray Rivers, and contrasts with the large, continuous palaeochannels that traversed the plain and connected directly to their trunk streams (Page et al., 2009; Pietsch et al., 2013).

The aim of this study is to establish the timing and magnitude of hydrologic and morphological adjustments of the lowland Macquarie River in the Late Quaternary. In doing so, we extend the alluvial palaeochannel chronology for the northern Murray-Darling basin, enabling comparison with nearby river systems. Six Macquarie palaeochannels were investigated using single-grain optically stimulated luminescence (SG-OSL) dating, focussing on those with the best preservation (clear features, longitudinal continuity) and encompassing a range of channel sizes and planforms. We combine these new analyses with two previously investigated sites on the late Holocene Macquarie River (Yonge and Hesse, 2009; Larkin, 2012) to investigate river response to climate-driven hydrologic changes that collectively have led to the decline and fall of the lower Macquarie River.

REGIONAL SETTING

The Macquarie River rises in the Great Dividing Range up to 1400 m asl, flowing northwest through a partly confined valley, before turning north at Narromine onto an alluvial plain ~80 km wide and ~240 km long (Figs. 1 and 2). The catchment area at Narromine is 26,000 km^2, and the river does not receive any further tributary input downstream.
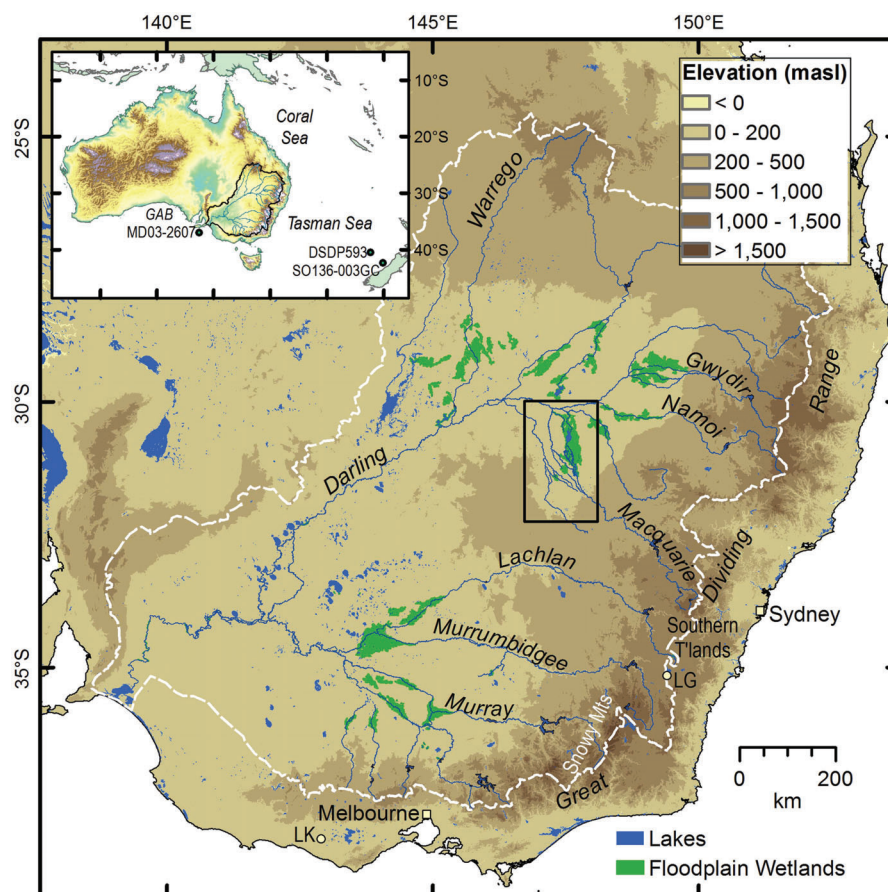

Figure 1. (color online) The Murray-Darling basin (dashed white outline) and major rivers, floodplain wetlands and lakes. The rectangle shows the location of Fig. 2. The inset map shows the locations of marine cores shown in Fig. 11. GAB, Great Australian Bight; LG, Lake George; LK, Lake Keilambete.

The average annual precipitation (nearly all as rain) is 650–1000 mm, decreasing to 400 mm at the Macquarie Marshes. Snow falls several times each year at altitudes above 1000 m but does not persist. Mean annual flow at Baroona gauge (upstream of Narromine) is $1.009 \times 10^9 \, m^3$, and mean peak annual discharge is 3017 m^3/s. Flow decreases downstream from Narromine, and at Oxley gauge (Fig. 2) the mean annual flow is only $0.301 \times 10^9 \, m^3$, and mean peak annual discharge only 277 m^3/s (http://realtimedata.water.nsw.gov. au/water.stm?ppbm=SURFACE_WATER&rs&3&rskm_url, accessed 12 Dec 2016).

The modern Macquarie River continues as a single sinuous channel until Oxley, then anastomoses over a short reach before entering the Macquarie Marshes (Fig. 3). Downstream

of the marshes, the river re-forms and joins the Barwon River. Within the marshes, channels avulse frequently (Ralph et al., 2016) and deposit sediment on the floodplains (Yonge and Hesse, 2009) but do not migrate much laterally.

Early surveys (1880s) of the Macquarie River show the river terminating in a wetland at the site we now call the "Terminus" (Ralph et al., 2016; Fig. 3). The surveys agree well with the first European account of the marshes by the explorer John Oxley in 1817. The Terminus channel was later abandoned by an avulsion that formed Monkeygar Creek (Ralph et al., 2011, 2016), but the old channel was preserved. The abandoned Terminus channel has an average width of 22 m and low sinuosity and is leveed and partly infilled with clays over the old bedload sand (Yonge and Hesse, 2009).

The so-called Old Macquarie is a reach of the river downstream of the abandoned Terminus that gathers outflowing water and forms a small, sinuous channel for 13 km before it again breaks down (Figs. 3 and 4G). This was the dominant channel of several in the southern Macquarie Marshes until avulsion at the Terminus redirected water eastward to Monkeygar Creek in the late nineteenth or early twentieth century, and construction of Marebone Weir upstream diverted flow to Bulgeraga Creek (Ralph et al., 2016; Figs. 2 and 3).

PREVIOUS WORK ON MACQUARIE RIVER PALAEOCHANNELS

Early research on the Macquarie DFS identified and dated by thermoluminescence (TL) four alluvial formations (Watkins, 1992; Watkins and Meakin, 1996) similar to the framework developed for the Murray and Murrumbidgee Riverine Plain (Page et al., 1996). All samples (except for the Trangie Formation) were taken from shallow ($\approx$1 m) pits (Watkins, 1992), but details of the sedimentology were not reported. Sediment adjacent to Marra Creek (Fig. 2) (Marra Creek Formation) was dated to 6.4 ± 1.7 ka (Watkins, 1992). Older Carrabear Formation sediment was dated to between 16 and 26 ka, and sediment of a yet older formation (Trangie) to the mid-Pleistocene (although these should be regarded as minimum ages; Price, D, personal communication, 2012). A fourth formation, the Bugwah, was inferred to date between the Marra and Carrabear Formations (Watkins and Meakin, 1996).

A later study using single-aliquot regenerative (SAR) OSL dating (Yonge and Hesse, 2009) found older ages inconsistent with the earlier chronology of Watkins (1992) and Watkins and Meakin (1996). Point bar sands of the Milmiland palaeochannel, correlated to the Bugwah Formation of Watkins and Meakin (1996), were found to be about 30 ka, much older than the 16–6 ka suggested by Watkins and Meakin (1996).

Watkins (1992) placed the onset of the modern fluvial regime at "about 10 ka," based on TL ages of 13.4 ka for the older Bugwah Formation, 9.4 ka for a source-bordering sand dune associated with it, and 6.4 ka for the suspended-
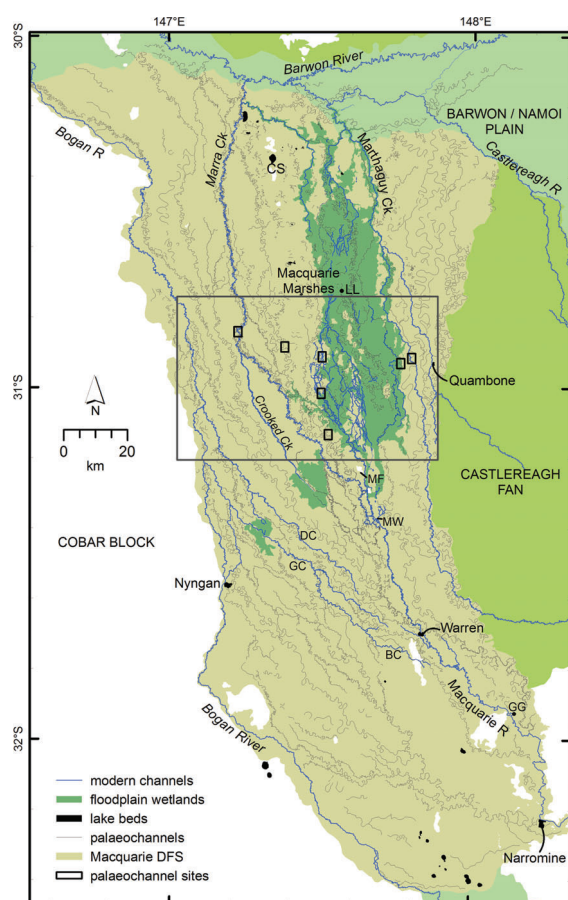
Figure 2. Macquarie distributive fluvial system showing the modern drainage system (blue) and palaeochannels (grey). Flow is from south (Narromine) to north. The Macquarie Marshes and other floodplain wetlands are shown as dark green. The large box indicates the position of Fig. 3. Small rectangles indicate the location of the field sites (Fig. 4). BC, Belaringar Creek; CS, Cuddie Springs archaeological site; DC, Duck Creek; GC, Gunningbar Creek; GG, Gin Gin; LL, Louden's Lagoon; MF, Mount Foster; MW, Marebone Weir. (For interpretation of the references to colour in this figure legend, the reader is referred to the web version of this article.)

Figure 3. Part of the large array of palaeochannels (grey lines) preserved on the surface of the Macquarie distributive fluvial systems (DFS). Modern channels shown in blue; flow is from 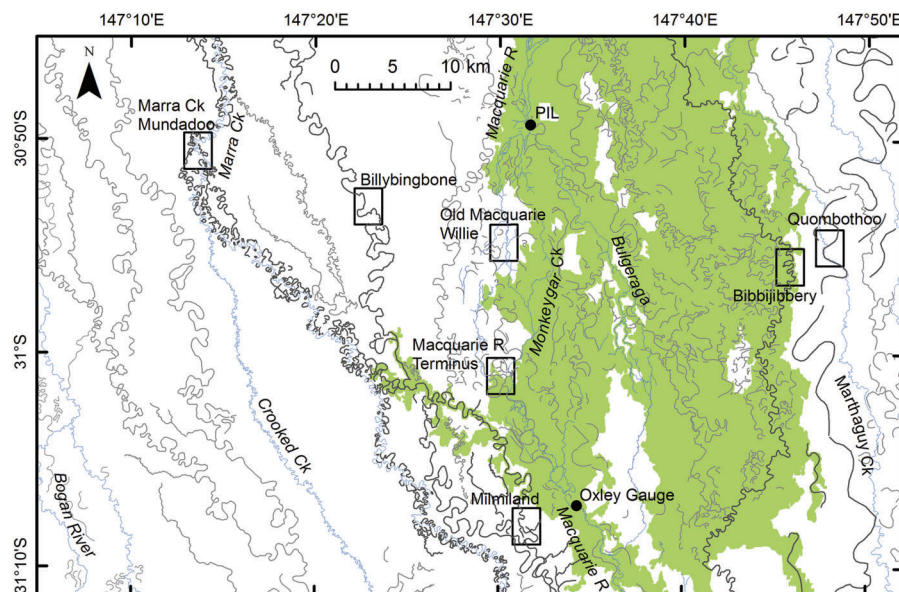south to north. Mapping was based on interpretation of the light detection and ranging digital elevation model (LIDAR DEM). Rectangles indicate the location of the field sites (Fig. 4). The green shaded area represents the area of frequent inundation within the Macquarie Marshes (from Thomas et al., 2011). PIL, Pillicawarrina. (For interpretation of the references to colour in this figure legend, the reader is referred to the web version of this article.)

load Marra Formation. Watkins and Meakin (1996) revised this to a "maximum recorded age" of 6.4 ka for the modern fluvial system based on the same ages. The onset of sedimentation in the marshes was dated to between 8.5 ka (OSL) and 4.9 cal ka BP (^{14}C) by Yonge and Hesse (2009), but the timing of the transition and the magnitude of the hydrologic changes leading to the Holocene system were not well constrained.

The floodplain in the now-abandoned Terminus marsh has characteristic floodplain wetland clays that overlie the silty and sandy clay deriving from an earlier, higher-energy, fluvial regime. The base of the wetland sediments is dated to 5.2 ka by SAR OSL and older than 4.9 cal ka BP by accelerator mass spectrometry ^{14}C of bulk organic material (Yonge and Hesse, 2009). This places initial marsh formation, and breakdown of the Macquarie, at about 5 ka. This transition is reflected in marsh sediment by loss of limnetic zooplankton and increasing diversity of terrestrial and aquatic vegetation before abandonment (Ralph et al., 2011).

The Old Macquarie channel and a related meander cutoff at Willie are underlain by sandy clay but otherwise infilled by smectite-rich clay typical of the marshes today (Larkin, 2012; Fig. 3). The steep-sided channel has a reach-average width of 15 m. SG-OSL ages from sand sieved from the clay infill are 2.3 ± 0.7 ka and 0.99 ± 0.14 ka, postdating the cutoff and predating the age of 0.8 ± 0.14 ka from the proximal floodplain of the adjacent modern channel (Larkin, 2012). The basal sandy clay layer in the cutoff gave an age of 4.8 ± 1.2 ka, close to the age of initiation of marsh sedimentation at the Terminus.

METHODS AND APPROACH

Palaeochannel mapping and morphometrics

Detailed palaeochannel mapping supported selection of study sites, assessment of channel morphology assessment, and determination of crosscutting relations among palaeochannels.

A 1 m light detection and ranging digital elevation model (LIDAR DEM; NSW Office of Environment and Heritage) was used to measure palaeochannel dimensions at the field sites (Fig. 4). A 5 m LIDAR DEM (NSW Spatial Services: http://elevation.fsdf.org.au, accessed 1 Aug 2017) was used to map palaeochannels at the eastern, western, and southern margins of the DFS beyond the limits of the 1 m DEM. SPOT imagery was used to identify palaeochannels in a small area in the northwestern corner of the DFS not covered by the LIDAR DEM.

The detail provided by the LIDAR DEM allowed us to map many palaeochannels not observable on SPOT imagery or aerial photographs and in greater detail than for other DFS in the Murray-Darling basin, enabling precise mapping and measurement of 81 individual palaeochannels (Supplementary Table S1) and assessment of crosscutting relationships. In combination with SG-OSL dating, we have used crosscutting relationships to infer a relative sequence of palaeochannel formation. Rankings of surface continuity and cross-sectional form were combined to derive a numerical index of palaeochannel preservation (Table 1). This index value gives a ranking from 2 (best preserved) to 6 (isolated traces) for palaeochannels with surface expression. The preservation index was used to supplement the
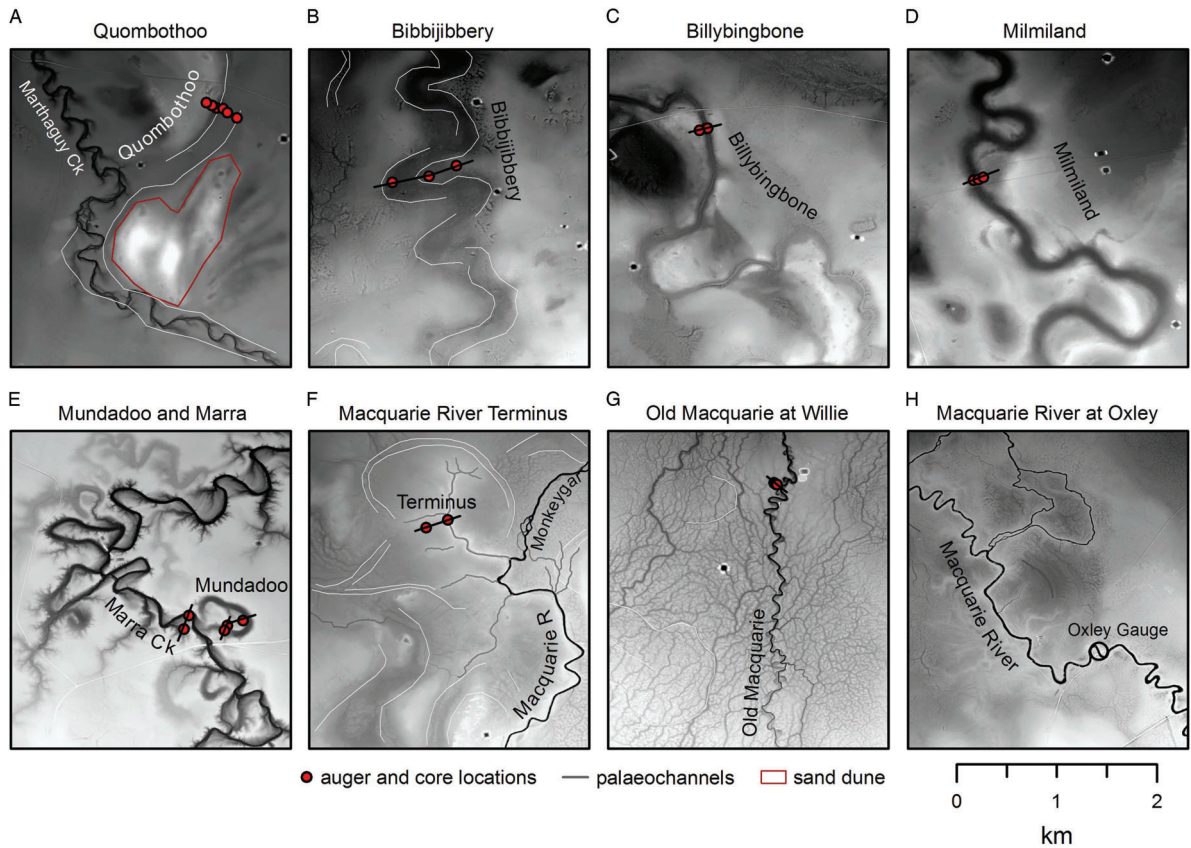
Figure 4. Extracts of the light detection and ranging digital elevation model (LIDAR DEM) showing the palaeochannel field sites (locations shown in Fig. 3). High elevations are white, and low elevations are black, but the grey scale is stretched in each extract to maximise the contrast and is not equivalent between extracts. Core and auger locations are indicated by circles, and palaeochannel traces (grey lines) are inferred from the LIDAR DEM (where not clear). Flow is from bottom to top. (For interpretation of the references to colour in this figure legend, the reader is referred to the web version of this article.)

Table 1. Palaeochannel preservation index scheme.

Channel longitudinal continuity	Value[a]	Continuity features (wavelength = L)	Channel form (cross section)	Value[a]	Cross-sectional features
Continuous	1	Continuous (>20 L)	Unfilled	1	Distinct bed and banks; able to transmit flow
Discontinuous	2	Reaches of continuous palaeochannel separated by reaches with absent or indistinct channel (20 > L > 1)	Partly filled	2	Partial preservation of banks; partly infilled (shallowing); transmits flow but reduced capacity; may be discontinuous shallow pools; commonly covered with terrestrial vegetation /trees
Isolated	3	Short reaches (e.g., oxbows) with no connection to other palaeochannel remnants (<1 L)	Trace	3	No depression; expressed as band of distinct soil/ sediment ± vegetation
Buried/ destroyed	4	No surface expression and/or no preservation	Buried/ destroyed	4	No trace at surface and/or no preservation

[a]The preservation index is derived by adding the value for continuity and the value for cross-sectional form.

dating and crosscutting relationships to infer the relative age sequence of palaeochannels.

Where possible for each mapped palaeochannel, we estimated bankfull width and meander wavelength. Bankfull width was measured at the inflection point between meander bends to reduce overestimation of width for formerly migrating palaeochannels. The reach-averaged bankfull width was calculated from eight individual measurements where possible. Rarely, a smaller number was used where palaeochannel preservation was poor. Meander wavelength was calculated by measuring the distance between inflection points along the reach over up to 10 wavelengths.

Palaeochannel sediment and OSL sampling locations

From the mapping, we identified four undated palaeochannels (Mundadoo, Billybingbone, Bibbijibbery, and Quombothoo) and two previously dated palaeochannels (Milmiland and Marra) (Figs. 2 and 3) for quartz SG-OSL dating. Each is generally well preserved (in terms of continuity and cross-sectional form) and can be related to the others by cross-cutting relationships. Although all have a meandering planform, they range in width, wavelength, and meander characteristics. Suitable sampling locations were found at an approximately equal distance downstream from the point where the Macquarie River debouches onto the alluvial plain at Narromine. All locations are covered by the LIDAR DEM.

Sampling for OSL dating targeted a single cross section on each palaeochannel and the shallowest bedload sediment beneath infill (where the infilling sediment is distinct in character from the bedload sediment), or proximal point bar sediments adjacent to the palaeochannel. The age of these deposits correspond to the time of channel abandonment. At a minimum of three points across the width of each palaeochannel, sediments were extracted using a Dormer 50-mm-diameter sand auger. Samples for OSL analysis were taken using stainless-steel tubes attached to the auger and driven vertically into the sediment. At Milmiland and Quombothoo palaeochannels, cores were taken with a Mori S15 crawler-mounted drill rig fitted with a Tone Ecoprobe 06 medium-frequency sonic drilling head. All cores were retrieved without exposing the sediment to light and were later subsampled under subdued red-light conditions for OSL analysis. Additional sediment from above, below, and surrounding each OSL sample was collected for dose-rate calculations using high-resolution gamma spectrometry (Table 2).

OSL sample processing

The OSL samples were prepared for analysis under subdued red light, with 180- to 212-μm-diameter quartz isolated using standard purification procedures, including 40% hydrofluoric acid for 45 min to etch the alpha-irradiated outer layers of the quartz grains (Aitken, 1998). Feldspar contamination was checked during analysis using an infrared wash (stimulation with IR diodes at 50°C for 100 s). For each sample, a preheat plateau test was conducted revealing a plateau of 260°C and the chosen preheat. A dose-recovery run (8 aliquots with signals removed at room temperature and bleached with blue diodes) at this preheat temperature tested the legitimacy of these measurement parameters, with all aliquots returning the surrogate dose within errors.

All OSL samples were analysed using an automated Risø TL/OSL-DA-20 reader (Bøtter-Jensen et al., 2003) fitted with an EMI 9235QA photomultiplier tube and with Hoya U-340 detection filters (290–370 nm transmission) to prevent recording scattered stimulation light. Optical stimulations were performed using a green laser (532 nm). Equivalent dose (D_e) was determined using a modified SAR protocol

Table 2. Optically stimulated luminescence (OSL) sample locations and depths.

Palaeochannel	Field code	HRGS (High Resolution Gamma Spectrometry) lab code	Location (latitude, longitude, elevation masl)	Burial depth (m)
Marra Creek (MC)	MC1	MQU14030	30.8451°S, 147.2302°E, 140 m	3.13
	MC2	MQU14031	30.8463°S, 147.2298°E, 141 m	3.89
Mundadoo (MDD)	MDD1	MQU14032	30.8460°S, 147.2337°E, 141 m	4.43
	MDD3	MQU14033	30.8455°S, 147.2351°E, 143 m	5.88
Milmiland (MIL)	MIL01-7	MQU14034	31.1324°S, 147.5187°E, 158 m	7.74
	MIL01-8	MQU14035	31.1324°S, 147.5187°E, 158 m	10.14
	MIL03	MQU14036	31.1321°S, 147.5196°E, 159 m	5.67
Billybingbone (BBB)	BBB1	MQU12008	30.8787°S, 147.3772°E, 155 m	6.18
	BBB2	MQU12009	30.8787°S, 147.3774°E, 155 m	7.40
	BBB3	MQU12010	30.8789°S, 147.3766°E, 156 m	3.65
Bibbijibbery (BIB)	BIB02	MQU12006	30.9289°S, 147.7613°E, 152 m	5.28
	BIB03	MQU12007	30.9294°S, 147.7580°E, 152 m	6.31
Quombothoo (QOB)	QOB02	MQU12011	30.9076°S, 147.8044°E, 153 m	3.10
	QOB04	MQU12014	30.9087°S, 147.8066°E, 150 m	6.26
	QOB05	MQU12015	30.9082°S, 147.8058°E, 150 m	6.00
	QOB06	MQU14037	30.9079°S, 147.8054°E, 154 m	8.57

after Murray and Wintle (2000) and Wintle and Murray (2006), with the first 0.2 s of luminescence decay used for signal integration and the last 0.3 s for background integration. Lithogenic radionuclide activity concentrations were determined using high-resolution gamma spectrometry, performed at the Environmental Research Institute of the Supervising Scientist, Darwin (Marten, 1992; Esparon and Pfitzner, 2010; Pfitzner, 2010). Dose rates were calculated using dose-correction factors from Adamiec and Aitken (1998), with beta-dose attenuation factors taken from Mejdahl (1979), and cosmic dose rates were calculated following the procedures of Prescott and Hutton (1994), factoring in latitude, altitude, and angle of zenith. Adjustments for moisture content (Aitken, 1985; Readhead, 1987) were calculated based on rounded in situ values measured from all samples in the absence of reliable information about long-term moisture content.

RESULTS

Palaeochannel mapping and crosscutting relationships

The mapping of palaeochannels and their crosscutting relationships and degree of preservation allowed the construction of a sequence of formation for 50 rivers and palaeochannels (Fig. 5). The dated palaeochannels can be fitted into this sequence to give a numerical time frame. The sequence is based primarily on the mapped crosscutting relationships. Secondarily, between palaeochannels constrained by clear crosscutting relationships or for palaeochannels not constrained by crosscutting relationships, we have considered the palaeochannel preservation to suggest possible relative ages. The remaining palaeochannels (not shown in Fig. 5) are mostly shorter and isolated reaches and are difficult to place in the sequence, because their continuity and crosscutting relationships cannot be inferred. Likewise, the southwestern portion of the DFS could not be interpreted easily, because the nearly parallel palaeochannels have few crosscutting relationships.

The palaeochannels we selected for OSL dating, therefore, constrain much of the sequence in the north and centre of the Macquarie DFS. A single TL age (WR25, Trangie Formation, 127 ± 16 ka) (Watkins, 1992) comes from an isolated trace palaeochannel in the south of the DFS that we have called "the Myall palaeochannel" to distinguish it from the broader alluvial surface with which it was identified by Watkins (Fig. 5). Other palaeochannels in the area, including Boggy Cowal (lpc1; Fig. 5, Supplementary Table S1) and Trangie Cowal (lpc2), are continuous and partly filled but of unknown age relative to our dated palaeochannels. A large number of palaeochannels in the central northern area in and around the Macquarie Marshes are older than the Bibbijibbery and Billybingbone palaeochannels and most likely older than the Quombothoo palaeochannel (Fig. 5).

The Bibbijibbery palaeochannel (Fig. 6B) is a continuous, partly filled palaeochannel that is very visible in the northeastern DFS. Its much smaller wavelength and amplitude and narrower channel contrast greatly with the nearby Quombothoo palaeochannel. A number of undated palaeochannels, especially in the south and west, may be older or of similar age to the Bibbijibbery palaeochannel. All of these palaeochannels are similar in size or smaller than the Bibbijibbery palaeochannel. The Billybingbone palaeochannel (Fig. 6C) has a similar morphology to the Bibbijibbery palaeochannel, but is slightly less infilled and continuous over a greater distance (total 160 km), and includes the Marebone palaeochannel (rpc 3) on the right bank of the modern Macquarie River. Short, straighter splays are evident in the lower reaches. The leveed Yarrawell palaeochannel, which forms an alluvial ridge bounding the western side of the Macquarie Marshes, is the only palaeochannel identified to have possibly formed in the period between the Bibbijibbery and Billybingbone palaeochannels. The Yarrawell palaeochannel is less well preserved than the Billybingbone palaeochannel but does not intersect it. However, the Yarrawell palaeochannel is clearly cut by the Milmiland palaeochannel at its upper end. The Milmiland palaeochannel (Fig. 6D) also crosscuts the Billybingbone palaeochannel and is of similar size and planform. While the Milmiland palaeochannel (including Five Mile Cowal, its upstream right-bank continuation) is a single-thread channel, the Bugwah Cowal/Yangunyah Cowal/Boomi Creek palaeochannel to the west is an older abandoned palaeochannel, with multiple (possibly successive) courses in its lower reaches (Fig. 6C).

The Mundadoo palaeochannel (Fig. 6E) is closely associated with Marra Creek (Fig. 6F). Both channels follow the same broad course, but the Mundadoo palaeochannel is found as a set of clearly larger (both in width and wavelength) cutoff bends and reaches. Both palaeochannels are confined laterally by the alluvial ridges of the Billybingbone and Bugwah/Yangunyah/Boomi palaeochannels, which may account for the absence of distributary channels along the Mundadoo or intermediate-age palaeochannels in this area. We speculate that the Boggy Cowal and perhaps the Trangie Cowal (superficial expression) palaeochannels date from the interval between the Milmiland and Mundadoo palaeochannels, based on their relative preservation (Fig. 4). A sand dune bordering Trangie Cowal at Weemabah (Fig. 6A) yielded TL ages of 61.8 ± 9.1 and 66.5 ± 4.5 ka (Supplementary Table S2). The dune is partly buried by fine-grained sediment, and it is likely that the visible channel of Trangie Cowal does not reflect the palaeochannel from which the dune was formed, but these ages do constrain the maximum age of the surficial Trangie Cowal palaeochannel. Marra Creek is the lower course of a palaeochannel system that can be traced to Ewenmar and Crooked Creeks from near Gin Gin at the upper end of the DFS. The intermediate reach, around Marebone Weir and Mount Foster, is one of a complex network of palaeochannels of similar size, apparently the product of multiple avulsions rather than the channel
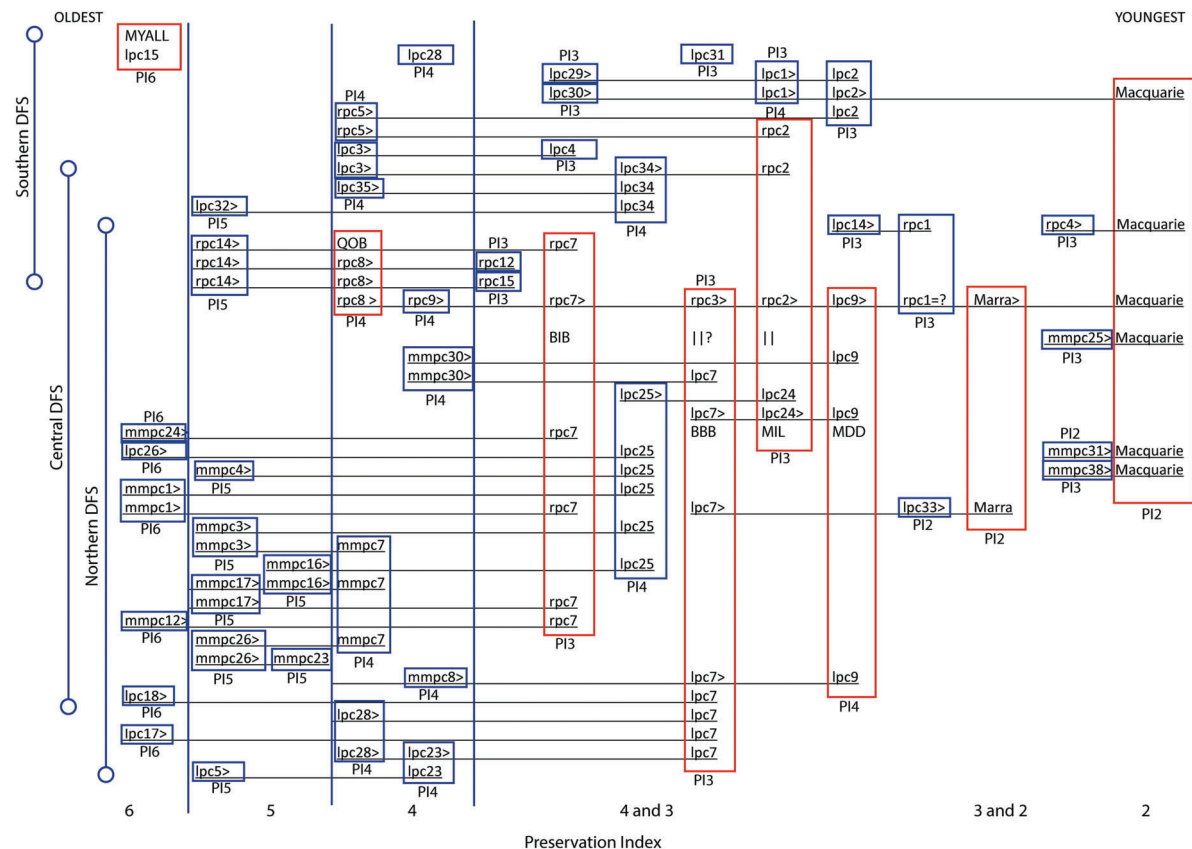
Figure 5. (colour online) Sequence of palaeochannel formation derived from luminescence ages, crosscutting relationships, and preservation index from oldest (left) to youngest (right). Individual palaeochannels are indicated by boxes (blue for undated channels or red where luminescence dating is available) and codes (rpc, lpc, or mmpc for left bank, right bank, and Macquarie Marshes palaeochannels, respectively). Crosscutting relationships (underlines) observed by mapping of the light detection and ranging digital elevation model (LIDAR DEM) are the primary criterion for arrangement of palaeochannels. Known relative age by crosscutting relationships is indicated by > or = symbols. Where not constrained (or between constraints) by crosscutting relationships or luminescence dating, the preservation index (PI above or below each box) has been used to suggest the relative age. As well as the modern Macquarie River, 49 palaeochannels are shown, including all 28 palaeochannels > 50 km in length and all 15 palaeochannels 25–50 km in length (Supplementary Table S1). Dated palaeochannels are indicated by codes: BBB, Billybingbone; BIB, Bibbijibbery; MDD, Mundadoo; MIL, Milmiland; QOB, Quombothoo (Table 2). Sequential maps derived from the framework of Fig. 4 show the channel evolution (Fig. 6). For example, the older palaeochannels of the central northern area are conspicuous to the west of the large Quombothoo palaeochannel (Fig. 6a). Source-bordering sand dunes are associated (albeit not exclusively) with meander plains of the Quombothoo palaeochannel and suggest the buried course of the palaeochannel to near the latitude of Warren. The upper reach of the Quombothoo palaeochannel is single thread, large, and sinuous with a few straighter, short, splay channels. In the lower reaches, up to three parallel Quombothoo palaeochannels occur and are most likely channels abandoned by rapid avulsion. Only the undated Euligal palaeochannel (lpc32) in the northwest approaches the Quombothoo palaeochannel in size. The poorer preservation of this palaeochannel suggests it may be older than the Quombothoo palaeochannel.

breakdown characteristic of the current Macquarie Marshes. Marra Creek clearly crosscuts the Mundadoo palaeochannel and is much smaller.

Marra Creek is presently a regulated channel fed by a canal from Marebone Weir on the Macquarie River (Fig. 6G). However, the LIDAR DEM reveals only small marsh channels naturally connecting it to the Macquarie floodplain before excavation of the canal. Previously, Marra Creek probably only carried high-stage overbank floodwaters from the Macquarie River and was therefore partly abandoned. This is a similar configuration to several left-bank palaeochannels of the Macquarie (including Crooked Creek, Duck Creek, Gunningbar Creek, and Belaringar Creek), which are now all connected by canals to the Macquarie to facilitate transfer of water for stock and irrigation across the DFS. In a similar way, the natural floodplain wetlands of the Macquarie and Crooked Creek have been partly canalised to facilitate water transfer but naturally are areas of channel contraction, termination, and overbank flow. Such areas, with their characteristic surface pattern of reticulate marsh channels (Yonge and Hesse, 2009) are only observed around the modern channel system and not the palaeochannels.
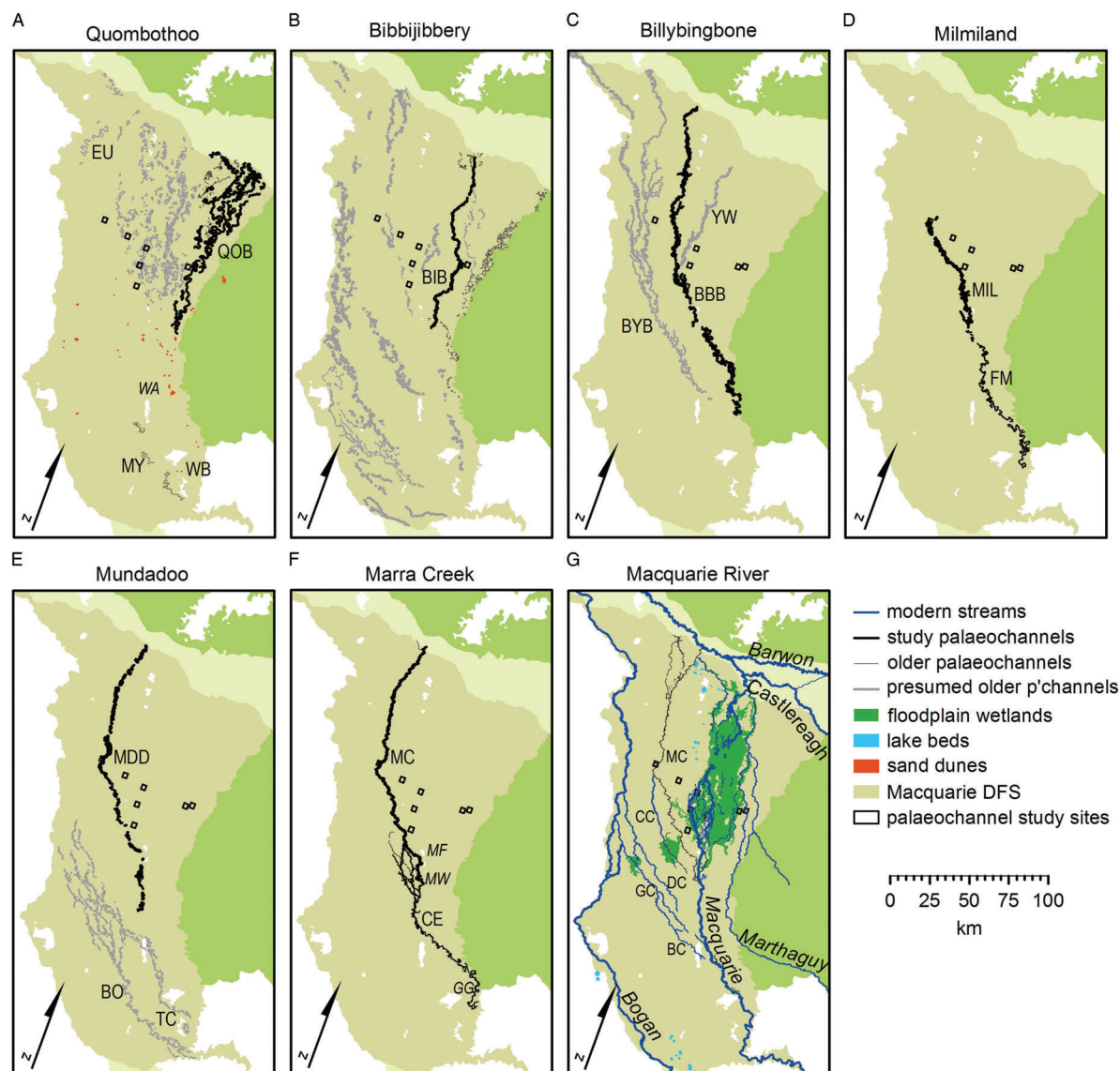
Figure 6. Sequential development of drainage on the Macquarie distributive fluvial system. (A–F) Each panel shows one dated palaeochannel (thick black lines) and older palaeochannels (thin black lines) formed since the time of the previous panel, confirmed by crosscutting relationships or assumed because of preservation status (grey lines). (G) The modern Macquarie River and other contemporary streams (blue) with modern floodplain wetlands (green). BBB, Billybingbone; BC, Belaringar Creek; BO, Boggy Cowal; BIB, Bibbijibbery; BYB, Bugwah/Yangunyah/Boomi; CC, Crooked Creek; CE, Crooked/Ewenmar; DC, Duck Creek; EU, Euligal; FM, Five Mile Cowal; GC, Gunningbar Creek; GG, Gin Gin; MC, Marra Creek; MDD, Mundadoo; MF, Mount Foster; MIL, Milmiland; MW, Marebone Weir; MY, Myall palaeochannel; QOB, Quombothoo; TC, Trangie Cowal; WA, Warren; WB, Weemabah source-bordering sand dune; YW, Yarrawell. Small squares show the location of field sites (Figs. 3 and 4). (For interpretation of the references to colour in this figure legend, the reader is referred to the web version of this article.)

Palaeochannel morphology, stratigraphy, and sedimentology

The Quombothoo palaeochannel (Fig. 7A) is a large, sinuous but discontinuous, broad, shallow, and partly infilled depression with elevated red sandy deposits on the inside of the meander bends. Sand dunes locally flank the channel downstream of

Marebone Weir, probably derived from point bar deposits (Fig. 6A). Meander wavelengths are 6 to 8 times larger than either the Billybingbone or Bibbijibbery palaeochannels and 21 times larger than the modern river at Oxley (Table 3). The surface expression shows that this palaeochannel has migrated across a belt up to 6 km wide. The palaeochannel is partly infilled by clay mixed with fine to coarse sand (Fig. 7A). Coarse

Table 3. Channel ages and dimensions for sample sites.

Palaeochannel	Median age[a] (ka)	Age 5th to 95th percentile[a] (ka)	Mean width[b] (m)	n	Mean wavelength[b] (m)	n	PC: modern width ratio	PC: modern wavelength ratio
Oxley (modern)	0		24 ± 0.8	8	212 ± 11	8		
Terminus[c]	3.4	0.5–5.6	22 ± 0.9	4	218	1	0.9	1.0
Willie	1.2	0.6–5.8	15 ± 0.7	8	152 ± 8	8	0.6	0.7
Marra	2.0	1.7–2.4	31 ± 2.2	8	291 ± 27	8	1.3	1.4
Mundadoo	5.6	4.8–6.4	86 ± 4.1	8	359 ± 24	7	3.7	1.7
Milmiland	21.7	19–24.3	114 ± 5.3	8	927 ± 68	8	4.8	4.4
Billybingbone	20.1	17.7–26.1	92 ± 5.3	9	759 ± 93	8	3.9	3.6
Bibbijibbery	34.1	27.1–41.2	125 ± 10.5	6	618 ± 53	8	5.3	2.9
Quombothoo	53.9	38.8–65.7	284 ± 9.4	8	4480 ± 212	8	12.1	21.1

[a]Median (50th percentile), 5th percentile, and 95th percentile ages from summed probability density functions (PDFs) of all accepted ages for each palaeochannel.
[b]Mean width and wavelength derived from light detection and ranging digital elevation model (LIDAR DEM) with standard error.
[c]The Terminus is the historically abandoned channel, downstream of Oxley, active until the early twentieth century. Its "median age" includes only numerical ages from sediment associated with the abandoned channel.

bedload was reached at approximately 6 m depth in the centre and concave bank of the palaeochannel and at 8.2 m depth on the convex bank. The deposits from the small inset palaeochannel on the convex bank of the broader palaeochannel are dominated by muddy coarse sand (Fig. 7A), but material below 2.4 m depth was not obtained due to hole collapse. We interpret this as a much later, small channel following the course of the palaeochannel, now infilled with sand derived from the surface sandy banks. The width of the palaeochannel estimated from the cross section is 250 m, although the concave bank is not well defined at the surface or from the lithostratigraphy. The average width of the Quombothoo palaeochannel from the LIDAR DEM in the sampled reach is 284 m (Table 3). The palaeochannel depth is at least 8.2 m and possibly as much as 10 m.

The Bibbijibbery palaeochannel (Fig. 7B) is a broad, shallow, continuous, and partly filled sinuous depression. There is little surficial evidence of channel migration other than being much wider at meander bends than at inflection points (Figs. 3 and 4). Coarse sandy loam bedload below around 6 m depth in the palaeochannel is overlain by smectite-rich clays containing some fine to medium sands, (Fig. 7B). A distinct sand layer below 5.3 m depth on the point bar is interpreted as bedload deposits from the migrating channel. The upper 3 m of the point bar core is dominated by clay, but the sand is finer and less abundant above 3 m depth. The average palaeochannel width in the sampled reach of Bibbijibbery is 125 m.

The Billybingbone palaeochannel is a shallow, partly filled, continuous, meandering (tortuously in places) depression with evidence of lateral migration and downstream translation (Figs. 3 and 4). Coarse sandy palaeo-bedload below 6–7.5 m depth is overlain by clay infill (Fig. 7C). The elevation of the bedload increases toward the inside of the meander bend, interpreted as bedload covered by point bar deposits and then fine-grained channel infill. At the channel margin, sand and muddy sand point bar, or ridge and swale, deposits (1.5 m depth) underlie fine-grained floodplain deposits. The average width in the sampled reach measured from the LIDAR DEM of Billybingbone palaeochannel is 92 m.

The Milmiland palaeochannel is a partly filled, meandering channel with well-defined banks. Clay was found in the base of the deepest core, overlain by alternating sand and gravel bedload layers from 10.4 to 7.7 m depth, in turn overlain by sandy clay to 5.9 m depth and clay infill above (Fig. 7D). Downstream, the palaeochannel is partly reoccupied by water escaping Buckiinguy marsh, and this water is contained within the palaeochannel until it meets Marra Creek. The average palaeochannel width is 114 m.

The Mundadoo palaeochannel is a series of large, partly filled, single cutoff meanders and reaches of meandering channel close to Marra Creek, but distinguished by its much larger dimensions (Fig. 3, Table 3). The palaeochannel is only partly filled with clay (Fig. 7E and F) above medium sands with some clay (sandy loam). The reach average palaeochannel width is 86 m.

Marra Creek, adjacent to the Mundadoo palaeochannel (Fig. 4), is a complex channel comprising reaches of reoccupied (and modified) Mundadoo palaeochannel and reaches of newer (Marra Creek–phase) palaeochannel. The Marra Creek–phase palaeochannel was in turn largely abandoned by the time of European occupation (thus meeting the definition of a palaeochannel) but has since been reoccupied by flows diverted by Marebone Weir. The Marra Creek–phase palaeochannel has distinctly smaller and less regular meanders than the Mundadoo palaeochannel. In these reoccupied reaches it is clearly underfit with evidence of oblique and vertical accretion within the channel margins. The Marra Creek–phase palaeochannel is narrow and steep-sided, with an average channel width of 31 m (Fig. 7G). Prominent ridges on the inside of the meander had sandy clay beneath a clay cover. Sand and gravel bars on the bed of Marra Creek are most likely derived from erosion of Milmiland-age (or older) palaeochannel deposits in the banks.

OSL dating results

Lithogenic radionuclide concentrations (Table 4) show that the thorium decay chains are in secular equilibrium (Olley
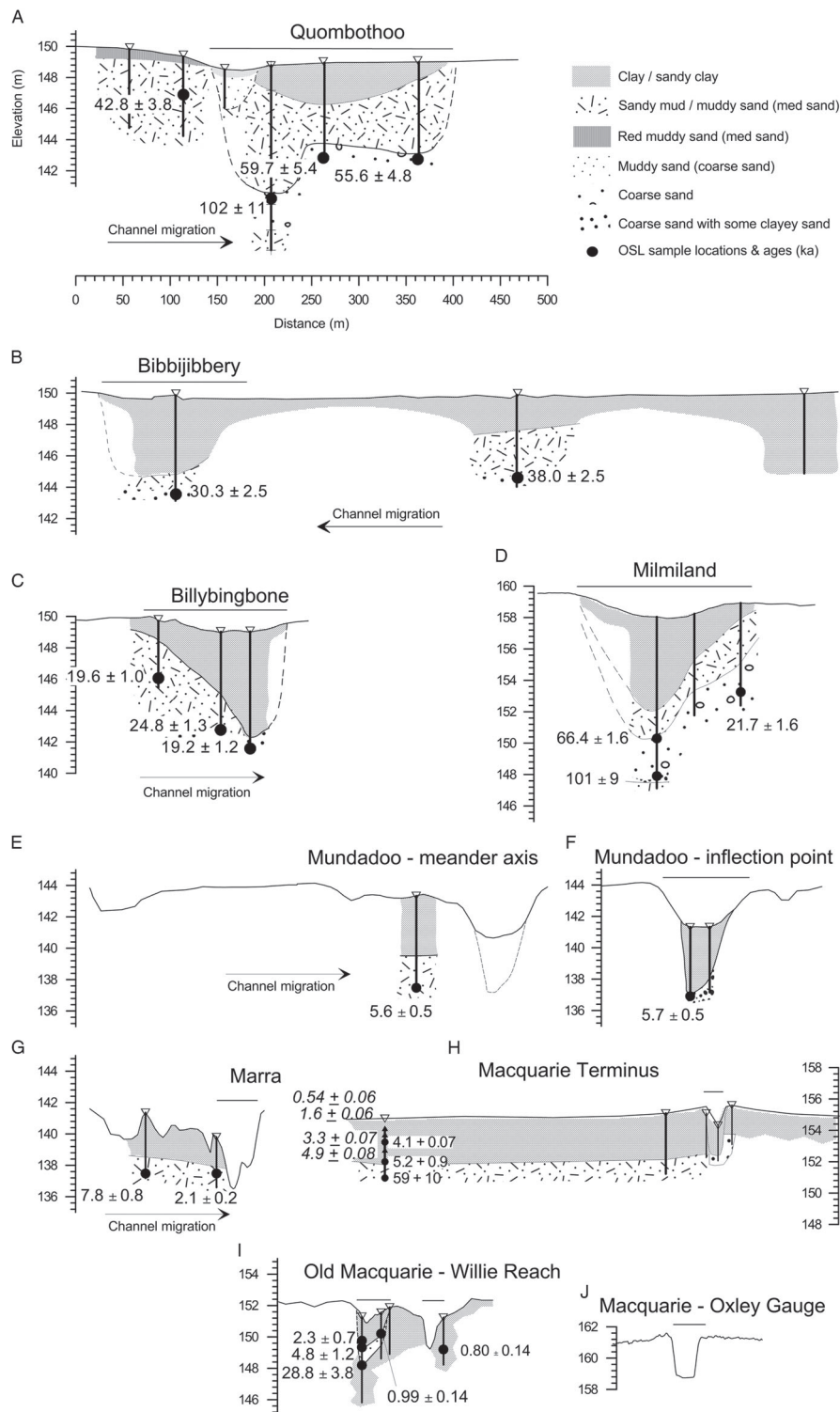
Figure 7. Macquarie palaeochannel cross sections showing lithostratigraphy, OSL sample location, and calculated ages (ka). All cross sections are shown at the same scale. Elevation is given in metres above sea level (Australian Height Datum). Inferred palaeochannel boundaries are shown by solid and dashed lines. Channels are arranged from oldest (A) to youngest (J). Oxley gauge (J) is located upstream of the anastomosing reach of the modern Macquarie River before the river breaks down into floodplain wetlands. The Terminus site (H) lies downstream of Oxley and was historically (nineteenth century) the terminal reach of the Macquarie River before it broke down and entered the reed beds (Yonge and Hesse, 2009). Old Macquarie at Willie (I) is a recent meander cutoff of the river downstream of the Terminus marshes where the river re-forms before again breaking down into wetlands further downstream (Larkin, 2012).

Table 4. Single-grain optically stimulated luminescence (SG-OSL) ages and analytical data of Macquarie palaeochannels.

| | | Dose rate | | | | | | | | | | | Equivalent dose | | | | |
| | | Nuclides[a] (Bq/kg) | | | | | | Cosmic dose rate[b] (Gy ka^{-1}) | Water content[c] (%) | | Total dose rate[d] (Gy/ka) | Number of grains[e] | | σ_D[f] | De[g] (Gy) | Age ± SD[h] (ka) |
OSL code	Dose rate lab code	^{238}U	^{226}Ra	^{210}Pb	^{228}Ra	^{228}Th	^{40}K		Field	Calculation		Measured	Accepted			
BBB1	MQU12008	19.9±3.0	16.0±0.3	<50	19.5±0.5	21.1±0.5	333±7	0.112±0.012	3.87	5±3	1.75±0.08	1000	207	29.5%	34.4±0.8	19.6±1.0
BBB2	MQU12009	10.0±2.6	11.6±0.3	<74	10.8±0.4	11.6±0.4	216±5	0.102±0.010	2.17	4±2	1.16±0.04	1000	213	45.5%	28.8±0.8	24.8±1.3
BBB3	MQU12010	20.2±3.6	32.4±0.4	56±28	28.0±0.7	32.2±0.8	436±9	0.141±0.015	5.49	6±4	2.47±0.13	1000	177	33.9%	47.3±1.1	19.2±1.2
BIB02	MQU12006	19.8±3.0	12.2±0.3	<46	15.7±0.5	17.5±0.5	337±7	0.120±0.013	5.38	6±4	1.64±0.09	1000	199	34.0%	62.5±2.0	38.0±2.5
BIB03	MQU12007	16.2±3.1	16.3±0.3	<68	22.8±0.6	24.8±0.6	381±8	0.108±0.012	7.04	7±5	1.90±0.12	1000	141	42.1%	57.5±3.0	30.3±2.5
QOB02	MQU12011	19.2±3.0	18.5±0.3	<92	25.6±0.6	28.3±0.7	361±7	0.131±0.017	17.67	18±8	1.76±0.15	1300	163	40.7%	75.5±1.8	42.8±3.8
QOB04	MQU12014	14.3±4.8	12.7±0.2	<43	17.1±0.2	18.2±0.5	305±4	0.097±0.012	18.30	18±8	1.36±0.11	1000	102	30.6%	81.1±2.3	59.7±5.4
QOB05	MQU12015	27.9±2.4	22.0±0.1	<23	20.3±0.2	21.4±0.4	306±3	0.108±0.013	5.18	10±7	1.70±0.13	1400	137	28.9%	94.7±3.0	55.6±4.8
QOB06	MQU14037	10±3	7.4±0.7	7±3	11.4±1.3	14.1±0.7	209±12	0.079±0.010	18.84	18±8	0.96±0.10	1000	182	21.6%	97.7±2.2	102±11
MIL03	MQU14036	12±3	9.1±0.7	7±3	15.4±1.4	11.3±0.7	311±15	0.118±0.012	2.54	5±3	1.38±0.09	900	170	31.7%	29.9±0.8	21.7±1.6
MIL01-7	MQU14034	19±2	16.0±0.5	19±2	17.7±0.9	16.0±0.5	312±10	0.087±0.011	16.25	16±8	1.46±0.13	1000	163	24.9%	96.7±3.3	66.4±6.6
MIL01-8	MQU14035	15±2	11.7±0.5	20±2	14.7±1.0	14.1±0.6	231±9	0.073±0.008	13.20	13±5	1.24±0.08	1000	109	43.4%	125.5±5.1	101±9.1
MDD1	MQU14032	10±2	8.7±0.5	14±2	11.9±1.0	12.6±0.5	238±10	0.132±0.014	4.71	5±3	1.29±0.07	1000	144	22.2%	7.24±0.19	5.60±0.45
MDD3	MQU14033	23±3	13.2±0.6	26±3	21.4±1.3	22.8±0.8	292±12	0.115±0.012	2.93	5±3	1.82±0.10	1000	232	34.3%	10.3±0.2	5.67±0.48
MC1	MQU14030	28±3	22.9±0.6	32±3	33.3±1.3	34.6±0.9	334±12	0.146±0.016	6.91	7±4	2.22±0.13	1000	189	34.7%	4.56±0.15	2.06±0.20
MC2	MQU14031	23±3	17.6±0.6	27±3	28.5±1.3	28.3±0.9	333±13	0.136±0.015	6.52	7±4	2.02±0.12	1000	174	22.6%	15.6±0.3	7.75±0.79

[a] Concentrations determined from high-resolution gamma spectrometry measurements of dried and powdered sediment sample.
[b] Time-averaged cosmic-ray dose rates (for dry sample), each assigned an uncertainty of ±10%.
[c] Water contents, expressed as (mass of water/mass of dry sample)×100. The "calculation" values were used to calculate the total dose rates and OSL ages.
[d] Mean±total (1σ) uncertainty, calculated as the quadratic sum of the random and systematic uncertainties. An internal dose rate of 0.03 Gy/ka is also included.
[e] Total number of grains processed and total number accepted.
[f] Dispersion of single-grain equivalent doses.
[g] Due to the fluvial environment and overdispersion of many samples, the minimum age statistical model (MAM) was used to determine the equivalent dose.
[h] Uncertainties at 68% (1σ) confidence interval.

et al., 1996) for the 16 Macquarie palaeochannel samples, with all but one falling within 10% of equilibrium and MIL03 within 20%. While the U-series results suggest disequilibrium for some samples (two are within 30% and one is within 50%), Olley et al. (1996) note that if the dose rates measured are assumed to have prevailed since burial, then the errors for this level of disequilibria are likely to be <3%.

The minimum age model (MAM) was considered the most appropriate model for determining palaeochannel ages, as all samples display equivalent dose (D_e) distributions that indicate heterogeneous bleaching, typical of fluvial sediments (Fig. 8). We assumed an overdispersion of 10% based on the spread of De in a modern analog sample.

We infer that the age of the Quombothoo palaeochannel is represented by three younger SG-OSL ages (42.8 ± 3.8 ka, 55.6 ± 4.8 ka, and 59.7 ± 5.4 ka) (Fig. 9). The deepest Quombothoo sample returned an age of 102 ± 11 ka, which we interpret as being from an older underlying unit.

The Bibbijibbery palaeochannel samples are from the upper palaeochannel sediments at two points along the meander axis. The younger sample (30.3 ± 2.5 ka) is near the apex of the meander bend, while the older sample (38.0 ± 2.5 ka) is beneath the floodplain deposits on the inside of the formerly migrating meander (Fig. 7B). These dates are taken to represent the period of activity of this palaeochannel and hence provide a maximum age for abandonment. The SG-OSL ages for the Billybingbone palaeochannel (19.2 ± 1.2 ka, 19.6 ± 1.0 ka, and 24.8 ± 1.3 ka) were taken at a depth immediately below fine-grained channel-filling muds (Fig. 7C) and, therefore, likely soon before abandonment.

Only one sample from the Milmiland palaeochannel (21.7 ± 1.6 ka) appears to give an age representing the time of channel activity. Two deeper samples are much older (66.4 ± 6.6 ka, 101 ± 9.1 ka) and do not overlap with the younger age at 2σ (Fig. 9). We interpret these samples to belong to an older unit not clearly identifiable in the stratigraphy. Both SG-OSL ages from the Mundadoo palaeochannel yielded similar ages (5.6 ± 0.5 ka and 5.7 ± 0.5 ka), distinctly older than one of the two ages from Marra Creek palaeochannel (2.1 ± 0.2 ka). The older age at Marra Creek (7.75 ± 0.8 ka), from the distal floodplain, we interpret as Mundadoo-age sediment preserved beneath the margin of the inset Marra floodplain.
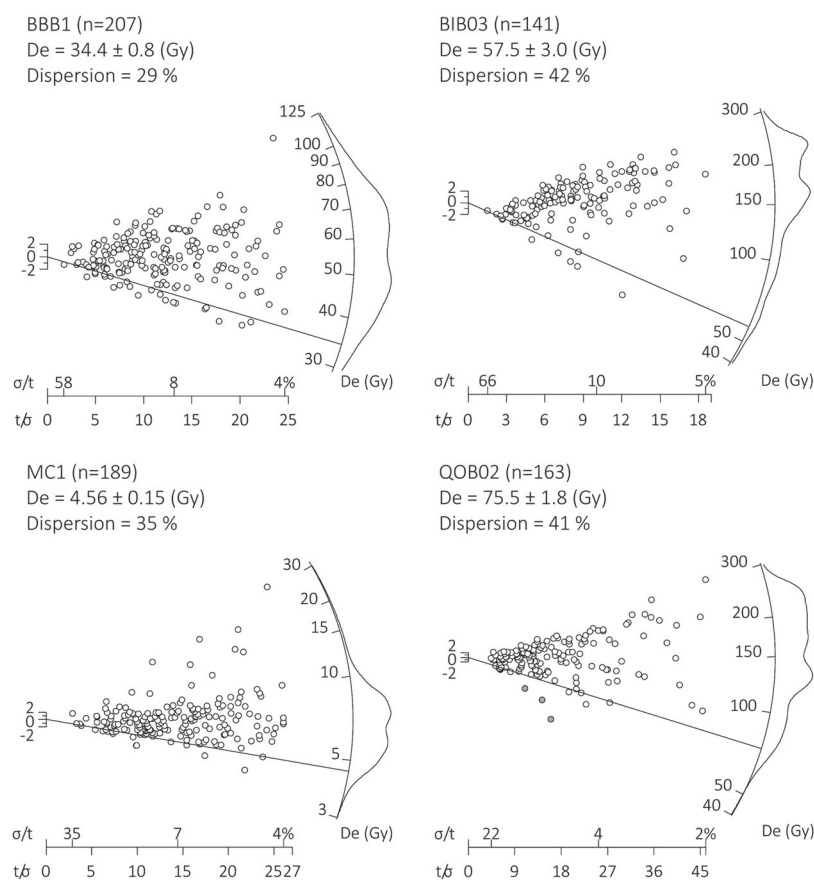

Figure 8. Selected radial plots (with KDE (kernel density estimate) on the radial scale or y-axis) for SG-OSL analyses showing the MAM De (Equivalent dose) result (solid line). All radial plots are shown in Supplementary Fig. S1.
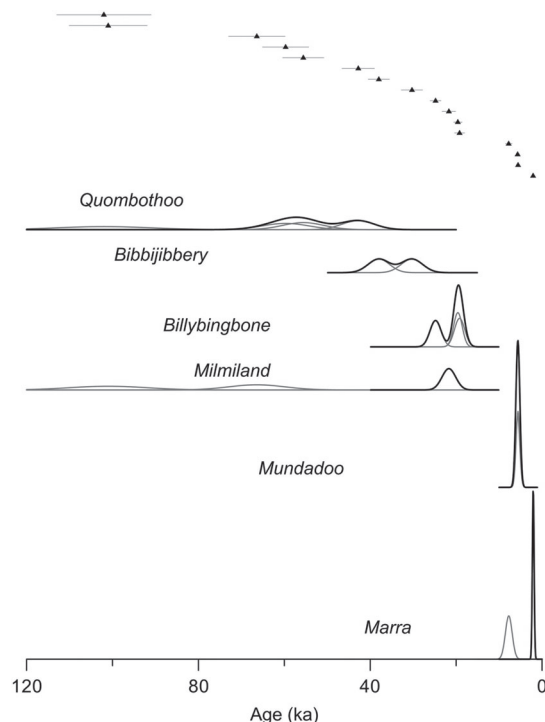
Figure 9. Probability density (PD) curves (all at the same vertical scale) and ranked age plot (top) for all OSL ages from the six palaeochannels. Individual age-determination PD curves are shown by grey lines, and the sum for each palaeochannel is shown by black lines. Several samples have been excluded from the sum, or accepted age, for Quombothoo, Milmiland, and Marra palaeochannels, where they appear to have reached older, underlying units (see text). Median (50th percentile) ages and 95% probability for each palaeochannel were calculated from these summed PD curves.

DISCUSSION

The chronological, sedimentological, and morphological data allow us to reconstruct the evolution of the Macquarie River over the last 54 ka. In combination with the results of earlier studies, we can infer the climate changes, and catchment hydrologic responses producing these changes.

Palaeochannel Chronology

In addition to the OSL chronology detailed earlier, crosscutting relationships indicate the relative age of some dated palaeochannels. The median OSL ages (Table 4) of the Quombothoo and Bibbijibbery palaeochannels confirm the mapped relationship showing that Quombothoo is the older palaeochannel. There is a small overlap of the age distributions at 2σ, suggesting a rapid transition from the very large Quombothoo palaeochannel (284 m width, median age 54 ka) to the narrower Bibbijibbery palaeochannel (125 m width, median age 34 ka) (Fig. 9).

Our SG-OSL ages for these palaeochannels are mostly younger than previous single aliquot ages. These differences are mostly due to our recognition of the scatter of equivalent doses (Fig. 8) and application of the MAM. Yonge and Hesse (2009) previously dated Milmiland Creek palaeochannel to ~ 30 ka by SA-OSL, but crosscutting relationships indicate that it is younger than the Billybingbone palaeochannel (median age 20.1 ka by SG-OSL MAM) and older than the Marra Creek palaeochannel. Based on the single accepted SG-OSL MAM age (Table 4), the age of 21.7 ka for the Milmiland palaeochannel overlaps broadly with the age of the Billybingbone palaeochannel. Upstream of the sample sites, the LIDAR DEM reveals that the Milmiland palaeochannel derives from the same system as the Billybingbone palaeochannel (Fig. 3). We infer that the Milmiland palaeochannel formed by avulsion from the Billybingbone, leading to the abandonment of that palaeochannel downstream. The new Milmiland palaeochannel cuts across the Billybingbone palaeochannel and is incised below the level of the Billybingbone plain in the area between the two sample sites. The very similar ages reflect the rapid avulsion process.

Sediment adjacent to the Marra Creek palaeochannel has a TL age of 6.4 ± 0.7 ka (Watkins, 1992), whereas our new SG-OSL age is 2.1 ± 0.2 ka (single accepted age), consistent with the older (by crosscutting relationship) Mundadoo palaeochannel (median age 5.6 ka). It is possible that Watkins (1992) dated underlying Mundadoo-age sediment (instead of the Marra Creek palaeochannel) as we suspect we did in the case of our older Marra sample.

Most palaeochannels are associated with thin sedimentary sequences representing lateral migration and point bar and/or oblique accretion rather than extensive vertical accretion. Deeper coring in the Milmiland and Quombothoo palaeochannels appears to have penetrated below the sediments associated with those palaeochannels (Fig. 7A and D). Yonge and Hesse (2009) also found older sediments (dated by single-aliquot OSL to 59 ± 10 ka and 42 ± 7 ka), not directly identifiable with a palaeochannel, beneath the Holocene Terminus and Buckiinguy marsh sediments. Using SG-OSL, Yu et al. (2015) found sediment dating to 28 ka at 1.5 m depth, beneath late Holocene marsh sediments at Louden's Lagoon (Fig. 2) in the northern Macquarie Marshes, and at Willie on the Old Macquarie (Larkin, 2012), a thin veneer of Late Holocene channel fill overlies older sandy clays dated to 28.8 ± 3.8 ka (Fig. 7J).

We have found older ages for the Macquarie palaeochannels than the previous chronology based on TL ages (Table 5). Watkins (1992) identified four phases of fluvial activity on the Macquarie plain on the basis of TL dating. The youngest, Marra Formation, including Marra Creek and the modern Macquarie River, was dated from 6 ka to the present. The Bugwah Formation (13.4–6 ka) as mapped includes both the Billybingbone (median age 20.1 ka) and Milmiland (21.7 ka) palaeochannels and, morphologically, would also likely include the Mundadoo (5.6 ka) and Bibbijibbery (34.1 ka) palaeochannels. The new SG-OSL ages suggest that the Bugwah Formation ages given by Watkins (1992) are too

Table 5. Comparison of palaeochannel ages with previous temporal frameworks.

	Watkins (1992)	Yonge and Hesse (2009)	This study (median ages)[a]
	Marra Formation < 6 ka	Macquarie River and Marshes Initiated 8.5–4.5 ka	Macquarie River and Marshes <5.5 ka Marra Creek palaeochannel 2.1 ka
Stratigraphic units[b]	Bugwah Formation 13.4–6 ka	Milmiland palaeochannel ≈30 ka	Mundadoo palaeochannel 5.6 ka Milmiland palaeochannel 21.7 ka Billybingbone palaeochannel 20.1 ka Bibbijibbery palaeochannel 34.1 ka
	Carrabear Formation 25.6–13.4 ka		Quombothoo palaeochannel 54 ka
	Trangie Formation mid-Pleistocene		n/a

[a]Palaeochannels mapped to respective formations by Watkins and Meakin (1996).
[b]From Watkins and Meakin (1996).

young. The older Carrabear Formation described by Watkins (1992) includes the Quombothoo palaeochannel, but the TL ages (13.4 ka and 25.6 ka; Watkins, 1992) are also far too young compared with the SG-OSL ages presented here for the Quombothoo palaeochannel (median age 53.9 ka). The even older Trangie Formation remains undated by OSL. It is possible that the systematically younger ages found by Watkins (1992) are due to shallow sampling from pits around 1 m deep. This may have led to sampling of postabandonment sediment or sediment affected by bioturbation following abandonment.

From our age assessments, we conclude that the Marra Creek palaeochannel formed and was abandoned in the late Holocene, and the Mundadoo palaeochannel in the mid-Holocene, and that the Milmiland and Billybingbone palaeochannels were active in the last glacial maximum (LGM), the Bibbijibbery palaeochannel during late Marine Oxygen Isotope Stage 3 (MIS 3), and the Quombothoo palaeochannel during early MIS 3.

We propose that the development of the southern Macquarie Marshes in conjunction with the modern hydrologic regime began about 5.6–5.2 ka. The historical Terminus of the Macquarie River formed after around 5.2 ka (Yonge and Hesse, 2009; Fig. 7I), shortly after the Mundadoo palaeochannel was active (5.6 ka). Although limited by few ages, we propose that abandonment of the Mundadoo palaeochannel resulted in the accumulation of sediment in the Terminus and nearby Buckiinguy marsh sediments (Yonge and Hesse, 2009), deposition by the Old Macquarie at Willie (Larkin, 2012; Fig. 7J), and the reduction in size of Marra Creek. This hydrologic regime is characterised by small, contracting channels, extensive overbank flooding, large expanses of floodplain wetlands, and little water and sediment from the Macquarie River making its way through to the Barwon River.

Decline of the Macquarie River

Combining the palaeochannel chronology with the palaeochannel dimensions (Fig. 10), it is possible to quantify the decline of palaeochannel width and infer a relative decline in bankfull discharge between the early MIS 3 Quombothoo palaeochannel and late MIS 3 Bibbijibbery palaeochannel, and the later further decrease of river discharge between the mid-Holocene Mundadoo and late Holocene Marra, Terminus and Willie (Old Macquarie) palaeochannels. The trend of decreasing river bankfull width (Fig. 10A) and meander size (wavelength) (Fig. 10B) between ≈54 ka and ≈2 ka is unequivocal, but quantifying palaeo-discharges is more problematic.

A range of approaches has been used previously to quantify palaeochannel morphometrics and to calculate palaeodischarge of Murray-Darling basin palaeochannels. Page and Nanson (1996) applied Manning's equation to the Murrumbidgee palaeochannels; and Dury's (1976) empirical relationship between meander wavelength and bankfull discharge has been applied to the Namoi (Young et al., 2002), Gwydir (Pietsch et al., 2013), and Lachlan (Kemp and Rhodes, 2010) palaeochannels. Dury (1976) also derived an empirical relationship between channel-bed width and bankfull discharge. Dury's equations have the advantage that fewer variables are required, and these can be measured accurately. However, his equations may not be directly applicable for the Macquarie palaeochannels; for example, whereas Dury (1976) found an approximate ratio of 11:1 for channel wavelength to bed width (L/W), the Macquarie
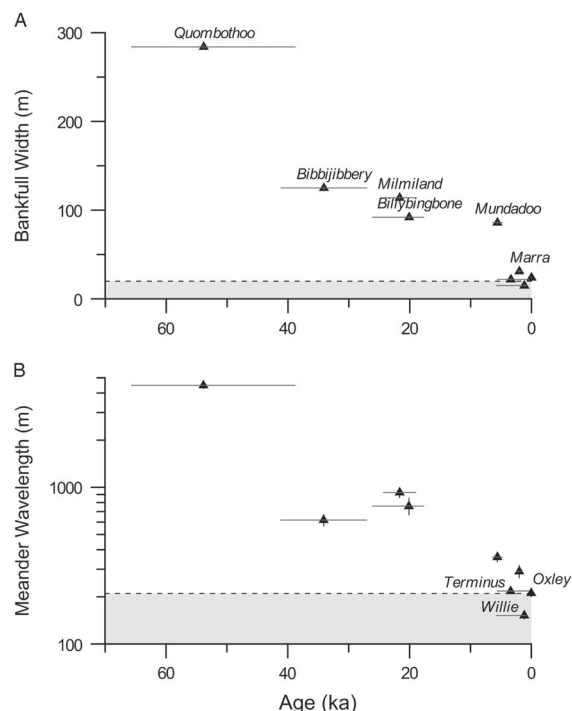
Figure 10. Palaeochannel age against palaeochannel bankfull width (A) and meander wavelength (B) for the Macquarie distributive fluvial systems (DFS). The 95% probability of combined optically stimulated luminescence (OSL) ages is shown. Standard error of width and wavelength measurements is shown but is mostly smaller than the symbol size. The dashed lines and shaded areas represent the proposed thresholds for channel stability and zones of channel breakdown and floodplain wetland formation.

palaeochannels have a L/W ratio of at least 15:1 (from data in Table 3). Because bankfull width is larger than bed width (which we could not derive reliably for infilled palaeochannels), the ratio L/W must be higher than 15:1 for these palaeochannels. This discrepancy is due to the unusual hydraulic geometry of Murray-Darling basin channels, which undergo a downstream loss of discharge on a declining slope (Kemp and Rhodes, 2010; Pietsch and Nanson, 2011). For these reasons, we have chosen not to estimate palaeo-discharge; rather, we simply infer that both meander wavelength and channel width positively correlate with river discharge, governed by poorly constrained power relationships.

Although the Macquarie River in the early twentieth century was a single-thread channel all the way to Oxley, we cannot be certain that this was the case for the palaeochannels. Therefore, each palaeochannel must be regarded as having been formed by bankfull discharges that were minima for the system as a whole. Nevertheless, palaeochannel mapping (Fig. 5) suggests that most of the palaeochannels were indeed continuous, single-thread channels rather than anastomosing channels. Where branching was observed, it was in the form of short, straight distributary channels and

splays escaping the leveed meandering channels, which terminated on the floodplain (Tooth, 2005).

There was a large decline in size of the Macquarie between the Quombothoo (median age 54 ka) and Bibbijibbery (median age 34 ka) palaeochannels. While the meander wavelength decreased sevenfold and the bankfull width by more than half (Fig. 10, Table 3), both palaeochannels maintained continuous, sinuous, laterally migrating channels across the Macquarie DFS to the floodplain of the Barwon River (trunk stream) downstream (Fig. 2). This decrease of bankfull discharge, while large, evidently was still within the range sufficient to maintain the same meandering fluvial style.

A second large decline in bankfull width and meander wavelength corresponded with abandonment of the Mundadoo palaeochannel and avulsion to the modern course of the lower Macquarie River about 5.5 ka. The diminished discharge associated with these reductions was probably integral to the breakdown of the formerly throughgoing river channel and formation of the Macquarie Marshes (Ralph and Hesse, 2010).

Collectively, these data indicate ongoing decline in the size and discharge of the Macquarie River since mid-MIS 3 and, in the late Holocene, a threshold change in fluvial style. The 285-m-wide Quombothoo palaeochannel was larger than any extant river in the Murray-Darling basin, even the lower Murray River (160–220 m downstream of its confluence with the Darling River). By contrast, the Macquarie River at Oxley is now just 24 m wide. Below Oxley, the river declines in width (and discharge) to 22 m at the Terminus before breaking down into unchannelled marshes, re-forming at the Old Macquarie (15 m wide at Willie), and then breaking down again. These data suggest, in the Macquarie DFS at least, that there is a threshold of around 20 m width (Fig. 10A) or 210 m wavelength (Fig. 10B) below which channels can no longer maintain themselves against the opposing forces of vegetation encroachment, sediment accumulation, and enhanced overbank flow and avulsion (Yonge and Hesse, 2009; Ralph and Hesse, 2010). Gauging data (at Oxley and downstream at Pillicawarrina; New South Wales Office of Water data, http://realtimedata.water.nsw.gov.au, accessed 12 Dec 2016) suggest that the bankfull discharge threshold is around 20 m^3/s. This equates to specific stream power of around 2–3 W/m on the lower Macquarie River (Ralph and Hesse, 2010).

Late Quaternary river response to climate-driven hydrologic change

River discharge is a complex and indirect proxy of climate. While it is useful to know the magnitude of the channel-forming flood, its relationship to average annual discharge, catchment runoff, or, ultimately, precipitation is complicated by the many links within the hydrologic system. In Australia, the large size of late Pleistocene (dominantly within MIS 2 and 3) palaeochannels compared with modern channels has
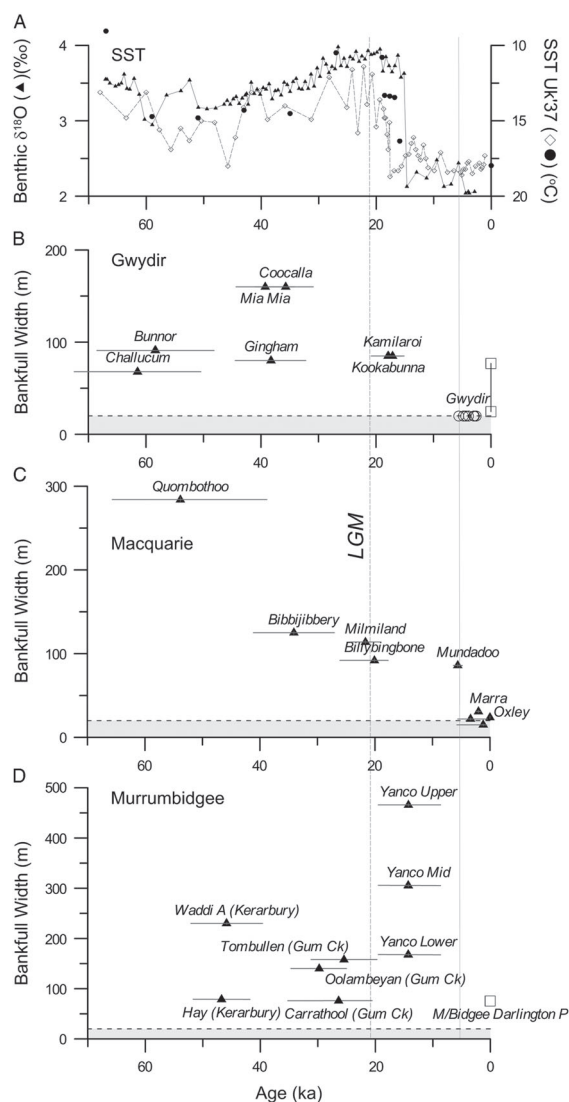
Figure 11. Sea-surface temperature and marine oxygen isotope record (A) compared with palaeochannel widths of the Gwydir (B), Macquarie (C), and Murrumbidgee (D) Rivers. Uk'37 sea-surface temperature (SST) records are from the Great Australian Bight core MD03-2607 (diamonds) (Lopes dos Santos et al., 2013) and eastern Tasman Sea core DSDP593 (circles) (McClymont et al., 2016), and the benthic foraminiferal oxygen isotope record is from the east Tasman Sea core SO136-003GC (triangles) (Ronge et al., 2015). Gwydir palaeochannel ages are from Pietsch et al. (2013), expressed as the median and 95th percentile range of summed ages for each identifiable palaeochannel with average width measurements (this study). Holocene Gwydir-phase ages are not identified with extant channels and are shown at a nominal width. Modern Gwydir river widths at Yarraman Bridge and downstream of Tyreel (squares) show the decrease in channel width just above the point of river breakdown. Murrumbidgee palaeochannel ages are from Page et al. (1996), expressed as the median and 95th percentile range of summed ages for each identifiable palaeochannel with average width measurements (this study). Three reaches of the Yanco palaeochannel are shown with the same pooled age. The modern Murrumbidgee

long been recognised (Butler, 1950; Pels, 1964a, 1964b; Bowler, 1967; Schumm, 1968). However, these large palaeochannels have not typically been associated with greater precipitation, as the landmark study of Galloway (1965) demonstrated the potential for temperature to influence runoff. Subsequently, several mechanisms have been proposed to account for large late Pleistocene (including LGM) palaeochannels. Many invoke lower temperatures in the upper catchment to both sustain larger snowpacks and enhance associated seasonal snowmelt and to reduce evapotranspiration and increase runoff efficiency (Page et al., 1996; Kemp and Rhodes, 2010; Reinfelds et al., 2014). This explanation has been commonly proposed for southern Murray-Darling basin rivers (Goulburn, Murray, Murrumbidgee, and Lachlan) that have small alpine areas within their catchments today (Langford-Smith, 1959, 1960; Bowler, 1978; Page et al., 1996, 2009; Kemp and Rhodes, 2010; Reinfelds et al., 2014). Alternatively, a northerly source of enhanced precipitation associated with a warm Coral Sea has been proposed to explain larger palaeochannels in the Gwydir catchment at times of lower sea level than today (Pietsch et al., 2013). Today, the Coral Sea is the largest moisture source for eastern and northern Australia (Gimeno et al., 2010), especially in summer.

We can begin to evaluate the ability of either of these mechanisms to explain the scale of the Macquarie palaeochannels by considering the catchment characteristics and timing of events. Modern Snowy Mountains hydrologic patterns (Reinfelds et al., 2014) translated to known LGM cooling would allow for a threefold increase in catchment runoff at lower altitudes. The LGM Billybingbone and Milmiland palaeochannels were four to five times larger (bankfull width and meander wavelength) than the equivalent modern Macquarie channel (Table 3). The log-linear relationship between these channel dimensions and bankfull discharge (Dury, 1976) predicts a bankfull discharge more than three times greater and therefore larger than that predicted by temperature change alone. Nevertheless, temperature could, and probably did, form part of the mix of factors operating to produce these systems. However, the observed pattern of palaeochannel size declining over time (Figs. 10 and 11) does not track the global temperature record and, therefore, temperature is not the only driver of the changes seen in the Macquarie or Gwydir catchments.

By contrast, the broad pattern of palaeochannel discharges described for the Murrumbidgee (Page and Nanson, 1996; Fig. 11D) shows large MIS 3 to early MIS 2 palaeochannels, but it is the late MIS 2 Yanco palaeochannel that is the largest on the DFS surface in its upper reach but declines markedly in width downstream. This is at least suggestive of a relationship between river discharge and temperatures in the southern Murray-Darling basin. On the basis of the available ages, there is no convincing case for synchronous palaeo-

River width at Darlington Point is shown for comparison. The vertical line at 5.5 ka marks the transition to the modern flow regime found in the Macquarie.

channel development in the Murrumbidgee, Macquarie, and Gwydir systems (most palaeochannels dated by between one and three ages, but with four ages for the Yanco palaeochannel), and this is especially true for the window around and following the LGM (Fig. 11).

A northern moisture source should have affected northern Murray-Darling basin catchments more than southern catchments. A northern moisture source in the Coral Sea may have been enhanced by warmer sea-surface temperatures (SSTs). There are some substantial similarities between the Macquarie record and the palaeohydrologic record from the Gwydir catchment (Pietsch et al., 2013) to its north (Fig. 11B): both preserve very large early to mid-MIS 3 palaeochannels, reduced but still substantial MIS 2 palaeochannels, and much smaller late Holocene channels that underwent breakdown and development of substantial floodplain wetlands. Within the limitations of the still relatively small number of OSL ages available for both systems, the ages of the Gwydir and Macquarie palaeochannels overlap at the 95% probability level (Fig. 11B and C). However, the largest palaeochannels preserved on the surface of the Gwydir DFS (Coocalla, Mia Mia) formed around 40–35 ka compared with the Quombothoo palaeochannel (Macquarie) at 54 ka. It is possible that moisture from the Coral Sea source was enhanced by warmer SSTs in MIS 3 compared with MIS 2. However, an SST record from the western margin of the Coral Sea shows a very muted temperature range over the last glacial cycle (<1.5°C) and early MIS 3 SST intermediate between interglacial and LGM values (Lawrence and Herbert, 2005). This suggests either very high sensitivity of precipitation to small SST changes within the MIS 3 window, but not in interglacials, or that additional factors remain to be identified. A possibility is that atmospheric circulation changes, independent of or in addition to SST, associated with the shoreline configuration and global climate at the time were responsible for enhanced tropical moisture reaching higher latitudes in eastern Australia.

The assembled palaeochannel and alluvial unit ages from several Murray-Darling basin and coastal New South Wales rivers have been used to suggest a history of punctuated but overall declining river discharge throughout the last glacial cycle and into the Holocene (Nanson et al., 2003). This includes an early Holocene interval (10–4.5 ka), identified as the Nambucca Phase, in which fluvial records are absent, interpreted as a phase of enhanced flow causing widespread erosion (Cohen and Nanson, 2007). An OSL-dated lakeshore record from Lake George in the Southern Tablelands of NSW (Fig. 1) confirms a period of high lake level (15–18 m depth) between 10 and 4.5 ka (Fitzsimmons and Barrows, 2010) and a record of water level and salinity from Lake Keilambete, Victoria (Fig. 1), confirms a period of high, fresh water between 8.8 and 7 ka, with prolonged contraction until around 4.5 ka, followed by low, fluctuating conditions (Wilkins et al., 2013). The large Mundadoo palaeochannel described here from the lower Macquarie DFS falls within the very last part of this interval, and a newly dated palaeochannel of the Lachlan River at Hunthawang also falls within

this gap (8.3–5.2 ka) but was the same width as the modern river (Kemp et al., 2017).

The Macquarie palaeochannels, as well as the other Murray-Darling basin palaeochannel records, show that the most profound change in river hydrology in the last 60 ka was within the Holocene. The general pattern of palaeochannel size reduction from the LGM or postglacial period to the Holocene has long been recognised (e.g., Ogden et al., 2001; Nanson et al., 2003), although Ogden et al. (2001) found poor agreement but also poor delineation of this transition in several Murray-Darling basin catchments. Our record from the Macquarie places the transition at around 5.5 ka. While the transition is not so clearly defined on the Gwydir, modern sediments were dated to the last 5.6 ka (Pietsch et al., 2013), consistent with the Macquarie. This transition, the transformation of each river at the end of a long decline, marks the onset of the modern hydrologic regime.

CONCLUSIONS

This study bolsters the fluvial chronology of the Macquarie DFS in the northern Murray-Darling basin by providing 16 SG-OSL ages from six morphologically distinct palaeochannels. Based on OSL dating, crosscutting relationships, and preservation index, 50 rivers and palaeochannels have been placed in a sequence for the Macquarie DFS, documenting the decline and fall of the Macquarie River in the late Quaternary. The new OSL ages have confirmed the high likelihood of heterogeneous bleaching in these fluvial samples, thereby improving upon the previously reported single-aliquot ages (Watkins, 1992; Yonge and Hesse, 2009) for Macquarie palaeochannels, which has wider relevance for palaeochannel studies and interpretations of DFS chronologies not only on DFS in Australia, but also elsewhere.

Our results substantially revise the chronology of morphological adjustment for the Macquarie River, in turn aiding comparisons with other Murray-Darling basin palaeochannel systems. The oldest dated Macquarie River palaeochannel (the Quombothoo, median age 54 ka) was 12 times wider and had 21 times greater meander amplitude than the modern river. Late MIS 3 and LGM (MIS 2) palaeochannels were five to seven times larger than the modern river. The transition to the modern river form (and by inference the modern hydrologic regime) followed abandonment of the smaller, but still substantial Mundadoo palaeochannel at 5.5 ka, marking the beginning of sediment accumulation at the historical terminus of the Macquarie River in the Macquarie Marshes.

There are similarities in timing and direction of change between this record and that of the Gwydir River in the northern Murray-Darling basin and, to some degree, with the Murrumbidgee River in the southern Murray-Darling basin. Together, these data support enhanced northern moisture sources, particularly during early and mid-MIS 3 in the northern Murray-Darling basin, in addition to suppressed

temperatures in controlling catchment runoff. Against this background of long-term decline, the most significant transition is the transformation of the previously continuous Macquarie River in the late Holocene to a discontinuous system forming the Macquarie Marshes. This threshold change appears to have occurred when the channel decreased to around 20 m bankfull width and 200 m meander wavelength. The historical trend described here for the Macquarie is common to many other lowland rivers in Australia, although the timing may differ. This work also shows that threshold responses to small changes around the critical flow levels required to sustain throughgoing channels can have profound impacts on fluvial geomorphology, tributary–trunk stream connectivity, and ecological status of rivers and wetlands.

SUPPLEMENTARY MATERIALS

To view supplementary material for this article, please visit https://doi.org/10.1017/qua.2018.48

ACKNOWLEDGMENTS

REFERENCES

Adamiec, G., Aitken, M.J., 1998. Dose-rate conversion factors: new data. *Ancient Thermoluminescence* 16, 37–50.

Aitken, M.J., 1985. *Thermoluminescence Dating*. Academic, London.

Aitken, M.J., 1998. *An Introduction to Optical Dating: The Dating of Quaternary Sediments by the Use of Photon-stimulated Luminescence*. Oxford University Press, Oxford.

Bøtter-Jensen, L., Andersen, C.E., Duller, G.A.T., Murray, A.S., 2003. Developments in radiation, stimulation and observation facilities in luminescence measurements. *Radiation Measurements* 37, 535–541.

Bowler, J.M., 1967. Quaternary chronology of Goulburn Valley sediments and their correlation in southeastern Australia. *Journal of the Geological Society of Australia* 14, 287–292.

Bowler, J.M., 1975. Deglacial events in southern Australia: their age, nature and palaeoclimatic significance. In: Suggate, R.P., Cresswell, M.M. (Eds.), *Quaternary Studies*. Royal Society of New Zealand, Wellington, pp. 75–82.

Bowler, J.M., 1978. Quaternary climate and tectonics in the evolution of the Riverine Plain, Southeastern Australia. In: Davies, J.L., Williams, M.A.J. (Eds.), *Landform Evolution in Australasia*. ANU Press, Canberra, Australia, pp. 70–112.

Butler, B.E., 1950. A theory of prior streams as a causal factor of soil occurrence in the riverine plain of S.E. Australia. *Australian Journal of Agricultural Research* 1, 231–252.

Cohen, T.J., Nanson, G.C., 2007. Mind the gap: an absence of valley-fill deposits identifying the Holocene hypsithermal period of enhanced flow regime in southeastern Australia. *The Holocene* 17, 411–418.

Dury, G.H., 1976. Discharge prediction, present and former, from channel dimensions. *Journal of Hydrology* 30, 219–245.

Esparon, A., Pfitzner, J., 2010. *Visual Gamma: Eriss Gamma Analysis Technical Manual. Internal Report 539*. Supervising Scientist, Darwin, Australia.

Fitzsimmons, K.E., Barrows, T.T., 2010. Holocene hydrologic variability in temperate southeastern Australia: an example from Lake George, New South Wales. *The Holocene* 20, 585–597.

Galloway, R.W., 1965. Late Quaternary climates in Australia. *Journal of Geology* 73, 603–618.

Gimeno, L., Drumond, A., Nieto, R., Trigo, R.M., Stohl, A., 2010. On the origin of continental precipitation. *Geophysical Research Letters* 37, L13804.

Hartley, A.J., Weissmann, G.S., Nichols, G.J., Warwick, G.L., 2010. Large distributive fluvial systems: characteristics, distribution, and controls on development. *Journal of Sedimentary Research* 80, 167–183.

Kemp, J., Pietsch, T.J., Gontz, A., Olley, J., 2017. Lacustrine-fluvial interactions in Australia's Riverine Plains. *Quaternary Science Reviews* 166, 352–362.

Kemp, J., Rhodes, E.J., 2010. Episodic fluvial activity of inland rivers in southeastern Australia: palaeochannel systems and terraces of the Lachlan River. *Quaternary Science Reviews* 29, 732–752.

Langford-Smith, T., 1959. Deposition on the Riverine Plain of south-eastern Australia. *Australian Journal of Science* 22, 73–74.

Langford-Smith, T., 1960. The dead river systems of the Murrumbidgee. *Geographical Review* 50, 368–389.

Larkin, Z.T., 2012. Late Holocene Channel Adjustment and Discontinuity in the Lower Macquarie River, Central New South Wales. Unpublished B. Env (Hons) thesis. Department of Environmental Sciences, Macquarie University, Sydney.

Lawrence, K.T., Herbert, T.D., 2005. Late Quaternary sea-surface temperatures in the western Coral Sea: implications for the growth of the Australian Great Barrier Reef. *Geology* 33, 667–680.

Lopes dos Santos, R.A., Spooner, M., Barrows, T.T., de Deckker, P., Sinninghe Damste, J.S., Schouten, S., 2013. Comparison of organic (UK'37, TEXH86, LDI) and faunal proxies (foraminiferal assemblages) for reconstruction of late Quaternary sea surface temperature variability from offshore southeastern Australia. *Paleoceanography* 28, 377–387.

Marten, R., 1992. *Procedures for Routine Analysis of Naturally Occurring Radionuclides in Environmental Samples by Gamma-Ray Spectrometry with HPGe Detectors. Internal Report 76*. Supervising Scientist for the Alligator Rivers Region, Canberra, Australia.

McClymont, E.L., Elmore, A.C., Kender, S., Leng, M.J., Greaves, M., Elderfield, H., 2016. Pliocene–Pleistocene evolution of sea surface and intermediate water temperatures from the Southwest Pacific. *Paleoceanography*, 31. http://dx.doi.org/10.1002/2016PA002954.

Mejdahl, V., 1979. Thermoluminescence dating: beta-dose attenuation in quartz grains. *Archaeometry* 21, 61–72.

Murray, A.S., Wintle, A.G., 2000. Luminescence dating of quartz using an improved single-aliquot regenerative-dose protocol. *Radiation Measurements* 32, 57–73.

Nanson, G.C., Cohen, T.J., Doyle, C.J., Price, D.M., 2003. Alluvial evidence of major Late-Quaternary climate and flow-regime changes on the coastal rivers of New South Wales. In: Gregory, K.J., Benito, G. (Eds.), *Palaeohydrology: Understanding Global Change*. Wiley, New York, pp. 233–258.

Nanson, G.C., Price, D.M., Short, S.A., 1992. Wetting and drying of Australia over the past 300 ka. *Geology* 20, 791–794.

Ogden, R., Spooner, N.A., Reid, M., Head, J., 2001. Sediment dates with implications for the age of the conversion from palaeochannel to modern fluvial activity on the Murray River and tributaries. *Quaternary International* 83–85, 195–210.

Olley, J.M., Murray, A.S., Roberts, R.G., 1996. The effects of disequilibria in the uranium and thorium decay chains on burial dose rates in fluvial sediments. *Quaternary Science Reviews* 15, 751–760.

Page, K., Nanson, G., Price, D., 1996. Chronology of Murrumbidgee River palaeochannels on the Riverine Plain, southeastern Australia. *Journal of Quaternary Science* 11, 311–326.

Page, K.J., Kemp, J., Nanson, G.C., 2009. Late Quaternary evolution of Riverine Plain palaeochannels, southeastern Australia. *Australian Journal of Earth Sciences* 56(S1), S19–S33.

Page, K.J., Nanson, G.C., 1996. Stratigraphic architecture resulting from Late Quaternary evolution of the Riverine Plain, southeastern Australia. *Sedimentology* 43, 927–945.

Pels, S., 1964a. The present and ancestral Murray River system. *Australian Geographical Studies* 2, 111–119.

Pels, S., 1964b. Quaternary sedimentation by prior streams on the Riverine Plain, south-west of Griffith, N.S.W. *Journal and Proceedings of the Royal Society of New South Wales* 97, 107–115.

Pels, S., 1966. Late Quaternary chronology of the Riverine Plain of southeastern Australia. *Journal of the Geological Society of Australia* 13, 27–40.

Pels, S., 1969. Radio-carbon datings of ancestral river sediments on the Riverine Plain of southeastern Australia and their interpretation. *Journal and Proceedings of the Royal Society of New South Wales* 102, 189–195.

Pfitzner, J., 2010. *Eriss HPGe Detector Calibration. Internal Report 576*. Supervising. *Scientist*. Darwin, Australia.

Pietsch, T.J., Nanson, G.C., 2011. Bankfull hydraulic geometry; the role of in-channel vegetation and downstream declining discharges in the anabranching and distributary channels of the Gwydir distributive fluvial system, southeastern Australia. *Geomorphology* 129, 152–165.

Pietsch, T.J., Nanson, G.C., Olley, J.M., 2013. Late Quaternary changes in flow-regime on the Gwydir distributive fluvial system, southeastern Australia. *Quaternary Science Reviews* 69, 168–180.

Prescott, J.R., Hutton, J.T., 1994. Cosmic ray contributions to dose rates for luminescence and ESR dating: large depths and long term variations. *Radiation Measurements* 23, 497–500.

Ralph, T.J., Hesse, P.P., 2010. Downstream hydrogeomorphic changes along the Macquarie River, southeastern Australia, leading to channel breakdown and floodplain wetlands. *Geomorphology* 118, 48–64.

Ralph, T.J., Hesse, P.P., Kobayashi, T., 2016. Wandering wetlands: the role of avulsion in historical floodplain wetland change and management. *Marine and Freshwater Research* 67, 782–802.

Ralph, T.J., Kobayashi, T., García, A., Hesse, P.P., Yonge, D., Bleakley, N., Ingleton, T., 2011. Paleoecological responses to avulsion and floodplain evolution in a semiarid Australian freshwater wetland. *Australian Journal of Earth Sciences* 58, 75–91.

Readhead, M.L., 1987. Thermoluminescence dose rate data and dating equations for the case of disequilibrium in the decay series. *International Journal of Radiation Applications and Instrumentation. Part D. Nuclear Tracks and Radiation Measurements* 13, 197–207.

Reinfelds, I., Swanson, E., Cohen, T., Larsen, J.R., Nolan, A., 2014. Hydrospatial assessment of streamflow yields and effects of climate change: Snowy Mountains, Australia. *Journal of Hydrology* 512, 206–220.

Ronge, T.A., Steph, S., Tiedemann, R., Prange, M., Merkel, U., Nurnberg, D., Kuhn, G., 2015. Pushing the boundaries: glacial/interglacial variability of intermediate and deep waters in the southwest Pacific over the last 350,000 years. *Paleoceanography* 30, 23–38.

Schumm, S.A., 1968. *River Adjustment to Altered Hydrologic Regimen—Murrumbidgee River and Paleochannels, Australia. U.S. Geological Survey Professional Paper 598*. Washington, DC.

Thomas, R.F., Kingsford, R.T., Lu, Y., Hunter, S.J., 2011. Landsat mapping of annual inundation (1979–2006) of the Macquarie Marshes in semi-arid Australia. *International Journal of Remote Sensing* 32, 4545–4569.

Tooth, S., 1999. Floodouts in Central Australia. In: Miller, A.J., Gupta, A. (Eds.), *Varieties of Fluvial Form*. Wiley, New York, pp. 219–247.

Tooth, S., 2005. Splay Formation along the lower reaches of ephemeral rivers on the Northern Plains of arid Central Australia. *Journal of Sedimentary Research* 75, 636–649.

Watkins, J., Meakin, N.S., 1996. Explanatory Notes—Nyngan and Walgett 1:250 000 Geological Sheets. Geological Survey of New South Wales, Sydney.

Watkins, J.J., 1992. Thermoluminescence dating of Quaternary sediments from the Nyngan—Walgett area. *Geological Survey of New South Wales, Quarterly Notes* 89, 23–29.

Weissmann, G.S., Hartley, A.J., Nichols, G.J., Scuderi, L.A., Olson, M., Buehler, H., Banteah, R., 2010. Fluvial form in modern continental sedimentary basins: distributive fluvial systems. *Geology* 38, 39–42.

Wilkins, D., Gouramanis, C., De Deckker, P., Fifield, L.K., Olley, J., 2013. Holocene lake-level fluctuations in Lakes Keilambete and Gnotuk, southwestern Victoria, Australia. *The Holocene* 23, 784–795.

Wintle, A.G., Murray, A.S., 2006. A review of quartz optically stimulated luminescence characteristics and their relevance in single-aliquot regeneration dating protocols. *Radiation Measurements* 41, 369–391.

Yonge, D., Hesse, P.P., 2009. Geomorphic environments, drainage breakdown, and channel and floodplain evolution on the lower Macquarie River, central-western New South Wales. *Australian Journal of Earth Sciences* 56, S35–S53.

Young, R.W., Young, A.R.M., Price, D.M., Wray, R.A.L., 2002. Geomorphology of the Namoi alluvial plain, northwestern New South Wales. *Australian Journal of Earth Sciences* 49, 509–523.

Yu, L., Garcia, A., Chivas, A.R., Tibby, J., Kobayashi, T., Haynes, D., 2015. Ecological change in fragile floodplain wetland ecosystems, natural vs human influence: the Macquarie Marshes of eastern Australia. *Aquatic Botany* 120, 39–50.

APPENDIX 3

WILEY

A nested hierarchical perspective to enhance interpretations and communication in fluvial geomorphology for use in water resources management: Lessons from the Okavango Delta, Botswana

Kirstie A. Fryirs[1] [iD] | Timothy J. Ralph[1] | Zacchary T. Larkin[1] | Stephen Tooth[2,3] | Marc Humphries[4] | Terence McCarthy[3] | Paul P. Hesse[1] | Edwin Mosimanyana[5]

[1]Department of Environmental Sciences, Macquarie University, North Ryde, NSW, Australia

[2]Department of Geography and Earth Sciences, Aberystwyth University, Aberystwyth, UK

[3]School of Geosciences, University of the Witwatersrand, Johannesburg, South Africa

[4]Molecular Sciences Institute, School of Chemistry, University of the Witwatersrand, Johannesburg, South Africa

[5]Okavango Research Institute, University of Botswana, Maun, Botswana

Correspondence
Kirstie A. Fryirs
Email: kirstie.fryirs@mq.edu.au

A key skill that geomorphologists possess is the ability to use multi-scale perspectives in their interpretations of landscapes. One way to gain these perspectives is with the use of nested hierarchical frameworks. In fluvial geomorphology, such frameworks help with assessment of large-scale controls (e.g., tectonic activity, climate change) on the pattern and dynamics of smaller-scale physical features (e.g., channels, floodplains, bars), and conversely illustrate how these smaller-scale features provide the building blocks from which to make interpretations of fluvial processes and dynamics over larger spatial and temporal scales. Given the rapid pace of technological developments, the range of relatively inexpensive tools available for visualising and mapping landscapes at different spatial scales is expanding exponentially. In this paper, which focuses on the World Heritage-listed Okavango Delta in Botswana, we demonstrate how various visualisations generated by different technologies at different spatial scales (catchment, landscape unit, reach, site and geomorphic unit) are providing critical baseline information to enhance interpretation and communication of fluvial geomorphology, with potential application in water resources management. In particular, our nested hierarchical approach could be used as an interactive communication tool for non-specialists and embedded within existing and future management plans for the Delta. The construction of nested hierarchies that synthesise information and analyses can be a valuable addition to the environmental manager's toolkit.

KEYWORDS
communicating geomorphology, geographical context, geomorphic mapping, reading the landscape, spatial analysis

1 | INTRODUCTION

Geomorphology is the scientific study of the characteristics, origin and development of landscapes. Geomorphic enquiry thus entails the description and explanation of earth surface processes, landforms and the broader landscape (Fryirs & Brierley, 2013). One of the fundamental skills of the geomorphologist lies in field interpretation of processes, process histories

and landscape evolution (Thornbush et al., 2014), and in the capacity to place site-specific perspectives and interpretations in their broader landscape context (Brierley et al., 2013; Gurnell et al., 2016). Consequently, geomorphology can be seen as an innately geographical science (Baker & Twidale, 1991; Church, 2010).

In recent years, there has been widening recognition that both global environmental change and human activities are increasing the magnitude and frequency of geomorphological hazards and placing increasing pressure on many aspects of ecosystem service delivery. This has led to a growing demand for geomorphology in many environmental management contexts, particularly river and water resources management (Brierley & Fryirs, 2008; Du Toit et al., 2003; Ralph et al., 2016). Among many issues, improved management of transboundary rivers in drylands has been identified as a key global challenge (Harris & Alatout, 2010; Turton et al., 2003; Varis et al., 2008). In the past, many such rivers have been misman-aged because decisions about channel management or water resource allocations have commonly been made in a piecemeal, isolated manner without considering the broader catchment perspective. Commonly, the lower parts of catchments are most impacted, such as where the construction of dams, sediment mining or land degradation in the upper reaches leads to alter-ations in downstream flow availability and quality, and sediment supply (Kgathi et al., 2006; Mueller & Marsh, 2002; Varis et al., 2008). Ongoing climate and land use changes may well exacerbate such problems (Pröpper & Gröngröft, 2015; Tur-ton et al., 2003). Effective, sustainable management of such rivers thus demands the application of geographical knowledge and reasoning, particularly by adopting multi-scale perspectives.

In this paper, we focus on the Okavango Delta, located in the northern Kalahari Desert of Botswana (Figure 1). The Delta is southern Africa's largest and most ecologically significant freshwater wetland (McCarthy, 2013), and in 2014 was inscribed as the 1,000th World Heritage site, partly because of its outstanding ecological diversity and hydrological charac-teristics. The Delta is supplied with water by the Okavango River, a transboundary river that arises in central Angola, crosses the narrow Caprivi Strip in Namibia, and then enters northwest Botswana where flow disperses along a network of anabranches and distributaries (Figure 1). Flow in the Okavango River is perennial but highly seasonal, largely being dependent on the intensity of summer rainfall in the headwaters (Government of Denmark and Republic of Botswana, 2006). The river is important for all three countries because there are few other permanent surface water resources in these parts of their territories. In particular, Botswana's tourism industry has grown substantially to become the country's second largest economic sector (~5% GDP) and is largely based around the Okavango Delta (BTDP, 1999; Mbaiwa, 2002; Rahm et al., 2006). However, the upstream countries of Namibia and Angola are reliant on the Okavango River for proposed
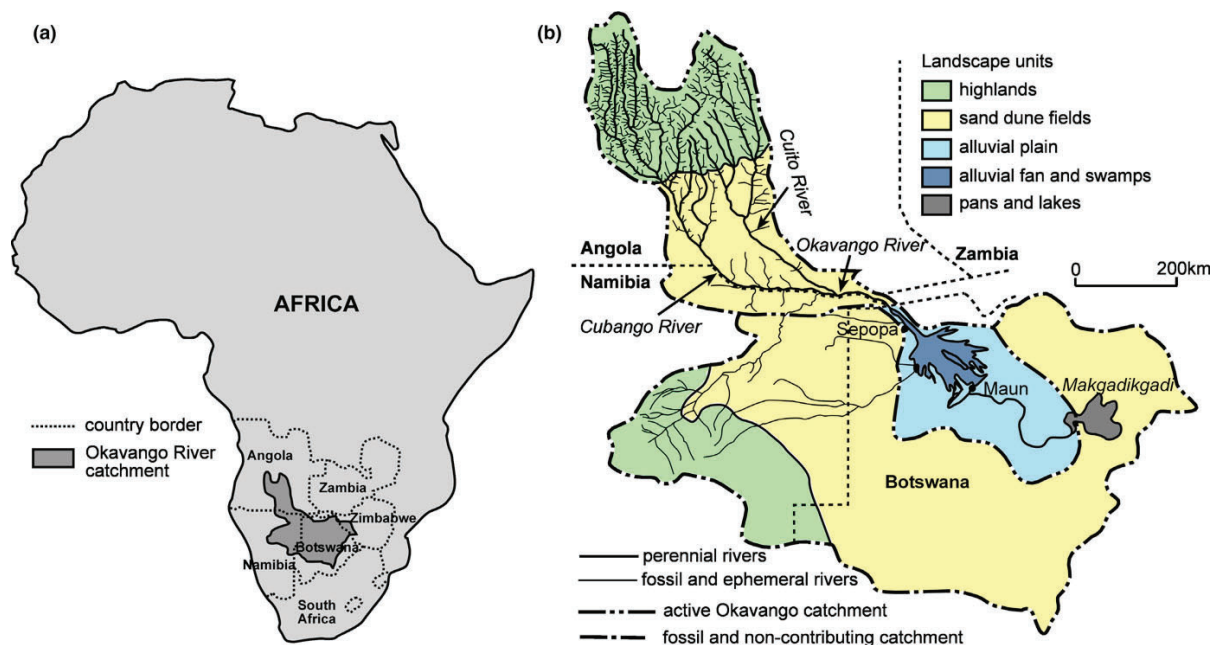

FIGURE 1   (a) Location of Botswana and the Okavango River catchment in southern Africa. (b) Okavango River catchment showing the drainage network that includes the Okavango Delta. Landscape units are also depicted. Basemap modified from figure 4 in Mendelsohn et al. (2010).

irrigation agriculture and hydropower developments. In recent years, for instance, Namibia has developed plans for a pipeline to divert water for drought relief, and for a hydropower dam upstream of the Delta (Kgathi et al., 2006; Mbaiwa, 2004; Mendelsohn et al., 2010). Prolonged civil war in Angola, which ended in 2002, has prevented significant water resources developments in the uppermost catchment, but continued agricultural expansion and potential hydropower generation are likely to impact on the river in the future (Kgathi et al., 2006; Mbaiwa, 2004; Pröpper & Gröngröft, 2015). Given these competing demands, management of the water resources in the Okavango catchment has had a long and contested history (Jansen & Madzwamuse, 2003; Mbaiwa, 2004; Rahm et al., 2006; Turton et al., 2003). The Permanent Okavango River Basin Water Commission (OKACOM) is the authority established in 1994 by Angola, Namibia and Botswana to manage the river basin (Mendelsohn et al., 2010; OKACOM, 2017).

Against this backdrop, the aims of this paper are to: (1) outline the importance of perspectives and visualisation in geomorphic interpretations of landscape, and in particular the value of a nested hierarchical perspective for gaining geographical context and communicating geomorphology; (2) document the range of data collection, visualisation and mapping tools used by our research team to build our nested hierarchy for study of the Okavango Delta;[1] (3) demonstrate how this hierarchical approach can be used to enhance geomorphic interpretations in the Panhandle region of the Delta; (4) discuss how the resulting multi-scale perspective can provide a useful tool for communicating geomorphology to non-specialists, potentially including practitioners and policy makers who work in water resources management in the Delta; and (5) outline the broader implications and potential developments of our research approach in transboundary river catchments and other environmental management contexts.

1.1 | Perspectives and visualisation in geomorphic interpretations of landscape

A key aim of the geomorphologist is to "read the landscape", namely by using field and other spatial datasets in order to build a picture and interpret the system under investigation (Fryirs & Brierley, 2013). This requires landscape observation from different perspectives and at different spatial scales, and the use of theory and concepts in spatial and temporal context (Bishop et al., 2012; Gregory & Lewin, 2015; Phillips, 1988). Field scientists in particular often develop an intuitive feel for landscape that may sit outside, but that may certainly overlap with and complement, formal abductive, inductive and deductive reasoning. These three routes to scientific explanation are essentially what geomorphologists aspire to do as part of more "mature explanation" in geosciences (Kleinhans, 2010, p. 290).

The spatial scale at which observations are made not only constrains what is seen, but dictates how and what is interpreted (Bishop et al., 2012). Maximising the range and number of perspectives on the landscape before going to the field, and more importantly while in the field, is therefore critical for providing geographical context for subsequent interpretations (Thornbush et al., 2014). For example, measuring the grain size characteristics of sand on a point bar provides a very different perspective from an aerial view of a sequence of meander bends from a helicopter, but both are necessary for a comprehensive, holistic interpretation of fluvial morphodynamics. Clearly, the lens through which we view a landscape is critical for understanding and interpreting it (Tooth et al., 2016).

With rapid technological advances, the range of tools for visualising and mapping the landscape, and for gaining multiple perspectives in the field, is expanding exponentially (e.g., Tooth, 2015; Williams et al., 2017) (Table 1). In many ways there has been a revolution in the way that geomorphological research is conducted (Bishop et al., 2012; Tooth et al., 2016). Whereas early geomorphologists might have headed out into the field with a map, a compass and a shovel, the backpack of the modern geomorphologist may be filled with a much greater range of technology. Commonly, Google Earth or other software with high-resolution satellite imagery is used on a tablet or mobile phone, unmanned aerial vehicles with cameras and other sensors are deployed at field sites to produce imagery and digital terrain models, terrestrial laser scanners (TLSs) survey millions of points in minutes, and cameras with panoramic and 360° recording capabilities provide wide-angle digital images and video footage (Table 1).

Nonetheless, there is still a real need for "old-fashioned" techniques that can be used to complement or enhance data gathered using new technology (Table 1). It is critical that the modern geomorphologist maintains an innate geographic ability to interpret the landscape by gathering new data and generating new visualisations, and supplements these with on-the-ground evidence from soil profiles or bank exposures dug with shovels, cores recovered with drill rigs or augers, and cross sections surveyed with total stations or automatic levels (Thornbush et al., 2014). The traditional way of doing things is often the only available option in remote or difficult terrain (e.g., densely vegetated or areas with no signal reception). Most importantly, we must remember that no new technology will do the geomorphic interpretation (Tooth, 2015).

TABLE 1 Examples of the range of techniques available to visualise and map landscapes across spatial scales

Technique	System component	Utility	Scale of observation	Observation extent (km²)	Graphic key of observation extent (km²)
1 Satellite imagery	Catchments, landscape units, reaches	Inundation, land cover	1:1,000,000 to 1:100	1,000,000 to 1 km²	
2 Aerial photographs and orthophoto mosaics	Catchments, landscape units, reaches, sites	Inundation, land cover, topography	1:1,000,000 to 1:1,000	1,000,000 to 10 km²	
3 Topographic maps	Catchments, landscape units, reaches, sites	Land cover, topography	1:1,000,000 to 1:1,000	1,000,000 to 10 km²	
4 Geomorphic maps	Reaches, sites, geomorphic units	Land cover, topography, geomorphic units	1:100,000 to 1:10	100,000 to 0.1 km²	
5 River and wetland maps	Reaches, sites, geomorphic units	Geomorphic units, hydraulic units	1:100,000 to 1:10	100,000 to 0.1 km²	
6 DGPS	Reaches, sites, geomorphic units	Topography, longitudinal profiles, cross sections, surface samples	1:100,000 to 1:10	10,000 to 0.1 km²	
7 Aerial laser and optical surveys	Reaches, sites, geomorphic units	Topography, longitudinal profiles, cross sections, surface samples	1:100,000 to 1:10	10,000 to 0.1 km²	
8 Terrestrial laser and optical surveys	Reaches, sites, geomorphic units	Topography, longitudinal profiles, cross sections, surface samples	1:1,000 to 1:10	100 to 0.1 km²	
9 Site maps	Sites, geomorphic units	Surface samples, profiles (pits, bank exposures and cores)	1:100 to 1:10	10 to 0.1 km²	

1.2 | Nested hierarchical perspectives on landscape and use in communicating geomorphology

One way to gain various perspectives is with the use of nested hierarchical frameworks (e.g., Brierley & Fryirs, 2000; Dollar et al., 2007; Frissell et al., 1986; Gurnell et al., 2016; Poole, 2002). Nested hierarchies provide a framework with which data can be synthesised, managed and used for targeted sampling and data collection at various spatial scales. In fluvial geomorphology, such frameworks have been used for decades and facilitate the assessment of large-scale controls on the pattern and dynamics of smaller-scale channel features, while also illustrating how smaller-scale features provide the building blocks from which to make interpretations of fluvial processes and changes over larger scales (Brierley & Fryirs, 2000, 2005; Fryirs & Brierley, 2013; Gurnell et al., 2016). Nested hierarchical frameworks are scaffolded such that structures and processes that operate over small spatial and temporal scales are constrained by, or nested within, boundaries set by structures and processes that operate over larger spatial and temporal scales (de Boer, 1992; Gumbricht & McCarthy, 2003; Phillips, 1988; Schumm & Lichty, 1965). These frameworks provide the means for making bottom-up, constructivist interpretations of forms and processes, while also enabling top-down analyses of their controls (Brierley, 1996; Brierley & Fryirs, 2005).

When used effectively, nested hierarchical frameworks provide an elegant way to frame geographical perspectives, organise scientific data and information, and make more insightful and sophisticated interpretations of landscape that are placed within appropriate spatial context (Dollar et al., 2007). Possibly more important, and less well explored to date, is the potential use of nested hierarchies as conceptual and visualisation tools for communicating geomorphology to non-specialist audiences, whether they be school children, landowners, practitioners or policy-makers (Brierley, 2009; Gregory & Lewin, 2015; Vervoort et al., 2014). Such perspectives, interpretations, and communication approaches can thus feed into river and water resources management (Brierley & Fryirs, 2005, 2008; Du Toit et al., 2003). In the sections below, we document the range of data collection, visualisation and mapping tools used by our research team in constructing the nested hierarchy and producing a visual product for use in the Okavango Delta.

2 | STUDY AREA

Geomorphologically, the Okavango Delta (Figure 1) is a large alluvial fan (c. 12,000 km^2) composed of two main geomorphic domains: the relatively confined (up to 12 km wide) depression known as the Panhandle, where the Okavango River and its anabranches meander through permanent swamps; and the broader (up to 120 km wide) Fan, where water and sediment are dispersed through several large stable sinuous to straight distributary channels that feed both permanent and seasonal swamps (Tooth & McCarthy, 2004). In the southern, peripheral region of the Delta, periodic high discharges enter the Boteti River, with flow sometimes continuing as far as the Makgadikgadi depression with its lacustrine basins (see Gumbricht et al., 2001).

Through the Panhandle, the Okavango River declines in size from ~90 to ~50 m wide, owing to water loss to surrounding swamps and to evapotranspiration (McCarthy, 2013; Tooth & McCarthy, 2004). The channel is highly sinuous and characterised by regular and irregular meanders, scroll bars, cutoffs and point bars. Dense vegetation (principally *Cyperus papyrus* and *Phragmites* spp.) lines the main channel and its anabranches, and plays a significant role in stabilising banks and regulating lateral flow losses from the channels. Bank erosion is most pronounced in the upper Panhandle where the river intersects an elevated (~5–10 m) scarp overlain by Kalahari sand. The river is anastomosing in the central Panhandle, where the Filipo channel breaks from the eastern bank of the Okavango River to create a branch that eventually rejoins the Okavango ~26 km downstream. Avulsion is common in this reach (McCarthy et al., 1992; Smith et al., 1997). Our overall research project is focusing in particular on characterising the avulsion dynamics in this reach, as well as the processes driving channel abandonment and failure, but here we focus more on the methodological and applied aspects of our project.

3 | APPROACH AND RESULTS

The various techniques available to geomorphologists (Table 1), and the images or data they produce, can be arranged in a hierarchical manner to capture and display the range of geographical perspectives for any given system. In our study of the Okavango Delta, we used the techniques and technology outlined in Table 2 to build a hierarchy of geomorphic information with five nested spatial scales (Figure 2): catchment; landscape unit; reach; site (sub-reach); and geomorphic unit

FIGURE 2   A nested hierarchical perspective for use in interpretation and communication of the fluvial geomorphology of the Okavango Delta. Sources of each visualisation are noted in Table 2. A version of this Figure is available as Supporting Information for viewing at larger size.
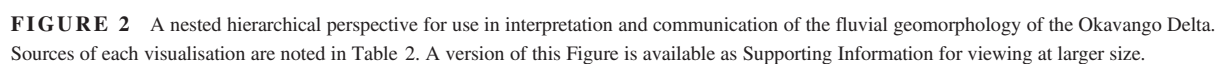
TABLE 2 Technique, technology and software used to capture data and thus visualise the landscape at different spatial scales in the nested hierarchy for the Okavango Delta

Spatial scale Image/data	Technique or technology used to produce image/data (brand, edition etc.)	Software used to process image/data
Catchment scale		
(a) Catchment map	Compiled from Landsat imagery in conjunction with a low-resolution differential GPS survey (30 m cell size)	Original: ESRI software Compilation and addition of landscape units: Macromedia Freehand MX
Landscape unit scale		
(b) Imagery	Google Earth (2.5 m cell size), Garmin Birdseye satellite imagery (sub-metre cell size)	Original: Google Earth Compilation: Macromedia Freehand MX
(c) Topography/digital elevation model	NASA Shuttle Radar Topography Mission (SRTM) 90 m data set	ESRI software
(d) Flow inundation map	NOAA AVHRR satellite data (1 km^2 resolution), ERS-ATSR and composite Landsat MSS/TM data	ESRI software
(e) Land cover classification	Landsat TM/MSS and MODIS imagery (30 m cell size)	ESRI software
Reach scale		
(f) Reach map with sites	Garmin Birdseye satellite imagery (as above), ESRI Basemap satellite imagery, Google Earth (2.5 m cell size), aerial photographs 1:40,000	ArcMap
Site scale		
(g) and (h) Panoramic photographs	Digital camera still photographs (12 megapixel)	Photoshop CS5 and Kolor Autopano Giga 3.5
(i) 3D digital elevation model using Structure from Motion (SfM)	Phantom 2 RPA, oblique RGB images	Agisoft PhotoScan Professional 1.2.6
(j) and (k) 360° panoramic photos and video	360fly camera with eight element glass ultra-fisheye lens (aperture: F2.5; field of view: 240°; focal length: 0.88 mm; video resolution: 1,504 × 1,504 29.97 fps)	360fly Desktop Director
(l) Cross sections	100 m measuring tape and clinometer, Garmin Birdseye satellite imagery (as above)	Microsoft Excel, Microsoft PowerPoint
Geomorphic unit scale		
(m) Sediment column	Geoscience Australia field texture guide	Microsoft PowerPoint
(m) Bank exposure and pit sediment sampling (OSL, bulk density, sedimentology)	Spade, Dormer push-tube sampler, mallet and anvil	Microsoft PowerPoint
(n) Channel velocity profiles	Universal Current Meter F1 with 4 m pole extension (measuring range: 0.025–10 m/s)	Microsoft Excel, Microsoft PowerPoint
(o) Channel cross sections	Sonar depth reader, Bushnell Laser 450 range finder (range: 5–999 m; accuracy: ±1 m)	Microsoft Excel, Microsoft PowerPoint
(p) Bedload sampling	Van Veen Grab bedload sampler	Microsoft PowerPoint
(q) Water levels	Trimble GPS Pathfinder ProXRT Receiver connected to a dual frequency GNSS antenna (accuracy: ±3–10 cm)	Trimble TerraSync software, Microsoft Excel

(landform). Our hierarchical framework differs slightly from existing frameworks (e.g., Brierley & Fryirs, 2005) in that we focus more on the site (sub-reach) scale and eliminate the smaller hydraulic unit (habitat) scale. This is because our research in the Okavango aims to analyse, interpret and communicate geomorphology mainly at the geographical scales of reaches and sites, and the analytical techniques we employed were chosen specifically to capture data and information most

relevant to these scales. While the structure of the nested hierarchy remains similar to the published examples from other geographical contexts (e.g., Brierley & Fryirs, 2000, 2005; Frissell et al., 1986), we have compiled the datasets and images in such a way that the content of each "box" is a visual illustrating the types of outputs produced from the mix of traditional and newer technologies (Figure 2). As addressed in the following sections, the resulting multi-scale perspectives allow us to enhance interpretations of the fluvial geomorphology of the Okavango Panhandle, and to communicate the insights to non-specialists, potentially including practitioners and policy-makers in water resources management. To aid with the communication aspects, we have constructed an interactive version of Figure 2 using the online presentation software suite, *Prezi*; this can be viewed at https://prezi.com/view/51UpgNhfKS1unm2NOM1L/ and in the Supporting Information, Data S1.

An outline of the five nested spatial scales in our hierarchy and the main resulting visual products is presented in the following sections.

3.1 | Catchment scale

Catchments (also called drainage basins or watersheds) are topographic and hydrological entities that have been described as the fundamental geomorphic unit (Chorley, 1969). Catchments can be divided into sub-catchments. Analyses at the (sub-)catchment scale set the context for smaller-scale investigations, particularly by providing valuable insights into the boundary conditions within which rivers operate (Brierley & Fryirs, 2005). For example, (sub-)catchment geology is a key control on the sediment transport regime, and (sub-)catchment morphometry (including size, shape, relief, drainage density and pattern, and connectivity) is a key control on the hydrological regime. When combined with analyses of regional climate, these (sub-)catchment-scale controls influence the flow–sediment–vegetation morphodynamics of rivers operating at finer scales in the hierarchy.

At the catchment scale, catchment maps were compiled and combined to produce Figure 2a and gain perspective on the size of the Okavango catchment (~156,250 km^2), the arrangement and shape of the sub-catchments (elongated in both the north and west), the drainage pattern (parallel and trellis like in the upper catchment, transitioning to dendritic and distributary in the Delta), the geological structure (e.g., position of faults), and the drainage density (higher upstream, lower downstream) (McCarthy, 2013). This perspective places the Okavango Delta in context, both in terms of position in the catchment and the morphometrics of the contributing (sub-)catchments.

3.2 | Landscape unit scale

Landscape units are sometimes called physiographic compartments or land systems units (Cooke & Doornkamp, 1990). They are areas of relatively homogenous topography, morphology and relief. Examples of landscape units are plateaus, escarpments, rounded hills, lowland plains and deltas. They are macro-landscape features that control, amongst other things, the slope and lateral confinement of rivers. Their position and pattern within a catchment dictate the sequencing of process zones (i.e., production, transfer and deposition zones; Schumm, 1977) and the pattern of valley settings within which river reaches occur at the next finer scale in the hierarchy (Fryirs et al., 2016).

At the landscape unit scale, several types of visual outputs were produced. Five different landscape units were identified based on their topography and morphometry (Figure 2a). These include highlands that extend up to 1,800 m above sea level, sand dunefields, alluvial plains, alluvial fan and swamps at around 1,000 m above sea level, and pans and lakes. This map provides a basis from which spatial terrain analysis could be undertaken to extract and analyse quantitative geomorphic metrics such as slope, valley confinement and profile concavity (Fryirs et al., 2016; Partridge et al., 2010; Perron & Royden, 2013). This map provides additional context for placing the Okavango Panhandle and Delta in topographic and landscape position. Google Earth and Garmin Birdseye satellite imagery provide a spectacular perspective of the alluvial swamps and fans in the Okavango Delta and neighbouring Kwando system, the adjacent alluvial plain and Kalahari sand dunefields, and various pans and lakes that dot the region (Figure 2b). NASA Shuttle Radar Topography Mission (SRTM) data were used to derive a digital elevation model (DEM) which highlights the morphology of the Panhandle, the pattern of ridges and depressions on the Delta surface, and sand dunes in the west (Figure 2c; McCarthy, 2013). A map of flow inundation (Figure 2d), produced from NOAA AVHRR satellite data (1 km^2 resolution) and ERS-ATSR and composite Landsat MSS/TM data, depicts the flooding frequency (in %) for different areas of the Panhandle and Fan. On this map, black areas are almost permanently inundated, with seasonal and quasi-seasonal flooding occurring in areas depicted in shades of grey (Gumbricht et al., 2004; McCarthy et al., 2003). Landsat satellite imagery was also used to map the

distribution of land cover and ecoregions (Figure 2e), as derived from a combined statistical and contextual rule-based post-classification (McCarthy et al., 2005).

3.3 | Reach scale

Reaches are sections of river along which flow and sediment load are sufficiently uniform to enable maintenance of near-consistent or characteristic forms and associated processes (Brierley & Fryirs, 2005; Kellerhals et al., 1976). Alternating patterns of reaches are referred to as segments (Frissell et al., 1986). For rivers, reaches are often differentiated by channel planform and the assemblages (packages) of finer-scale geomorphic units (landforms) that comprise them.

At the reach scale in the Panhandle, Google Earth and Garmin Birdseye satellite imagery (along with aerial photographs, not shown) were the primary means of visualisation (Figure 2f). Other pre-existing geomorphic maps of the Panhandle were also used (not shown, but for examples see Smith et al., 1997 and McCarthy, 2013). These maps are invaluable as tools for analysing the morphology of the Panhandle relative to adjacent landscape units, channel planform attributes, and the relative extent of channels and floodplains, and also provide insight into the distribution and morphology of palaeochannels, permanent swamps and various active channels. When accompanied with air photograph sets or a temporal sequence of Google Earth images, analyses of historical channel avulsion and migration can be undertaken.

3.4 | Site and geomorphic unit scales

In our study, sites were defined at the sub-reach scale and may occur along river channels and on floodplains. To capture the range of geomorphic units that make up river reaches requires analysis of numerous sites. Selecting the correct sites to undertake more detailed analysis, that are representative, or that capture the range of variability, is critical if interpretations are to adequately reflect the morphodynamics occurring in the system.

Geomorphic units, also called landforms, are the building blocks of rivers and the surrounding landscapes Evans (2012). Each geomorphic unit is created by certain process–form interactions at particular positions in landscapes, and units may have differing material properties (Brierley & Fryirs, 2005; Fryirs & Brierley, 2013). Units may comprise erosional or depositional forms, and the mix of geomorphic units (called an assemblage) that occurs along a river reach is dictated by the range of processes occurring along that reach. This range of processes determines river behaviour. When considering the global diversity of rivers, there is a spectrum of in-stream and floodplain geomorphic units that occur in different types of river reaches and valley settings. Channel geomorphic units range from bedrock-influenced features such as cascades and rapids, through to mid-channel depositional features such as longitudinal bars, to bank-attached depositional features such as benches or point bars, to fine-grained sculpted features such as scour pools and planar riffles (see Fryirs & Brierley, 2013; Wheaton et al., 2015). Floodplain geomorphic units also span a spectrum from homogenous, discontinuous pockets with limited relief, to complex, more continuous surfaces that may comprise landforms such as levees, backswamps, chute channels and crevasse splays.

At the site and geomorphic unit scale in the Okavango Panhandle, the set of techniques and methods used was the most extensive. At the site scale, the most impressive and transformative perspectives were those gained from the air. Aerial surveys from a helicopter (Figure 2g,h) provided an unparalleled perspective of individual sites and their geomorphic unit assemblages, as well as their position relative to other sites, reaches and landscape units. Additional perspectives were gained from Unmanned Aerial Vehicle (UAV)-derived data and analysis using Structure from Motion (SfM),[2] which allows for 3D digital terrain analysis at a much greater level of detail than manual topographic surveys (Figure 2i). At these scales, we also utilised a range of other visualisation techniques, including panoramic and 360° cameras mounted to boats to gain live video and still images of the trunk stream and tributary networks (Figure 2j,k). These videos were calibrated against GPS and topographic survey data to gain insights into downstream changes in channel width along the Panhandle. By capturing continuous video footage from a helicopter, a longitudinal perspective of floodplain and channel/palaeochannel character across the Panhandle was gained and was used to place still, oblique aerial photography in context. Floodplain transects were surveyed using tape and clinometer survey techniques (Figure 2l), but alternatively could have been completed using a digital theodolite, automatic level or TLS.

The perspectives gained and mapping undertaken at coarser scales in the nested hierarchy were used to select locations in the Panhandle for more detailed geomorphic unit analysis. At this scale, more traditional techniques complement analyses undertaken using new technology, both in the field and in the laboratory. Standard sediment analysis was used to document the sedimentology of floodplains from pit and bank exposures. These data are visualised by constructing sediment columns (logs) (Figure 2m). Sediment samples were collected for treatments, including bulk density and grain sizing.

Samples for optically stimulated luminescence (OSL) dating were extracted using coring and augering equipment (Figure 2m). When analyses are completed, these data will be added to the sediment columns to assess vertical trends in sedimentology, quantify sedimentation rates in different parts of the Okavango Panhandle, and interpret overall geomorphic development. At numerous locations along the Okavango River and its anabranches, channel cross sections were surveyed and a velocity meter used to determine flow characteristics (Figure 2n). Velocity data are presented as isovel maps (Figure 2o) and are used to calculate relative discharges through different channels. Bed load sampling was undertaken in each channel to assess sediment transport characteristics (Figure 2p). A Trimble GPS Pathfinder ProXRT Receiver connected to a dual frequency GNSS antenna was used at multiple sites in the Panhandle to determine channel water levels (Figure 2q). When compared with historical water levels and calibrated against gauged discharge data, water-level changes will be mapped and used to aid interpretations of geomorphic adjustments.

4 | INTERPRETATIONS AND DISCUSSION

4.1 | Using the hierarchical approach to enhance geomorphic interpretations in the Okavango Panhandle

One challenge for the modern day geomorphologist is to know where to focus data collection to address the right questions (Lisenby & Fryirs, 2017). Vast amounts of data can now be easily generated using new technologies, but the risk is that data are gathered in the absence of a fundamental research question or hypothesis. Without careful consideration of what data are being collected, and at what scale and resolution, the problem of extracting information that captures the essence of character or functionality of a landscape is thus simply transferred from the field to the computer laboratory. This runs the risk of vital parts of the puzzle being missed or misinterpreted, without any new insights being generated. In our study, we have developed an organisational framework (the nested hierarchy) for the Okavango Delta that contains essential data and information for undertaking more detailed interpretations and explanations of the fluvial geomorphology. Using our interactive version of Figure 2 in *Prezi* we can dynamically visualise the Okavango from a range of different geographical perspectives, and at different scales in the hierarchy. Here we briefly discuss an application of this approach to assess patterns and processes of channel change that are a critical part of the fluvial geomorphology of the Panhandle, including those changes occurring at the landscape scale and at the finer scales of reaches and sites.

Previous on-the-ground observations and measurements have shown that there is a significant overall downstream decrease in the size of the Okavango River and its distributaries through the Panhandle and Fan (Tooth & McCarthy, 2004). To date, however, it has been unclear whether the channel decreases in size in a predictable manner downstream or whether there are variations in channel size at a finer scale. With the use of our hierarchical framework and additional high-resolution data gathered using new technology, we can enhance our insights and interpretations. At the landscape unit scale, the Okavango River trunk stream has a nearly constant longitudinal gradient in the Panhandle (Figure 3a). Relatively coarse-resolution channel width analyses derived from field measurements by Tooth and McCarthy (2004) show that the river has a broadly uniform downstream decrease in width over a reach ~85 km long (Figure 3b). Higher-resolution measurements in the same reach using 2004 Google Earth imagery, however, show that channel width is highly variable, both decreasing and increasing, while the overall downstream width decrease is still observed (Figure 3c). The overall downstream channel width decrease is therefore not a simple linear relationship, but shows a step change from 1.2 to 0.26 m/km at 70 km downstream from Shakawe. The step-like manner in which channel width changes in this reach is due to finer-scale reach or site controls, including losses or gains of water at channel bifurcations of confluences (Figure 2h), development of point bars (Figure 3d,e), and low levees that flank parts of the channel that do not have floating aquatic vegetation along their margins (Figure 3f).

At the reach scale (Figure 2f), some channels in the Panhandle are more sinuous than others and it is clear that some channel sections have become connected or disconnected due to meander bend cutoff (Figure 3g) and avulsion. Techniques employed at reach and site scales, including oblique aerial photography and video footage, reveal that vegetation (e.g., *Vossia cuspidata*) encroaches far into the channels in certain locations. Confirmation is provided by UAV-derived 3D terrain data using SfM (Figure 2i), which show vegetation bordering and encroaching into the channel on the inside of some bends, and in straight reaches downstream of major bifurcation points where flow has divided between two channels. Boat-level observations of channel form, and cross-section measurements of channel width, flow velocity and discharge provide additional data to confirm the patterns and processes of channel size change (Figure 2j). At the geomorphic unit scale, channel cross-sectional area, flow velocity and bedload measurements can be compared, highlighting the links between channel size, flow and sediment transport (Figure 2n,o,p). For instance, downstream channel size changes are largely the
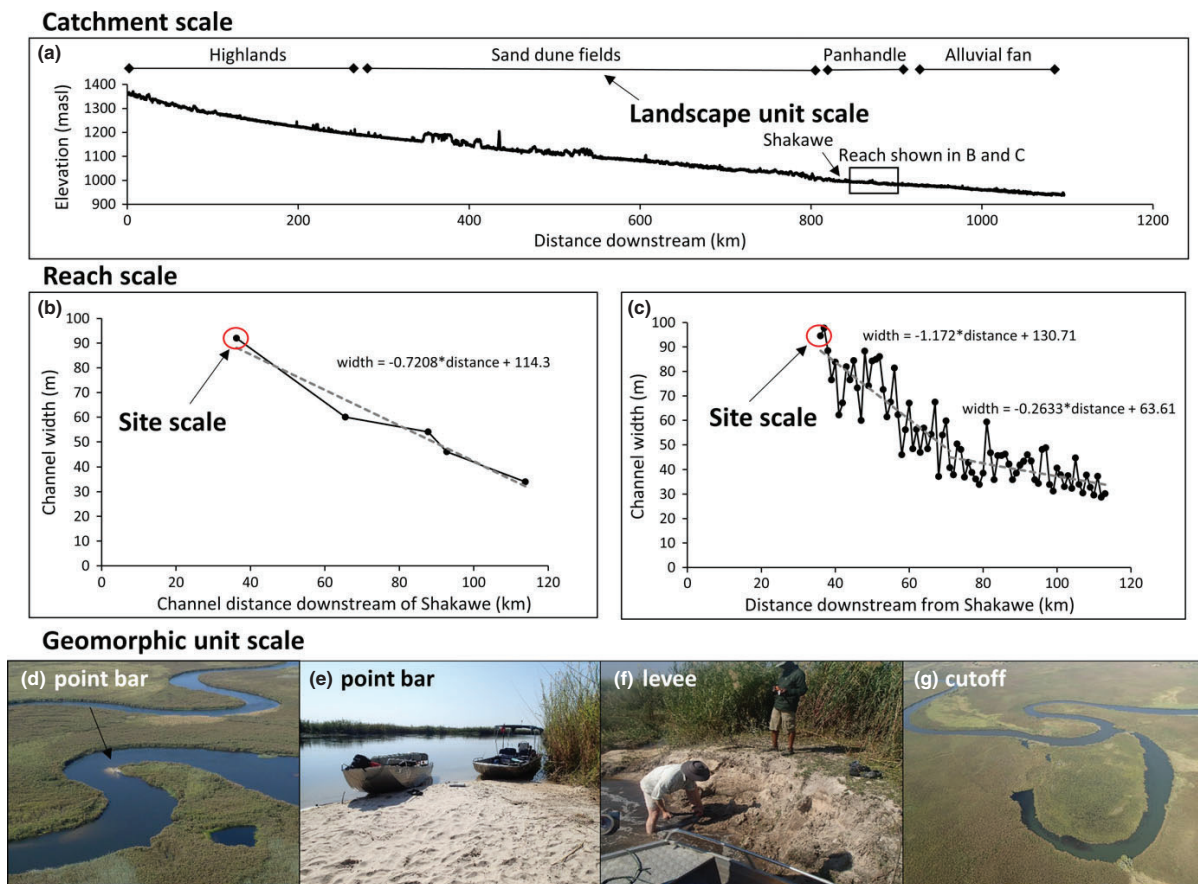
FIGURE 3 Hierarchical framework highlighting how the use of new technology can enhance our understanding of the Okavango River in the Panhandle. (a) Longitudinal profile of the Okavango River extracted from SRTM data (30 cm cell size). (b) Reach scale pattern of downstream decrease in channel width as measured by Tooth and McCarthy (2004). Note the approximately constant rate of overall width decrease. (c) High-resolution channel width data from the same reach as (b), obtained using Google Earth satellite imagery from the year 2004. Note the high level of variability in channel width and the step change in the rate of overall width decrease that is not apparent in Tooth and McCarthy's (2004) coarser resolution data. (d) Image of a point bar from the air. Flow direction is from middle right to lower left. (e) Image of a point bar on the ground, looking downstream. (f) Image of a breached levee on the main channel. During floods, flow direction is away from the camera. (g) Image of a meander cutoff from the air. Flow direction is from left to right. A version of this Figure is available as Supporting Information for viewing at larger size.

result of increases or decreases in channel width, with depth and velocity showing fewer changes (Tooth & McCarthy, 2004). In markedly narrowing channels, however, sediment transport rates decrease, which leads to partial infilling. This promotes increasing diversion of flow through the porous, vegetated channel margins, leading to decreases in flow velocity and further vegetation encroachment. Ultimately, this can lead to channel abandonment and avulsion (McCarthy et al., 1992; McCarthy, 2013). In summary, for this reach in the Panhandle, a multi-scale perspective has provided a higher-resolution dataset that can be used to enrich previous interpretations into downstream channel size changes and their role in avulsion.

4.2 | Using the hierarchical approach to communicate geomorphology and better inform water resources management in the Okavango Delta

One overarching benefit of adopting a multi-scale perspective through the development of a nested hierarchical framework is to help non-specialists and decision-makers understand more fully how various parts of the system fit together and interact across scales, thereby enhancing insight into the functionality of the system as a whole (Brierley, 2009; Gregory & Lewin, 2015; Vervoort et al., 2014). In the Okavango catchment, for instance, there is a current, pressing need to

understand the impacts of climate change, land use changes and water resource developments (e.g., dams, weirs, extensive extraction) in Angola, Namibia and Botswana on total annual flow volumes, seasonal flow variability, water quality, and sediment and nutrient loads in the Delta (Government of Denmark and Republic of Botswana, 2006; Kgathi et al., 2006; Pröpper & Gröngröft, 2015). These natural and human drivers, operating in large part at the catchment and landscape unit scales, influence the reach, site and geomorphic unit scale relationships between flow, sediment, vegetation and other biota that underpin the ecological diversity and other ecosystem services in the Delta (Hamandawana & Chanda, 2010; Jansen & Madzwamuse, 2003; Mendelsohn et al., 2010). Analyses by Andersson et al. (2006) and Pröpper and Gröngröft (2015) of the impacts of climate change and development scenarios on the Okavango catchment indicate that in the long term, climate change will considerably reduce mean annual flow and increase flow variability, but in the short to medium term, the impacts of potential increases in irrigated agriculture, hydropower dam building and flow diversion are likely to be much more marked. An obvious impact of dam building and large irrigation diversions will be reduced peak flooding in the Okavango Panhandle and Fan, thereby threatening the maintenance of complex wetland ecosystems. Due to the pronounced dry season experienced in the south of the catchment during winter, such developments may also exacerbate natural seasonal variability, which may have ramifications for wetland ecosystems and human communities in an already water-stressed environment (Jansen & Madzwamuse, 2003; Kgathi et al., 2006; Pröpper & Gröngröft, 2015). A less obvious, but no less insidious, impact of dam or weir building is a reduction in downstream sediment flux. As noted above, sedimentation within channels in the Delta plays a role in channel avulsion, for this promotes loss of water from the channel to the surrounding swamps, facilitating a decrease in flow velocity, vegetation encroachment and ultimately channel failure (Government of Denmark and Republic of Botswana, 2006). Avulsion leads to water, sediment and nutrient dispersal, rejuvenating parts of the wetlands and promoting biodiversity (Kgathi et al., 2006; McCarthy & Ellery, 1998; McCarthy et al., 2012). Other abandoned channels may become filled with fine sediment to create topographically elevated ridges that often give rise to tree-covered islands, and these also play a fundamental role in the functioning of the Okavango through their influence on water salinity, nutrient concentrations and habitat diversity (McCarthy et al., 2012). Overall, a significant change in sediment flux from the upstream catchment may translate to changes in sedimentation rates linked to avulsion processes in the Delta.

At reach, site and geomorphic unit scales, therefore, it is important to recognise that the relationships between flow, sedimentation and vegetation growth that underpin processes such as avulsion ultimately create a complex mosaic of landforms within a broader context, and so cannot be assessed and managed in isolation or without spatial context (Kgathi et al., 2006; Mendelsohn et al., 2010). In transboundary rivers in particular, recognition and accommodation of these multi-scale linkages in catchment development planning is thus essential to avoid cross-border and within-country conflicts (Harris & Alatout, 2010; Mendelsohn et al., 2010; Turton et al., 2003). Throughout the Delta in Botswana, for instance, many local communities and tour companies site their accommodation on river frontages and require access to the channels for transport (Jansen & Madzwamuse, 2003; Pröpper & Gröngröft, 2015). Any potential changes to channel location that may result from avulsion are seen as a threat, and so efforts are commonly made to clear channels and keep them "locked" in position, without any consideration of the potential consequences for reaches downstream where similarly close relationships between channel position, local communities and tourism companies may exist (Kgathi et al., 2006; Mendelsohn et al., 2010). Adopting a multi-scale perspective and constructing nested hierarchies may help people to recognise that local (e.g., site and short reach scale) geomorphological processes can thus have important effects at the longer reach or landscape unit scale. Attempts to restrict the movement of avulsion-prone channels may succeed in the short term, but are likely to fail in the medium to long term and also risk imposing "unnatural" flow regimes in parts of the wetlands. While this is generally recognised in regional and national management plans for the Delta, there tends to be only tacit acknowledgement of the importance of adopting such perspectives at the local scale (Jansen & Madzwamuse, 2003; Mendelsohn et al., 2010; Pröpper & Gröngröft, 2015; Turton et al., 2003). Formal use of hierarchical frameworks potentially can help such multi-scale, geographical perspectives to be embedded more fully in decision-making and planning, including projects, monitoring and management plans developed under OKACOM (Mendelsohn et al., 2010).

4.3 | Possible developments of the hierarchical approach for communicating geomorphology and using scientific insights in management

We recognise that Figure 2 is a static characterisation of the Okavango at each scale, but our interactive version using *Prezi* introduces a new element of dynamic observation through a flexible and navigable system of multimedia files (maps, photographs and videos). In an era of rapid technological developments, such approaches and syntheses provide new and

exciting ways of contextualising and visualising landscapes, and communicating geomorphology (Tooth et al., 2016). Within and beyond the Okavango catchment, this has many potential benefits for end user engagement and other outreach activities (Vervoort et al., 2014). For instance, while new technology allows faster data capture over larger areas and with greater precision than ever before, the use of a nested hierarchy provides the framework for synthesising and visualising pre-existing and new datasets in an integrated, coherent manner. This opens up great opportunities for public communication of geomorphology, such as how river systems are structured and function at, and across, different spatial scales (cf. Vervoort et al., 2014). In addition, these technologies are helping to democratise parts of the research process through citizen science, particularly by allowing people to generate their own place-based knowledge and engage more fully in environmental management practice (Brierley, 2009; Brierley et al., 2006; Haywood et al., 2016; Vervoort et al., 2014).

In the Okavango Delta, the intent is for Figure 2 to provide geographical and geomorphological context for the various datasets, but we envisage that it could also be used as a template upon which temporal analyses are added as we gather additional data regarding the timeframes of adjustments. Indeed, detailed 3D hierarchies could be produced for each of the catchment, landscape unit, reach, site and geomorphic unit scales to visualise geomorphic changes over time, as well as the varying timeframes (millions of years to days) over which these changes occur. This approach could complement and extend previous approaches adopted by studies in and around the Delta that have investigated landscape and land cover dynamics but by necessity have had to rely on static imagery at a restricted range of spatial scales for temporal analysis (e.g., Hamandawana & Chanda, 2010).

While beyond the scope of this paper, and well beyond the extent of the data and information currently available for the Okavango, in other landscapes where high-resolution and extensive databases and resources already exist, there is significant potential for even more sophisticated multi-media, nested hierarchy visualisations to be produced. In these situations, a user would be able to zoom into the figure and access images, videos, animations and models showing different features at different scales and resolutions. Such technology can be used to provide not only geographical context across spatial scales but also context over time (Brierley et al., 2013; Montgomery, 2008; Phillips, 2015). Such approaches that synthesise existing and new datasets into an interactive and visual product have the potential to be highly effective in communicating geomorphology as part of more sustainable environmental management practices, particularly for transboundary rivers (cf. Armitage et al., 2015).

5 | CONCLUSION

This paper has demonstrated how at different scales in a nested hierarchy, various data collection, visualisation and mapping techniques have been used to gain geographical perspective and build a comprehensive picture of the Okavango catchment and Delta, and the Panhandle in particular. While the reality of most fieldwork is a focus on conducting relatively detailed analyses at finer scales in the hierarchy (reach, site and geomorphic unit scales), we found it invaluable to gain a much broader perspective (catchment to reach scales) both prior to, and during, fieldwork. In particular, obtaining a large-scale aerial perspective, whether derived from air photographs, remotely piloted aircraft or a helicopter, provides the context for making better informed and more insightful geomorphic interpretations of the landscape. Constraining analyses to too fine a scale, and/or failing to gain a broader perspective, runs the risk of misinterpretations. Our use of a nested hierarchical framework is certainly enhancing our ongoing analyses and interpretations of the fluvial geomorphology of the Okavango Delta, and also has potential to improve communication of geomorphology and engagement in water resources management. Moreover, given the rapid pace of technological advances that are enabling ever more detailed geographical and geomorphological data acquisition, multi-media nested hierarchical visualisations have significant potential for further developments, both within the Okavango Delta and beyond. Such developments are not only important scientifically but also provide a critical geographical perspective with which to engage a broader community and manage the environment.

and Aberystwyth University. We also thank Ineelo Mosie for assistance in the field and Mike Murray-Hudson for insights on the Okavango. We thank two anonymous reviewers and the Editor, Prof Keith Richards, for their comments on this paper.

ENDNOTES

[1] The Okavango crosses the Namibian panhandle (the Caprivi Strip); the narrow stretch of the Okavango after it has entered Botswana, and upstream from the delta, is referred to as the Okavango Panhandle in Botswana, and in this paper.

[2] An UAV is an Unmanned Aerial Vehicle, or drone. Structure-from-Motion (SfM) is a relatively inexpensive photogrammetric technique that can recover a 3D surface from multiple images obtained as a camera is moved around a survey area, without the need for detailed a priori information on camera geometry or a set of introduced targets (see Westoby et al., 2012).

ORCID

Kirstie A. Fryirs (iD) http://orcid.org/0000-0003-0541-3384

REFERENCES

Andersson, L., Wilk, J., Todd, M. C., Hughes, D. A., Earle, A., Kniveton, D., Layberry, R., Savenije, H. H. G. (2006). Impact of climate change and development scenarios on flow patterns in the Okavango River. *Journal of Hydrology*, *331*, 43–57.

Armitage, D., de Loe, R. C., Morris, M., Edwards, T. W., Gerlak, A. K., Hall, R. I., Huitema, D., Ison, R., Livingstone, D., MacDonald, G., Mirumachi, N., Plummer., & Wolfe, B. B. (2015). Science-policy processes for transboundary water governance. *Ambio*, *44*(5), 353–366.

Baker, V. R., & Twidale, C. R. (1991). The reenchantment of geomorphology. *Geomorphology*, *4*(2), 73–100.

Bishop, M. P., James, L. A., Shroder, J. F., & Walsh, S. J. (2012). Geospatial technologies and digital geomorphological mapping: Concepts, issues and research. *Geomorphology*, *137*(1), 5–26.

de Boer, D. H. (1992). Hierarchies and spatial scale in process geomorphology: A review. *Geomorphology*, *4*(5), 303–318.

Botswana Tourism Development Programme (BTDP) (1999). *Tourism economic impact assessment*. Gaborone, Botswana: Department of Tourism.

Brierley, G. J. (1996) Channel morphology and element assemblages: A constructivist approach to facies modelling. In P. Carling & M. Dawson (Eds.), *Advances in fluvial dynamics and stratigraphy* (pp. 263–298). Chichester, UK: Wiley Interscience.

Brierley, G. J. (2009). Communicating geomorphology. *Journal of Geography in Higher Education*, *33*(1), 3–17.

Brierley, G. J., & Fryirs, K. (2000). River styles, a geomorphic approach to catchment characterization: Implications for river rehabilitation in Bega catchment, New South Wales, Australia. *Environmental Management*, *25*(6), 661–679.

Brierley, G. J., & Fryirs, K. A. (2005). *Geomorphology and river management: Applications of the river styles framework*. Oxford, UK: Blackwell Publications.

Brierley, G. J., & Fryirs, K. A. (Eds.) (2008). *River futures: An integrative scientific approach to river repair*. Washington, DC: Island Press.

Brierley, G. J., Fryirs, K., Cullum, C., Tadaki, M., Huang, H. Q., & Blue, B. (2013). Reading the landscape: Integrating the theory and practice of geomorphology to develop place-based understandings of river systems. *Progress in Physical Geography*, *37*(5), 601–621.

Brierley, G. J., Hillman, M., & Fryirs, K. (2006). Knowing your place: An Australasian perspective on catchment-framed approaches to river repair. *Australian Geographer*, *37*(2), 131–145.

Chorley, R. J. (1969). The drainage basin as the fundamental geomorphic unit. In R. J. Chorley (Ed.), *Water, earth, and man*. London, UK: Methuen and Co., Ltd.

Church, M. (2010). The trajectory of geomorphology. *Progress in Physical Geography*, *34*(3), 265–286.

Cooke, R. U., & Doornkamp, J. C. (Eds.) (1990). *Mapping geomorphology*. Oxford, UK: Clarendon Press.

Dollar, E. S. J., James, C. S., Rogers, K. H., & Thoms, M. C. (2007). A framework for interdisciplinary understanding of rivers as ecosystems. *Geomorphology*, *89*(1), 147–162.

Du Toit, J. T., Biggs, H. C., & Rogers, K. H. (2003). *The Kruger experience: Ecology and management of savanna heterogeneity* (pp. 536). Washington, DC: Island Press.

Evans, I. S. (2012). Geomorphometry and landform mapping: What is a landform? *Geomorphology*, *137*(1), 94–106.

Frissell, C. A., Liss, W. J., Warren, C. E., & Hurley, M. D. (1986). A hierarchical framework for stream habitat classification: Viewing streams in a watershed context. *Environmental Management*, *10*(2), 199–214.

Fryirs, K. A., & Brierley, G. J. (2013). *Geomorphic analysis of river systems: An approach to reading the landscape*. Chichester, UK: John Wiley and Sons.

Fryirs, K. A., Wheaton, J. M., & Brierley, G. J. (2016). An approach for measuring confinement and assessing the influence of valley setting on river forms and processes. *Earth Surface Processes and Landforms*, *41*, 701–710.

Government of Denmark and Republic of Botswana. (2006). *Okavango management plan: Hydrology and Water resources, morphology and sediment transport* (pp. 49). Maun, Botswana: Harry Oppenheimer Okavango Research Centre.

Gregory, K. J., & Lewin, J. (2015). Making concepts more explicit for geomorphology. *Progress in Physical Geography*, *39*(6), 711–727.

Gumbricht, T., & McCarthy, T. S. (2003) Hierarchical processes and patterns sustaining the Okavango: An integrated perspective for policy and management. *Environmental Monitoring of Tropical and Subtropical Wetlands. Maun (Botswana): Harry Oppenheimer Okavango Research Center*. Okavango Report Series 1 181-196.

Gumbricht, T., McCarthy, T. S., & Merry, C. L. (2001). The topography of the Okavango Delta, Botswana, and its tectonic and sedimentological implications. *South African Journal of Geology*, *104*, 243–264.

Gumbricht, T., Wolski, P., Frost, O., & McCarthy, T. S. (2004). Forecasting the spatial extent of the annual flood in the Okavango delta. *Botswana Journal of Hydrology*, *290*, 178–191.

Gurnell, A. M., Rinaldi, M., Belletti, B., Bizzi, S., Blamauer, B., Braca, G., Buijse, A. D., Bussettini, M., Camenen, B., Comiti, F., Demarchi, L., García de Jalón, D., González del Tánago, M., Grabowski, R. C., Gunn, I. D. M. (2016). A multi-scale hierarchical framework for developing understanding of river behaviour to support river management. *Aquatic Sciences*, *78*(1), 1–16.

Hamandawana, H., & Chanda, R. (2010). Natural and human dimensions of environmental change in the proximal reaches of Botswana's Okavango Delta. *The Geographical Journal*, *176*, 58–76.

Harris, L. M., & Alatout, S. (2010). Negotiating hydro-scales, forging states: Comparison of the upper Tigris/Euphrates and Jordan River basins. *Political Geography*, *29*(3), 148–156.

Haywood, B. K., Parrish, J. K., & Dolliver, J. (2016). Place-based and data-rich citizen science as a precursor for conservation action. *Conservation Biology*, *30*(3), 476–486.

Jansen, R., & Madzwamuse, M. (2003). The Okavango Delta management plan project: The need for environmental partnerships. In A. Turton, P. Ashton & E. Cloete (Eds.), *Transboundary rivers, sovereignty and development: Hydropolitical drivers in the Okavango river basin*. Pretoria, South Africa: African Water issues Research Unit (AWIRU) and Green Cross International (GCI).

Kellerhals, R., Church, M., & Bray, D. I. (1976). Classification and analysis of river processes. *Journal of the Hydraulics Division. Proceedings of the American Society of Civil Engineers*, *102*(HY7), 813–829.

Kgathi, D. L., Kniveton, D., Ringrose, S., Turton, A. R., van der Post, C. H. M., Lundqvist, J., & Seely, M. (2006). The Okavango; a river supporting its people, environment and economic development. *Journal of Hydrology*, *331*, 3–17.

Kleinhans, M. G. (2010). Sorting out river channel patterns. *Progress in Physical Geography*, *34*(3), 287–326.

Lisenby, P., & Fryirs, K. (2017). 'Out with the Old?' Why coarse spatial datasets are still useful for catchment-scale investigations of sediment (dis)connectivity. *Earth Surface Processes and Landforms*, *42*, 1588–1596.

Mbaiwa, J. (2002). The socio-economic and environmental impacts of tourism development on the Okavango Delta, north-western Botswana. *Journal of Arid Environments*, *54*, 447–467.

Mbaiwa, J. (2004). Causes and possible solutions to water resource conflicts in the Okavango River Basin: The case of Angola. *Namibia and Botswana Physics and Chemistry of the Earth*, *29*, 1319–1326.

McCarthy, T. S. (2013). The Okavango Delta and its place in the geomorphological evolution of Southern Africa. *South African Journal of Geology*, *116*, 1–54.

McCarthy, T. S., & Ellery, W. N. (1998). The Okavango Delta. *Transactions of the Royal Society of South Africa*, *53*, 157–182.

McCarthy, T. S., Ellery, W. N., & Stanistreet, I. G. (1992). Avulsion mechanisms on the Okavango fan, Botswana: The control of a fluvial system by vegetation. *Sedimentology*, *39*, 779–795.

McCarthy, J., Gumbricht, T., & McCarthy, T. S. (2005). Ecoregion classification in the Okavango Delta, Botswana, from multitemporal remote sensing. *International Journal of Remote Sensing*, *26*, 4339–4358.

McCarthy, J., Gumbricht, T., McCarthy, T. S., Frost, P., Wessels, K., & Seidel, F. (2003). Flooding patterns of the Okavango wetland in Botswana between 1972 and 2000. *Ambio*, *32*, 453–457.

McCarthy, T. S., Humphries, M. S., Mahomed, I., Le Roux, P., & Verhagen, B. (2012). Island forming processes in the Okavango Delta. *Botswana Geomorphology*, *179*, 249–257.

Mendelsohn, J. M., dervan Post, C., Ramberg, L., Murray-Hudson, M., Wolski, P., & Mosepele, K. (2010). *Okavango delta: Floods of life*. Windhoek, Namibia: RAISON.

Montgomery, D. R. (2008). Dreams of natural streams. *Science*, *319*, 291–292.

Mueller, G. A., & Marsh, P. C. (2002). *Lost, a desert river and its native fishes: A historical perspective of the lower Colorado River*. US Fish and Wildlife Service, Information Technology Report, 2002-0010.

OKACOM (2017). *The permanent Okavango river basin water commission (OKACOM)*. Retrieved from http://www.okacom.org

Partridge, T. C., Dollar, E. S. J., Moolman, J., & Dollar, L. H. (2010). The geomorphic provinces of South Africa, Lesotho and Swaziland: A physiographic subdivision for earth and environmental scientists. *Transactions of the Royal Society of South Africa*, *65*(1), 1–47.

Perron, J. T., & Royden, L. (2013). An integral approach to bedrock river profile analysis. *Earth Surface Processes and Landforms*, *38*(6), 570–576.

Phillips, J. D. (1988). The role of spatial scale in geomorphic systems. *Geographical Analysis*, *20*(4), 308–317.

Phillips, J. D. (2015). Badass geomorphology. *Earth Surface Processes and Landforms*, *40*(1), 22–33.

Poole, G. C. (2002). Fluvial landscape ecology: Addressing uniqueness within the river discontinuum. *Freshwater Biology*, *47*(4), 641–660.

Pröpper, M., & Gröngröft, A. (Eds.) (2015). *The Future Okavango (TFO): Findings, scenarios and recommendations for action; research project final synthesis report 2010–2015*. Germany: University of Hamburg.

Rahm, D., Swatuk, L., & Matheny, E. (2006). Water resource management in Botswana: Balancing sustainability and economic development *Environment. Development and Sustainability*, *8*, 157–183.

Ralph, T. J., Hesse, P. P., & Kobayashi, T. (2016). Wandering wetlands: Spatial patterns of historical channel and floodplain change in the Ramsar-listed Macquarie Marshes. *Australia Marine and Freshwater Research*, *67*, 782–802.

Schumm, S. A. (1977). *The fluvial system*. New York, NY: John Wiley and Sons.

Schumm, S. A., & Lichty, R. W. (1965). Time, space and causality in geomorphology. *American Journal of Science*, *263*, 110–119.

Smith, N. D., McCarthy, T. S., Ellery, W. N., Merry, C. L., & Rüther, H. (1997). Avulsion and anastomosis in the Panhandle region of the Okavango fan. *Botswana Geomorphology*, *20*, 49–65.

Thornbush, M., Allen, C. D., & Fitzpatrick, F. A. (Eds.) (2014). *Geomorphological fieldwork*. Amsterdam, the Netherlands: Elsevier.

Tooth, S. (2015). Spotlight on. Google Earth as a resource. *Geography*, *100*(1), 51–56.

Tooth, S., & McCarthy, T. S. (2004). Controls on the transition from meandering to straight channels in the wetlands of the Okavango Delta. *Botswana Earth Surface Processes and Landforms*, *29*, 1627–1649.

Tooth, S., Viles, H. A., Dickinson, A., Dixon, S. J., Falcini, A., Griffiths, H. M., Hawkins, H., Lloyd-Jones, J., Ruddock, J., Thorndycraft, V. R., & Whalley, B. (2016). Visualizing geomorphology: Improving communication of data and concepts through engagement with the arts. *Earth Surface Processes and Landforms*, *41*(12), 1793–1796.

A. Turton, P. Ashton, & E. Cloete. (Eds.). (2003). *Transboundary rivers, sovereignty and development: Hydropolitical drivers in the Okavango river basin*. Pretoria, South Africa: African Water issues Research Unit (AWIRU) and Green Cross International (GCI).

Varis, O., Tortajada, C., & Biswas, A. K. (2008). *Management of transboundary rivers and lakes* (pp. 304). Berlin, Germany: Springer. Retrieved from https://doi.org/10.1007/978-3-540-74928-8

Vervoort, J. M., Hoogstra, M. A., Kok, K., van Lammeran, R., Bregt, A. K., & Janssen, R. (2014). Visualizing stakeholder perspectives for reflection and dialogue on scale dynamics in social-ecological systems. *Human Ecology Review*, *20*(2), 157–181.

Westoby, M. J., Brasington, J., Glasser, N. F., Hambrey, M. J., & Reynolds, J. M. (2012). 'Structure-from-Motion' photogrammetry: A low-cost, effective tool for geoscience applications. *Geomorphology*, *179*, 300–314.

Wheaton, J. M., Fryirs, K. A., Brierley, G., Bangan, S. G., Bouwes, N., & O'Brien, G. (2015). Geomorphic mapping and taxonomy of fluvial landforms. *Geomorphology*, *248*, 273–295.

Williams, R. G., Tooth, S., & Gibson, M. (2017). The sky is the limit: Reconstructing physical geography from an aerial perspective. *Journal of Geography in Higher Education*, *41*(1), 134–146.

SUPPORTING INFORMATION

Additional supporting information may be found online in the Supporting Information section at the end of the article.

Data S1. A nested hierarchical perspective for use in interpretation and communication of the fluvial geomorphology of the Okavango Delta.

How to cite this article: Fryirs KA, Ralph TJ, Larkin ZT, et al. A nested hierarchical perspective to enhance interpretations and communication in fluvial geomorphology for use in water resources management: Lessons from the Okavango Delta, Botswana. *Geogr J*. 2018;184:192–207. https://doi.org/10.1111/geoj.12250